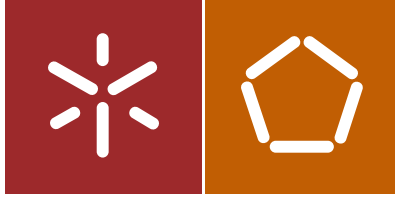


Universidade do Minho  
Escola de Engenharia

Sílvia Manuela Ferreira da Cruz

INKJET PRINTING TECHNOLOGY  
FOR FLEXIBLE PRESSURE SENSORS



Universidade do Minho  
Escola de Engenharia

Sílvia Manuela Ferreira da Cruz

INKJET PRINTING TECHNOLOGY  
FOR FLEXIBLE PRESSURE SENSORS

Tese de Doutoramento  
Ciência e Engenharia de Polímeros e Compósitos

Trabalho efectuado sob a orientação do  
Professor Doutor Júlio César Machado Viana  
Professor Doutor Luís Alexandre Machado da Rocha

## DECLARAÇÃO

**Nome**

Sílvia Manuela Ferreira Da Cruz

**Título:**

INKJET PRINTING TECHNOLOGY FOR FLEXIBLE PRESSURE SENSORS

**Orientador(es):**

Professor Doutor Júlio César Machado Viana

Professor Doutor Luís Alexandre Machado da Rocha

**Ano de conclusão:** 2015

**Designação do Ramo de Conhecimento do Doutoramento:**

Programa Doutoral em Ciência e Engenharia de Polímeros e Compósitos

É AUTORIZADA A REPRODUÇÃO PARCIAL DESTA TESE APENAS PARA EFEITOS DE INVESTIGAÇÃO, MEDIANTE DECLARAÇÃO ESCRITA DO INTERESSADO, QUE A TAL SE COMPROMETE.

Universidade do Minho, 27 de Fevereiro de 2015

Assinatura:

## STATEMENT OF INTEGRITY

I hereby declare having conducted my thesis with integrity. I confirm that I have not used plagiarism or any form of falsification of results in the process of the thesis elaboration.

I further declare that I have fully acknowledged the Code of Ethical Conduct of the University of Minho.

University of Minho, \_\_\_\_\_

Full name: Sílvia Manuela Ferreira da Cruz

Signature: \_\_\_\_\_





*To my family,  
Para a minha família,*

*Nothing in life is to be feared, it is only to be understood. Now is the time to understand more,  
so that we may fear less.*

*Marie Curie (1867-1934)*



---

# Acknowledgments

Over these three years, I have learned a lot, and one of them was that a PhD is not an individual journey. For this reason, I would like to express my gratitude to numerous persons that contributed to the achievement of this thesis.

Firstly, I would like to express my gratitude to my supervisors Professor Júlio César Machado Viana and Professor Luís Alexandre Machado Rocha for their patience, support, teaching and guidance. Professor Júlio Viana has been a mentor and advisor to me during my under-graduate years and my Master's thesis. He has showed me how to do good science, and how the scientific community operates. For helping me grow as a student and as researcher, I cannot thank them enough. I want to thank Professor Luís Rocha for his steadfastness and persistence ideas. He has given me independence to manage my work, but still, he readily provides help through insightful comments and guide with more clever ideas.

To my friends, Gabriela Azevedo, Alexandra Sepúlveda, Bruno Oliveira, Paulo Teixeira and Carlos Nuno Barbosa and, Seyyed Sabet with who I have create great friendships bonds, and somehow helped me during this long journey. To Daniel Dias for his contribution and collaboration on experimental *hardware and software*. Thanks also to academic staff and technicians of the Department of Polymer Engineering. To all the persons and entities that contributed to the work, but are not directly mentioned here, my sincere gratefulness and appreciation.

To the hosting institution, the Institute of Polymer and Composites/I3N of the University of Minho for the facilities and equipment provided for this research. I hereby acknowledge the scientific project "TICE-Healthy - Sistemas de Saúde e Qualidade de Vida", project n.º 13842, co-financed by FEDER which made possible the realization of this work.

Finally, I would like to dedicate this thesis to those who gave me their ultimate support, my family. To my parents and brother, for being present when I most needed them. For their encouraging words and incentive when I was discouraged. To Hugo who has helped me the most and with whom I have the happiness to share everything in my life. For his patience towards my unpredictable research schedules. To my newborn Ana Carolina, for her unending love when my full attention was most needed.

My family has helped me tremendously in completing this journey.



## **‘Inkjet Printing Technology for Flexible Pressure Sensors’**

Conductive ink has extraordinary properties. The printing of patterns with conductive inks on polymer surfaces gives them new properties and functionalities, making them ideal for several diverse application areas. These printed polymeric materials can be embedded in a system to perform a given function, e.g., to change their electrical resistivity as a response to an applied deformation.

The use of printed electronics on the fabrication of flexible pressure sensors is of particular interest. Flexible Pressure Sensor (FPS) technology provides more accurate reading and contact area thanks to its ability to fold/roll, when compared to other traditionally used materials. However, they remain unsatisfactory and inaccessible to the general population. Developing a more intelligent and efficient sensor, capable of being integrated in complex environments, with improved properties, lighter and more robust, elastically deformable with quick back response, which does not sacrifice the freedom of motion, and equally important, economically attractive and suitable for mass production, is essential.

Inkjet Printing Technology (IPT) has evolved in a way that ceased to be known only as a manufacturing tool in the paper and newspapers industry and it became one of the most important technologies in organic, flexible electronics and printing polymeric substrates, as well as a topic in scientific research. This technology has attracted the attention of the industrial community over the past due to a number of features, which makes a compelling argument for an interesting alternative to the conventional Printed Electronics (PE) technologies.

But, there are many challenges in the use of direct printing. Most polymers are hydrophobic showing a low surface energy. Therefore, they are difficult to adhere to other materials. A new developed method for the surface treatment of polymeric substrates in order to increase their surface energies is presented. This novel surface treatment of thermoplastic polymers was applied to the inkjet printing of Thermoplastic Polyurethane (TPU) substrates with conductive inks, and significant improvements on the printability were obtained.

Still, to reach the spatial geometry of the printed pattern, electrical conductivity, resolution and durability, several studies were performed and depending on the material involved, a specific know-how is required. A compromise between several criteria must be performed in order to select the proper substrate and conductive ink to get the desired sensor performance (achieve the desired sensor characteristics like resolution and bandwidth).

The focus of this thesis is the development of a new generation of good performance and lower cost thin flexible pressure sensors. The applied research was focused from a materials science point of view (selectively applying commercially available and compatible materials or defining viable material alternatives), with resource to a Drop-on-Demand inkjet printer with a piezoelectric printhead to process the materials, and exploring it's potential to be integrated into electronic applications.

Three different inks with different characteristics were studied. After inkjet printing parameters definition and depending on the ink and substrate, the characterization of the printed system was conducted for pattern resolution, adhesion of the ink to the substrate, and electromechanical properties evaluation.

The design, fabrication and experimental results of a FPS system and its readout electronics interface are also presented here. The developed sensing platform for postural imbalance monitoring consists of an array of flexible capacitive pressure sensors, in the millimeter range and uses a simple manufacturing process (enabling a reasonable density of sensors in the active zone). Thus, it is possible to achieve good performance results (comparable to existing solutions in the industry), with the particularity of offering an economically viable alternative, allowing its use in rehabilitation activities. The results obtained are very promising and encouraging. The developed pressure platform could be successfully inkjet printed and was fully functional.

## **‘Tecnologia de Impressão a Jato de Tinta para Sensores de Pressão Flexíveis’**

As tintas condutoras têm propriedades extraordinárias. A impressão de padrões com tintas condutoras na superfície de polímeros atribui-lhes novas propriedades e funcionalidades, tornando-os ideais para diversas áreas de aplicação. Estas tintas impressas em substratos poliméricos podem ser incorporados num sistema para realizar uma dada função, i.e., a sua resistividade elétrica muda em resposta à deformação exercida.

O uso da eletrônica impressa na fabricação de sensores de pressão flexíveis tem particular interesse. A tecnologia de sensores de pressão flexíveis permite maior precisão de leitura e maiores áreas de contato graças à sua capacidade para dobrar/enrolar, quando comparados aos materiais tradicionalmente utilizados. No entanto, estes sensores continuam a ser incipientes e inacessíveis a população em geral. Desenvolver um sensor inteligente e eficiente, capaz de integrar ambientes complexos, com propriedades, de tamanho ainda mais reduzido, leves e robustos, deformáveis e com elasticidade, com rápida resposta, e que não sacrifique a liberdade de movimentos, economicamente atrativos e adequados para produção à escala industrial é essencial.

A tecnologia de impressão a Jato de Tinta evoluiu de tal forma que deixou de ser conhecida apenas como uma ferramenta de produção na indústria do papel e de jornais e, tornou-se uma das tecnologias mais importantes na eletrônica flexível e na impressão de substratos poliméricos, bem como um tópico pesquisa científico. Nos últimos anos, esta tecnologia atraiu a atenção da comunidade industrial principalmente devido a uma série de características que a torna num argumento convincente como uma alternativa interessante as tecnologias convencionais para a eletrônica impressa.

No entanto, são muitos os desafios do uso de impressão direta. A maioria dos polímeros são hidrofóbicos, apresentando uma baixa energia de superfície. Por esta razão são difíceis de aderir a outros materiais. Um novo tratamento da superfície foi desenvolvido para os substratos poliméricos, a fim de aumentar as suas energias de superfície. Na superfície do substrato de termoplástico poliuretano (TPU) com o novo tratamento de superfície, tintas condutoras foram impressas e melhorias significativas na capacidade de impressão foram observados.

Ainda assim, a obtenção a geometria especial da estrutura impressa, condutividade elétrica, resolução de impressão e durabilidade, exigiu estudo, e dependendo dos materiais envolvidos, um *know-how* específico é necessário. Será um compromisso entre vários critérios de forma a seleccionar o substrato e a tinta condutora ideal para obter a performance desejada do sensor (atingir as características desejadas do sensor como a resolução e largura de banda).



O foco deste trabalho reside no desenvolvimento de uma nova geração de sensores de pressão flexíveis com bom desempenho e baixo custo. O estudo focou-se no ponto de vista da ciência dos materiais (aplicação seletiva de materiais comercialmente disponíveis e compatíveis, ou definir alternativas viáveis), utilizando uma impressora jato de tinta com sistema *Drop-on-Demand* com uma cabeça de impressão piezoelétrica para processar os materiais, e explorar o seu potencial para ser integrado em aplicações eletrônicas.

Foram estudadas três tintas com características diferentes. Após a definição dos parâmetros de impressão a jacto de tinta de acordo com a tinta e o substrato, o sistema impresso foi caracterizado para uma avaliação da resolução de impressão, adesão da tinta ao substrato, e das propriedades eletromecânicas.

O *design*, fabricação e resultados experimentais de um sensor de pressão flexível e sua interface eletrônica de leitura também foram aqui apresentados. O sensor de pressão flexível desenvolvido para monitorização do desequilíbrio postural consiste numa matriz de sensores capacitivos de pressão flexíveis, no intervalo milímetro, e, usa um processo de fabrico simples (permitindo uma densidade razoável de sensores na zona ativa). Assim, é possível conseguir bons resultados de desempenho (comparáveis às soluções existentes na indústria), com a particularidade de oferecer uma alternativa economicamente viável, permitindo o seu uso em atividades de reabilitação. Os primeiros resultados obtidos são muito promissores e encorajadores. A plataforma de pressão desenvolvida pode ser produzida com sucesso por impressão a jato de tinta e demonstrou ser totalmente funcional.

---

# Table of Contents

	Page
<i>Acknowledgements</i> .....	v
<i>Abstract</i> .....	vii
<i>Resumo</i> .....	ix
<i>Table of Contents</i> .....	xi
<i>List of Figures</i> .....	xvi
<i>List of Tables</i> .....	xxiii
<i>List of Abbreviation</i> .....	xxiv
<i>List of Symbols</i> .....	xxviii
<b>Chapter 1. Introduction</b> .....	<b>1</b>
1.1. Context.....	3
1.2. Printed Electronics (PE) .....	3
1.3. Motivation and Objectives.....	6
1.4. Research approach.....	8
1.5. Thesis outline.....	10
REFERENCES.....	12
<b>Chapter 2. Overview on Printing Technology for Printed Electronics</b> .....	<b>15</b>
2.1. Contact printing techniques.....	17
2.1.1. Screen Printing.....	17
2.1.2. Flexography.....	19
2.1.3. Gravure printing.....	20
2.1.4. Soft lithography.....	22
2.2. Non-contact printing techniques.....	25
2.2.1. Laser Direct Writing (LDW) .....	25
2.2.2. Aerosol printing.....	26
2.2.3. Inkjet printing Technology.....	27
2.3. Historical overview on Inkjet Printing Technology.....	28
2.4. IPT mode technology systems.....	30
2.4.1. Continuous Inkjet (CIJ) Mode Technology.....	31
2.4.2. Drop-On-Demand (DoD) System.....	32
2.4.2.1. Acoustic method.....	33
2.4.2.2. Electrostatic method.....	33

2.4.2.3. Thermal method.....	34
2.4.2.4. Piezoelectric method.....	34
2.4.2.5. Microelectromechanical Systems (MEMS) manufacturing method.....	35
2.5. Process phenomena.....	36
2.5.1. Drop formation.....	36
2.5.2. Drop impact phenomena.....	38
2.6. Process variables.....	41
2.7. Materials and potential applications.....	42
2.8. Advantages and Challenges of IPT.....	44
2.8.1. Ink properties .....	46
2.8.2. Process control.....	47
2.8.3. Ink compatibility.....	47
2.8.4. Compatibility between ink and substrate.....	48
2.8.5. Substrate surface treatment.....	49
2.9. Flexible pressure sensors.....	51
2.10. IPT of conductive inks on polymeric substrates for FPS manufacturing.....	53
2.11. Summary.....	54
REFERENCES.....	56
<b>Chapter3. Materials and Methods.....</b>	<b>69</b>
3.1. Material selection.....	71
3.1.1. Substrates.....	71
3.1.1.1. Poly(4,4'-oxydiphenylene-pyromellitimide).....	71
3.1.1.2. Polyethylene terephthalate (PET).....	72
3.1.1.3. Polydimethylsiloxane (PDMS).....	72
3.1.1.4. Thermoplastic polyurethane (TPU).....	73
3.1.2. Micro and nanosized particles.....	74
3.1.2.1. Clay Particles (CP).....	74
3.1.2.2. Silica Particles (SP) .....	75
3.1.3. Conductive inks for IP.....	75
3.1.3.1. Poly (thiophene - 3- [2 - (2-methoxyethoxy)ethoxy] - 2,5 - diyl), sulfonated (P3HT) .....	75
3.1.3.2. Poly (3,4-ethylenedioxythiophene) - poly (styrenesulfonate) (PEDOT:PSS) .....	77
3.1.3.3. Silver-based ink.....	80

3.2. Substrates preparation method.....	82
3.2.1. PDMS fabrication.....	82
3.2.2. TPU Compression moulding procedure.....	83
3.2.3. Substrate cleaning.....	84
3.3. Technology – Xennia Carnelian.....	84
3.3.1. Printhead Mount.....	86
3.3.2. Motion System.....	88
3.3.3. Drop-spacing and resolution.....	89
3.3.4. Jet controls.....	90
3.3.5. Check of the printed pattern quality.....	92
3.3.6. Printhead working principal.....	92
3.4. Characterization Techniques.....	93
3.4.1. Critical Substrate Superficial Tension (ST) measurements.....	94
3.4.2. Thermalgravimetric analysis (TGA) of the conductive inks.....	95
3.4.3. Detail characterization of the surface treated substrates and of the printed ink.....	95
3.4.3.1. Adhesion tests.....	95
3.4.3.2. Optical Microscopy (OM).....	97
3.4.3.3. Scanning electron microscopy (SEM).....	97
3.4.3.4. Atomic force microscopy (AFM).....	97
3.4.3.5. Electrical conductivity measurements.....	98
3.4.3.6. Measurement of piezo-resistive effect of the printed ink.....	100
REFERENCES.....	103

***Chapter 4. Inkjet Printing of Poly (thiophene-3-[2-(2-methoxyethoxy)ethoxy]-2,5-diyl) sulfonated conductive ink (P3HT).....109***

4.1. Inkjet printing of polymer conductive ink.....	111
4.1.1. Material's properties.....	111
4.1.2. Ink Preparation.....	113
4.1.3. Preliminary Inkjet printing.....	113
4.1.3.1. Surface roughness control.....	114
4.1.4. Inkjet printing on modified substrate.....	119
4.2. Adhesion and electrical resistivity characterization of printed substrates.....	123
4.2.1. Adhesion tests.....	123
4.2.2. Electrical resistivity measurements.....	124
4.3. Summary.....	125

REFERENCES.....	127
<b>Chapter 5. Inkjet Printing of the Poly (3,4-ethylenedioxythiophene) - poly (styrenesulfonate) (PEDOT:PSS) conductive ink.....</b>	<b>129</b>
5.1. Inkjet printing of the polymer conductive ink.....	131
5.1.1. Material's properties.....	131
5.1.2. Ink Preparation.....	133
5.1.3. Preliminary Inkjet printing.....	133
5.1.4. Inkjet printing on the modified substrate.....	134
5.2. Adhesion and electrical characterization of the printed substrates.....	138
5.2.1. Adhesion test.....	138
5.2.2. Electrical resistivity.....	139
5.2.3. Piezo-resistive measurements.....	140
5.3. Summary.....	145
REFERENCES.....	147
<b>Chapter 6 - Inkjet Printing of the silver based ink.....</b>	<b>149</b>
6.1. Inkjet printing of polymer conductive ink.....	151
6.1.1. Material's properties.....	151
6.1.2. Ink preparation.....	155
6.1.3. Preliminary Inkjet printing.....	155
6.1.4. Inkjet printing on the TPU substrate.....	158
6.2. Adhesion and electrical resistivity characterization of printed substrates.....	161
6.2.1. Adhesion tests.....	161
6.2.2. Electrical resistivity measurements.....	162
6.3. Summary.....	164
REFERENCES.....	166
<b>Chapter 7 - Ink-Jet Printed Pressure Sensing Platform for Health Monitoring.....</b>	<b>167</b>
7.1. Introduction.....	169
7.2. System Overview.....	171
7.3. Sensor Modeling.....	172
7.4. Manufacturing Process.....	175
7.4.1. Flexible Membranes with Conductive Inks.....	175
7.4.2. Flexible PCB's.....	177
7.4.3. Prototype Sensor Assembly.....	178
7.5. Electronics Interface.....	178

7.6. Experimental Results and Discussion.....	179
7.7. Summary.....	184
REFERECES.....	189
<b>Chapter 8 – Conclusions and Future Work.....</b>	<b>191</b>
8.1. Conclusions.....	193
8.2. Future work.....	197
<b>Appendix.....</b>	<b>199</b>
A1. Other fabrication techniques.....	200
A2. Piezoelectric heads.....	202
A.2.1. Shear mode.....	202
A.2.2. Bend mode.....	202
A.2.2.3. Push mode.....	203
A.2.2.4. Squeeze mode.....	204
A3. Inkjet Printer information.....	205
A4. Datasheet of the printhead.....	208
A5. Datasheet of the substrates.....	210
A6. Datasheet of the nanoparticles.....	218
A7. Datasheet of the inks.....	220
A8. Characterization Kit and Comparison Chart.....	224
A9. Adhesive datasheet.....	226
A10. Pressure Chamber accessories.....	227
A11. List of Publications.....	231



---

# List of Figures

	Page
Figure 1.1-New applications for Printable Electronics.....	4
Figure 1.2 - The market in 2013 for printed Flexible sensors.....	4
Figure 1.3 - Block diagram of the physiological computing approach.....	8
Figure 1.4 - Schematic outline of the work presented in this thesis.....	10
Figure 2.1 - Schematic of Screen printing (at left).Flat-bed screen printing of silver paste showing the squeegee during a printing cycle showing how the ink is forced through.....	17
Figure 2.2 – Schematic of Rotary screen printing (left). A photograph of rotary screen printing of conducting graphite ink onto a clear polyester foil (right).....	18
Figure 2.3 - Screen-printing: a) Biosensor inks on the Left; b) Flexible EL on the right; c) Top view photograph of a pressure sensitive test device (not to scale). The force probe is applied to the center of the printed disk. ....	18
Figure 2.4 – Schematic of flexographic printing system.....	19
Figure 2.5 - The anilox roller disengaged from the anilox showing the negative print of the motif after ink pick out from the printing cylinder (left). The printing cylinder with the relief carrying the ink (in this case a silver paste) during printing. The final printed pattern on the web can be observed in the background (right).....	20
Figure 2.6 – Gravure printing process. ....	21
Figure 2.7 - Detail of Gravure Cylinder engraving and a comparison of printability of 200 $\mu\text{m}$ nominal line by using two different engraving approaches.....	21
Figure 2.8 - Gravure printed wireless power antenna. This could allow sensor networks such as RFID tags, price tags, smart logos, signage, and sensors could be fully interconnected and driven by DC power of less than 0.3 W.....	22
Figure 2.9 - Schematic illustration of the four major steps implied in soft lithography and is four major techniques: (a) replica molding (REM), (b) microtransfer molding ( $\mu\text{TM}$ ), (c) micromolding in capillaries (MIMIC), and (d) solvent-assisted micromolding (SAMIM).....	23
Figure 2.10 - Schematic illustration of the major steps in soft lithography technologies: (a) replica molding (REM), (b) microtransfer molding ( $\mu\text{TM}$ ), (c) micromolding in capillaries (MIMIC), and (d) solvent-assisted micromolding (SAMIM).....	24
Figure 2.11-Structure layers of a tactile sensing array manufactured by Lithography.....	24



Figure 2.12 - Schematic of the LIFT process.....	26
Figure 2.13 - Optical microscopy images of the microarrays of LIFT spotted droplets containing the human cDNAs in a); SEM images of laser direct written silicon wires for field effect transistor sensors in b). Boron-doped silicon wires are fabricated using laser direct writing in combination with chemical vapor deposition.....	26
Figure 2.14 - At left is a schematic of aerosol jet printing process. At right is a printed silver structures into 500 $\mu\text{m}$ deep trenches through aerosol jet printing.....	27
Figure 2.15 – At left a schematic of the Inkjet printing technology. At right a jet printed IPT pattern on flexible polymer substrate with a polyaniline ink.....	28
Figure 2.16 – The Siphon recorder. The first practical continuous inkjet device.....	29
Figure 2.17 - Drawing of the first drop-on-demand piezoelectric inkjet device patented in 1950 (US Patent 2,512,743).....	30
Figure 2.18 – Printing Technologies respective methods and specialized companies.....	31
Figure 2.19 - IPT processing scheme. This system uses both the binary deflection and multiple deflection systems.....	32
Figure 2.20 – DoD system – Acoustic method.....	33
Figure 2.21 – DoD system – Electrostatic method.....	33
Figure 2.22 - DoD system - Thermal Method.....	34
Figure 2.23 - Behind DoD system – Piezoelectric method.....	35
Figure 2.24 – DoD system – MEMS printhead.....	36
Figure 2.25– Stroboscopic images of inkjet printing droplets: a) drop formation for a Newtonian fluid; b) effect of addition to the ink of a small amount of high molecular weight polymer.....	37
Figure 2.26 - Influence of polymer concentration and molecular weight on the drop formation dynamics: a) glycerol/water; b) 0.3%100000 poly(ethylene oxide); c) 0.1%300000 poly(ethylene oxide); d) 0.05%1000000 poly(ethylene oxide); e) 0.043%5000000 poly(ethylene oxide).....	38
Figure 2.27 – Drop impact morphology on a dry surface.....	39
Figure 2.28 - Schematic representation of the spreading of a liquid drop with time. ( $d^*$ is the non-dimensional diameter of the drop, and $t^*$ the non-dimensional time after impact. The labelling of the axes is approximate.....	41
Figure 2.29 – Typical ink formulation.....	44
Figure 2.30 – Challenge critical areas.....	46
Figure 2.31 – Ink behaviour on substrate.....	48
Figure 2.32 - Contact angle: a) High surface energy with a contact angle $<90^\circ$ ; b) Low surface energy with a contact angle $>90^\circ$ .....	49

Figure 2.33 - Optical microscope photographs of PI film contact angle: a) without treatment. [contact angle: 46.2°]; b) after low pressure plasma treatment [contact angle: 14.5°]	50
Figure 2.34 - Illustration of a capacitive pressure sensor based on the parallel arrangement.	52
Figure 3.1 - Structure of poly-oxydiphenylene-pyromellitimide, "Kapton"	71
Figure 3.2 - Chemical structure of polyethylene terephthalate"	72
Figure 3.3 - The chemical formula of Polydimethylsiloxane. a) Chemical structure combining both organic and inorganic groups; b) Structural representation of the shielding of the main chain (Si-O groups) by the methyl groups.	72
Figure 3.4 - Molecular structures of most common industrial isocyanates.	73
Figure 3.5 - Schematic diagram of a regioregular polythiophene based polymers.	76
Figure 3.6 - Poly(thiophene-3-[2-(2-methoxyethoxy)ethoxy]-2,5-diyl), sulfonated solution 2% in ethylene glycol monobutyl ether/water, 3:2, electronic grade.	77
Figure 3.7 - Molecular structure of Poly (3,4-ethylenedioxythiophene)-poly (styrenesulfonate).	79
Figure 3.8 - Fabrication process flow for the development of a flexible PDMS substrate.	83
Figure 3.9 - Compression moulding procedure for TPU substrates fabrication.	83
Figure 3.10 - Cleaning effect on the wettability. Cleaning the glass substrates results in a better wetting with polar liquids.	84
Figure 3.11 - Xennia Carnelian Inkjet Printer.	85
Figure 3.12 - Schematic of the main components of the Carnelian system.	85
Figure 3.13 - Printhead mount: a) printhead; b) detail figure of the printhead rotation system.	87
Figure 3.14 - Digital foto of a Dimatix Sapphire QS-256/10 AAA print head.	88
Figure 3.15 - Print head and motion plate direction movements.	89
Figure 3.16 - Pattern resolution in X-Axis and Y- Axis.	90
Figure 3.17 - Steps for testing the inkjet printing parameters.	93
Figure 3.18 - The TQC Cross Cut Adhesion Test KIT (CC2000) ate the left and Cutting tool accessory ate right.	96
Figure 3.19 - Schematic representation of a Van der Pauw configuration used in the measurements of the two characteristics resistance $R_A$ and $R_B$ .	99
Figure 3.20 - Digital image of the experimental test setup. a) Sample assembly jig with four ohmic contact probes from the resistivity measurement system.	100
Figure 3.21 - Standard (according to ISO527- 2:1993) geometry shape (in mm) used for the	

piezo-resistive tests. ....	101
Figure 3.22 - Piezo-resistive measurements setup: a) metal grip isolation; b) IC Capture 2.0 interface.....	102
Figure 4.1 – P3HT mass loss analysis for optimal annealing temperature evaluation.....	112
Figure 4.2 – Printed substrates: a) Inspection camera image of a clean PDMS substrate with flooding of the P3HT ink; b) Digital image of TPU with drop formation of the P3HT ink (few seconds after printing).....	114
Figure 4.3 - SEM images of neat TPU: a) top substrate surface; b) cross section by cryogenic fracture. ).....	115
Figure 4.4 - SEM images the substrate with CP after 15 min at 120°C: a) fracture surface of TPU with CP; b) PET surface with CP.....	115
Figure 4.5 - Result structure of the SP-polymer interaction created by mechanical deposition.....	116
Figure 4.6 - SEM images of the top surface of the SP-TPU substrate SP without thermal treatment.....	117
Figure 4.7 - SEM images of SP-TPU: a) Top substrate surface b) Fractured surface; c) detail of Figure 4.7b).....	117
Figure 4.8 – AFM topographical images of the TPU surface: a) neat TPU and b) SP-TPU. The image size is 10 $\mu\text{m}$ x10 $\mu\text{m}$ .....	118
Figure 4.9 – Drop of water on the: a) neat TPU substrate; b) SP-TPU substrate.....	118
Figure 4.10 – Image of the P3HT printed in the SP-TPU substrate: a) before annealing; b) after annealing.....	119
Figure 4.11 – SEM images of SP-TPU with inkjet printed P3HT ink: a) and b) Top and fractured cross section substrate surface, respectively, with one layer of ink; c) and d) Top and fractured cross section substrate surface, respectively, with four layers of ink; e) and f) Top and fractured cross section substrate surface, respectively, with nine layers of ink.....	121
Figure 4.12 - SEM images of SP-TPU fractured surface with inkjet printed P3HT ink: a) nine layers; b) ten layers.....	122
Figure 4.13 – Printed SP-TPU surface with six layers of P3HT: a) SEM image; b) AFM topographic image (image size is 10 $\mu\text{m}$ x10 $\mu\text{m}$ ).....	122
Figure 4.14 – OM images of the printed substrate after the Cross-cut Tape test: a) remaining ink on the substrate; b) detail of Figure 4.14a); and c) image of the remaining ink on the adhesion tape. ).....	123
Figure 4.15 – Sheet resistance measurement, through Van der Pauw method, according to the number of P3HT layers).....	124

Figure 5.1 - PEDOT mass loss analysis for optimal annealing temperature evaluation.....	132
Figure 5.2 - Digital image of TPU with drop formation of the PEDOT:PSS ink (few seconds).....	133
Figure 5.3 - Digital images of the PEDOT:PSS ink printed in the SP-TPU substrate: a) Before annealing; b) After annealing.....	135
Figure 5.4 - Detail of the interface between ink and modified substrate.....	136
Figure 5.5 - SEM images of SP-TPU top substrate surface.....	136
Figure 5.6 - SEM images of SP-TPU substrate with inkjet printed PEDOT:PSS ink: a) top surface with five layers of ink; b) fractured cross section surface with five layers of ink; c) top surface with six layers of ink; d) fractured cross section surface with six layers of ink; e) top surface with seven layers of ink; f) fractured cross section surface with seven layers of ink.....	137
Figure 5.7 - AFM topographic image of the printed SP-TPU surface with six layers of PEDOT. The image size is 10 $\mu\text{m}$ x 10 $\mu\text{m}$ .....	138
Figure 5.8 – OM images of the printed substrate after the Cross-cut Tape test: a) remain ink on the substrate; b) detail of Figure 5.8 a); c) remaining ink on the adhesion tape.....	139
Figure 5.9 - Sheet resistance measurement, according to the number of PEDOT:PSS layers. ....	140
Figure 5.10 – Typical TPU Stress vs. Strain Curve.....	141
Figure 5.11 – Mechanical properties of the SP-TPU substrate (for comparison) and SP-TPU substrate inkjet printed (with 6 layers of PEDOT:PSS).....	141
Figure 5.12 - Electrical resistance vs. Homogeneous Stress.....	142
Figure 5.13 - Electrical resistance vs. Homogeneous Strain.....	143
Figure 5.14 – Curve profile of the PEDOT:PSS measured resistance changes during tensile mechanical tested, with an initial resistance ( $R_0$ ) of $\pm 295.85 \Omega$ .....	144
Figure 6.1 – Silver-based ink mass loss analysis for optimal annealing temperature evaluation.....	152
Figure 6.2 – TGA measurements vs. Surface Resistivity ( $\rho_s$ ).....	153
Figure 6.3 – Temperature and time influence on the sintering of the Silver-based ink on glass substrate. Detail SEM image of the printed ink with 1 hour sintering at 130 $^{\circ}\text{C}$ .....	154
Figure 6.4 – Schematic of the printing pattern to test the resolution for Ag lines printing. ....	155
Figure 6.5 - Example of flooding of one layer of the printed silver-based ink (with drop spacing of 28.22 $\mu\text{m}$ (900 DPI)) on a clean PI substrate.....	152

Figure 6.6 - OM images of the sintered silver-based ink printed on a PI substrate after the Cross-cut tape test: a) remain ink on the substrate; and b) image of the remaining ink on the adhesion tape.....	157
Figure 6.7 – Image of clean TPU substrate: a) one layer of printed silver-based ink lines with drop spacing of 254 $\mu\text{m}$ (100 DPI); b) flooding of one layer of the silver-based ink (with drop spacing of 28.22 $\mu\text{m}$ (900 DPI)).....	158
Figure 6.8 - Printed silver-based ink (with a drop spacing of 84.67 $\mu\text{m}$ ) in the TPU substrate (before sintering): a) Image of the printed pattern of testing lines; b) SEM images with detail of one layer line with width of $\pm 400 \mu\text{m}$ .....	159
Figure 6.9 – Image of a printed sample: a) Before sintering; b) After sintering.....	160
Figure 6.10 – SEM images of the TPU substrate fracture cross section with one layer of inkjet printed silver-based ink: a) before sintering; and b) after sintering.....	160
Figure 6.11 - AFM topographic images of the printed TPU surface with one layer of silver-based ink: a) without sintering; and b) with sintering. The image size is 10 $\mu\text{m}$ x 10 $\mu\text{m}$ .....	161
Figure 6.12 - OM images of the printed TPU substrate (before sintering) after the cross-cut tape test: a) remain ink on the TPU substrate; and b) remaining ink on the adhesion tape.....	161
Figure 6.13- OM images of the printed TPU substrate (after sintering) after the cross-cut tape test: a) remain ink on the TPU substrate; and b) remaining ink on the adhesion tape.....	162
Figure 6.14 – SEM image of the printed ink, before sintering.....	162
Figure 6.15– SEM images with a detail of the cracked Silver based ink on TPU substrate, after sintering at 130 $^{\circ}\text{C}$ .....	163
Figure 6.16 - SEM image of the TPU printed substrate after sintering at 150 $^{\circ}\text{C}$ : a) with detail of the cracked Silver-based ink; b) physical contact between nanoparticles forming a silver network.....	164
Figure 7.1 - Sensorial platform scheme (the dimensions are in cm).....	171
Figure 7.2 - 3D view of a square (side length = 2a) pressure sensor.....	172
Figure 7.3 - Cross section of a generic deflectable diaphragm.....	173
Figure 7.4 - Iterative algorithm to compute the capacitive changes of flexible capacitive pressure sensors.....	175
Figure 7.5 -Sensor elements manufacturing process in which: a) Flexible PCB (the geometry of copper conductors and the capacitor dielectric were defined using a PCB flexible process); b) Flexible substrate (the electrodes of the capacitors are inkjet printed on the TPU using conductive ink) and c) Assembled prototype sensor where the two flexible substrates with	

electrodes (one for the TOP and a second one for the BOTTOM (Figure 7.6), were assembled using conductive glue to the flexible PCB, Figure 7.7).....	176
Figure 7.6- Conductive electrodes: a) Drawing pattern for electrodes definition; b) Inkjet printed flexible substrates (with conductive inks electrodes on a 1.5mm thick TPU substrate). .....	177
Figure 7.7 - The top side (on the left) and bottom side (on the right) of the flexible PI substrate and the respective dielectric areas. The PCB size is 124 mm x 95 mm.....	178
Figure 7.8 - Schematic of the sensing-array system.....	179
Figure 7.9 - 3D illustration of the used pressure chamber to measure the capacitive changes of the flexible pressure sensors.....	179
Figure 7.10 – Digital image of the test setup.....	180
Figure 7.11 - Assembled Prototype Sensors (left) and the reading system (right).....	180
Figure 7.12 - Sensors response to pressure.....	181
Figure 7.13 - Layout and electrical schematic of the connections for sensor reading, including cross-coupling capacitances (Cc).....	182
Figure 7.14 - Experimental results and comparison with analytical model.....	182
Figure 7.15 - Sensor response for increase/decrease pressure cycles.....	183
Figure 7.16 - Noise measurement during 64 hours.....	183
Figure 7.17 - Example of sensor repeatability with/without load.....	184



---

# List of Tables

	Page
Table 2.1 – Main differences between printing techniques.....	44
Table 3.1 - Substrates identification their main properties.....	74
Table 3.2 - CP detail technical specification.....	74
Table 3.3 –Silica (SiO <sub>2</sub> ) particles detail technical specification.....	75
Table 3.4 - Plexcore® physical properties.....	77
Table 3.5 - Main physical Properties of EDOT monomer.....	78
Table 3.6 – Orgacon™ Physical Properties.....	80
Table 3.7 – Major ink requirements for IPT.....	81
Table 3.8 - Ag-IJ10 silver-based ink.....	82
Table 3.9 – Resolution setting according to rotation angle.....	90
Table 3.10 - Surface energy components for the test liquids.....	94
Table 4.1 - Plexcore® OC RG-1100 physical properties.....	111
Table 4.2 – ST of the Substrates vs. ST of the ink (35-38 mN/m).....	112
Table 4.3 - Main printhead settings used for P3HT ink.....	119
Table 5.1 – Orgacon™ Physical Properties.....	131
Table 5.2 – ST of the Substrates and of the PEDOT:PSS ink.....	132
Table 5.3 - Main printhead settings used for PEDOT:PSS ink.....	134
Table 6.1 - Ag-IJ10 silver-based ink physical properties.....	151
Table 6.2 - ST of the Substrates and of the silver-based ink (28-35 mN/m).....	154
Table 6.3 - Main printhead settings used for silver-based ink printing.....	158
Table 7.1– Number of deaths by Accidents (unintentional injuries) cause: fall (selected from 113 causes), by age: United States, 2010.....	170
Table 7.2 – Main design parameters of the pressure sensor.....	174
Table 7.3 – Comparison of different pressure sensors.....	185
Table 7.4 - Comparison with commercial sensors.....	185
Table 8.1 – Summary of the results.....	196





---

# List of Abbreviations

<b>Abbreviations</b>	<b>Designation</b>
1D	One Dimension
2D	Two Dimensions
3D	Three Dimensions
$\mu$ CP	Microcontact Printing
$\mu$ TM	Micro Transference Molding
<b>A</b>	
AFM	Atomic Force Microscopy
ASTM	American Society for Testing and Materials
<b>B</b>	
BDO	1,4-butanediol
BET	Brunauer-Emmett-Teller
<b>C</b>	
CAD	Computer-aided-design
CAPDAC	Computer-Aided Piping Design & Construction
CDC	Capacitance Digital Converter
CIJ	Continuos InkJet
CP	Clay Particles
CPP	Central Plantar Pressure
<b>D</b>	
DC	Direct Current
DPI	Dots Per Inch
DNA	Deoxyribonucleic Acid
DoD	Drop-on-demand
<b>E</b>	
ECG or EKG	Electrocardiography
<b>F</b>	
FET	Field-effect transistor
FPCB	Flexible Printed Circuit Board
FPMS	Flexible Pressure Mapping System
FPS	Flexible Pressure Sensors

FS	Full Scale
<b>G</b>	
GPIB	General Purpose Interface Bus
<b>H</b>	
HS	Hard Segments
<b>I</b>	
I <sup>2</sup> C	Inter-Integrated Circuit
IC	Image Acquisition
IEEE	Institute of Electrical and Electronics Engineers
IMS	Industrial Mentholated spirits/ethanol
IPA	Isopropyl Alcohol
IP	Inkjet Printing
IPT	Inkjet Printing Technology
<b>L</b>	
LCVD	Laser Chemical Vapor Deposition
LDW	Laser direct writing
LDW+	Laser Direct Write addition
LDW-	Laser Direct Write subtraction
LDWM	Laser Direct Write Modification
LEEP	Laser-Enhanced Electroless Plating
LIFT	Laser-induced Forward Transfer
<b>M</b>	
M3D	Maskless Mesoscale Materials Deposition
MATLAB	Matrix Laboratory
MDI	4,4'-diphenylmethane diisocyanate
MEMS	MicroElectroMechanical System
MIMIC	Micromolding in Capillaries
<b>O</b>	
OFETs	Organic Field-Effect Transistors
OLEDs	Organic Light Emitting Diodes
OPDs	Organic PhotoDiodes
OM	Optical Microscopy
OTFTs	Organic Thin Film Transistors
OWRK	Owens, Wendt, Rabel and Kaelble method
<b>P</b>	

P3HT	Poly(thiophene-3-[2-(2-methoxyethoxy)ethoxy]-2,5-diyl), sulfonated
PCB	Printed Circuit Board
PDMS	Poly (dimethyl) siloxane
PE	Printed Electronics
PEDOT:PSS	Poly (3,4 - ethylenedioxythiophene): poly (4 -styrenesulfonate)
PEN	Polyethylene naphthalate
PET	Polyethylene terephthalate
PI	Polyimide
PMMA	Polymethylmethacrylate
PU	Polyurethane
PVDF	Polyvinylidene fluoride
PZT	Piezoelectric Zirconate Titanate
<b>R</b>	
R	Roughness of the surface
R2R	Roll-to-Roll
REM	Replica Molding
RFID	Radio-Frequency Identification
rpm	Rotation per minute
rr-P3HT	Regioregular poly 3-hexylthiophene
<b>S</b>	
SAMIM	Solvent Assisted Micromolding
SEM	Scanning Electron Microscopy
SP	Silica Particles
SP-TPU	Silica Particles - Thermoplastic Polyurethane
SS	Soft Segments
ST	Superficial Tension
<b>T</b>	
TDI	Toluene Diisocyanate
TGA	Thermogravimetric Analysis
TPU	Thermoplastic Polyurethane
<b>U</b>	
USB	Universal Serial Bus
UV	Ultraviolet
<b>X</b>	
X-Axis	Horizontally direction

**Y**

Y-Axis

Horizontal shift

**Z**

Z-Axis

Vertically direction

# List of Symbols

<b>Symbols</b>	<b>Description</b>	<b>SI</b>
A	Area of the electrodes	[m]
Ag	Silver	[-]
Au	Gold	[-]
Au-Pd	Gold - Palladium	[-]
C	Carbon	[-]
$C$	Capacitance	[F]
$C_0$	Rest capacitance	[F]
$C_c$	Cross-coupling capacitances	[F]
Cu	Copper	[-]
$C_{10}H_8O_4$	Ethylene terephthalate	[-]
$(CH_3)_2SiO$	Methylated linear siloxane	[-]
CTE	Coefficient of Thermal Expansion	[ppm/°C]
$d^*$	Drop diameter (spreading factor)	[m]
$d_0$	Gap between the electrodes	[m]
d	Distance between electrodes	[m]
$D$	Drop initial diameter	[m]
E	Young's Modulus	[Pa]
GF	Gauge Factor	[-]
$H_2O$	Water	[-]
H	Hydrogen	[-]
h	Hour	[-]
$I$	Current	[A]
L	Evaluation length	[nm]
$l_c$	Length of the capacitor electrodes	[m]
n	Number of repeating monomer units	[-]
N	Nitrogen	[-]
O	Oxygen	[-]
$Oh$	Ohnesorge number	[-]
$P_0$	Inside pressure	[Pa]
$P_{out}$	Outside pressure	[Pa]
pH	Decimal logarithm of the reciprocal of the hydrogen ion activity	[-]
$R_0$	Initial resistance	[Ω]

$R$	Measured resistance	[ $\Omega$ ]
$R_a$	Arithmetic average of the absolute values of the roughness profile ordinates	[nm]
$R_A$ and $R_B$	Characteristic resistances associated with the corresponding terminals. Van der Pauw method	[ $\Omega$ ]
$Re$	Reynolds number	[-]
$RMS, R_q$	Root mean square average of the roughness profile ordinates	[nm]
$R_s$	Sheet Resistance	[ $\Omega/sq$ ]
$RT$	Room Temperature	[%]
$RH$	Relative Humidity	[ $^{\circ}C$ ]
$Si$	Silicone	[-]
$SiO_2$	Silicone dioxide	[-]
$t^*$	Time after drop impact	[s]
$T_g$	Glass transition temperature	[ $^{\circ}C$ ]
$V$	Voltage	[V]
$W_0$	Deflection	[m]
$W_c$	Width of the capacitor electrodes	[m]
$We$	Weber number	[-]
$Z$	Inverse of Ohnesorge number: $Z = Oh^{-1}$	[-]
$Z(X)$	Profile height function	[nm]
$\Delta ST$	Difference between ST	[mN/m]
$\gamma$	Surface energy	[mN/m]
$\gamma_{sl}$	Interfacial tension solid-liquid	[mN/m]
$\gamma_{sv}$	Interfacial tension solid-vapour	[mN/m]
$\gamma_{lv}$	Interfacial tension liquid-vapour	[mN/m]
$\eta$	Viscosity	[Pa.s]
$\epsilon_0$	Permittivity of the free space	[F/m]
$\epsilon_r$	Relative permittivity of the material between the plates (dielectric)	[-]
$\nu$	Poisson's ratio	[-]
$\pi$	3,14	[-]
$\rho_s$	Surface Resistivity	[ $\Omega$ ]
$\rho$	Density	[g/cm <sup>3</sup> ]

# Chapter 1

## **Introduction**

In this chapter a general introduction about Printed Electronics is presented. The motivation for developing this study as well as the proposed objectives and the specific tasks of this research work are also presented. At the end of the chapter the approach followed in this thesis, the outline and a flow chart illustration of the experimental sequence are presented for an overview of the performed work.





## 1.1. Context

Nowadays, humans are highly dependent on the use of sensors and, therefore, they can be found in work and leisure application areas. The availability of good information processing capabilities and sensors enable smarter sensing systems and find application in new areas, such as physical monitoring. The interest on flexible pressure mapping systems for use on non-planar surfaces grew tremendously in recent years [1.1, 1.2] in areas such as aerospace and automotive [1.3], biomedical [1.4], robotics [1.5-1.7] and particularly in clinical applications for motion analysis [1.8-1.10].

The exchange of knowledge and experiences between different fields of science has speed up the evolution of sensors technology. An example of this, results from the combination of different polymeric materials (as compared to traditional silicon based substrates) combined with new coating and printing techniques. The use of flexible polymers has many advantages compared to traditional hard circuits including: higher contact area, capability to fold/roll, among others, and therefore, they start to have a key role in the development of new conductive circuits. The printing of patterns on the surface of polymers, assigns them with new properties and functionalities.

## 1.2. Printed Electronics (PE)

When an electrical device is created through a printing process, it is designated Printed Electronics (PE). Over 20 years, the manufacturing industry has been using various printing techniques to produce, e.g., antennas, sensors, membrane switches and keypads [1.11] (Figure 1.1). This list is continually increasing. Today's users demands (for lower cost, flexible and smarter products), is a decisive factor for the selection of PE fabrication technologies, and therefore, PE is contributing to novel and better products.

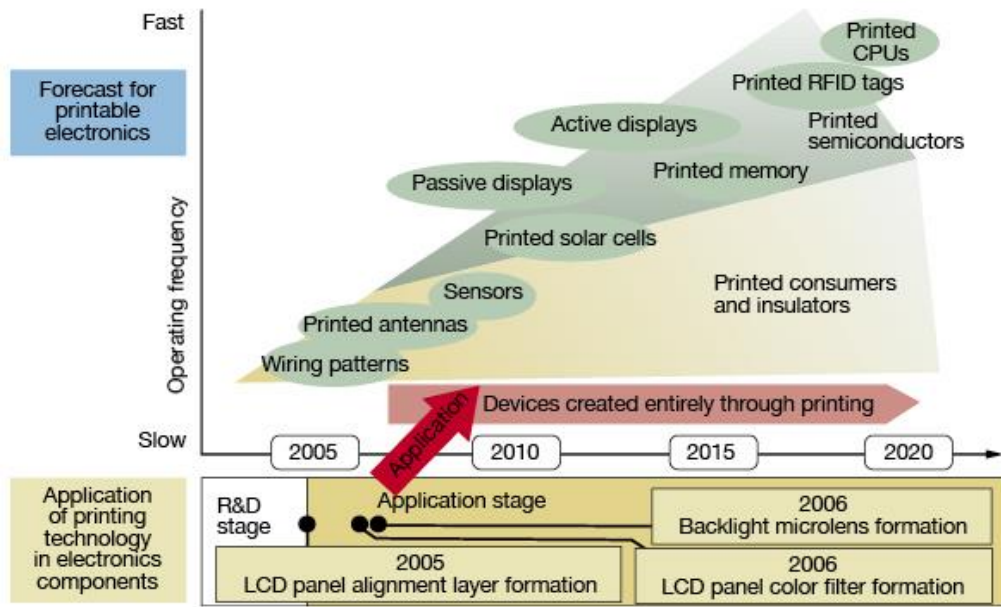


Figure 1.1-New applications for Printable Electronics (source Nikkei Electronics, March 2007)

What, in the past was part of a science fiction movie, today is translated from a science project to an industrial process. In the next few years, thanks to better and flexible materials combined with PE, commercial applications diversity will continue to emerge (Figure 1.2). Latest reports manifest an encouraging progress of “Flexible Applications Based on Printed Electronics Technologies 2013” [1.12]. In 2007, a market of \$1.2 billion was estimated [1.13] and the printed and flexible electronics market is expected to grow from \$176 million in 2013 to \$950 million in 2020 [1.12].

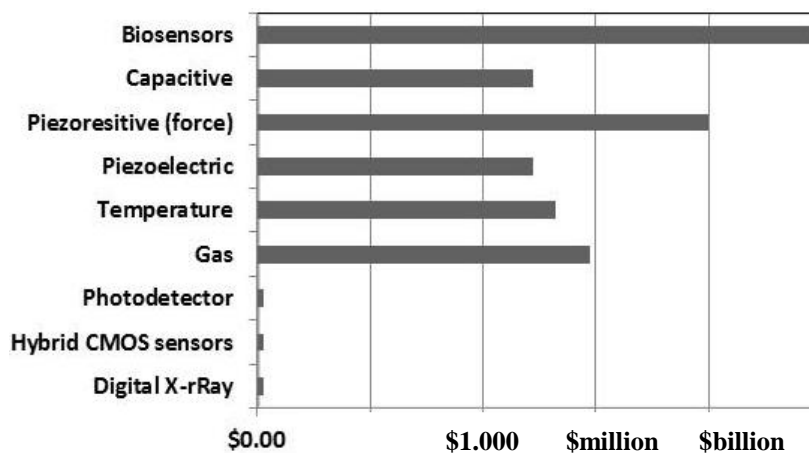


Figure 1.2 - The market in 2013 for printed Flexible sensors (Adapted from: IDtechEx webinar 2013).

For the fabrication of a PE device, many are the possible printing technologies and materials to be employed in the manufacturing process. Over the years, printing technologies, e.g. Screen Printing, Flexography, Gravure printing, Soft Lithography, and Inkjet Printing are the elected by the electronic manufacturing industry. Mainly, these technologies consist in patterning of structures, by depositing ink on a substrate. Each technology is selected according to the type of electronic components or devices (small, thin, lightweight, flexible, inexpensive and disposable, etc.), the production cost, and volume.

The essential aspects for the success of any type of printed electronic device is the processability, performance and long-term reliability [1.11] of the materials used [1.14]. The pastes, inks or coatings can be based both on organic and inorganic materials [1.14]. Inorganic inks normally contain metallic (e.g. copper, gold, silver, aluminum) nano-particles dispersed in a retaining matrix and they are used in the fabrication of passive components and transistor electrodes [1.14]. Organic inks are based on organic materials, such as polymers (conductors, semiconductors and dielectrics). The inks based on high conductive polymers are employed in batteries, electromagnetic shields, capacitors, resistors and inductors, sensors, etc., while inks based on organic semiconductors are employed as active layers of active devices such as, Organic PhotoDiodes (OPDs), Organic Light Emitting Diodes (OLEDs), Organic Field-Effect Transistors (OFETs), organic solar cells, sensors, etc. [1.14]. Due to the wide range of printing technologies, the materials must meet certain requirements depending on the type of printing being performed and on the application. The PE technologies are divided in:

- contact techniques (e.g. screen printing, flexography, gravure printing and soft lithography), in which the printing plate is in direct contact with the substrate;
- non-contact techniques (e.g. Laser direct writing, Aerosol printing, inkjet printing), where only the inks gets in contact with the substrate.

In the next Chapter, the main features of some contact and non-contact printing techniques and examples of PE applications are discussed, with greater prominence to Inkjet Printing Technology.

### 1.3. Motivation and Objectives

High resolution conductive flexible polymeric circuits are devices that use insulating polymers as substrates. These conductive flexible polymers are a new class of materials that are prepared for a wide range of applications, such as photovoltaic solar cells, transistors molecular devices, and sensors.

Currently, the methods used for defining electrical circuits resort to using masks and chemicals to attack specific areas, creating conductive regions on a substrate. These techniques involve the use of expensive raw materials, generate large chemical pollutants and waste materials. The use of large solvent quantities represents an important drawback for industries, due to environmental and cost issues. Adding to this, the complexity of the fabrication process prevents their automation to industrial level. The growing need for electrical circuits requires simpler manufacturing and innovative techniques that can produce large-scale and low cost.

Inkjet printing technology (IPT) has attracted attention [1.15] as an alternative method to traditional manufacturing techniques. This technology allows the direct and accurate deposition of the fluid, without contact with the material to be printed. Compared to other deposition methods, IPT enables the production with low waste and with the possibility to use various types of substrates, reducing cost and production time. For these reasons, IPT is more directed to the manufacture of devices with superior resolution. It is a competitive technology with a simple method, relatively low cost and offers the required manufacturing versatility to allow customization.

However, direct printing has its limitations. IPT is a technology that is yet to prove its technological viability in the printed polymers industry. Substrates, printing ink, and drop placement accuracy [1.16] are the main challenges for IPT. Most commercial available conductive inks, even some equipment accessories, often do not meet all the needed requirements.

This technology is new and shows great promise. However, there are still challenges that need to be addressed in order to better understand and control IPT operation. There is still insufficient data, methodologies or normative specifications documented, mentioning the most suitable process parameters according to the IPT application. Before moving to the IPT process itself, and the parameters of manufacture (equipment, process speed, amount of ink, resolution, maintenance, etc.), it is of paramount importance a thorough investigation of the properties of materials to be used, in particular, the physical-chemistry formulation of the inks, the surface

properties of the substrate, etc., and the compatibility of both, to ensure that there is ink absorption by the substrate.

IPT has become an important topic in scientific research and technology [1.17]. While some researchers [1.18] explore the effect of solvents in paints and optimization of their adhesion and spreading, as well as the performance, quality and electric properties of the printed layer, other researchers [1.19] focus on understanding and optimization of the behaviour of the ink droplet in different temperature conditions and substrates surface. The printing of different inks on different substrates (the absorption from different substrates) are topics that need to be further explored, since scarce information and studies are documented. Therefore, it is necessary to explore and understand the interactions between ink/substrate on IPT in order to increase the range of new end-use applications. The need for products and the lack of information and knowledge in IPT justifies the intensive research of this technology.

The optimization of the printed pattern fabrication using IPT has a key role in the development of new conductive circuits, and it is a major target of this study. Print resolution and uniformity of the printed layer are key aspects and it requires identification and control of the processing variables. The understanding and integration of this knowledge about IPT is a scientific and technological challenge and a motivation for innovative solutions in printed systems with enhanced electrical-mechanical properties. The work presented focus on materials science (selectively applying commercially available and compatible materials or defining viable material alternatives), materials processing using inkjet printing technology and exploring its potential into electronic and instrumentation applications.

The need for increasingly intelligent and efficient sensors, with the ability to be integrated in complex environments, encouraged the development of a flexible pressure sensor using the direct print technology - Inkjet Printing Technology - for a simpler and low cost manufacture method for large scale industrial production.

The final stage of work is the integration of the selected material on the development of a pressure sensor resorting to IPT with a simpler structure design. Therefore, the **goal** of this work is to **develop an array of flexible pressure sensors built from a printed electrodes platform** (Figure 1.3) with specific characteristics (resolution and dynamic range) in order to give the desired transducer functionalities and requirements:

- With reading and resolution accuracy;
- Capable of making field readings in real time;
- Capable of static and dynamic measurement in the whole range of movement:

- Cost-effective: high performance with low cost.

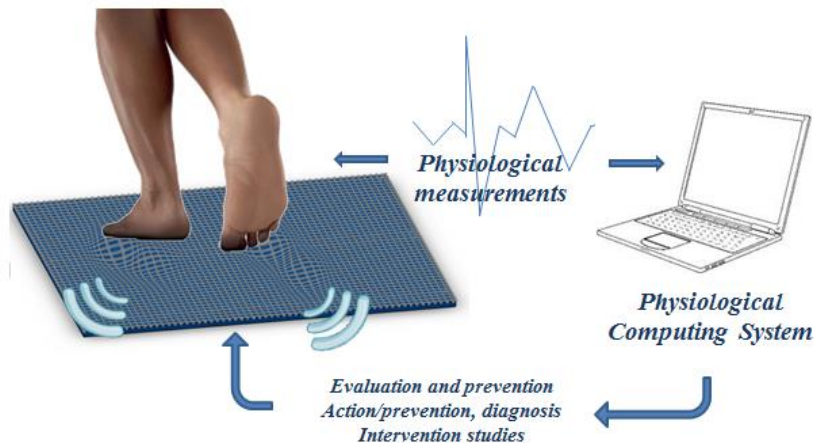


Figure 1.3 - Block diagram of the physiological computing approach.

Listed below are the key contributions of this work to pressure sensor array design and fabrication, as well as key experiments demonstrating the capabilities of IPT:

- Development of a printed pattern with transducer properties for use in the pressure sensor array.
- Characterization and modelling of the response of the pressure sensor array to all pressure signals.
- Demonstration of the sensor's ability to mobility monitoring.
- Demonstration of the IPT as a viable technology for large scale manufacturing of these sensors without the involvement of expensive raw materials, generation of large chemical pollutants and waste materials, therefore, reducing the final cost.

#### 1.4. Research approach

This section describes the research approach used to achieve the goals of this Thesis. The research is initially concentrated on ink and substrate compatibility, their interactions, and on processing the materials by inkjet printing. The applied research, focus on the development of a sensing platform manufactured by IPT, on selectively applying commercially available and compatible materials and/or defining viable material alternatives. Therefore, the requirements for the fulfilment of the above objectives are listed as follows and a scheme representing the research strategy is illustrated in Figure 1.4:

- Substrate & conductive ink selection for the fabrication of the flexible sensing cells (compatibility between ink/substrate adhesion);

- Study of the Inkjet printer working principle for enhanced printing resolution and uniformity of the printed layer;
- Demonstrate the reliability of the flexible printed structure in terms of **mechanical performance** and applicability of the selected materials to the application;
- Pressure sensor operation requires a platform structure that is capable to mechanically respond to applied stress while preserving the integrity of the printed structures. Demonstration that the ink is capable of accompanying the flexibility and deformations along with the substrate without breaking or losing adhesion;
- Achievement of the desired **electrical properties**. Define an ink composition compatible with the substrate and to define a printed layer thickness to impart the desired conductivity. The type and amount of used ink is directly related to the electrical performance;
- Demonstration of piezo-resistive effect of the conductive printed material without the disruption of the ink for sensing applications;
- Design, development and test of a prototype of a flexible pressure sensor, meeting the requirements of the envisaged application. Establish the limits of such conductive material for such application. Demonstrate the applicability of the printed solution in an array of sensors platform;
- Demonstration of the applicability of the selected **manufacturing technology** and its potential to meet the needs of the electronic industry.



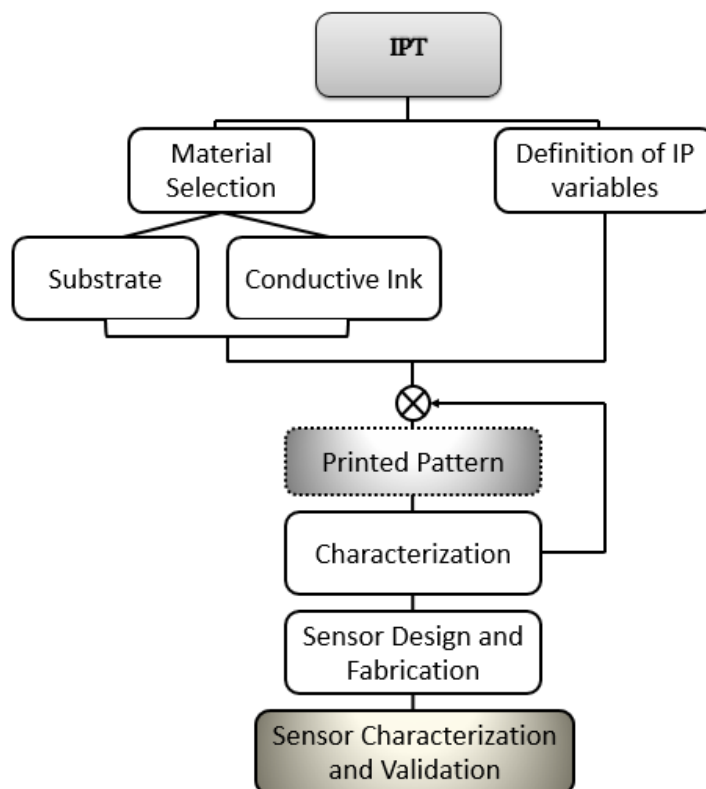


Figure 1.4 Schematic outline of the work presented in this thesis.

## 1.5. Thesis outline

This thesis is divided in eight Chapters. In order to have an overview of this research work, hereafter the thesis outline is presented with a brief description:

**Chapter 1** presents the context and a general overview on Printed electronics. The motivation and objectives of the present work are given, as well as an outline of the thesis approach.

**Chapter 2** focus on the description of the widely used printing techniques for sensor manufacturing. Greater prominence is given to Inkjet Printing Technology to evidence the importance of this technology as key-technology for the printed electronics industry. A background and a review on prior work is presented along with materials used, developed applications and potential of this technology. Finally, advantages and challenges are discussed.

The next chapter gives detailed information concerning the fabrication procedure followed in this work. Thus, **Chapter 3** gathers the description of the main physical and chemical properties of the employed materials. A detailed description of the used IPT (printing technique and equipment characteristics) is provided. Afterwards, a description of the experimental techniques employed for the characterization of the printing patterns is given.

**Chapter 4, Chapter 5** and **Chapter 6** correspond, each one, to the work performed with the three different inks. Here, all the results concerning the fabrication and the characterization of printed patterns are concentrated and a summary of the main results achieved is given.

The subsequent **Chapter 7** is fully dedicated to the design and fabrication of the pressure sensor array system. This chapter has three sections: The sensor design, the production and the testing and validation of the functional prototype sensor.

**Chapter 8** concludes the thesis, summarizes the present work and the performance attributes of the pressure sensor array, and provides directions for future research.

**REFERENCES**

- [1.1] M. Nir, D. Zamir, I. Haymov, L. Ben-Asher, O. Cohen, B. Faulkner, and F. de la Vega, "Electrically conductive inks for inkjet printing," in *The chemistry of inkjet inks*, Shlomo Mag., Jerusalem: World Scientific Publishing Co. Pte. Ltd., 2010, pp. 225–254.
- [1.2] Engel J, Chen N, Tucker C, Liu C, Kim S-H, and D. Jones, "Flexible multimodal tactile sensing system for object identification. Proceedings of the IEEE Sensors 2006, Exco, Daegu, Korea," pp. 563–566, 2006.
- [1.3] "Pressure Profile Systems, Inc. Online <<http://www.pressureprofile.com/technology-capacitive.php>>."
- [1.4] C.-C. Chiang, C.-C. K. Lin, and M.-S. Ju, "An implantable capacitive pressure sensor for biomedical applications," *Sensors Actuators A Phys.*, vol. 134, no. 2, pp. 382–388, 2007.
- [1.5] E. Pritchard, M. Mahfouz, B. Evans, S. Eliza, and M. Haider, "Flexible capacitive sensors for high resolution pressure measurement," in *Sensors, 2008 IEEE*, 2008, pp. 1484–1487.
- [1.6] M. Y. Cheng, C. L. Lin, and Y. J. Yang, "Tactile and shear stress sensing array using capacitive mechanisms with floating electrodes," in *Micro Electro Mechanical Systems (MEMS), 2010 IEEE 23rd International Conference on*, 2010, pp. 228–231.
- [1.7] S. K. Yeung, E. M. Petriu, W. S. McMath, and D. C. Petriu, "High sampling resolution tactile sensor for object recognition," *IEEE Trans. Instrum. Meas. - IEEE TRANS INSTRUM MEAS*, vol. 43, pp. 277–282, 1994.
- [1.8] E. M. Petriu, W. S. McMath, S. S. K. Yeung, and N. Trif, "Active Tactile perception of objects surface geometric profiles," *IEEE Trans. Instrum. Meas. - IEEE TRANS INSTRUM MEAS*, vol. 41, pp. 87–92, 1992.
- [1.9] "Xsensor Technology Corporation." [Online]. Available: <http://www.xsensor.com>.
- [1.10] T. V Papakostas, "Tactile sensor: stretching the limits," in *Intelligent Environments, 2007. IE 07. 3rd IET International Conference on*, 2007, pp. 472–476.
- [1.11] T. Adcock and D. Fenner, "Printed Electronics : Traditional Technology Addresses Today's Smaller, Faster, Lower Cost Requirements," <<http://www.henkel.com/electronics.htm>>, 2012. .
- [1.12] "Sensors: Electronics & Computers <<http://www.sensormag.com/electronics-computers/news/flexible-printed-electronics-applications-grow-11580>>," 2013. .
- [1.13] L. Kersey, V. Ebacher, V. Bazargan, R. Wang, and B. Stoeber, "The effect of adhesion promoter on the adhesion of PDMS to different substrate materials," *Lab Chip*, vol. 9, no. 7, pp. 1002–1004, 2009.
- [1.14] L. Basiricó, "Inkjet Printing of Organic Transistor Devices," University of Cagliari, 2012.

[1.15] B. News, ““Scientists use inkjet printing to produce solar cells,”” *BBC News Technology*. [Online]. Available: <http://www.bbc.co.uk/news/technology-13977038>.

[1.16] A. Hudd, “Inkjet Printing Technologies. In: Magdassi S., Ed. *The Chemistry of Inkjet Inks.*,” New Jersey-London\_Singapore :World Scientific, 2010, pp. 3–18.

[1.17] A. Kamyshny, J. Steinke, and S. Magdassi, “Metal-based Inkjet Inks for Printed Electronics,” *Open Appl. Phys. J.*, vol. 4, pp. 19–36, 2011.

[1.18] K.-Y. Shin, S.-H. Lee, and J. H. Oh, “Solvent and substrate effects on inkjet-printed dots and lines of silver nanoparticle colloids,” *J. Micromechanics Microengineering*, vol. 21, no. 4, p. 45012, 2011.

[1.19] L. Boon Keng and H. Xiao, “Transient contact angle of evaporating inkjet droplet on trans-parent polymer substrate,” in *Electronics Packaging Technology Conference (EPTC), 2010 12th*, 2010, pp. 240–245.



# Chapter 2

## **Overview on Printing Technology for Printed Electronics**

Printing polymers with conductive inks has been demonstrated to be highly efficient in the generation of sensing applications. There are many possible techniques for printing polymers. In this chapter, a briefly description of the most common techniques use at the industrial level is given for an overall vision and, a better understanding and evaluation of its different features. Greater prominence to Inkjet Printing Technology (IPT), their features and value is provided. An overview of IPT is presented to evidence the importance of this technology as key-technology for the printed electronics industry. The characteristics of printing technologies, such as the basic printing principles of operation are outlined. A background and a review on prior work is presented along with used materials, developed applications and potential of this technology. At the end, the process requirements, the advantages and challenges are also presented.



## 2.1. Contact printing techniques

The contact printing techniques are the predominant printing processes in the current days. However, the contact printing techniques involve limitations around the resolution and range of the used materials (substrates, inks, solvents). Some of the contact printing techniques are briefly described next.

### 2.1.1. Screen Printing

Screen Printing is a traditional printing technique used to graphical reproduce over any material (epidermis [2.1], paper, glass, metal [2.2], ceramic [2.3], wood, textiles [2.1][2.4], plastic [2.1] [2.5]). This technique is costly due to use of metal masks (stencil) and due to its high waste of production material (including the ink), it is also a slow and non-automated process. The biggest limitation is reflected in the level of resolution when compared with other methods. This printing technique may be performed in a planar system (Figure 2.1) or in a roll-to-roll system (Figure 2.2). The planar system uses the screen printing stencil, which is in direct contact with the substrate; the blade moves and helps defining the ink layer to be deposited on the substrate, the squeegee containing supports the blade [2.6]. The ink passes into the standard image in the stencil to the substrate and defines the final image [2.7].

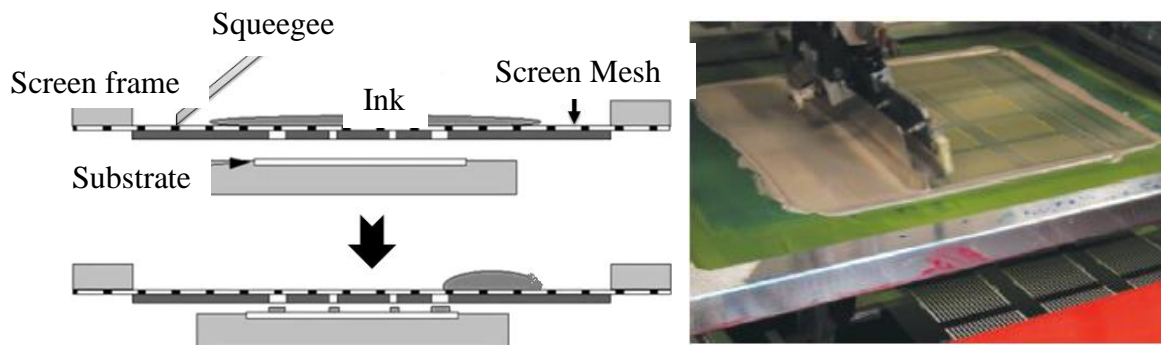


Figure 2.1 - Schematic of Screen printing (at left) (Adapted from[2.8]). Flat-bed screen printing of silver paste showing the squeegee during a printing cycle showing how the ink is forced through (Reprinted from [2.9], Copyright (2012), with permission from Elsevier).

In the screen printing roll-to-roll process, the squeegee is replaced by a roller, and the ink is placed inside this roll [2.9]. The blade continues to exist, but inside the roll. This last one, forces the ink through the mesh. The substrate is supported by a platen that allows the process to be continuous, offering the most efficient production to the system.



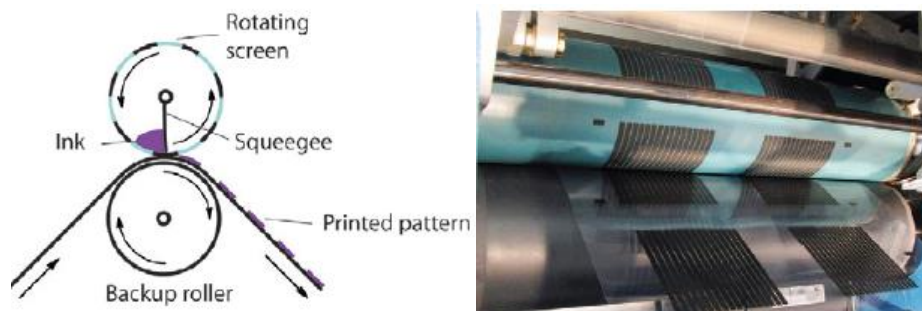


Figure 2.2 – Schematic of Rotary screen printing (left). A photograph of rotary screen printing of conducting graphite ink onto a clear polyester foil (right) (Reprinted from [2.9], Copyright (2012), with permission from Elsevier).

Screen printing is a technology that has been often used for pressure sensor manufacturing [2.10 - 2.13]. Figure 2.3 shows some examples of pressure sensors manufactured by Screen printing. Screen printing inks viscosity are between 0.1 to 10 Pa.s [2.6]. The printed ink film thickness goes from 20 nm to 100  $\mu\text{m}$  [2.6]. Inks may dry through solvent evaporation or by UV- or electron beam-cured. Screen printing limitations lies in its maximum resolution (usually under 50 lines per centimeter) and its speed (is low in comparison to other conventional printing processes) [2.6]. Figure 2.3 shows some examples of printed systems by screen-printing technology.

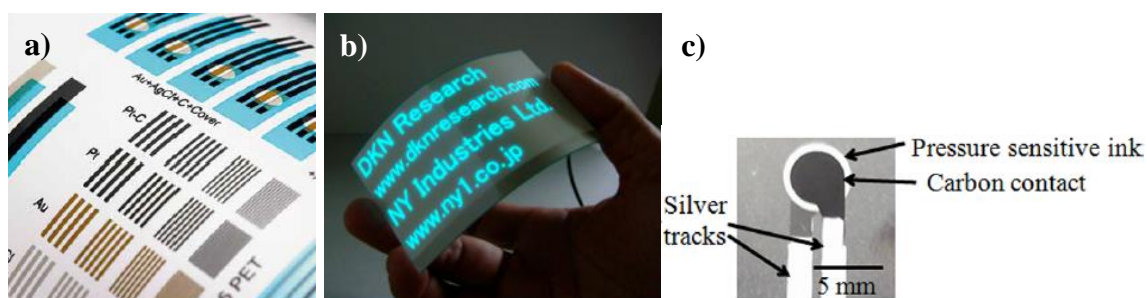


Figure 2.3 - Screen-printing: a) Biosensor inks on the Left (Reprinted from [2.14] ); b) Flexible electronic on the right (Reprinted from [2.15] with permission. Copyright line © 2008 IEEE); c) Top view photograph of a pressure sensitive test device (not to scale). The force probe is applied to the center of the printed disk [2.16].

### 2.1.2. Flexography

The flexography printing is a R2R (Roll-to-Roll) direct printing technology, where final pattern stands out from the ink transfer made through small depressions that retain the ink on the printing plate cylinder (see 1 in Figure 2.4) [2.17]. This set is located around a late cylinder (2) to ensure a continuous [2.17] high speed printing process (Figure 2.4). The ceramic anilox roller (4) [2.17], covered with micro-cavities on its surface, allows the collection of ink, and then its transfer to the printing plate cylinder (Figure 2.5). A closed chamber (5) supplies the ink to the anilox roller (4) [2.6]. A doctor blade (6) removes excess ink from the cylinder and prevents the output from the ink supplier chamber [2.6]. The rotation of the anilox cylinder, in direct contact with the printing plate, continuously rotate in contact with the substrate [2.17].

The viscosities of flexographic inks vary from 0.01 to 0.1 Pa.s. Inks may be water-based, solvent-based or UV-curing. The printed ink film thickness goes from 6 to 8  $\mu\text{m}$ . However, situations as Halo effect (patterns with excess ink) occur due to the compression between the printing plate and the substrate, despite the low pressure applied. These leads to limitations on image size stability and resolution [2.6].

This printing technique is commonly used for the fabrication of products, such as, on-label battery testers, drug delivery patches, printed batteries and other e-label applications [2.18].

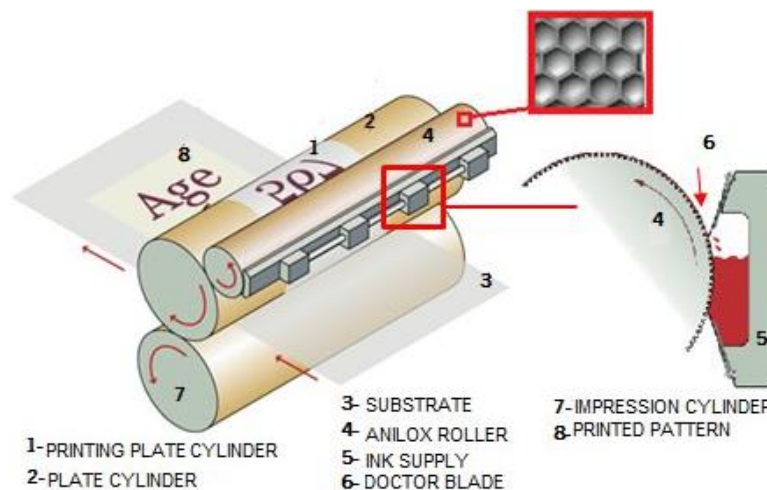


Figure 2.4 – Schematic of flexographic printing system. Adapted from [2.19].

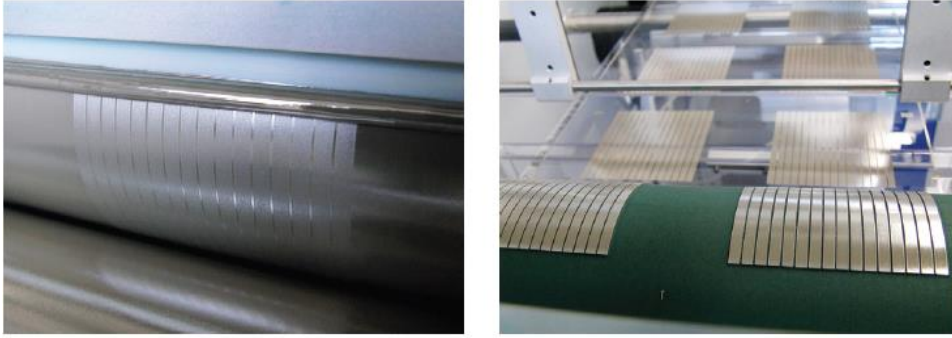


Figure 2.5- The anilox roller disengaged from the anilox showing the negative print of the motif after ink pick out from the printing cylinder (left). The printing cylinder with the relief carrying the ink (in this case a silver paste) during printing. The final printed pattern on the web can be observed in the background (right). (Reprinted from [2.9], Copyright (2012), with permission from Elsevier).

Flexography is a technique still under study for pressure sensors manufacturing. Julin [2.20] has study the suitability of flexography printing and new electrode materials in the manufacture of flexible piezoelectric pressure sensors. He has developed a flexo-printed piezoelectric Polyvinylidene fluoride (PVDF) pressure sensor. Although fabricated samples showed sensitivities, the sheet resistance presented high values and a lot of variance was observed in his results. He reported a non-uniform structure and some difficulties on achieving a uniform pressure sensor with flexo-printing.

### 2.1.3. Gravure printing

The gravure printing process is the reverse process to flexography where the image to be printed is negative (Figure 2.6). The ink is transferred from the small engraved cavities on the cylinder surface forming the pattern (resulting from chemical etching processes or, laser engraving). The ink is received directly by the container or by an additional roller (often an anilox roll) to the gravure plate, where the pattern image is located and where the ink is temporarily stored in the cavities. A flexible metal blade removes the excess ink, leaving the surface clean [2.21].

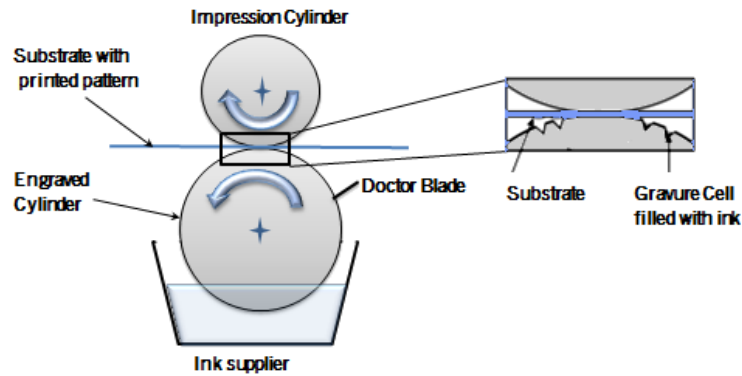


Figure 2.6 – Gravure printing process. A adapted from [2.22].

Figure 2.7 shows a detail of Gravure Cylinder engraving and a comparison of printability of 200  $\mu\text{m}$  nominal line by using two different engraving approaches. Nano silver ink was able to produce continuous lines with both types of engraving; however, the lines were different in width (measured  $248 \pm 6 \mu\text{m}$  and  $269 \pm 7 \mu\text{m}$  for type A and type B engraving, respectively). For silver flake ink, engraving B resulted in very smooth line edge and line width of  $263 \pm 5 \mu\text{m}$ .

This technique is suitable for printing with inks of low viscosity and high manufacturing speeds (up to 15 m/s) can be achieved. This process normally uses water-based inks, solvent-based inks or UV-curable inks with viscosities of 0.01-0.05 Pa.s [2.6]. The printed ink film thickness goes from 8 to 12  $\mu\text{m}$  [2.6]. A careful optimization of the process and of the materials is important because the final print quality is highly dependent on the properties of the ink, namely, their rheological behavior, the solvent evaporation rate, viscosity, and curing.

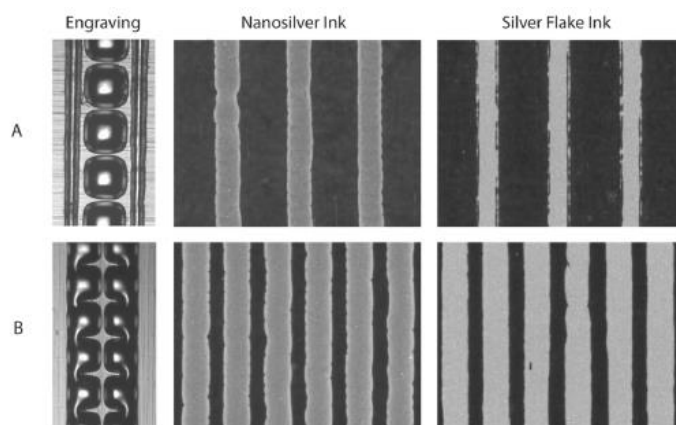


Figure 2.7 - Detail of gravure cylinder engraving and a comparison of printability of 200  $\mu\text{m}$  nominal line by using two different engraving approaches. (Reprinted, with permission, from [2.23], Copyright © 2011 IEEE).

Widely used in magazine printing, gravure printing is also heavily employed for certain electronics products such as medical Electrocardiography (ECG or EKG) pads and high-volume Radio-Frequency Identification (RFID) applications [2.18, 2.24] (Figure 2.8). However this process is not viable to applications with flexible substrates. It presents two limitations: The first lies in the high pressure required to print that deforms the substrate; the second lies in the fact that the printing image is built from separate cells, when printing a straight line, a jagged line is observed [2.6, 2.21].

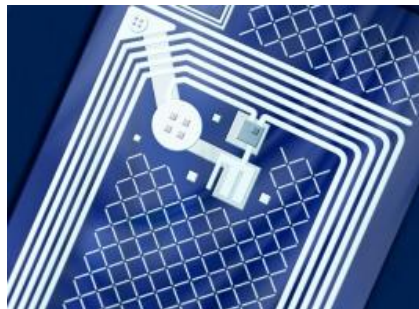


Figure 2.8 - Gravure printed wireless power antenna. This could allow sensor networks such as RFID tags, price tags, smart logos, signage, and sensors could be fully interconnected and driven by DC power of less than 0.3 W [2.25].

#### **2.1.4. Soft lithography**

Soft lithography technology encompasses several printing techniques, such as microcontact printing ( $\mu$ CP) [2.26], replica molding (REM), micro transference molding ( $\mu$ TM), micromolding in capillaries (MIMIC), and solvent assisted micromolding (SAMIM) [2.27] (Figure 2.9 and Figure 2.10). These techniques allow the fabrication of micro- and nanostructures of high quality. The key element of these techniques lies in the elastomeric stamp or mold, which transfers the pattern to the substrate [2.27]. Usually the master is prepared using either e-beam or photolithography. From this master, several stamps can be molded. The stamp is made of elastomeric polymers, most commonly of poly (dimethylsiloxane) (PDMS). The material of interest is deposited on the stamp and transferred on the substrate.

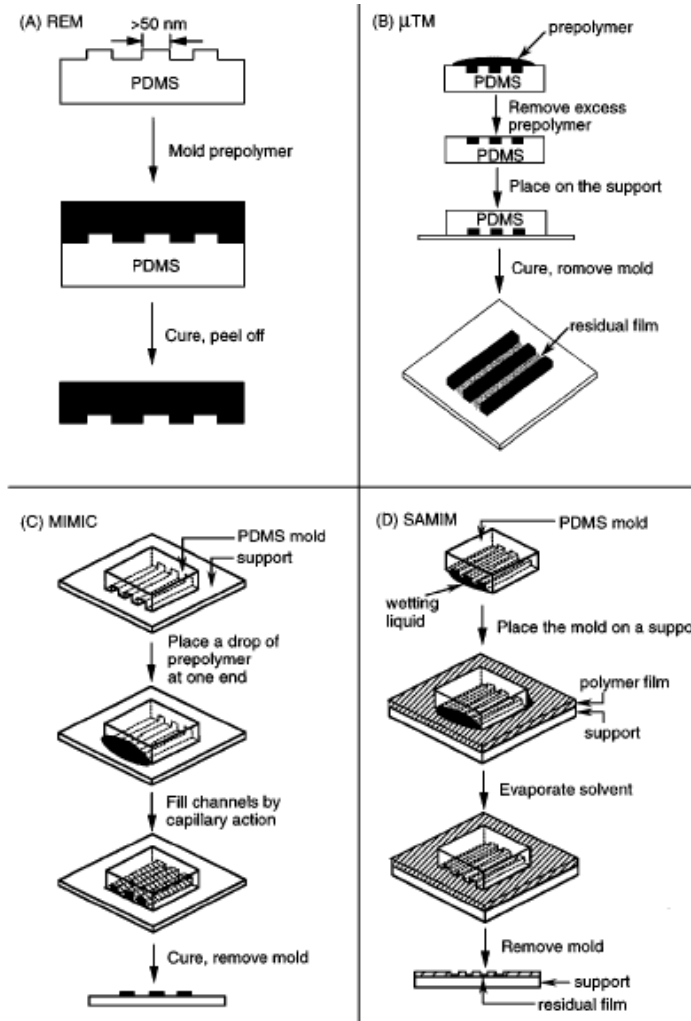


Figure 2.9 - Schematic illustration of the four major steps implied in soft lithography and is four major techniques: (a) replica molding (REM), (b) microtransfer molding ( $\mu$ TM), (c) micromolding in capillaries (MIMIC), and (d) solvent-assisted micromolding (SAMIM). (Reprinted from [2.27] with permission. Copyright © 1998 WILEY-VCH Verlag GmbH).

Soft lithography provides a convenient, effective, and low-cost method for the formation and manufacturing of micro- and nanostructures [2.28] systems. In this set of technologies, an elastomeric stamp with patterned relief structures on its surface is used to generate patterns and structures with feature sizes ranging from 30 nm to 100  $\mu$ m [2.27]. However, soft lithography doesn't offer better economic advantage when compared to the printing techniques described before due to the rapid throughput of roll-to-roll printing techniques as flexography and gravure printing [2.29].



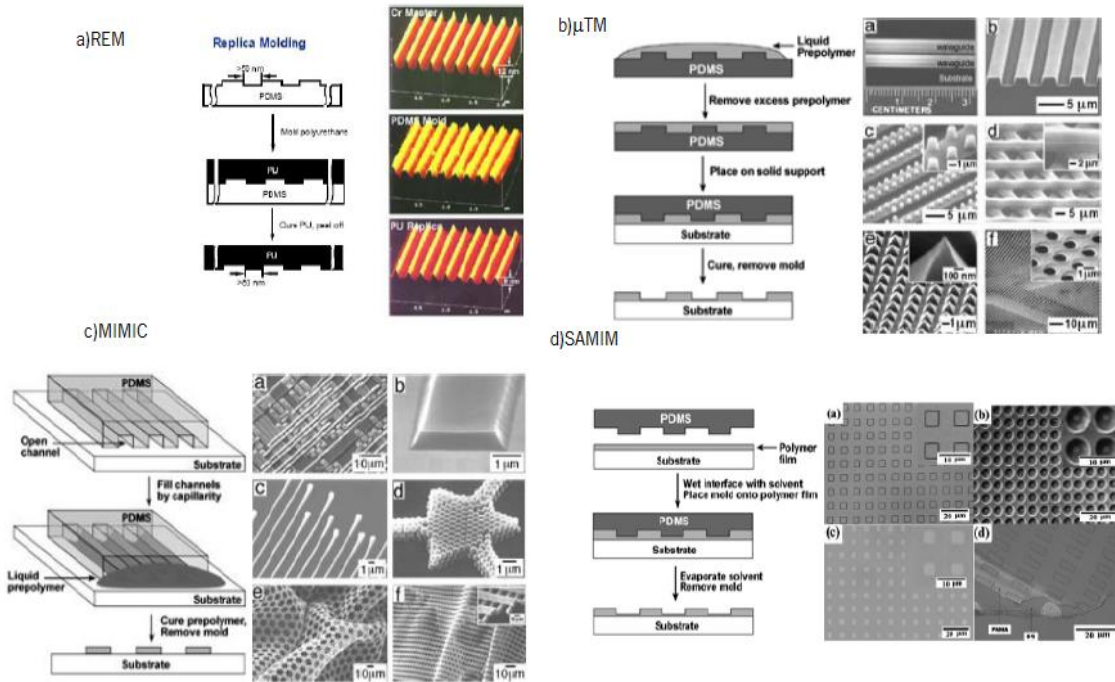


Figure 2.10 - Schematic illustration of the major steps in soft lithography technologies: (a) replica molding (REM), (b) microtransfer molding ( $\mu$ TM), (c) micromolding in capillaries (MIMIC), and (d) solvent-assisted micromolding (SAMIM) (Reprinted from [2.30]).

This technology has been used for the fabrication of pressure sensors [2.31 - 2.33]. Yang et al. [2.31, 2.32] developed a capacitive tactile and shear –stress sensing array (Figure 2.11) using this technology and using a flexible printed circuit board (FPCB). It should be noted that although the proposed design reduces the complexity of the capacitor structure, the fabrication included several manufacture steps, and with the involvement of photolithography technology.

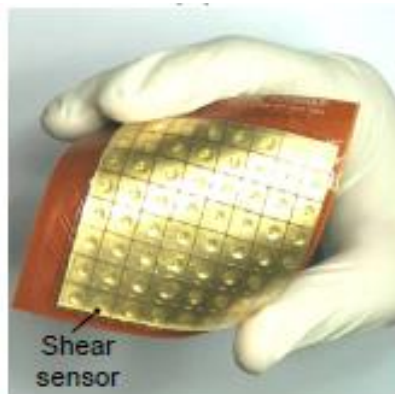


Figure 2.11 – Structure layers of a tactile sensing array manufactured by Lithography © [2010] IEEE. Reprinted, with permission, from [2.31].

## 2.2. Non-contact printing techniques

Compared to the contact printing techniques, the non-contact printing techniques have the advantage of the substrate only getting in contact with the ink. This lowers the risks of contamination and damaging the substrate and the patterns alignment is more accurate. This last one is an indispensable functionality to pattern multilayered devices.

The contact techniques also stumble upon some difficulties when completing multilayered devices [2.34] are need. Non-Contact printing technologies require low processing temperature, grant a green light to work with all kinds of substrates, such as, wood, glass, metals and most interesting, rubbers, polymers, which have limited processing temperatures, risking to be damaged and deformed when subjected to thermal stresses and high temperature processes. There's no need for physical master of the to-be-printed image. Non-contact techniques only requires a digital image (gathering all need information in a digital form), simplifying the switch process without no additional cost [2.35].

### 2.2.1. Laser Direct Writing (LDW)

Laser direct-writing techniques enable the realization of 1D to 3D structures by laser-induced deposition of metals, semiconductors, polymers, ceramics, without using masks and without physical contact between a tool or nozzle and the substrate material. Operated by a computer, the laser pulses are manipulated to control the composition, structure, and properties of individual three-dimensional volumes of materials, across length-scales, spanning six orders of magnitude, from nanometers to millimeters [2.36]. The ability to process complex or delicate material systems and achieved resolution, enables LDW to fabricate structures that are not possible to generate using other fabrication techniques [2.36]. Within LDW, there are three writing techniques: In the first, Laser Direct Write addition (LDW+) technique, the material can be deposited from gaseous, liquid and solid precursors (e.g.: Laser Chemical Vapor Deposition (LCVD)) or by transfer, by means of a laser beam, from an optically transparent support onto a parallel substrate (e.g.; Laser-induced forward transfer (LIFT), Figure 2.12 and Figure 2.13) [2.29]. These techniques entail high cost due to the use of sophisticated equipment (e.g. reaction chamber associated with vacuum equipment), it is not possible to deposit organic substrates, and it can only be printed on flat substrates, parallel to the material of support. In the second, Laser Direct Write subtraction (LDW-) technique, the material is removed by ablation (ex: photochemical, photothermal, or photophysical ablation [2.37], laser scribing, cutting, drilling, or etching) [2.38]. An industrial application example is



the high-resolution manufacturing and texturing of stents or other implantable biomaterials; Finally, the third technique is Laser Direct Write Modification (LDWM), where the material is modified (thermally or chemically) to produce a desired effect [2.36] (e.g.: Laser-Enhanced Electroless Plating (LEEP)). The substrate is submerged in a chemical solution that contains the metallic ions required for the deposition. A laser beam is responsible for local temperature rise, decomposing the liquid and leading to the deposition of a metallic layer on the substrate surface. This technique disadvantage relies in its disability to create 3D structures.

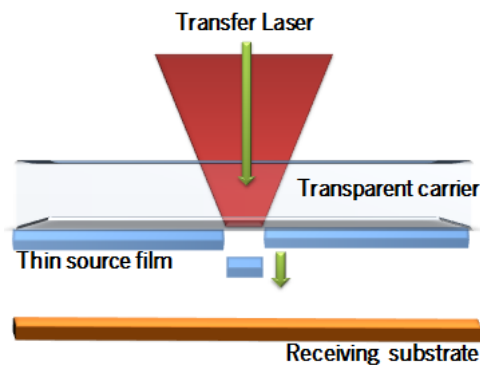


Figure 2.12 - Schematic of the LIFT process (Adapted from [2.39]).

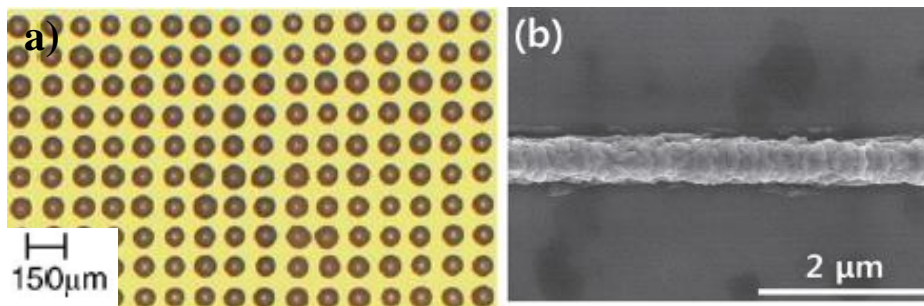


Figure 2.13 - Optical microscopy images of the microarrays of LIFT spotted droplets containing the human cDNAs (Reprinted from Publication [2.40] Copyright (2005), with permission from Elsevier.) in a); SEM images of laser direct written silicon wires for field effect transistor sensors in b). Boron-doped silicon wires are fabricated using laser direct writing in combination with chemical vapor deposition (Reprinted form [2.41]. Copyright [2013], with permission from AIP Publishing LLC).

### 2.2.2. Aerosol printing

Aerosol Jet Printing (also known as Maskless Mesoscale Materials Deposition or M3D) is another material deposition technology for printed electronics developed by Optomec (Figure 2.14) [2.42]. The ink (solutions and nanoparticle suspensions based on metals, alloys, ceramics,

polymers, adhesives or biomaterials) is placed into an atomizer, where it aerosolizes in liquid particles (between 20 nm and 5  $\mu\text{m}$  diameter depending on the ink viscosity). Then the ink is transported into the deposition head by a nitrogen flow, the aerosol being focused by jet stream onto the substrate. Complex design could be printed (e.g., displays, thin film transistors and solar cells) [2.42]. Complex conformal surfaces (3D Printed Electronics) are also possible, thanks to ability to control position in z-direction of the writing head over substrate.

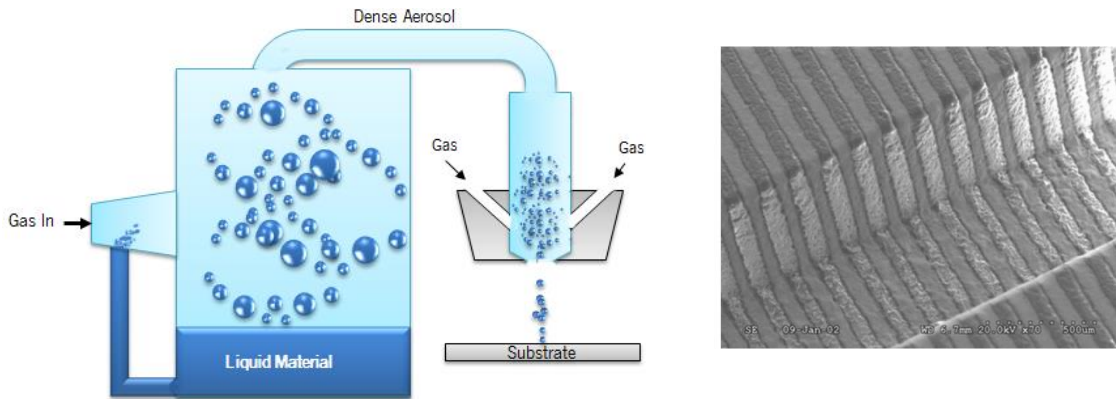


Figure 2.14 - At left is a schematic of aerosol jet printing process. Adapted from [2.42]. At right is a printed silver structures into 500  $\mu\text{m}$  deep trenches through aerosol jet printing [2.43].

### 2.2.3. Inkjet printing Technology

In Inkjet Printing Technology (IPT), a content stored in a digital format is transferred by a direct deposition of droplet fluid or powder (from small openings in printheads for each specific case), under the gravity force and air resistance, to a specified position of the substrate to create printing patterns (Figure 2.15). In the case of fluids, it dries through the evaporation of the solvent, chemical changes (for example the cross-linking of polymers) or crystallization. Eventually, a post-processing treatment is required, as thermal annealing or sintering (heating to elevated temperatures) [2.44]. For greater accuracy and versatility in the production of conductive circuits, the control of the printer is made by a computer. When compared to other deposition methods, IPT enables the possibility of using various substrates (rigid or flexible, smooth or rough surfaces) [2.45 - 2.47], with lower production time due to high processing velocities, mass production with low consumption of raw materials [2.47, 2.48] and low levels of waste. IPT works entirely without the use of masks and without contact between the printhead and the substrate. Inkjet printing stands out for being an one-step process, with a simple operating principle, with the possibility of using low cost raw materials, with a speed of production overcoming some of the flaws of traditional patterning technologies and with a

compact equipment, that represent a great advantage when compared to other deposition methods and offering low cost fabrication technology [2.49].

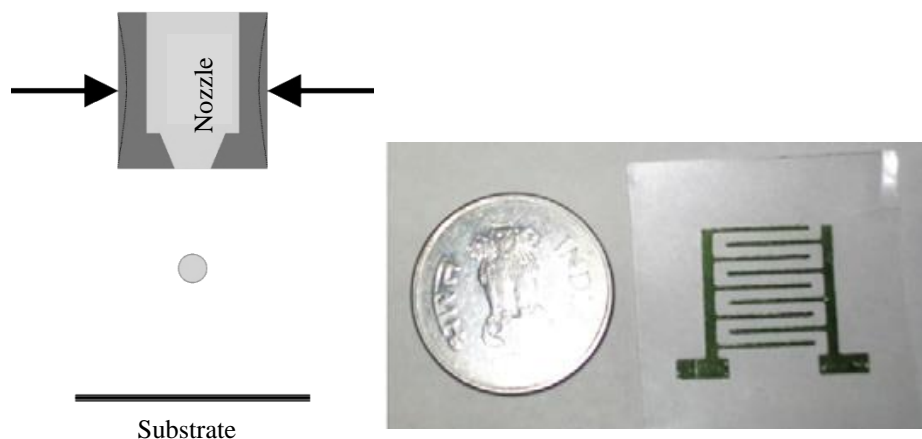


Figure 2.15 – At left a schematic of the Inkjet printing technology. At right a jet printed IPT pattern on flexible polymer substrate with a polyaniline ink (Reprinted from [2.50] Copyright (2013), with permission from Elsevier).

In recent years, the interest in this printing technology has increasing due to the great range of applications. In the field of flexible pressure sensors it is just taking the first steps. Only a few examples of IPT pressure sensors have been reported so far in the literature. Due to a number of features, IPT potential makes a compelling argument for an interesting alternative to the conventional PE technologies. For this reason, IPT was the technology selected for this research work and a in-depth overview on IPT is given. The interested reader may find in the Appendix A1 further review of the printing techniques.

### 2.3. Historical overview on Inkjet Printing Technology

The first inkjet printing device (Figure 2.16), using electrostatic forces was invented by William Thomson [2.51], and later developed by Lord Kelvin in 1858. It was used for automatic recordings of telegraph messages and was patented in 1867 (UK Patent 2147/1867). A siphon produces a continuous stream of ink on a moving paper and a driving signal moves the siphon horizontally back and forward. Since then, the evolution of technology for ink printing never stopped. The Belgian physicist Joseph Plateau and English physicist Lord Rayleigh are the fathers of modern inkjet technology. The first publication on the constitution of jets of liquid from circular orifices belongs to Plateau in 1856 [2.52]. Lord Rayleigh with a series of founding papers used acoustic energy to form uniform drops. The groundwork for the description of the role of surface tension forces was laid by Young in 1804 [2.53] and Laplace in 1805 [2.54].

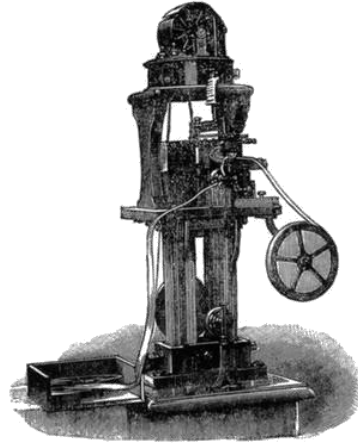


Figure 2.16 – The Siphon recorder. The first practical continuous inkjet device [2.55].

Still, it took many decades before applications of the physical principles of drop formation were used in commercial working devices. In 1951, the first practical continuous inkjet device was patented (US Patent 2,566,433) based on the English physicist Lord Rayleigh by Elmqvist of the Siemens-Elcoma company [2.56]. In the early 1960s Sweet of Stanford University patented a version of the printing process known as the Continuous Inkjet (CIJ) printing process (US Patent 3,596,275), and launched the Inkjet Oscillograph as first CIJ device. Videojet 9600 (1968) was the first commercial CIJ printing product [2.57]. New and more advanced equipment continued to emerge.

In 1940s Hansell of the Radio Corporation of America invented the first drop-on-demand (DoD) device where a piezoelectric disc, by means of pressure waves, causes a spray of ink drops. A piezoelectric disc (5) generates pressure waves in the solid cone (1), which cause a spray of ink drop from the nozzle (2) (Figure 2.17). No further developments into commercial product occurred until 1960. The first piezoelectric printer to reach the market was the Siemens PT-80, in 1977, which used the squeeze mode. The first companies to develop the first DoD equipment based on the electrostatic system were Casio, the Teletype and Paillard [2.57].

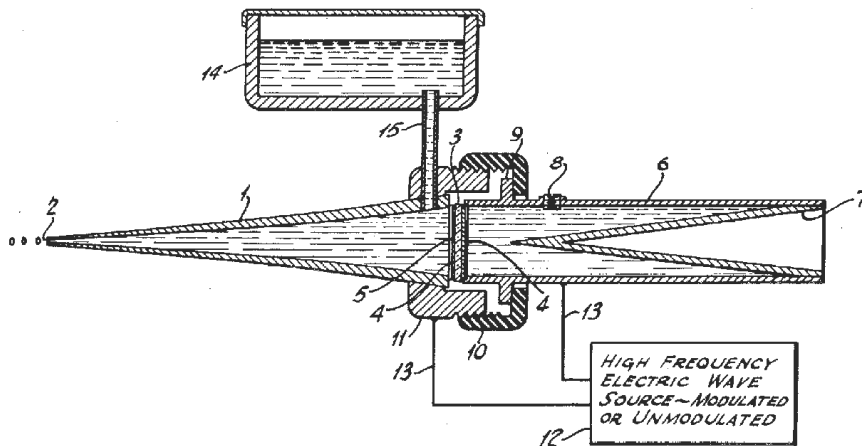


Figure 2.17 - Drawing of the first drop-on-demand piezoelectric inkjet device patented in 1950 (US Patent 2,512,743) [2.57].

The DoD system thermal printing was invented by Sperry Rand in the 60s, but only in the 70s Canon and HP used this technology. Canon launched its first printer in 1981 and HP released the first low cost ink jet printer in 1984 [2.57].

In recent years, this technology has evolved so that it became the most important printing technology in the world. The increase of the printing resolution leads to an increased number of applications and to more complex circuits. A recent application of this technology is the construction of conductive lines for the production of micro and nano-devices. IPT has been selected for the production of several devices, such as, integrated circuits [2.58, 2.59], transistors [2.60 - 2.62], conducting polymer devices [2.58], structural polymers and ceramics [2.63], biomaterials, printed scaffolds for growth of living tissues [2.58, 2.64] and MicroElectroMechanical System (MEMS) [2.63] sensors.

#### 2.4. IPT mode technology systems

The IPT can operate in two different modes: Continuous InkJet (CIJ) and Drop-On-Demand (DoD) [2.47]. The method for controlling the droplet movement is quite different between the two systems. Today, countless solutions in terms of equipment exist and several companies (Microdrop, Microfab and Fujifilm) are known for high technology and resolution, other by their commercial and simpler solutions (Epson, Hewlett-Packard and Canon). Figure 2.18 presents an overview of the two operation methods.

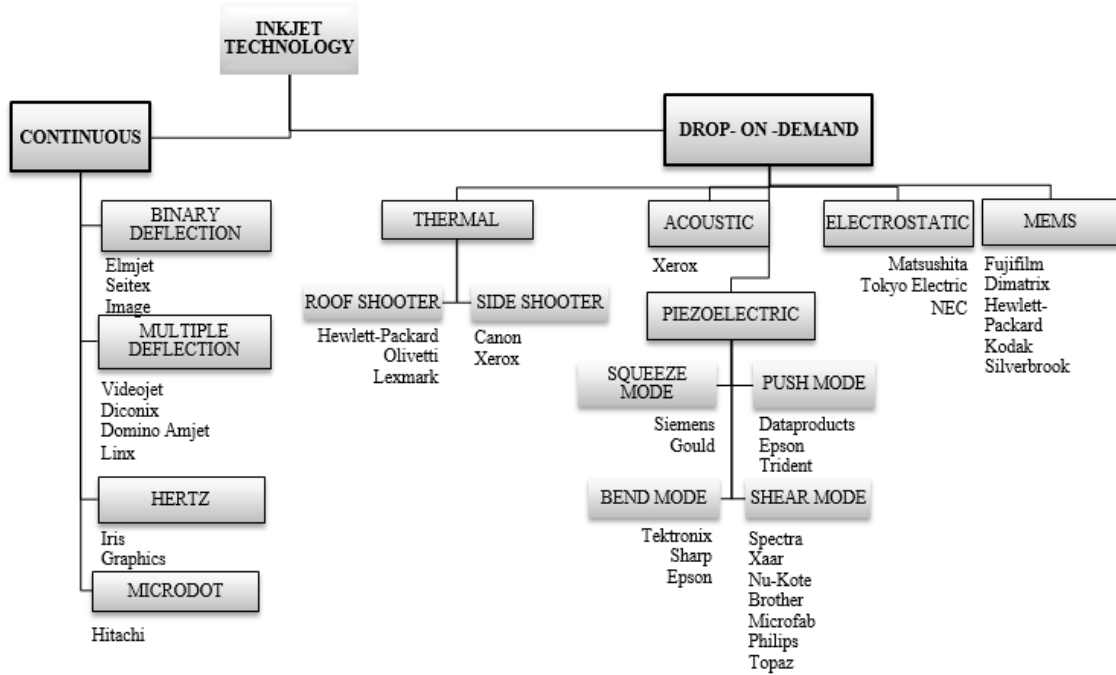


Figure 2.18 – Printing Technologies respective methods and specialized companies. Adapted from [2.56] and from [2.65].

### 2.4.1. Continuous Inkjet (CIJ) Mode Technology

In the CIJ system, the formation and ejection of the droplet is continuous in all nozzles of the printer. In the traditional CIJ, a piezoelectric transducer is coupled to the print head to provide a periodic excitation [2.66]. After leaving the nozzle, an electric field determines and controls the trajectory of the droplet to the desired position on the substrate.

Within this technology, the droplets can be diverted by binary or multiple deflection systems. On the binary system, the droplets are directed to a single pixel location on the substrate or to the gutter, for later recycling or reuse of the ink. In the multiple deflection system, the droplets are charged and deflected to the substrate at different levels, this way creating multiple pixels. Hertz et al. [2.67] used the binary continuous ink jet and developed a method consisting in the formation of a layer of irregularly droplets of ink size. In the Hertz method, the droplets are dispersed in a straight line to a gutter so as to converge into the recirculation system. This method also introduced a new procedure and methodology relatively to the use of volatile solvents that allows a quick drying and adherence to the substrate materials. Figure 2.19 shows the IPT processing scheme using both the binary deflection and multiple deflection systems.

Compared to the DoD system, the CIJ system benefits from the ability to combine the printing speed (on the order of 25 m/s) with the possibility of achieving extended distances and the ability to divert droplets independent of gravity [2.68].

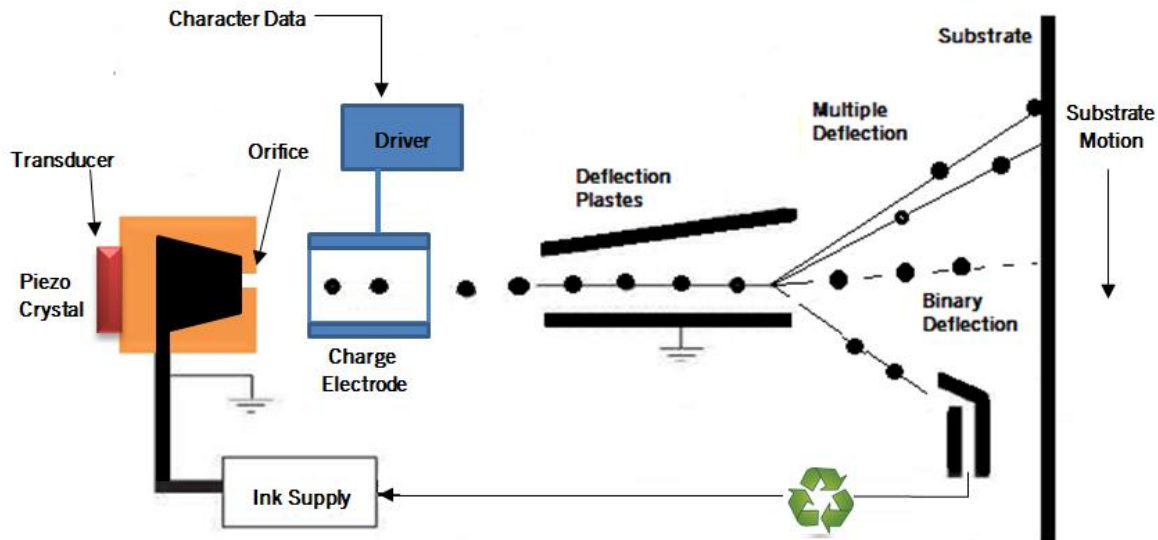


Figure 2.19 - IPT processing scheme. This system uses both the binary deflection and multiple deflection systems. Adapted from [2.69].

CIJ technology is typically used for large industrial productions of bar codes and labels of food products or medicines. This process can be comparatively fast, with the advantage of circumscribing large printing areas with a single pass and its printing heads have a long duration. The droplet size can reach values such as 20  $\mu\text{m}$ , with a standard size of 150  $\mu\text{m}$  [2.70].

However, in the manufacture of electronic products, the CIJ produces droplets of inadequate resolution due to the long distance between print head and the substrate [2.6]. Other less positive factors, reside in the high cost of initial investment in such equipment, the lower resolution compared to some DoD systems, the need to use low viscosity electrolyte inks (with viscosity in the range of 3-6 mPa.s), resulting in some final ink waste [2.71].

#### 2.4.2. Drop-On-Demand (DoD) System

In the DoD technology, the printhead ejects a single droplet only when activated. The printer is based on several injector nozzles in the printhead and the droplets are ejected in parallel to each other producing an inkjet at each pulse. Characters are constructed from successive pulses, which largely differentiate from CIJ. The DoD technology works with a Computer-aided-design (CAD) image file, high speed, scalability and high frequency multiple nozzles. The

method that is used to generate this impulse defines the subcategories of the primary DoD. They are: the acoustic, the electrostatic, the thermal, the piezoelectric, and an additional method, sometimes controversial, the MEMS [2.65] method. This last method is more related to the fabrication process, since the drop generation is based on thermal or piezo printheads.

**2.4.2.1. Acoustic method**

In the acoustic method, a high frequency transducer positioned behind an acoustic lens is used (Figure 2.20). To operate the system an acoustic wave is launched through the lens. When a wave greater than the surface tension of the ink is created, the pressure expel the ink droplets [2.72].

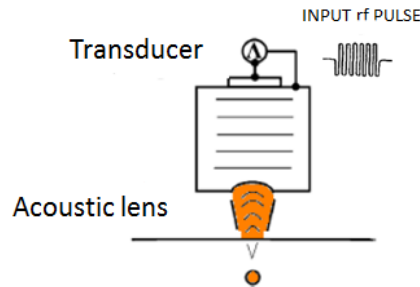


Figure 2.20 – DoD system – Acoustic method (Adapted form [2.73]).

**2.4.2.2. Electrostatic method**

In the electrostatic method the ink drops are jetted by the influence of an electrostatic field. This field, acting between an electrode and the orifice, attracts free charges within the ink (sometimes described as a liquid toner) to the surface such that a droplet is produced when the electrostatic pull exceeds the surface tension of the ink (Figure 2.21). Since this technique is based on the attraction of free charges, the ink must be conductive.

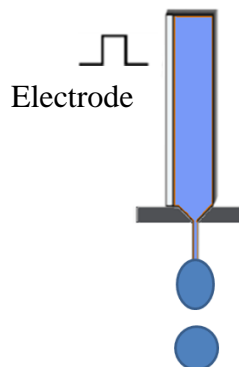


Figure 2.21– DoD system – Electrostatic method. Adapted from [2.65].



The electrostatic system allows printing a significantly concentrated formulation [2.65]. The droplet size is defined by the voltage applied at the time of ejection, not by the size of the output nozzle of the ejector [2.65]. The main limitations of this method is the requirement of conductive inks and the high cost of implementing the printing system [2.65].

### 2.4.2.3. Thermal method

The thermal method uses an electric heater within the nozzle, which rapidly increases the temperature of ink to create a vapor bubble which, in expansion, ejects an ink droplet through the nozzle orifice [2.47] and places it precisely on a surface to form patterns or images (Figure 2.22). As advantages, this method includes the fact that it creates very small droplets, allowing reduced nozzles size and therefore a more compact equipment with reduced costs. The main disadvantages are related to the restriction of the fluid used. Water-based inks are usually desirable [2.70], since the fluid has to be vaporized and has to sustain high temperatures. With an inappropriate choice of the fluid, high temperatures can cause a hard coating and thus reduce equipment efficiency and significantly reduce the lifetime of the print head, making it impractical for electronic circuits printing. This method was developed for desktop printers, designed to be cheap, silent and easy to use on flat surfaces that maintain a fixed orientation.

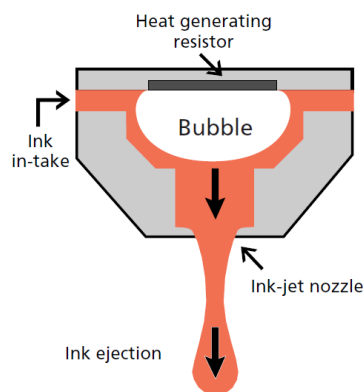


Figure 2.22 - DoD system - Thermal Method. Adapted from [2.71].

### 2.4.2.4. Piezoelectric method

In the piezoelectric method (Figure 2.23) a piezoelectric crystal expands in response to a stress wave (electric current) creating a pressure within the ink vessel [2.47]. The volume of the ink vessel is reduced and by mechanical pressure the droplet is ejected from the nozzle.

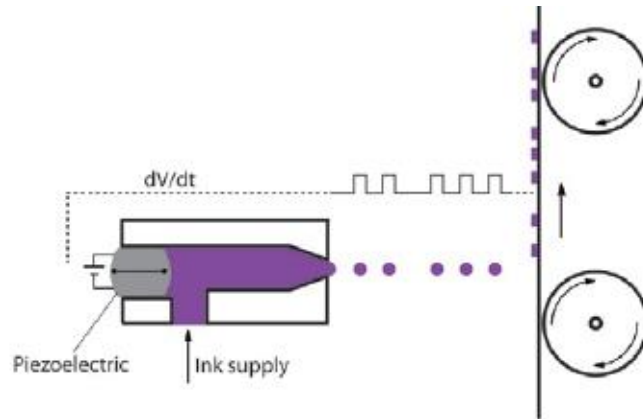


Figure 2.23 - Behind DoD system – Piezoelectric method (Reprinted from [2.9] Copyright (2012), with permission from Elsevier).

The piezoelectric method offers major benefits for electronic circuits' production. Regarding the application of this technology, in the printing of conductive circuits, the method piezo-DoD is preferable to CIJ, primarily because DoD enables higher positioning accuracy of each ink droplet. The piezoelectric heads can be grouped based on how the electric current deforms the piezoelectric crystal, in other words: Shear mode, Bend mode, Push mode and Squeeze mode [2.66]. The piezoelectric crystals are mostly made of Zirconate Titanate (PZT). The selected technology for this study was DoD system - piezoelectric heads. The different DoD system - piezoelectric heads are described in detail in Appendix A.2

#### 2.4.2.5. Microelectromechanical Systems (MEMS) manufacturing method

MEMS is a technology where the devices are fabricated at micro scale and electrically operated. This allows their integration into microscale systems. The print heads manufactured based on this technology are used mainly in thermal and piezo printing (Figure 2.24). It's possible to manufacture printing heads increasingly small and identical to the conventional ones in terms of performance or even more efficient. This efficiency is translated in higher speeds, lower heat losses, and greater control over the size of the ink droplets, higher print quality and greater stability through print heads life [2.74].

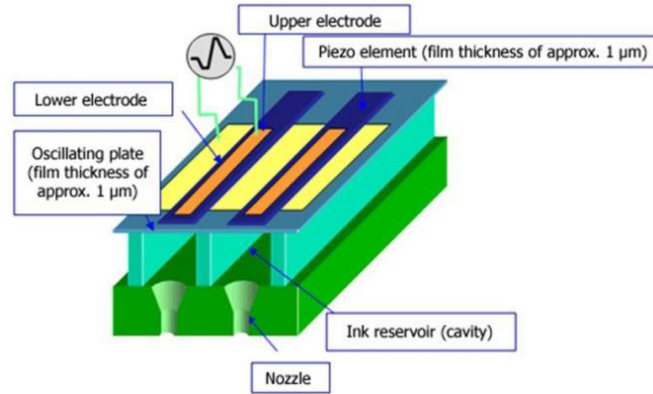


Figure 2.24 – DoD system – MEMS printhead [2.75].

## 2.5. Process phenomena

### 2.5.1. Drop formation

Printing parameters, such as, the compatibility between the materials (ink-substrate), the temperature of the printhead, and print speed can affect the printing process and, of course, the quality and properties of the final printing. Several issues are to be considered, such as, the physical-chemical characteristics of the ink (e.g., surface tension, viscosity, concentration, pH (acidic or basic solutions), type of vehicle (solvent), evaporation rate, particle size, solids content, etc.), which constitute the most crucial features of inkjet printing technology. The shape of the drop, as it is jetted from the nozzle, straightly depends on the surface tension (typically from 28 mN/m to 350 mN/m) and the viscosity of the ink (also temperature dependent) [2.47].

Viscosity values lower than 20 mPa.s are recommended in order to allow droplet ejection from the nozzle. The viscous forces to inertial and surface tension forces relation is expressed by the dimensionless Ohnesorge number ( $Oh$ ) [2.76]:

$$Oh = \frac{\sqrt{We}}{Re} = \frac{\eta}{\sqrt{\rho D \sigma}} \quad \text{Equation 2.1}$$

where,  $\eta$  is the viscosity,  $\rho$  is the density and  $\sigma$  is the surface tension of the ink and  $D$  is a length parameter, normally the nozzle diameter. The Ohnesorge number is related to the Reynolds ( $Re$ ) and Weber ( $We$ ) numbers.  $Re$  number is the ratio of the inertial and the viscous forces and the  $We$  number is the ratio of the inertial force to the surface tension [2.77]:

$$Re = \frac{\rho V D}{\eta} \quad \text{Equation 2.2}$$

$$We = \frac{\rho V^2 D}{\sigma} \quad \text{Equation 2.3}$$

where,  $V$  is the fluid velocity. The inverse of Ohnesorge number:  $Z = Oh^{-1}$  is also very common. As predicted by Fromm [2.78], the drop formation occurs only for  $Z > 2$ . According to Reis and Derby [2.79] the range is  $1 < Z < 10$ , where for  $Z < 1$  viscous dissipation in the fluid prevents drop ejection, and for the upper limit unwanted satellite drops formation occurs [2.80, 2.82].

Between the polymer-based inks, the drop formation dynamics depends upon the concentration and the molecular weight of the polymer. Even with a small amount of polymer added to the ink, the ejection of a droplet involves the formation of a filament connecting the ejected droplet to the nozzle of the printer (Figure 2.25). With an increasing of the molecular weight of the polymer, the increase of viscoelastic forces also occur.

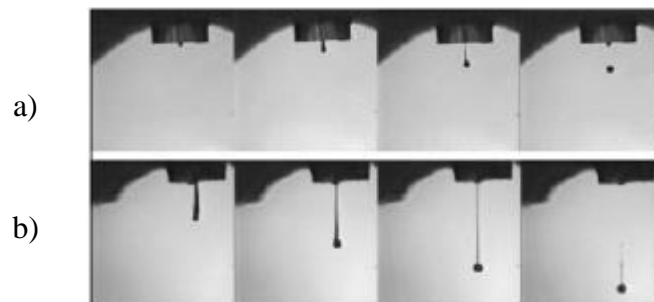


Figure 2.25 – Stroboscopic images of inkjet printing droplets: a) drop formation for a Newtonian fluid; b) effect of addition to the ink of a small amount of high molecular weight polymer [2.83].

With the increase of the concentration or molecular weight of polymer, the satellite drops occurrence decreases. The satellite drops happens when a filament becomes a tail, breaking up from the main drop along its axis to form a satellite drop (Figure 2.26). The higher the concentration or molecular weight of polymer, the less droplets without satellites is formed. If the concentration/molecular weight of polymer is higher than a certain value, the capillary force is not able to break the filament, forcing the drop to retract to the nozzle.

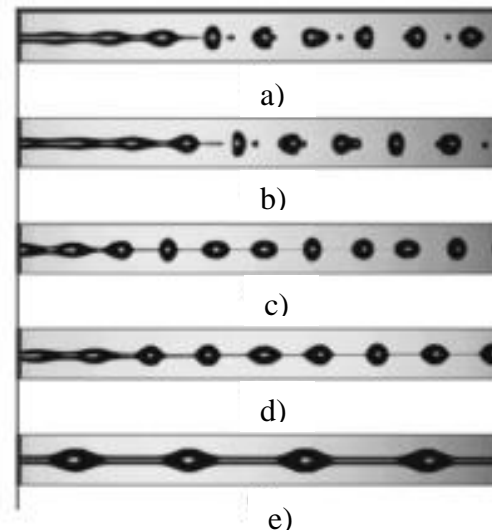


Figure 2.26 - Influence of polymer concentration and molecular weight on the drop formation dynamics: a) glycerol/water; b) 0.3% 100000 poly(ethylene oxide); c) 0.1% 300000 poly(ethylene oxide); d) 0.05% 1000000 poly(ethylene oxide); e) 0.043% 5000000 poly(ethylene oxide) [2.84].

### 2.5.2. Drop impact phenomena

In order to optimize the printing performance, especially in electronic inkjet applications, where high resolution of printed structures are desirable, the fluid impact phenomena's of the drop on a dry surface has enormous importance. As reported by Yarin [2.77] the variables involved are numerous: the drop velocity, its direction with respect to the substrate, the drop size, the ink properties, the wettability and the roughness of the substrate and the non isothermal effects (e.g. solidification and evaporation of solvent) greatly affect the drop impact on the substrate.

Rioobo and Tropea. [2.85] reported six possible drop impact phenomena when a droplet strikes a solid dry surface, namely, *Deposition*, *Prompt splash*, *Corona Splash*, *Receding break-up*, *Partial rebound* and *Complete rebound* (Figure 2.27):

- The *Deposition* is considered when the drop, during the impact, deforms without breaking up in smaller drops, and stays attached to the substrate surface.
- The *Prompt splash* occurs in rough surfaces. From the drop impact, in the beginning of the spreading, new droplets are formed at the contact line.
- The *Corona splash* occurs if the drop impact on a rough surface is very fast, forming a corona during the spreading phase, eventually breaking into droplets.
- If the surface is non wettable the *Receding break-up* scenario occurs, in other words, the drop after the impact breaks up into a number of fingers, each of them capable

to further breakup. The droplets are left on the surface during the retraction of the drop.

- e. Finally, if the surface is super hydrophobic, the ***Partial rebound*** occurs when part of the drop stays attached to the surface and,
- f. The ***Complete rebound*** occurs when the entire drop lifts off the surface.

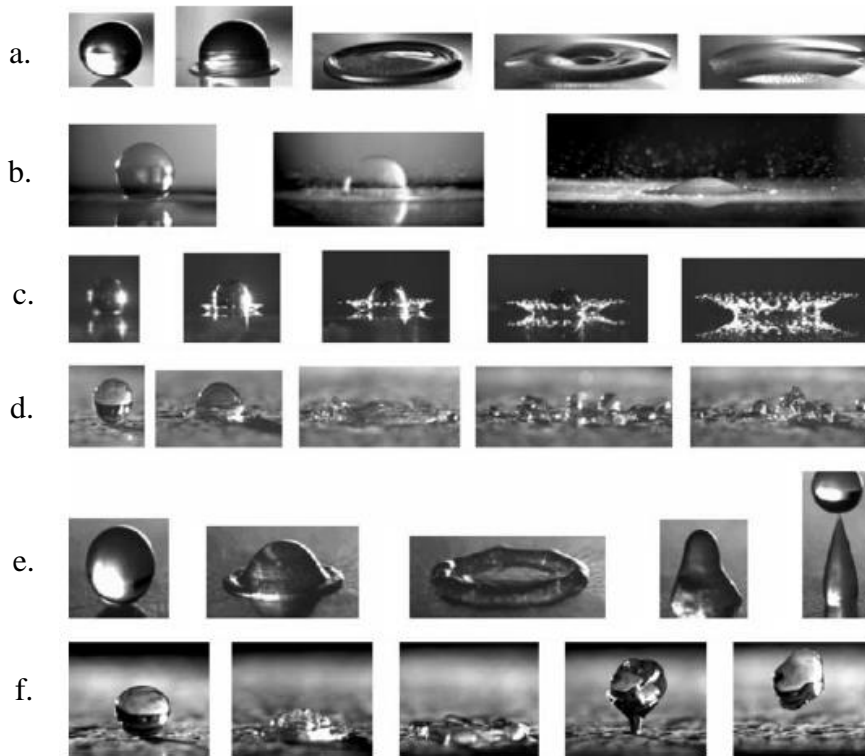


Figure 2.27 – Drop impact morphology on a dry surface [2.85].

In inkjet electronic applications, splashing is an unwanted effect because it could compromise drop precision and resolution. According to Rioobo et al. [2.86] the diameter spreading of a drop onto a substrate may develop in four different phases (Figure 2.28):

- The kinematic phase,
- the spreading phase,
- the relaxation phase,
- the wetting/equilibrium phase.

As shown in Figure 2.28, the axis  $t^*$  represents the time after impact, calculated through the drop velocity  $V$  and the spherical drop initial diameter  $D$  [2.86]:

$$D \left( t^* = t \left( \frac{V}{D} \right) \right), \quad \text{Equation 2.4}$$

where  $d^*$ , known as spreading factor, is the drop diameter, defined as the ratio between the contact zone diameter and  $D$ ,  $t^*$  and  $d^*$  are non-dimensional parameters. In the kinematic phase, the spreading factor increases according to a power law  $d^* \sim t^{*1/2}$ , being dependent only upon the drop velocity and its initial diameter. The spreading phase is characterized by a constant increase of  $d^*$  with  $t^*$ . At the beginning of this phase ( $t^* \sim 0.1$ ) the viscosity of the fluid strongly affects the spreading: the lower is the viscosity the larger is  $d^*$ . At the beginning, the surface tension has a moderate effect, whereas, at the end of the phase ( $t^* \sim 1$ ), the surface tension begins to affect the spreading, becoming crucial in the relaxation phase. Herein, the equilibrium contact angle is determined by the wettability of the surface and the balance between the inertial and viscous forces (Re number), thereby the drop continues to expand or retract. Finally, for  $t^* > 10$ , in a well wetted surface by the liquid, the drop continues to spread according to the power law  $t^{*1/10}$  [2.45]. Splashing (Figure 2.27 b.), is an unwanted effect in IPT electronic applications and is highly dependent on the high precision of the drop placement. The starting-point for spreading on a dry surface can be expressed in terms of another dimensionless group  $K = We \cdot Oh^{-2/5}$ , depending on the roughness of the surface  $R$  ((roughness amplitude)/  $D$ ). Cossali reported [2.87] that splashing occurs if:

$$K > 649 + 3:76R^{-0.63} \quad \text{Equation 2.5}$$

Qualitatively, splashing is favored by large drops size, high velocity, low surface tension and viscosity of the ink and high roughness of the substrate [2.45].

Figure 2.28 summarizes the temporal development of the spreading film diameter after the instant of impact, i.e. shows the different phase of the drop spreading with time on a solid surface.

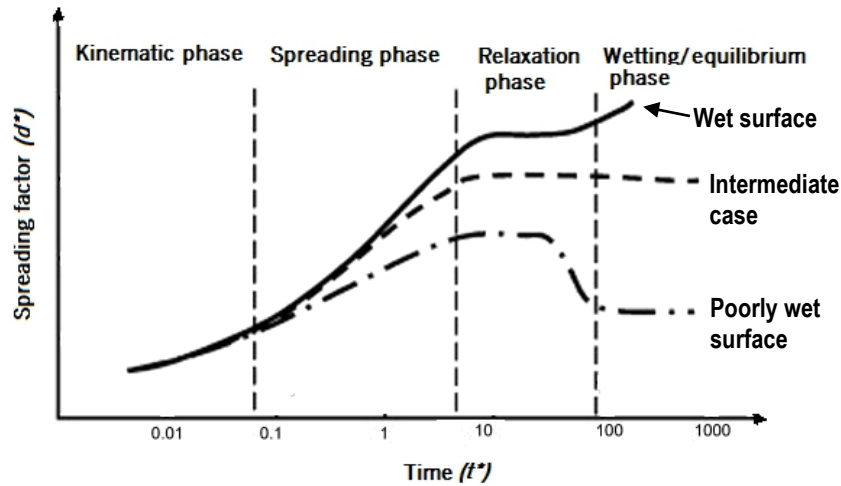


Figure 2.28 - Schematic representation of the spreading of a liquid drop with time. ( $d^*$  is the non-dimensional diameter of the drop, and  $t^*$  the non-dimensional time after impact. The labelling of the axes is approximate (Adapted from [2.86]).

## 2.6. Process variables

The control of ink drop, the printhead temperature, the sintering or cure of the ink, and the printing control of each layer are key parameters to ensure the quality of a multilayer printed structure. Furthermore, it is also important to evaluate the properties of the substrate, such as, the work temperature, its barrier properties against humidity, electrical, optical, mechanical and chemical properties. It is also important to consider the receptivity of the ink to the substrate or with previously printed layers, in the case where a different ink has been used. The droplet size can vary depending on the interactions between the ink and the substrate. The droplet size sets the width of the printed line, establishing the pattern space and the electric design limits, and defines the final specifications of the printed pattern and application system (e.g., resolution, bandwidth in the case of a printed transducer). Thereby, during the manufacturing step, the pattern characteristics are dependent on the materials and their interaction (i.e., the properties of the ink must be chosen in advance to understand its behavior during or after the printing process over a given substrate). Sintering and cure of conductive materials are essential because it defines its chemical, electrical and physical performance and reliability of the printed layers over the long term.



## 2.7. Materials and potential applications

IPT is a relatively new technology with a grown interest from the scientific community [2.58] and is considered to be in an early stage of development [2.88].

Additionally, IPT is adaptable for patterning on a high variety of substrates (glass, plastic [2.89 - 2.91], paper [2.73, 2.92, 2.93], textile [2.66], etc.). In the IPT, a content stored in a digital format is transferred by a direct deposition of ink droplets or powder, proteins and minerals [2.58,2.64], conductive polymers [2.60,2.94-2.96] and nanoparticles [2.59,2.89,2.90, 2.97,2.98] in soluble form, intended for a wide range of applications: transducers [2.60], transistors [2.62, 2.72,2.99], structural polymers and ceramics [2.58], biomimetic and biomedical materials [2.64], and even printed scaffolds for growth of living tissues [2.58], as well as for building 3D electric circuits [2.69], MEMS [2.97], and sensors [2.70, 2.90, 2.91].

Extensive studies searching for new flexible materials (substrates and inks), more economic processes and greater freedom of design are delivering novel improvements in this field of research, providing studies with increasingly intelligent sensors, able to be integrated in complex systems and environments [2.90, 2.97].

Various types of polymers have been proposed as substrates (e.g.: Poly(dimethylsiloxane) (PDMS) [2.100], Polyimide (PI) [2.101, 2.102], Polyethylene terephthalate (PET) [2.102, 2.16], Polyethylene naphthalate (PEN)[2.103], Polyurethane (PU) [2.104], etc.. Due to their mechanical properties (e.g., high elasticity and flexibility), the high processability of thin films, their ability to withstand high processing temperatures and their low production cost, polymers are a material with great potential for use as the flexible substrate in electronic applications. Their major drawback lies on the low surface energy which requires a prior treatment of its surface before printing. Polymers are great electrical "insulators" and the printing of conductive patterns on their surface, assigns them with new properties and functionalities. Within the class of polymers, the selection of the type of substrate suitable for each specific application, must meet a series of requirements: physical, mechanical, chemical, thermal and optical (resistant, bright and transparent, dimensional stability, chemical resistance), biocompatibility, flexibility, and most important, the compatibility with the conductive inks.

Along with IPT, the conductive inks are gathering more and more attention over the past two decades. They present excellent properties and tremendous potential. When properly transferred to the substrate, they can revolutionize industry and consequently human's life. Conductive inks have been elected to incorporated several applications due to their suitability for printing substrates, its processing simplicity and mechanical flexibility, but also due to its

ability to assign new properties, capabilities and complex functionalities. After the experimental evidence of conductive inks, the interest of the scientific community rose exponentially due to their unparalleled application possibilities. These emerging inks are penetrating the market enabling new applications based on their attributes of conductivity, inkjet printability and flexibility, justifying the growing market, represented in \$2.86 billion market in 2012 and forecasted to rise to \$3.36 billion in 2018 [2.105]. Compared to the more commonly used materials (non-flexible inks containing metallic particles (e.g. copper, gold, silver, aluminum) printed on rigid substrates; nano-particles dispersed in a retaining matrix) used in pressure sensors they give the advantage to extend the application areas.

The most common types of inks are water, oil or solvents based inks. The general form of the ink consist of a mixture of compounds (pigments or dyes, resins, solvents, fillers, humectant and additives), in liquid or solid state (Figure 2.29). In the specific case of conductive inks, what makes its electrical conductivity and distinguishes them from common ink [2.106] is the fact that it contains in the composition conductive particles. The incorporation of conductive polymers, carbon (C) [2.107, 2.108] or metallic particles are the most common selections. The Poly (thiophene – 3 - [2 - (2 - methoxyethoxy) ethoxy] - 2,5 - diyl), sulfonated (P3HT) [2.107-2.111], and the Poly (3,4 - ethylenedioxythiophene): poly (4 -styrenesulfonate) (PEDOT:PSS) [2.95, 2.101] are two types of conductive polymers with a growing interest in printed electronics due to its relatively low cost. However, when compared to inks with metallic particles (e.g., silver (Ag) [2.59, 2.98, 2.112, 2.113], copper (Cu) [2.105, 2.114], and gold (Au) [2.115]), these conductive polymers don't have such a high conductivity. Both types of ink are known to be the most suitable for Inkjet Printing and the particle size should be of the nanometer scale, and the interest of this inks to be used for inkjet printing applications has greatly increase in recent years [2.115 - 2.118].

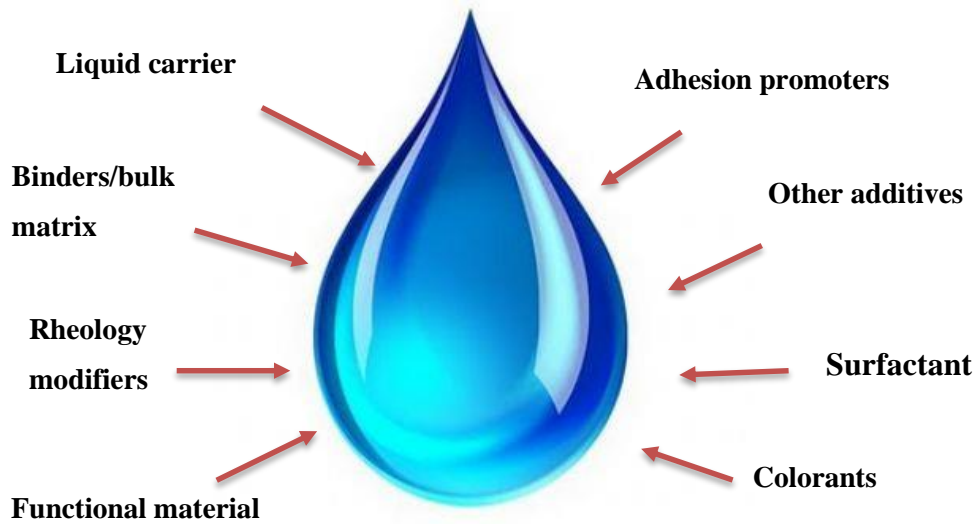


Figure 2.29 – Typical ink formulation.

In this work, three different ink were studied according to their composition and potential application use: i) two conductive polymer based inks (e.g. P3HT and PEDOT:PSS), ii) a silver based ink. Information about the inks used is presented in Chapter 3.

## 2.8. Advantages and Challenges of IPT

Over the years, IPT has demonstrated added value compared to the traditional techniques that are typically more complex and time consuming, requiring multiple step processes and expensive facilities. The jetted patterns are controlled by the printer software. This technology allows digital controlled deposition of ink droplets with less waste production that is harmful to the environment [2.119, 2.46] and less ink lost, since it doesn't require the use of high resolution masks, generally very expensive. Table 2.1 shows the main differences between different printing techniques.

Table 2.1 – Main differences between printing techniques (Source: WMU CAPE).

	Resolution	Ink film thickness	Printing speed
Screen	50 $\mu\text{m}$	3-60 $\mu\text{m}$	8 m/s
Inkjet	1 $\mu\text{m}$ or less* [2.120][2.121]	0.05-0.5 $\mu\text{m}$	2.5 m/s
Flexography	20 $\mu\text{m}$	0.5-2 $\mu\text{m}$	5 m/s
Gravure	15 $\mu\text{m}$	0.5-8 $\mu\text{m}$	15 m/s

\* With optimization between ink & substrate.

The main advantages of IPT are:

- reduce number of manufacturing steps;
- no special processing conditions are needed;
- without resorting to the use of masks;
- without production of large quantities of chemical waste;
- wide range of materials that can be deposited (ex.: print bioactive fluids, which cannot tolerate exposure to photolithography and etching chemicals present in conventional techniques [2.60]);
- wide range of possible substrates.

Compared to the screen printing paste, the inkjet ink has lower viscosity, contains smaller conductive particles (e.g., in case of a conductive ink for sensor applications) and incorporates additives to prevent their aggregation (in order to avoid blocking the printhead). Therefore, the dispersion of particles in the inkjet ink matrix is of utmost importance.

IPT of conductive inks can provide faster, innovative fabrication, high quality and low cost productions. For all the aforementioned advantages, the IPT is surely considered the most promising technique in the non-contact techniques printed electronics technology, for production of some of the electronic devices, namely, flexible displays, radio frequency identification tags (RFID), sensors, OLEDs, batteries, and printed circuit boards (PCB).

However, like every kind of printing technique, IPT presents some limitations and critical issues which have to be taken into consideration during the deposition process, in order to achieve the best printing quality. The major challenge in IPT lies in the ink physical properties with a suitable formulation, in particular its viscosity and superficial tension [2.47, 2.122]. The inks are selected depending on the application, the type of the substrate, the type of technology, equipment, and printhead technology. It is well understood that conductive ink is a key parameter to enhance the conductivity properties, however its proper formulation is quite difficult to attain. Figure 2.30 shows the main critical areas of the IPT processing variables and used materials.

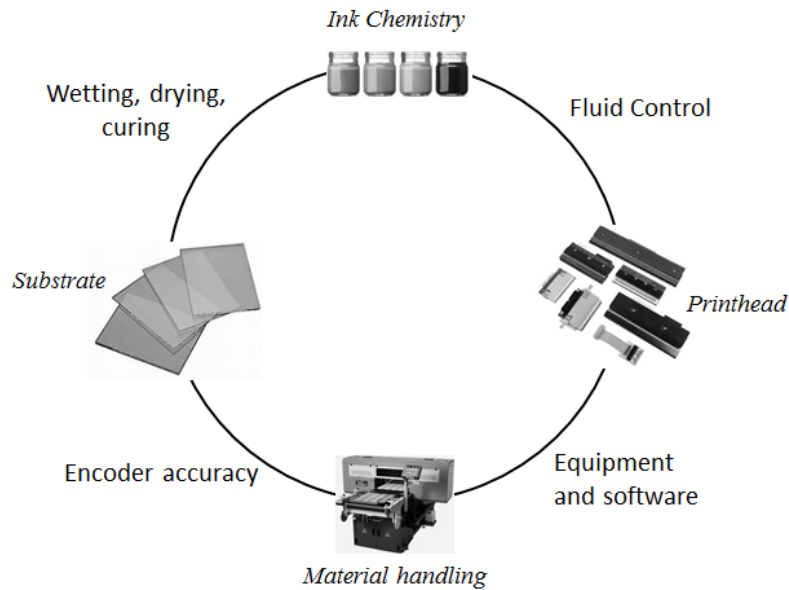


Figure 2.30 – Challenge critical areas.

### 2.8.1 Ink properties

The ink formulation should be based on the limits imposed by the process, the adhesion to the substrate and final application. Fast drying and stain resistant ink are elected, capable of passing through the nozzle-jet ink without obstruction, and should allow fast cleaning of machine parts, with minimal effort. The inks used in IPT have a particular set of physical specifications, where the viscosity should lie between 0.002 and 0.1 Pa.s, the surface tension between 25 and 35 mN/m, and the amount of humectant between 10-20% [2.80].

However, not all commercially available conductive inks can be used to print polymeric substrates. Few are the companies who have commercially available conducting inkjet inks [2.88]. The existing inks on the market are still poorly developed for IPT and such physical-chemical characteristics not only determine the ejection of the ink, but also the quality of the printed patterns and final resolution. So, the optimization of the inks and interaction between ink and the substrate strongly affects the final resolution and constitutes the main research challenge in order to achieve repeatability of inkjet printed patterns and devices. There's no sufficient data, methodologies or documented normative specifications, reporting the most suitable process variables for the various applications of the different materials. While some researchers [2.123] explore the effect of solvents on the optimization of the inks (their adhesion and spreading, as well as, performance, quality, and electric properties of the printed layer),

other researchers [2.124] are focused on understanding and optimizing the behavior of the ink droplet in different conditions of temperature and substrate surfaces.

Presently, in consequence of the poor variety of available commercial inks, in terms of physical-chemical characteristics adjusted for inkjet printed and according to the final application, the achievement of quality and repeatability of inkjet printed patterns and devices forces to include a prior step before printing (specially when an automation for medium to high-volume production batches is need) namely, an optimization of different types of conductive inks for the different applications or by optimizing the IPT process variables (depending on the used ink and final application).

### **2.8.2. Process control**

Process parameters of IPT, responsible for the deformation of droplets in a uniform and controlled way and absorption by different substrates are areas that still need to be further explored, since few studies and information are documented.

Purge procedures are essential and necessary in order to avoid undesired nozzle clogging. The cleaning frequency depends on the inks physical properties (such as density, viscosity, volatility and shelf life). These actions may cause small material and time waste. The ink with solvents with higher volatility, require higher cleaning frequency. But sometimes permanent damage of nozzles is inevitable. These procedures are described in more detail in Chapter 3.

### **2.8.3. Ink compatibility**

Another aspect that can pose a problem during printing is the incompatibility between different inks used in multilayered structures or between layers of the same ink. An incompatibility between layers can cause redissolution, resuspension, or remelting of each previously deposited layer of ink in the new printed layer, depriving uniform and uncontaminated layers [2.80]. Equally relevant, are the different post-processing treatments as sintering, annealing or simply drying in air required for each ink, which defines the final morphology and uniformity of the printed pattern and the manufacturing time [2.60]. An optimized ink formulation, according to equipment and target application, as well as the substrate treatment processes constitutes the main successful factors to achieve high resolution and repeatability of the inkjet printed patterns and devices.

### 2.8.4. Compatibility between ink and substrate

Most polymers are hydrophobic with low surface energy. Therefore, they are difficult to adhere to other materials.

The transfer and distribution of the ink on a substrate depends on the wettability and adhesion capabilities, besides other factors of paramount importance which plays a relevant role at their interface. The adhesion between two materials is the sum of a number of mechanical, physical, and chemical forces between them. Such attractive forces at the interface depend on the mechanism of adhesion involved, that include mainly:

- Substrate properties (chemical composition, surface porosity, wettability, etc.).
- Conductive ink properties (chemical composition, rheological behaviour, the rate of solvent evaporation, etc.).
- The Superficial Tension (ST) of the ink, and the surface energy of the substrate that will receive the ink; or better the difference between them.
- Functional groups and their intermolecular forces present in the ink/polymer system.

Surface wettability, spreadability and adhesion are the most important requirements in the printing process, and both are directly dependent on the fluid contact angle (Figure 2.31). A good surface wettability happens if the fluid spreads evenly over the surface without the formation of droplets. When this happens, the surface is said to be wettable. When a droplet is formed, the surface is said to be non-wettable, implying that cohesive forces associated with the fluid are greater than the forces associated with the interaction of the fluid with the surface.

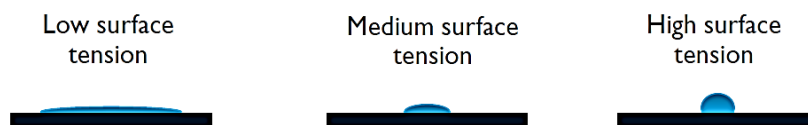


Figure 2.31 – Ink behaviour on substrate.

To achieve a good ink adhesion to the substrate it is necessary to have compatible surface energies between them. ST refers to the amount of cohesive forces between liquid molecules. The surface energy describes the degree of energy with which the molecules of the surface of a solid draw and allow adherence of the fluid. Often, ST and surface energy are interrelated, since both measure the ability of molecules to attract and to adhere to each other. In IPT, the spheroidal shape of the liquid emerging from the nozzle is defined by the ST of the liquid. The adhesion between two surfaces (ink, substrate) occurs when these come into contact and develop strength in order to maintain a stable interface. Adhesion between a solid and a liquid

exists when the solid surface energy exceeds the liquid ST. The major challenge on the use of polymers is their low surface energy. This represents a great challenge in terms of wettability, spreadability and ink adhesion to the substrate.

A simple quantitative method for defining the relative degree of interaction of a liquid with a solid surface is by measuring the contact angle of liquid droplet on the solid substrate (Figure 2.32). A contact angle less than  $90^\circ$  indicates that the substrate is readily wetted by the test liquid, while an angle greater than  $90^\circ$  shows that the substrate will resist wetting.

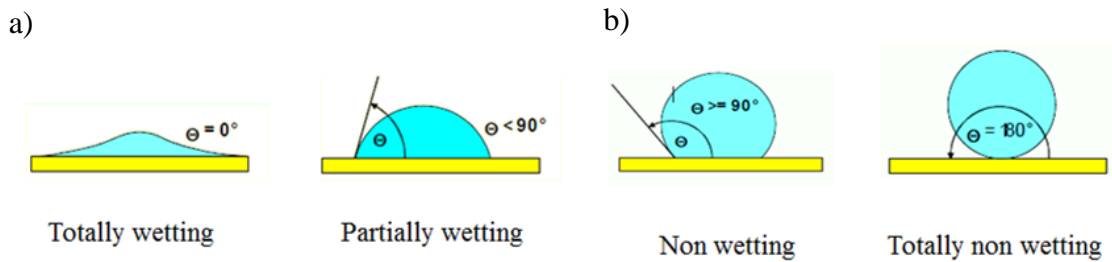


Figure 2.32 - Contact angle: a) High surface energy with a contact angle  $< 90^\circ$ ; b) Low surface energy with a contact angle  $> 90^\circ$ .

A liquid with a surface tension lower than the surface energy of the substrate will spread over its surface and there will be a strong adhesion between the substrate and the liquid film. The unit of measurement which is used for ST is the surface millinewton per meter (mN/m) (Typically, ST ranges from 28 mN/m to 350 mN/m).

### 2.8.5. Substrate surface treatment

In situations where the substrate is polymeric, surface treatments are normally required to promote compatibility and to improve adhesion forces by increasing the surface tension of the polymer, thus changing their hydrophilicity, increasing the surface contact area. Many adhesion-enhancing techniques have been explored in the literature, such as chemical roughening of the surface [2.125], resorting to the use of a primer (by dipping, brush or spray the substrate that can chemically alter the surface, e.g. silane coupling agents [2.126]), but within the framework of printing polymer surface, corona discharge [2.127, 2.128], plasma treatment [2.129 - 2.133], and flame treatment [2.127] are the most common methods.

Plasma treatments are used to change the surface energy, creation of functional groups, induce mechanical roughness on the surface and eliminate surface contaminants such as silicone mold release, dirt, dust, grease, oils, and fingerprints. This contaminants also inhibit



the shape of the drops, hence image quality [2.134] and the adhesion. Although, the surface treatment is temporary, i.e., the surface treatment enhances the compatibility of the surface with the ink, but the exposure to air induces hydrophobic recovery [2.135]. Therefore, it is recommended to bond, coat, ink, or decorate the product as soon as possible after surface treatment. In other words, it was found that the transformation to hydrophilic surface is temporary. The plasma surface treatment increases the compatibility of the surface with the ink, but subsequent exposure to air induces the hydrophobic recovery.

This adhesion improvement has been the subject of several studies: McDonald et al. [2.135] published a study of PDMS atmospheric plasma treatment. It was showed that after the polymer surface treatment, adhesion and wettability increased, but a continuous exposure to air (5 to 30 minutes depending on the substrate) resulted in recovery of their hydrophobic nature. Plasma treatments performed on PET showed that different operational parameters such as energy, time, pressure, and gas flow rate lead to different results [2.130]. Figure 2.33, shows the results of the effect of plasma treatment with low pressure in the adhesion between PI and the liquid [2.131]. A dramatic decrease of the contact angle was achieved when the PI was treated with atmospheric plasma. The results revealed an increase in the strength of adhesion between the PI and the coated layer with the increasing of the treatment time [2.136].

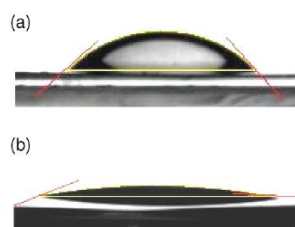


Figure 2.33 - Optical microscope photographs of PI film contact angle: a) without treatment. [contact angle: 46.2°]; b) after low pressure plasma treatment [contact angle: 14.5°] [2.131]. Copyright (2008), with permission from Elsevier).

An increment in the roughness of the polymer surface caused by a chemical treatment is another option. These methods are preferred industrially over the plasma processes due to the much lower cost. The chemical treatment changes the surface characteristics (physical and chemical) in order to improve adhesion. In chemical treatment solutions, the adhesion is achieved by increasing the total area of interface between both layers leading to structural changes (by increasing the interface roughness) and interactions between the fluid molecules and the substrate.

Both on industrial and scientific studies polymer surface treatment has been used to promote the polymer receptivity to the ink. The adoption of such a solution, in addition to the inclusion of an extra step in the manufacturing process, increases the time and cost of production. Given the hydrophobicity of the polymers, a surface treatment to improve its adhesion ST and the ink is vital, but more economic solutions are required.

## 2.9. Flexible pressure sensors

Flexible Pressure Sensors (FPS) are transducers that measure pressure distribution on the sensing element, with the particularity of being flexible. These sensors can be configured as an array of sensors elements to force or pressure that are embedded in a substrate constituting a pressure mapping system (FPMS). The force or pressure sensors are connected to electronic circuits responsible for the signal acquisition from the transducers (several times per second) and communication to a device (typically a computer). Specialized software enables reading of data in real time providing 2D or 3D representation of the measured signals. Analysis tools acquire the pressure peak, the center of pressure or force, the output signal with respect to time and various statistical parameters, thus visualizing the magnitude and distribution of forces applied to the pressure mapping systems.

Flexible polymer detection systems provide a better contact area and therefore more accurate readings thanks to its ability to fold/roll compared to traditional hard circuits. In medical applications a wide variety of configurations is needed and therefore it requires the pressure sensors to be flexible (bendable to a few degrees). Also, the sensitive area should be as small as possible. Depending on the spatial resolution required for the intended application, the diameter for the sensitive area of the sensor can range from 1 mm<sup>2</sup> to 1 cm<sup>2</sup> [2.137]. A high precision, reproducibility and selectivity are other essential requirements for the sensors. Flexible sensors have the capacity to follow all the movements, capacity to stretch to some degree (to measure correctly the applied forces) and have low thickness (thick sensors tend to provide erroneous readings [2.137]). FPMS offers the possibility of obtaining pressure readings measured in the contact surface, revealing information which is not readable to the naked eye.

FPMS have gained increasing importance in application areas such as intelligent packaging/security [2.138], wearable applications [2.139], aerospace and automotive engineering [2.140], in biomedical [2.100, 2.141], robotics [2.31, 2.142 - 2.144] and healthcare [2.13 - 2.145].

The types of sensors available to measure pressure or force at the interface between two objects, are divided by the working range and the characteristics: size, shape and construction

materials. Currently, the most used transduction mechanisms for these pressure sensors are piezo-resistive and capacitive. The capacitive sensors are sometimes preferred over piezo-resistive because they have no significant internal wear or breakage under load. Due to the typical low deviation, the frequency which the capacitive sensors must be calibrated is also reduced. Generally, the capacitance changes are in the range of pico-Farads (pF) or even lower values, making it crucial to use a highly sensitive, accurate, and stable [2.137] electronic reading circuit.

Capacitive transduction in flexible pressure sensors is based on the capacitance variation between two parallel plates, assembled on non-conductive flexible material or on an elastomer with high dielectric constant, when a force or pressure is applied. When this pressure is applied, the plates move closer to one another, and the capacitance value between them increases (Figure 2.34).

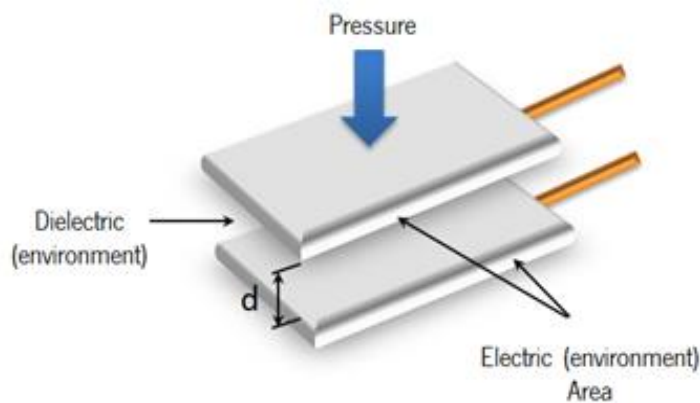


Figure 2.34 - Illustration of a capacitive pressure sensor based on the parallel arrangement.

The capacitance is given by Equation 2.6:

$$C = \frac{\epsilon_0 \epsilon_r A}{d}, \quad \text{Equation 2.6}$$

where,  $\epsilon_0$  is the permittivity of the free space,  $\epsilon_r$  is the relative permittivity of the material between the plates (dielectric),  $A$  is the area of the electrodes, and  $d$  is the distance between electrodes.

## 2.10. IPT of conductive inks on polymeric substrates for FPS manufacturing

Polymeric substrates have been reported in the literature addressing several application areas. In the specific case of capacitive pressure sensor applications, polymeric substrates such as PET [2.33], PI [2.13, 2.31, 2.32, 2.146, 2.147] and PDMS [2.31, 2.33, 2.100, 2.146 - 2.148] are the most commonly used. Lee *et al.* [2.146] developed a flexible capacitive pressure sensor for plantar pressure measurement, using a flexible printed circuit film as a sensor substrate and PDMS as dielectric layer. Cheng *et al.* [2.31, 2.32] developed a tactile sensor with PDMS using a highly reliable capacitive mechanism. Someya *et al.* [2.149, 2.150] developed a flexible pressure sensor matrix with organic field-effect transistors for artificial skin applications. However, the required manufacturing process to fabricate the standard sensor involves multiple factoring steps and the use of several and different material layers (gold, PET, PEN and PDMS), which consequently leads to high time consumption, large material waste and high manufacturing costs. When the goal is large area sensing platforms, manufacture premium prices constitute a problem for a faster wide spread of new products.

Currently, the most commonly used fabrication processes resort to complex processing, e.g., photolithography [2.31, 2.32, 2.146 - 2.148, 2.151], screen-printing [2.10], spin-coating [2.33, 2.148, 2.100]. These techniques involve the use of expensive raw materials, generate large chemical pollutants, waste materials and have resolution limitations. Adding to this, the complexity of the fabrication process most often prevents the process automation to an industrial level.

In recent years, the interest for IPT to sensor fabrication has attracted attention [2.48][2.63] [2.72][2.152] due to the great range of applications and a number of attributes that makes a compelling argument for an interesting alternative to the conventional PE technologies. IPT of an intrinsically conducting polymer [2.50] onto a flexible substrate for humidity and gas sensing applications [2.153, 2.154], respectively, are two of many of the rapidly emerging IPT examples that may be found in the literature. In the field of flexible pressure sensors, the first steps are being taken. Only a few examples of IPT pressure sensors combining IPT polymer conductive ink (PEDOT:PSS and P3HT) or Silver ink [2.139, 2.155], printed on polymer substrate (PET and PI, respectively) have been reported so far in the literature. Someya *et al.* [2.156, 2.157] has developed a flexible pressure sensors using organic field-effect transistor FET active matrices. Polyimide precursors and silver nanoparticles were patterned on a polyimide film by using an ink-jet printing system and cured at 180 °C to form gate dielectric layers and electrodes for organic FETs, respectively. In order to define the device dimensions, epoxy partitions were prepared by a screen printing system. The designed structure presents some complexity and the

fabrication step resorted to different manufacturing technologies. Polyimide precursors and silver nanoparticles were patterned on a polyimide film by using an ink-jet printing system and cured at 180 °C to form gate dielectric layers and electrodes for organic FETs, respectively. In order to define the device dimensions, epoxy partitions were prepared by a screen printing system. Basiricó et al. [2.158] has propose a totally IPT flexible organic field effect transistors (OFETs) assembled on plastic films as sensors for mechanical (pressure and bending) variables using a PEDOT:PSS as electrodes and a P3HT as a semiconductor. The results obtained are promising despite the lower charge carrier mobility measured (believed to be strongly correlated to the final deposited film morphology). An improvement, either by a proper optimization of the polymeric ink and/or by an accurate optimization of deposition parameters is expected.

### **2.11. Summary**

IPT is a new and promising manufacturing direct printing technique. The main advantages of the proposed technology lie in its simplicity and low cost operating principle, on the low cost of raw materials and on the speed of production, overcoming the flaws of traditional patterning technologies. In spite of intensive work performed over the last years, IPT full potential has yet not been achieved. The print quality is directly related to the quality, type and amount of used ink. The inks surface tension and its viscosity determine the speed, the size and stability of the ejected droplet and the form that the droplet reaches the substrate. The available ink formulations are not developed according to the receiving substrate and desired application, but still, the technological viability is evident for low-cost and high-volume manufacturing.

Application of a direct inkjet printing process, maintaining a good dispersion of the available commercial ink, providing a promising adhesion of the ink on the hydrophobic polymeric substrates and achieving the desired performance it's still a subject of study. For the development of an array of flexible pressure sensors to be built from printed electrodes an inkjet printer with DoD system and piezoelectric head was selected in this work. Within the selected printhead characteristic the drop-volume (10 pL), and firing frequency are fixed parameters. The processing variables are: head speed; drop spacing; printhead temperature; height position. Three distinct types of inks were selected according to their content nature (e.g., two different conductive polymer ink, and silver nanoparticles based ink) and potential application use. For the fabrication of the sensor, two polymeric inks, P3HT and PEDOT, and a silver-based ink were tested. The properties and performance of the commercially available conductive inks were evaluated in order to check their potential for untreated substrate surface printing. The

inks were compared based on their adhesion to the substrate and electrical conductivity. Four different flexible polymeric materials, namely, Polyimide (PI), Polyethylene terephthalate (PET), Poly(dimethyl)siloxano (PDMS), and Thermoplastic polyurethane (TPU) were analyzed with particular attention to the substrate mechanical (high elasticity and flexibility), chemical and optical properties (resistant, brightness and transparency, dimensional stability) surface porosity and processing temperatures. Special attention was given to its compatibility and receptivity of the ink. The polymer with the greatest potential (according to above criteria) to be used as substrate, was selected.

**REFERENCES**

- [2.1] M. Li, Y.-T. Li, D.-W. Li, and Y.-T. Long, "Recent developments and applications of screen-printed electrodes in environmental assays--a review.," *Anal. Chim. Acta*, vol. 734, pp. 31–44, Jul. 2012.
- [2.2] J. Li, T. Peng, and C. Fang, "Screen-printable sol – gel ceramic carbon composite pH sensor with a receptor zeolite," vol. 455, pp. 53–60, 2002.
- [2.3] J. P. Metters, R. O. Kadara, and C. E. Banks, "Fabrication of co-planar screen printed microband electrodes.," *Analyst*, vol. 138, no. 9, pp. 2516–21, May 2013.
- [2.4] I. S. Conference, "B. Antunovic, 'The Influence of the Materials and Printing Technologies in Digital Printing of Textiles on Colorimetric Values' in Printing Future Days -International Student Conference," in *3rd International Student Conference on Print and Media Technology*, 2009, p. 389.
- [2.5] J. Gonzalo-Ruiz, M. Asunción Alonso-Lomillo, and F. Javier Muñoz, "Screen-printed biosensors for glucose determination in grape juice.," *Biosens. Bioelectron.*, vol. 22, no. 7, pp. 1517–21, Feb. 2007.
- [2.6] A. Blayo and B. Pineaux, "Printing processes and their potential for RFID printing," *Proceedings of the 2005 joint conference on Smart objects and ambient intelligence: innovative context-aware services: usages and technologies*. ACM, Grenoble, France, pp. 27–30, 2005.
- [2.7] R. Nogueira, J. Octavio, A. Paschoal, M. Linardi, and R. Cuenca, "Catalyst layer optimization by surface tension control during ink formulation of membrane electrode assemblies in proton exchange membrane fuel cell," *J. Power Sources*, vol. 196, pp. 4680–4685, 2011.
- [2.8] "The Gwent Group<[http://www.gwent.org/gem\\_thick\\_film.html](http://www.gwent.org/gem_thick_film.html)>." .
- [2.9] R. Søndergaard, M. Hösel, D. Angmo, T. T. Larsen-Olsen, and F. C. Krebs, "Roll-to-roll fabrication of polymer solar cells," *Denmark, Rev. Elsevier*, vol. 15, pp. 36–49, 2012.
- [2.10] E. Ochoteco, J. Castellanos-Ramos, R. Navas-González, H. Macicior, T. Sikora, and F. Vidal-Verdú, "Tactile sensors based on conductive polymers," *Microsyst. Technol.*, no. 5, pp. 765–776, 2010.
- [2.11] J. A. Sanchez-Duran, J. A. H. Lopez, F. Vidal-Verdu, and E. Ochoteco, "Experimental evaluation of the incidence of tactile sensor limitations on application parameters," in *Progress in Organic Coatings*, 2009, pp. 175–178.
- [2.12] T. V Papakostas, J. Lima, and M. Lowe, "A large area force sensor for smart skin applications," in *Sensors, 2002. Proceedings of IEEE*, 2002, vol. 2, pp. 1620–1624 vol.2.
- [2.13] T. V Papakostas, "Tactile sensor: stretching the limits," in *Intelligent Environments, 2007. IE 07. 3rd IET International Conference on*, 2007, pp. 472–476.

- [2.14] “Dupont Microcircuit materials, ‘New Dimensions in Printed Electronics’, USA, 2010. <[http://www2.dupont.com/MCM/en\\_US/assets/downloads/prodinfo/Printed\\_Electronics.pdf](http://www2.dupont.com/MCM/en_US/assets/downloads/prodinfo/Printed_Electronics.pdf)>,” 2010. .
- [2.15] “Advanced Screen Printing ‘Practical Approaches for Printable & Flexible Electronics’,” *IEEE*, pp. 205–208, 2008.
- [2.16] A. J. Webb, M. Szablewski, D. Bloor, D. Atkinson, A. Graham, P. Laughlin, and D. Lussey, “A multi-component nanocomposite screen-printed ink with non-linear touch sensitive electrical conductivity.,” *Nanotechnology*, vol. 24, no. 16, p. 165501, Apr. 2013.
- [2.17] D. Deganello, J. A. Cherry, D. T. Gethin, and T. C. Claypole, “Patterning of micro-scale conductive networks using reel-to-reel flexographic printing,” *Thin Solid Films*, vol. 518, no. 21, pp. 6113–6116, 2010.
- [2.18] T. Adcock and D. Fenner, “Printed Electronics : Traditional Technology Addresses Today ’ s Smaller , Faster , Lower Cost Requirements,” <<http://www.henkel.com/electronics.htm>>, 2012. .
- [2.19] “Imagem digital<<http://gusgsm.com/flexografia>>.” .
- [2.20] T. Julin, “FLEXO-PRINTED PIEZOELECTRIC PVDF PRESSURE,” Tampere University of Technology, 2011.
- [2.21] E. Hrehorova, A. Pekarovicova, and P. D. Fleming, “Gravure Printability of Conducting Polymer Inks,” *Final Progr. Proc.*, vol. 4, pp. 107–110, 2006.
- [2.22] “<http://www.prismpak.com/Printing-Options-s/103.htm>.”
- [2.23] E. Hrehorova, M. Rebros, A. Pekarovicova, B. Bazuin, A. Ranganathan, S. Garner, G. Merz, J. Tosch, and R. Boudreau, “Gravure Printing of Conductive Inks on Glass Substrates for Applications in Printed Electronics,” *J. Disp. Technol.*, vol. 7, no. 6, pp. 318–324, 2011.
- [2.24] H. Park, H. Kang, Y. Lee, Y. Park, J. Noh, and G. Cho, “Fully roll-to-roll gravure printed rectenna on plastic foils for wireless power transmission at 13.56 MHz.,” *Nanotechnology*, vol. 23, no. 34, p. 344006, Aug. 2012.
- [2.25] N. Flaherty, “Researchers Print Wireless Power Antennas for Less Than A Penny,” *EE Times*, 2012.
- [2.26] C.-X. Liu and J.-W. Choi, “Patterning conductive PDMS nanocomposite in an elastomer using microcontact printing,” *J. Micromechanics Microengineering*, vol. 19, no. 8, p. 085019, Aug. 2009.
- [2.27] Y. Xia and G. M. Whitesides, “Soft Lithography,” *Angew. Chemie Int. Ed.*, vol. 37, no. 5, pp. 550–575, Mar. 1998.
- [2.28] D. Qin, Y. Xia, and G. M. Whitesides, “Soft lithography for micro- and nanoscale patterning.,” *Nat. Protoc.*, vol. 5, no. 3, pp. 491–502, Mar. 2010.



- [2.29] L. Basiricó, “Inkjet Printing of Organic Transistor Devices,” University of Cagliari, 2012.
- [2.30] Miao Liu, “A Customer Programmable Microfluidic System.,” University of Central Florida. Orlando, Florida, 2008.
- [2.31] M. Y. Cheng, C. L. Lin, and Y. J. Yang, “Tactile and shear stress sensing array using capacitive mechanisms with floating electrodes,” in *Micro Electro Mechanical Systems (MEMS), 2010 IEEE 23rd International Conference on*, 2010, pp. 228–231.
- [2.32] M. Y. Cheng, B. T. Liao, X. H. Huang, and Y. J. Yang, “A flexible tactile sensing array based on novel capacitance mechanism,” in *Solid-State Sensors, Actuators and Microsystems Conference, 2009. TRANSDUCERS 2009. International, 2009*, pp. 2182–2185.
- [2.33] C. Hailin and P. Tingrui, “Microfabrication of conductive PDMS on flexible substrates for biomedical applications,” in *Nano/Micro Engineered and Molecular Systems, 2009. NEMS 2009. 4th IEEE International Conference on*, 2009, pp. 731–734.
- [2.34] T. Kawase, T. Shimoda, C. Newsome, H. Sirringhaus, and R. H. Friend, “Thin Solid Films,” *5th Int. Conf. Nano-Molecular Electron.*, vol. 438–439, 2, p. 7,21, 2003.
- [2.35] Y. Neuvo and S. Ylönen, *Bit Bang Rays to the Future*. 2009.
- [2.36] C. B. Arnold and A. Piqué, “Laser Direct-Write Processing,” *MRS Bull.*, vol. 32, no. January, pp. 9–15, 2007.
- [2.37] D. Bauerle, *Laser Processing and Chemistry*. Springer. 2000.
- [2.38] W. Steen and J. Mazumder, *Laser Material Processing*. 2010, p. 558p.
- [2.39] “University of southampton-Optoelectronics Research Centre <<http://www.orc.soton.ac.uk/lift.html>>.”
- [2.40] M. Colina, P. Serra, J. M. Fernández-Pradas, L. Sevilla, and J. L. Morenza, “DNA deposition through laser induced forward transfer.,” *Biosens. Bioelectron.*, vol. 20, no. 8, pp. 1638–42, Feb. 2005.
- [2.41] W. Nam, J. I. Mitchell, C. Tansarawiput, M. Qi, and X. Xu, “Laser direct writing of silicon field effect transistor sensors,” *Appl. Phys. Lett.*, vol. 102, no. 9, p. 093504, 2013.
- [2.42] “Optomec -Production Grade #D Printers <<http://www.optomec.com>>.”
- [2.43] V. Zöllmer, M. Müller, M. Renn, M. Busse, I. Wirth, D. Godlinski, and M. Kardos, “Printing with aerosols,” *Eur. Coatings J.*, vol. 49, no. 511, p. 46, 2006.
- [2.44] J. Perelaer, U. S. Schubert, and F. Jena, “Inkjet Printing and Alternative Sintering of Narrow Conductive Tracks on Flexible Substrates for Plastic Electronic Applications,” in *Radio Frequency Identification Fundamentals and Applications, Design Methods and Solutions*, no. February, C. Turcu, Ed. Croatia: InTech, 2010, pp. 265–286.

- [2.45] K. K. B. Hon, L. Li, and I. M. Hutchings, "Direct writing technology—Advances and developments," *CIRP Ann. - Manuf. Technol.*, vol. 57, no. 2, pp. 601–620, Jan. 2008.
- [2.46] M. Nir, D. Zamir, I. Haymov, L. Ben-Asher, O. Cohen, B. Faulkner, and F. de la Vega, "Electrically conductive inks for inkjet printing. In: Magdassi S, Ed. The chemistry of inkjet inks.," World Scie., New Jersey-London-Singapore, 2010, pp. 225–54.
- [2.47] B. J. de Gans, P. C. Duineveld, and U. S. Schubert, "Inkjet Printing of Polymers: State of the Art and Future Developments," *Adv. Mater.*, vol. 16, no. 3, pp. 203–213, 2004.
- [2.48] F. V. López, A. Diez, and A. Odriozola, "Inkjet Printing of Conductive and Resistive Coatings," *Int. Polym. Process.*, vol. 22, no. 1, pp. 27–32, 2007.
- [2.49] B. Andò and S. Baglio, "Inkjet-Printed Sensors: A Useful Approach for Low Cost, Rapid Prototyping," no. October, pp. 36–40, 2011.
- [2.50] M. V. Kulkarni, S. K. Apte, S. D. Naik, J. D. Ambekar, and B. B. Kale, "Ink-jet printed conducting polyaniline based flexible humidity sensor," *Sensors Actuators B Chem.*, vol. 178, pp. 140–143, Mar. 2013.
- [2.51] W. Thompson, "The Siphon, recorder 1858 (UK Patent 2147/1867).," 1858.
- [2.52] J. A. F. Plateau, "On the recent theories of the constitution of jets of liquid issuing from circular orifices," *Philosophical Magazine*, vol. 12, p. 286, 1856.
- [2.53] T. Young, "An Essay on the Cohesion of Fluids," *Philos. Trans. R. Soc. London*, vol. 95, pp. 65–87, 1805.
- [2.54] P.-S. de Laplace, "Sur l'action capillaire. In Mécanique Céleste: Supplément au Livre X. (Courcier, Paris, 1805)," pp. 349–498.
- [2.55] J. A. Nollet, *Recherches sur les causes particulieres des phénomènes électriques*. Paris: Freres Guerin, 1749.
- [2.56] H. P. Le, "Progress and Trends in Ink-jet Printing Technology," *Oregon J. Imaging Sci. Technol.*, vol. 42, 1998.
- [2.57] H. Wijshoff, "Structure- and fluid-dynamics in piezo inkjet printheads. Netherlands; Océ Technologies B.V.," 2008.
- [2.58] P. Calvert, "Inkjet Printing for Materials and Devices," *Chem. Mater.*, vol. 13, no. 10, pp. 3299–3305, Oct. 2001.
- [2.59] A. Kamyshny, J. Steinke, and S. Magdassi, "Metal-based Inkjet Inks for Printed Electronics," *Open Appl. Phys. J.*, vol. 4, pp. 19–36, 2011.
- [2.60] H. Al-chami, "Inkjet Printing of Transducers," University of British Columbia, 2010.
- [2.61] R. M. Meixner, D. Cibis, K. Krueger, and H. Goebel, "Characterization of polymer inks for drop-on-demand printing systems," *Microsyst. Technol.*, vol. 14, no. 8, pp. 1137–1142, May 2008.

- [2.62] L. Basiricò, P. Cosseddu, B. Fraboni, and A. Bonfiglio, “Inkjet printing of transparent, flexible, organic transistors,” *Thin Solid Films*, vol. 520, no. 4, pp. 1291–1294, Dec. 2011.
- [2.63] C. Griggs, J. Sumerel, and D. Ph, “Opportunities for Inkjet Printing in Industrial Applications,” *Industrial + Specialty Printing* <<http://www.industrial-printing.net>>, no. C, 1899.
- [2.64] P. CALVERT, Y. YOSHIOKA, and G. JABBOUR, “INKJET PRINTING FOR BIOMIMETIC AND BIOMEDICAL MATERIALS,” in *Learning from Nature How to Design New Implantable Biomaterials*, Academic Publishers, 2004, pp. 169–180.
- [2.65] A. Hudd, “Inkjet Printing Technologies. In: Magdassi S., Ed. The Chemistry of Inkjet Inks.,” New Jersey-London\_Singapore :World Scientific, 2010, pp. 3–18.
- [2.66] H. Ujiie, “Digital Printing of Textiles.” Woodhead Publishing.
- [2.67] “<https://www.google.com/patents/US6509917>.” .
- [2.68] L. Smith, A. Söderbärg, and U. Björkengren, “Continuous ink-jet print head utilizing silicon micromachined nozzles,” *Sensors Actuators A Phys.*, vol. 43, no. 1–3, pp. 311–316, 1994.
- [2.69] M. Junfeng, M. R. Lovell, and M. H. Mickle, “Formulation and processing of novel conductive solution inks in continuous inkjet printing of 3-D electric circuits,” *Electron. Packag. Manuf. IEEE Trans.*, vol. 28, no. 3, pp. 265–273, 2005.
- [2.70] V. Marinov, “Direct-write technologies for rapid prototyping applications: sensors, electronics, and integrated power sources by A. Piqué and D. B. Chrisey (eds.), Academic Press, New York, 2002, ISBN 0-12-174231-8, 726pp,” *Int. J. Adapt. Control Signal Process.*, vol. 19, no. 9, pp. 741–743, 2005.
- [2.71] V. Cabbill, “Introduction to Digital Printing Technology. Graphic Artists,” *Pre-Press Pers.*, 1998.
- [2.72] K. E. Paul, W. S. Wong, S. E. Ready, and R. a. Street, “Additive jet printing of polymer thin-film transistors,” *Appl. Phys. Lett.*, vol. 83, no. 10, p. 2070, 2003.
- [2.73] B. Hadimioglu, S. A. Elrod, D. L. Steinmetz, M. Lim, J. C. Zesch, B. T. Khuri-Yakub, E. G. Rawson, and C. F. Quate, “ACOUSTIC INK PRINTING,” in *IEEE. ULTRASONICS SYMPOSIUM*, 1992, pp. 929–936.
- [2.74] B. C. Menzel, A. Bibl, and P. H. Spectra, “MEMS Solutions for Precision Micro-Fluidic Dispensing Application.”
- [2.75] C. Burke, “The Inkjet Printhead for Kodak easyshare Aio Printers. Rochester, Kodak, 2007.”
- [2.76] G. H. Mckinley, M. Renardy, and V. Tech, “Wolfgang von Ohnesorge Biography of Wolfgang von Ohnesorge Family background and early years,” 2011, pp. 1–17.

- [2.77] A. L. Yarin, “DROP IMPACT DYNAMICS: Splashing, Spreading, Receding, Bouncing...,” *Annu. Rev. Fluid Mech.*, vol. 38, no. 1, pp. 159–192, Jan. 2006.
- [2.78] J. . Fromm, “Numerical Calculation of the Fluid Dynamics of Drop-on-Demand Jets,” *IBM J. Res. Dev.*, vol. 28, no. 3, pp. 322 – 333, 1984.
- [2.79] N. Reis and B. Derby, “Ink Jet Deposition of Ceramic Suspensions: Modeling and Experiments of Droplet Formation,” in *MRS Proceedings*, 2000.
- [2.80] U. Caglar, “Studies of Inkjet Printing Technology with Focus on Electronic Materials,” Universidade de Tampere, 2009.
- [2.81] N. Reis, C. Ainsley, and B. Derby, “Ink-jet delivery of particle suspensions by piezoelectric droplet ejectors,” *J. Appl. Phys.*, vol. 97, no. 9, p. 094903, 2005.
- [2.82] B. Derby and N. Reis, “Inkjet Printing of Highly Loaded Particulate Suspensions,” in *MRS Bulletin*, 2000, pp. 815–818.
- [2.83] E. I. Haskal, M. Büchel, J. F. Dijkman, P. C. Duineveld, E. A. Maulenkamp, C. A. H. A. Mutsaers, A. A. Sempel, P. Snijder, E. I. Vulto, P. van der Weijer, and S. P. H. M. Winter, “Society for,” in *Proceedings of the 22nd International Display Research Conference*, 2002.
- [2.84] Y. Christanti and L. . Walker, “Effect of fluid relaxation time of dilute polymer solutions on jet breakup due to a forced disturbance,” *J. Rheol. (N. Y. N. Y.)*, vol. 46, no. 3, pp. 733–748, 2002.
- [2.85] R. Rioboo and C. Tropea, “Outcomes from a drop impact on solid surfaces.,” *At. Sprays*, vol. 11:, pp. 155–165, 2001.
- [2.86] R. Rioboo, M. Marengo, and C. Tropea, “Time evolution of liquid drop impact onto solid, dry surfaces,” *Exp. Fluids*, vol. 33, no. 1, pp. 112–124, Jul. 2002.
- [2.87] G. E. Cossali, a. Coghe, and M. Marengo, “The impact of a single drop on a wetted solid surface,” *Exp. Fluids*, vol. 22, no. 6, pp. 463–472, Apr. 1997.
- [2.88] M. Nir, D. Zamir, I. Haymov, L. Ben-Asher, O. Cohen, B. Faulkner, and F. de la Vega, “Electrically conductive inks for inkjet printing.,” in *The chemistry of inkjet inks*, Shlomo Mag., Jerusalem: World Scientific Publishing Co. Pte. Ltd., 2010, pp. 225–254.
- [2.89] D. Kim, S. Jeong, B. K. Park, and J. Moon, “Direct writing of silver conductive patterns: Improvement of film morphology and conductance by controlling solvent compositions,” *Appl. Phys. Lett.*, vol. 89, no. 26, 2006.
- [2.90] L. Huang, Y. Huang, J. Liang, X. Wan, and Y. Chen, “Graphene-based conducting inks for direct inkjet printing of flexible conductive patterns and their applications in electric circuits and chemical sensors,” *Nano Res.*, vol. 4, no. 7, pp. 675–684, Mar. 2011.
- [2.91] M. V. Kulkarni, S. K. Apte, S. D. Naik, J. D. Ambekar, and B. B. Kale, “Ink-jet printed conducting polyaniline based flexible humidity sensor,” *Sensors Actuators B Chem.*, vol. 178, pp. 140–143, Mar. 2013.

- [2.92] A. Määttänen, U. Vanamo, P. Ihalainen, P. Pulkkinen, H. Tenhu, J. Bobacka, and J. Peltonen, “A low-cost paper-based inkjet-printed platform for electrochemical analyses,” *Sensors Actuators B Chem.*, vol. 177, pp. 153–162, Feb. 2013.
- [2.93] Y. Zheng, Z. He, Y. Gao, and J. Liu, “Direct Desktop Printed-Circuits-on-Paper Flexible Electronics,” *Sci. Rep.*, vol. 3, pp. 1–7, May 2013.
- [2.94] P. Morvillo, I. A. Grimaldi, R. Diana, F. Loffredo, and F. Villani, “Study of the microstructure of inkjet-printed P3HT:PCBM blend for photovoltaic applications,” *J. Mater. Sci.*, vol. 48, no. 7, pp. 2920–2927, Oct. 2012.
- [2.95] C.-C. Tseng, Y.-H. Chou, T.-W. Hsieh, M.-W. Wang, Y.-Y. Shu, and M.-D. Ger, “Interdigitated electrode fabricated by integration of ink-jet printing with electroless plating and its application in gas sensor,” *Colloids Surfaces A Physicochem. Eng. Asp.*, vol. 402, pp. 45–52, May 2012.
- [2.96] U. S. Bhansali, M. a. Khan, and H. N. Alshareef, “Organic ferroelectric memory devices with inkjet-printed polymer electrodes on flexible substrates,” *Microelectron. Eng.*, vol. 105, pp. 68–73, May 2013.
- [2.97] S. B. Fuller, E. J. Wilhelm, and J. M. Jacobson, “Ink-jet printed nanoparticle microelectromechanical systems,” *J. Microelectromechanical Syst.*, vol. 11, no. 1, pp. 54–60, 2002.
- [2.98] D. Zhai, T. Zhang, J. Guo, X. Fang, and J. Wei, “Water-based ultraviolet curable conductive inkjet ink containing silver nano-colloids for flexible electronics,” *Colloids Surfaces A Physicochem. Eng. Asp.*, vol. 424, pp. 1–9, May 2013.
- [2.99] T. Sekitani, Y. Noguchi, U. Zschieschang, H. Klauk, and T. Someya, “Organic transistors manufactured using inkjet technology with subfemtoliter accuracy,” *Proc. Natl. Acad. Sci. USA*, vol. 105 no. 13, pp. 4976–4980, 2008.
- [2.100] C.-C. Chiang, C.-C. K. Lin, and M.-S. Ju, “An implantable capacitive pressure sensor for biomedical applications,” *Sensors Actuators A Phys.*, vol. 134, no. 2, pp. 382–388, 2007.
- [2.101] B. J. Kang, C. K. Lee, and J. H. Oh, “All-inkjet-printed electrical components and circuit fabrication on a plastic substrate,” *Microelectron. Eng.*, vol. 97, no. 4023, pp. 251–254, Sep. 2012.
- [2.102] F. Molina-Lopez, D. Briand, and N. F. de Rooij, “All additive inkjet printed humidity sensors on plastic substrate,” *Sensors Actuators B Chem.*, vol. 166–167, pp. 212–222, May 2012.
- [2.103] U. Caglar, K. Kaija, and P. Mansikkamaki, “Analysis of Mechanical Performance of Silver Inkjet-Printed Structures,” in *2nd IEEE International Nanoelectronics Conference (INEC 2008)*, 2008, pp. 851–856.
- [2.104] M. Suzuki, T. Takahashi, and S. Aoyagi, “Flexible Tactile Sensor Using Polyurethane Thin Film,” pp. 315–324, 2012.

- [2.105]K. Haffarzadeh and H. Zervos, “Conductive Ink Markets 2012-2018 Silver & Copper Inks & Pastes and Beyond,” 2012.
- [2.106]S. S. Azim, A. Satheesh, K. K. Ramu, S. Ramu, and G. Venkatachari, “Studies on graphite based conductive paint coatings,” *Prog. Org. Coatings*, vol. 55, no. 1, pp. 1–4, 2006.
- [2.107]C.-T. Lin, C.-H. Hsu, C.-H. Lee, and W.-J. Wu, “Inkjet-Printed Organic Field-Effect Transistor by Using Composite Semiconductor Material of Carbon Nanoparticles and Poly(3-Hexylthiophene),” *J. Nanotechnol.*, vol. 2011, pp. 1–7, 2011.
- [2.108]C.-T. Lin, C.-H. Hsu, I.-R. Chen, C.-H. Lee, and W.-J. Wu, “Enhancement of carrier mobility in all-inkjet-printed organic thin-film transistors using a blend of poly(3-hexylthiophene) and carbon nanoparticles,” *Thin Solid Films*, vol. 519, no. 22, pp. 8008–8012, Sep. 2011.
- [2.109]S. P. Speakman, G. G. Rozenberg, K. J. Clay, W. I. Milne, A. Ille, I. A. Gardner, E. Bresler, and J. H. G. Steinke, “High performance organic semiconducting thin films : Ink jet printed polythiophene [ rr -P3HT ],” *Org. Electron.*, vol. 2, pp. 65–73, 2001.
- [2.110]Y. Yang, W. Guo, Y. Zhang, Y. Ding, X. Wang, and Z. L. Wang, “Piezotronic effect on the output voltage of P3HT/ZnO micro/nanowire heterojunction solar cells.,” *Nano Lett.*, vol. 11, no. 11, pp. 4812–7, Nov. 2011.
- [2.111]J. B. Chang, “Functionalized polythiophene thin-film transistors for low-cost gas sensor arrays,” University of California at Berkeley, 2006.
- [2.112]F. Xue, Z. Liu, Y. Su, and K. Varahramyan, “Inkjet printed silver source/drain electrodes for low-cost polymer thin film transistors,” *Microelectron. Eng.*, vol. 83, no. 2, pp. 298–302, Feb. 2006.
- [2.113]B. J. Perelaer, A. W. M. de Laat, C. E. Hendriks, and U. S. Schubert, “Inkjet-printed silver tracks: low temperature curing and thermal stability investigation,” *J. Mater. Chem.*, vol. 18, no. 27, p. 3209, 2008.
- [2.114]C. M. Hong, M. Inc., and S. Wagner, “Inkjet printed copper source/drain metallization for amorphous silicon thin-film transistors,” *Electron Device Lett. IEEE*, vol. 21, no. 8, pp. 384 – 386, 2002.
- [2.115]S. Molesa, D. R. Redinger, D. C. Huang, and V. Subramanian, “High-quality inkjet-printed multilevel interconnects and inductive components on plastic for ultra-low-cost RFID applications.,” vol. 769, pp. 1–6, 2003.
- [2.116]J. . Szczech, D. R. Megaridis, Constantine M. Gamota, and J. Zhang, “Fine-line conductor manufacturing using drop-on demand PZT printing technology,” *Electron. Packag. Manuf. IEEE Trans.*, vol. 25, no. 1, pp. 26 – 33, 2002.
- [2.117]Y. Yoshioka and G. E. Jabbour, “Desktop inkjet printer as a tool to print conducting polymers,” *Synth. Met.*, vol. 156, no. 11–13, pp. 779–783, Jun. 2006.

- [2.118]E. Menard, M. a Meitl, Y. Sun, J.-U. Park, D. J.-L. Shir, Y.-S. Nam, S. Jeon, and J. a Rogers, "Micro- and nanopatterning techniques for organic electronic and optoelectronic systems.," *Chem. Rev.*, vol. 107, no. 4, pp. 1117–60, Apr. 2007.
- [2.119]V. Subramanian, "Printed electronics. In: Magdassi S, Ed. The Chemistry of inkjet inks," W. S. 2010, Ed. New-Jersey-London-Singapore, 2010, pp. 283–317.
- [2.120]Y.-Y. Noh, N. Zhao, M. Caironi, and H. Sirringhaus, "Downscaling of self-aligned, all-printed polymer thin-film transistors.," *Nat. Nanotechnol.*, vol. 2, no. 12, pp. 784–9, Dec. 2007.
- [2.121]C. W. Sele, T. von Werne, R. H. Friend, and H. Sirringhaus, "Lithography-Free, Self-Aligned Inkjet Printing with Sub-Hundred-Nanometer Resolution," *Adv. Mater.*, vol. 17, no. 8, pp. 997–1001, Apr. 2005.
- [2.122]Dongjo Kim, Sunho Jeong, Bong Kyun Park, and J. Moon, "Direct writing of silver conductive patterns-Improvement of film morphology and conductance by controlling solvent compositions," *Appl. Phys. Lett.* 89, 264101, vol. 89, no. 26, 2006.
- [2.123]K.-Y. Shin, S.-H. Lee, and J. H. Oh, "Solvent and substrate effects on inkjet-printed dots and lines of silver nanoparticle colloids," *J. Micromechanics Microengineering*, vol. 21, no. 4, p. 45012, 2011.
- [2.124]L. Boon Keng and H. Xiao, "Transient contact angle of evaporating inkjet droplet on trans-parent polymer substrate," in *Electronics Packaging Technology Conference (EPTC), 2010 12th*, 2010, pp. 240–245.
- [2.125]S. Siau, A. Vervaet, A. Van Calster, I. Swennen, and E. Schacht, "Influence of wet chemical treatments on the evolution of epoxy polymer layer surface roughness for use as a build-up layer," *Appl. Surf. Sci.*, vol. 237, no. 1–4, pp. 457–462, Oct. 2004.
- [2.126]B. Arkles, Y. Pan, and Y. M. Kim, "The Role of Polarity in the Structure of Silanes Employed in Surface Modification," vol. 5, 2009.
- [2.127]M. Strobel, V. Jones, C. S. Lyons, M. Ulsh, M. J. Kushner, R. Dorai, and M. C. Branch, "A Comparison of Corona-Treated and Flame-Treated Polypropylene Films," *Plasma Polym.*, vol. 8, no. 1, pp. 61–95, 2003.
- [2.128]L.-A. O'Hare, S. Leadley, and B. Parbhoo, "Surface physicochemistry of corona-discharge-treated polypropylene film," *Surf. Interface Anal.*, vol. 33, no. 4, pp. 335–342, 2002.
- [2.129]P. W. Rose and H. W. Chang, "Gas Plasma Treatment of Spectra Fiber.," *SAMPE Q.*, vol. 19, 1988.
- [2.130]R. Morent, N. de Geyter, and C. Leys, "Effects of operating parameters on plasma-induced PET surface treatment," *Nucl. Instruments Methods Phys. Res. Sect. B*, vol. 266, pp. 3081–3085., 2008.
- [2.131]J. S. EOM and S. H. KIM, "Plasma surface treatment of polyimide for adhesive Cu/80Ni20Cr/PI flexible copper clad laminate," *Elsevier, Amsterdam, PAYS-BAS (1967) (Revue)*, vol. 516, no. 14, pp. 4530–4534, 2008.

- [2.132]J. Lai, B. Sunderland, J. Xue, S. Yan, W. Zhao, M. Folkard, B. D. Michael, and Y. Wang, "Study on hydrophilicity of polymer surfaces improved by plasma treatment," *Appl. Surf. Sci.*, vol. 252, no. 10, pp. 3375–3379, 2006.
- [2.133]L. P. Yeo, B. K. Lok, Q. M. P. Nguyen, C. W. Lu, and Y. C. Lam, "Selective surface modification of PET substrate for inkjet printing," *Int. J. Adv. Manuf. Technol.*, vol. 71, no. 9–12, pp. 1749–1755, Jan. 2014.
- [2.134]S. Mohanty, C. Ylitalo, and O. S. Woo, "Modeling Drop Shape on Contaminated Surfaces or Surfaces with Physical Structures," *Langmuir*, vol. 20, no. 6, pp. 2277–2281, 2004.
- [2.135]J. C. McDonald and G. M. Whitesides, "Poly(dimethylsiloxane) as a Material for Fabricating Microfluidic Devices," *Acc. Chem. Res.*, vol. 35, no. 7, pp. 491–499, 2002.
- [2.136]S. LEE, J. WU, and T. LIN, "The properties of copper deposited on polyimide by nitrogen and oxygen plasma pre-treatment.," *Appl. Surf. Sci.*, vol. 252, pp. 1818–1825, 2005.
- [2.137]C. M. A. Ashruf, "Thin flexible pressure sensors," *Sens. Rev.*, vol. 22, no. 4, pp. 322–327, 2002.
- [2.138]K. Lawrie, A. Mills, and D. Hazafy, "Simple inkjet-printed, UV-activated oxygen indicator," *Sensors Actuators B Chem.*, vol. 176, pp. 1154–1159, Jan. 2013.
- [2.139]Y. Li, R. Torah, S. Beeby, and J. Tudor, "An all-inkjet printed flexible capacitor for wearable applications," 2012, no. April, pp. 25–28.
- [2.140]"Pressure Profile Systems, Inc.," [Online]. Available: <http://www.pressureprofile.com/index-automotive1.php>.
- [2.141]K. S. Jansson, M. P. Michalski, S. D. Smith, R. F. LaPrade, and C. a Wijdicks, "Tekscan pressure sensor output changes in the presence of liquid exposure.," *J. Biomech.*, vol. 46, no. 3, pp. 612–4, Feb. 2013.
- [2.142]E. Pritchard, M. Mahfouz, B. Evans, S. Eliza, and M. Haider, "Flexible capacitive sensors for high resolution pressure measurement," in *Sensors, 2008 IEEE*, 2008, pp. 1484–1487.
- [2.143]E. M. Petriu, W. S. McMath, S. S. K. Yeung, and N. Trif, "Active Tactile perception of objects surface geometric profiles," *IEEE Trans. Instrum. Meas. - IEEE TRANS INSTRUM MEAS*, vol. 41, pp. 87–92, 1992.
- [2.144]S. K. Yeung, E. M. Petriu, W. S. McMath, and D. C. Petriu, "High sampling resolution tactile sensor for object recognition.," *IEEE Trans. Instrum. Meas. - IEEE TRANS INSTRUM MEAS*, vol. 43, pp. 277–282, 1994.
- [2.145]"Xsensor Technology Corporation." [Online]. Available: <http://www.xsensor.com>.



- [2.146]K. F. Lei, K.-F. Lee, and M.-Y. Lee, “Development of a flexible PDMS capacitive pressure sensor for plantar pressure measurement,” *Microelectron. Eng.*, vol. 99, pp. 1–5, Nov. 2012.
- [2.147]X. Riedl, C. Bolzmacher, R. Wagner, and K. Bauer, “A Novel PDMS Based Capacitive Pressure Sensor,” pp. 2255–2258, 2010.
- [2.148]H. Li, C. X. Luo, H. Ji, Q. Ouyang, and Y. Chen, “Micro-pressure sensor made of conductive PDMS for microfluidic applications,” *Microelectron. Eng.*, vol. 87, no. 5–8, pp. 1266–1269, 2010.
- [2.149]T. Someya, T. Sekitani, S. Iba, Y. Kato, and H. Kawaguchi, “A large-area, flexible pressure sensor matrix with organic field-effect transistors for artificial skin applications,” in *National Academy of Sciences of the USA. Advance Online Publication*, 2004, pp. 101, 27.
- [2.150]T. Someya, Y. Kato, T. Sekitani, S. Iba, Y. Noguchi, Y. Murase, H. Kawaguchi, and T. Sakurai, “Conformable, flexible, large-area networks of pressure and thermal sensors with organic transistor active matrixes,” *Proc. Natl. Acad. Sci. U. S. A.*, vol. 102, no. 35, pp. 12321–5, Aug. 2005.
- [2.151]H. Kim, S. Lee, and K. Yun, “Capacitive tactile sensor array for touch screen application,” *Sensors Actuators A. Phys.*, vol. 165, no. 1, pp. 2–7, 2011.
- [2.152]B. News, ““Scientists use inkjet printing to produce solar cells,”” *BBC News Technology*. [Online]. Available: <http://www.bbc.co.uk/news/technology-13977038>.
- [2.153]U. Altenberend, F. Molina-Lopez, A. Oprea, D. Briand, N. Bârsan, N. F. De Rooij, and U. Weimar, “Towards fully printed capacitive gas sensors on flexible PET substrates based on Ag interdigitated transducers with increased stability,” *Sensors Actuators B Chem.*, vol. 187, pp. 280–287, Oct. 2013.
- [2.154]V. Matic, L. Liedtke, T. Guenther, A. Buelau, A. Ilchmann, J. Keck, B. Polzinger, W. Eberhardt, and H. Kueck, “Inkjet printed differential mode touch and humidity sensors on injection molded polymer packages,” *IEEE SENSORS 2014 Proc.*, pp. 2234–2237, Nov. 2014.
- [2.155]“MICRO PIRANI PRESSURE SENSOR FABRICATED BY INKJET PRINTING OF SILVER NANOPARTICLES,” in *Transducers 2013, Barcelona, SPAIN*, 2013, no. June, pp. 1783–1786.
- [2.156]Y. Noguchi, T. Sekitani, and T. Someya, “Organic-transistor-based flexible pressure sensors using ink-jet-printed electrodes and gate dielectric layers Organic-transistor-based flexible pressure sensors using ink-jet-printed electrodes and gate dielectric layers,” *Appl. Phys. Lett.*, vol. 253507, no. 89, pp. 14–17, 2006.
- [2.157]T. Someya, T. Sakurai, T. Sekitanil, and Y. Noguchil, “Printed Organic Transistors for Large-Area Electronics,” in *IEEE Polytronic 2007 Conference*, 2007, pp. 6–11.
- [2.158]L. Basiricò, P. Cosseddu, A. Bonfiglio, R. Neelgund, and H. W. Tyrer, “Inkjet printed arrays of pressure sensors based on all-organic field effect transistors,” in *32nd Annual*

*International Conference of the IEEE EMBS Buenos Aires, Argentina, 2010, pp. 2111–2114.*



# Chapter 3

## **Materials and Methods**

In this chapter, relevant information regarding material, characteristics of the equipment, the experimental methods, and the characterizations techniques used is presented. In a first section, some fundamentals on the main physical and chemical properties of the materials used, and evaluated for the fabrication of the printed patterns, are reported; in a second section, information about the printer employed and material preparation is presented. Finally, the last section reports a brief description of the principal characterization techniques used and experimental conditions. IPT technology requires a fundamental investigation of the properties of inks and of the substrates, the compatibility between them, and exploration of differentiating solutions in order to optimize the fabrication process.



### 3.1. Material selection

Substrate & conductive ink selection methodology for fabrication of flexible sensors involves two important topics: i) Selection of a flexible material with a combination of unique properties (physical, mechanical, chemical) for the fabrication of a flexible support; and ii) Study of different available inks based on the limits imposed by the printing process, resulting on the selection of the appropriated physicochemical (the superficial tension, rate of solvent evaporation and drying the particle size) ink formulation for IPT. This selection also depends on the relation between ink/substrate adhesion, limit of the ink/substrate flexibility, the final electrical properties while meeting the desired mechanical properties without the disruption of the ink.

#### 3.1.1. Substrates

Four different flexible polymeric materials, namely, Polyimide (PI), Polyethylene terephthalate (PET), Poly(dimethyl) siloxano (PDMS), and Thermoplastic polyurethane (TPU) were analyzed with particular attention to the substrate mechanical (high elasticity and flexibility), chemical and optical properties (resistant, brightness and transparency, dimensional stability), surface porosity and processing temperatures. Special attention was given to its compatibility and receptivity of the ink. The polymer with the greatest potential (according to above criteria) to be used as substrate, was selected. Their description and main properties are presented next.

##### 3.1.1.1. Poly (4,4' – oxydiphenylene - pyromellitimide)

Kapton, a poly(4,4'-oxydiphenylene-pyromellitimide) (Figure 3.1) is the brand name of a polyimide (PI) film, first developed by DuPont [3.1]. The film of PI HN from Kapton® has a unique combination of properties that make them ideal for applications in many different industries. It has excellent physical and mechanical properties and electrical insulation at high temperatures (1012  $\Omega$ .cm at 200°C). It also has a good dimensional stability and chemical resistance.

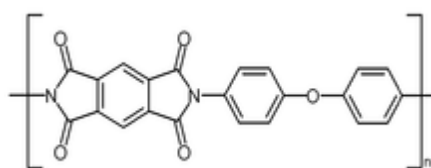


Figure 3.1 - Structure of poly-oxydiphenylene-pyromellitimide, "Kapton".

### 3.1.1.2. Polyethylene terephthalate (PET)

PET is the most used thermoplastic polyester and consists of polymerized units of monomer ethylene terephthalate, with repeating  $C_{10}H_8O_4$  units (Figure 3.2). In particular, the very thin PET film Mylar® from DuPont is a biaxially oriented thermoplastic with a unique combination of physical, chemical, thermal, optical (resistant, bright and transparent, dimensional stability, chemical resistance) and mechanical properties ideal for a wide range of electronic applications.

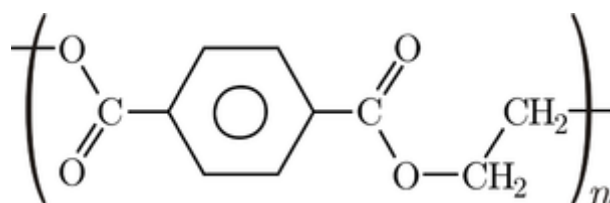


Figure 3.2 - Chemical structure of polyethylene terephthalate.

### 3.1.1.3. Polydimethylsiloxane (PDMS)

Consists of fully dimethyl siloxane polymers containing repeating units of the formula  $(CH_3)_2SiO$  [3.2] (Figure 3.3). PDMS Sylgard® 184 from Dow Corning® is an elastomer resulting from the combination of a siloxane base and a curing agent. It is a homogeneous material, isotropic, biocompatible, optically transparent, chemically inert, thermally stable, with high elasticity and high flexibility [3.2]. The PDMS also allows great freedom of design, which combined with the excellent properties, makes it a widely used polymer.

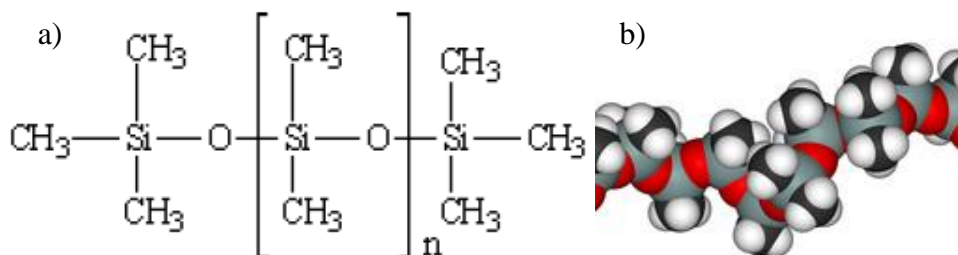


Figure 3.3 - The chemical formula of Polydimethylsiloxane. a) Chemical structure combining both organic and inorganic groups; b) Structural representation of the shielding of the main chain (Si-O groups) by the methyl groups.

### 3.1.1.4. Thermoplastic polyurethane (TPU)

Thermoplastic polyurethane elastomer belongs to the class of thermoplastic elastomers that combine the mechanical properties of vulcanized rubber with the processability of thermoplastic polymers. They can be repeatedly melted and processed due to the absence of the chemical networks that normally exist in rubber. TPU are linear segmented block copolymers having hard segments (HS) and soft segments (SS) [3.3]. TPU are based on the exothermic reaction of polyisocyanates with polyol molecules, containing hydroxyl groups. Relatively few basic isocyanates and a range of polyols of different molecular weights and functionalities are used to produce the whole spectrum of polyurethane materials. Two types of diisocyanates are employed in polyurethane preparations, aromatic and aliphatic ones. Most commonly used chemical structures are the aromatic diisocyanates; toluene diisocyanate (TDI), and 4,4'-diphenylmethane diisocyanate (MDI) (Figure 3.4) [3.3].

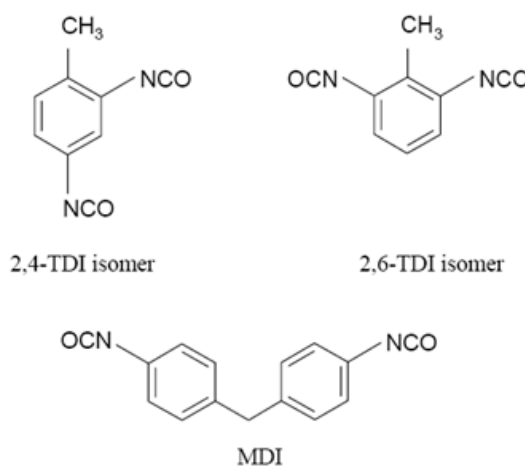


Figure 3.4 - Molecular structures of most common industrial isocyanates.

TPU are usually made from pure MDI which is reacted with a substantially linear polyether or polyester diol [3.3] and with a chain-extending diol of a low molecular weight, such as 1,4-butanediol, (BDO) in either a one-step or a two-step reaction process [3.4]. The polyester diols are usually the condensation products of adipic acid and one or more simple aliphatic diols ranging from ethylene glycol to 1,6-hexanediol. TPU are used in applications where a product requires excellent tear strength, abrasion resistance, flexible fatigue resistance and resistant to radiation exposure. Mechanical properties of the polyester TPU are generally higher ( $E=7.5\text{MPa}$ ). Service temperatures range from  $-50\text{ }^{\circ}\text{C}$  to  $130\text{ }^{\circ}\text{C}$  and all have excellent adhesion properties. These materials generally offer better strength and rigidity properties than conventional thermoset rubbers and their high elasticity confers exceptional dynamic flex properties.



The materials used here are commercial grades available in different physical forms. The main features of each of the materials used are summarized in Table 3.1.

Table 3.1 - Substrates identification their main properties.

Substrate	PI	PET	PDMS	TPU
Supplier	DuPont	DuPont	Dow Corning®	Huntsman
Grade	HN Kapton®	Mylar®	Sylgard® 184	Avalon 65AB
Physical form	Film	Film	Base+Cure agent free*	Processed film
Thickness (mm)	0.025	0.023		1.5
Density (g/cm <sup>3</sup> )	1.42	1.39	1.03	1.18
Vol.Res.(Ω.cm)	1.5x10 <sup>17</sup>	1.0x10 <sup>19</sup>	1.2x10 <sup>14</sup>	3.0x10 <sup>14</sup>
Modulus (MPa)	2.5x10 <sup>3</sup>	4.1x10 <sup>3</sup>	1	7
WorkTemp.(°C)	Up to 400	-50 -150	-45- 200	130

\*Two colorless components in the liquid state (a silicone base and a curing agent) with free final dimensions and geometry.

Note: The tabulated values are from the producer data sheet (Appendix A.5).

### 3.1.2. Micro and nanosized particles

Ink/substrate adhesion is a key performance characteristic for the fabrication of IPT systems. During this work, some methods using nanosized particles were employed in order to improve the ink/substrate adhesion.

#### 3.1.2.1. Clay Particles (CP)

Nanofil 5 (distearyl-dimethyl-ammonium ion exchanged bentonite), supplied by Süd-Chemie AG- Germany, is an organic modified nanodispersed layered silicate with platelet structure [3.5]. Table 3.2 lists the main properties of Nanofil 5.

Table 3.2 - CP detail technical specification.

Name	Average diameter of the primary particle size [μm]	Average Agglomeration size [μm]	Platelet thickness [nm]	Bulk density [gl <sup>-1</sup> ]	Specific weight [g.cm <sup>-3</sup> ]	Intercalation
Nanofil 5	8	≈8-12	1	150	≈ 1.8	Distearyldimethyl-ammonium chloride

Note: The tabulated values are from the producer data sheet (Appendix A.6)

### 3.1.2.2. Silica Particles (SP)

SP consists on spherical particles having an average diameter of the primary particle size of 12 nm and an average agglomeration size of 100 nm [3.6]. Chemically speaking, they are made of silicon and oxygen atoms. AEROSIL 200 is highly dispersed, hydrophilic fumed silica that is produced by high-temperature hydrolysis of silicon tetrachloride in an oxyhydrogen gas flame. The primary particles are spherical and free of pores. AEROSIL 200 consists entirely of amorphous silicon dioxide. It starts to sinter and turn into glass above 1200°C. Crystallization only occurs after thermal treatment. One gram of AEROSIL 200 contains approximately 1 mol of silanol groups [3.7]. Table 3.3 lists main properties of AEROSIL 200.

Table 3.3 –Silica (SiO<sub>2</sub>) particles detail technical specification.

Name	Average diameter of the primary particle size [nm]	Average Agglomeration* size [nm]	Specific surface area [m <sup>2</sup> g <sup>-1</sup> ]	Tapped density [g l <sup>-1</sup> ]	Behaviour toward water
AEROSIL 200	12	≈100	200 ± 25	≈ 50	Hydrophilic

Note: The tabulated values are from the producer data sheet (Appendix A.6). \*Specific surface according to BET.

### 3.1.3. Conductive inks for IP

Three different inks, P3HT, PEDOT and a silver-based ink have been study elements for sensor fabrication (electrical paths and electrodes). The properties and performance of the commercially available conductive inks were evaluated in order to check their potential for untreated substrate surface printing. The inks were compared based on their adhesion to the substrate and electrical conductivity. Their main properties and experimental evaluation using IPT are discussed in Chapter 4, Chapter 5 and Chapter 6.

#### 3.1.3.1. Poly (thiophene-3-[2-(2-methoxyethoxy) ethoxy]-2,5-diyl), sulfonated (P3HT)

Regioregular polythiophene has been widely used in organic electronics. Organic electronics have a tremendous potential for applications in flexible electronics because of its low cost, solubility (thanks to the 3-substituted alkyl-chain in the polythiophene core [3.8]); exceptional spectroscopic and electronic properties, low-temperature process, highly ordered structure, self-assembled, semi-crystallinity in its solid states [3.9], regioregular compatibility to large-area fabrications and industrial mass production technologies. In the

chemical structure of the regioregular polythiophenes, the backbone of the polymer is formed by thiophene rings and a chemical side-chain group can be attached on each thiophene ring along the polymer (Figure 3.5). An end-group or a secondary copolymer chain can be added to each end of the polythiophene.

All these features make polymer semiconductors suitable for several printing technologies, such as, spin coating [3.10, 3.11], screen printing [3.12] and inkjet printing [3.8, 3.13 - 3.15]. For this reason, various organic electronic devices have been proposed and implemented: thin film diode [3.13]; organic thin film transistors (OTFTs) [3.11, 3.14, 3.15], photodiodes, Organic Field-Effect Transistor (OFETs) [3.16, 3.17], solar cells [3.18, 3.19], organic light-emitting diodes (OLEDs) [3.10], and sensors [3.8, 3.20].

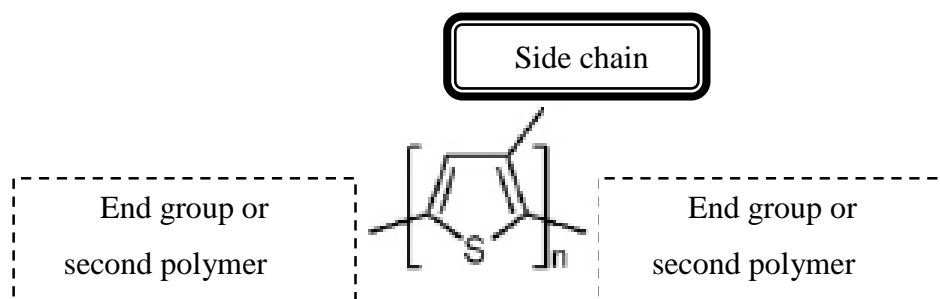


Figure 3.5 - Schematic diagram of a regioregular polythiophene based polymers.

The regioselective polymerization techniques used for synthesizing P3HTs allow fine control of the absolute structure of the polymeric materials, which support a variety of functionalities, thus enabling a greatly expanded platform for polymer design [3.21]. For example, Plextronics has developed an inherently doped sulfonated solution of Poly(thiophene-3-[2-(2-methoxyethoxy) ethoxy]-2,5-diyl) [3.22].

The electronic grade Plexcore<sup>®</sup> OC RG-1100, Sulfonated polythiophene ink from Plextronics (Aldrich Prod. No. 699799) (Figure 3.6) is the trade name of the P3HT (2% in 1,2-propanediol/isopropanol/water, 3:2:1) organic semiconductor polymer based ink used for the experimental activities presented in this thesis. Plexcore<sup>®</sup> OC RG-1100 belongs to a set of organic conductive inks originally designed for spin-coating applications, but may also be applied to the ink printing technologies. The inks are ideal for integration into various printed electronic applications. The physical properties of the ink are reported in Table 3.4.

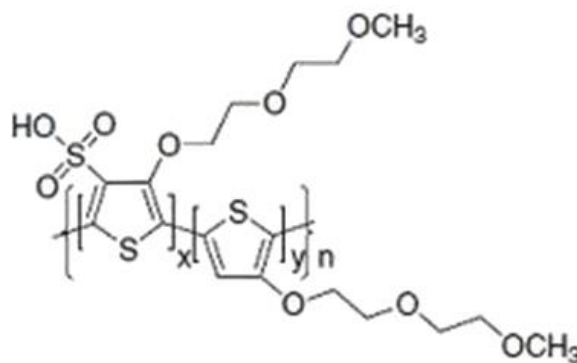


Figure 3.6- Poly(thiophene-3-[2-(2-methoxyethoxy)ethoxy]-2,5-diyl), sulfonated solution 2% in ethylene glycol monobutyl ether/water, 3:2, electronic grade [3.22].

Plexcore<sup>®</sup> OC offers [3.22]:

- A reduced acidity, preventing anode degradation and ensuring improved device lifetime;
- Tunable properties such as work function, resistivity, surface energy, and viscosity, enabling researchers to optimize device performance;
- Compatible with multiple solvent systems and aqueous-based solutions, facilitating a variety of processing techniques.

Table 3.4 - Plexcore<sup>®</sup> physical properties [3.23] .

Conductor component	Conductive Polymer
Solid content (wt%)	2
Concentration	0.8% in H <sub>2</sub> O
Electrical Resistivity (Ω.m)	0.25-2.5
pH	2.2-2.8
Viscosity (mPa.s)	7-13
Surface tension (mN/m)	35 - 38

Note: The tabulated values are from the producer data sheet (Appendix A.7).

### 3.1.3.2. Poly (3,4-ethylenedioxythiophene) - poly (styrenesulfonate) (PEDOT:PSS)

Conductive polymers are classified into two different categories: extrinsically or intrinsically conductive polymers. The extrinsically conductive polymers normally involve a blend of conductive and nonconductive polymers, as well as metallic particles suspended in the polymer matrix [3.24]. Essentially, they consist of highly conductive additives incorporated into polymer compounds, meaning that they are extrinsically enhanced to be conductive.

Relatively to the intrinsically conductive polymers, also called “synthetic metals”, they consist of a network of alternating single and double carbon bonds. It’s this alternation of bonds that produces conjugated  $\pi$ -bonds, resulting in a intrinsically conductive material [3.25].

The molecule at hand, PEDOT, was developed during the second half of the 1980s, by scientists at the Bayer AG research laboratories in Germany [3.25, 3.26] as an intrinsically conductive polymer. PEDOT, a polythiophene derivative based on 3,4-ethylenedioxythiophene or EDOT monomer, is composed of an aromatic thiophene ring with the carbon atoms in position 3 and 4, connected by means of a double ethereal bridge (Figure 3.7). Table 3.5 presents the main physical properties of the monomer.

Table 3.5 - Main physical Properties of EDOT monomer [3.25].

Viscosity (20°C)	11 mPa.s
Density (20°C)	1.34 g/cm <sup>3</sup>
Melting point	10.5°C
Boiling point (1013 mbar)	225°C
Vapor pressure (20°C)	0.05 mbar
Vapor pressure (90°C)	10 mbar
Solubility in water (20°C)	2.1 g/l
Flash point	104°C
Ignition temperature	360°C

PEDOT stands out for its high transparency [3.27, 3.28] when deposited in thin, oxidized films, high conductivity [3.27, 3.28], very high chemical stability in the oxidized state, processability and simplicity of production [3.26]. Although, it was found to be an insoluble and infusible polymer, limiting its employment in printed electronic techniques. This problem was subsequently surrounded through the use of a water-soluble polyelectrolyte, poly(styrene sulfonic acid) (PSS), as the charge-balancing dopant during polymerization to yield PEDOT:PSS [3.26, 3.29]. This combination resulted in a water-soluble polyelectrolyte system with high conductivity (ca. 10 S/cm), high visible light transmissivity, and excellent stability [3.26, 3.29]. These unique properties make PEDOT an excellent material for various

applications such as in electrochromics devices [3.30], sensors [3.31 - 3.33], biosensors [3.34, 3.35], actuators [3.36], capacitors [3.36 - 3.38], and photovoltaic cells [3.36], etc.

All these features make polymer semiconductors suitable for several printing technologies, such as, spin coating [3.39, 3.40], screen printing [3.41] and inkjet printing [3.34, 3.42].

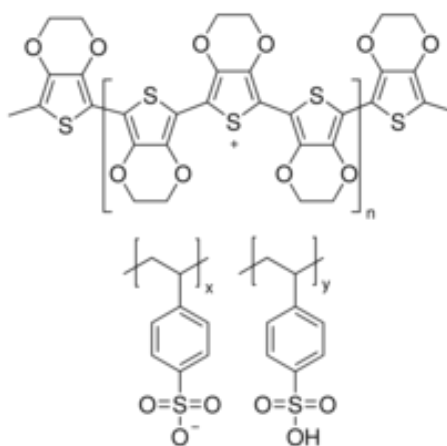


Figure 3.7 - Molecular structure of Poly (3,4-ethylenedioxythiophene)-poly (styrenesulfonate) [3.29].

Undoubtedly, PEDOT is the most widely used conductive polymer [3.43]. Chemical variations of PEDOT often appears [3.44], by altering the main chain ring sequence, the nature of the dioxy substituents, or the counterionic component [3.43, 3.44]. This new polymers appear due to the need of higher conductivity, transparency, lower surface energy, higher viscosity, and/or greater chemical homogeneity [3.45].

The Orgacon™ IJ-1005 from Agfa is the trade name of the used PEDOT:PSS. Is a water (0.8% in H<sub>2</sub>O) based electronic conductive polymer dispersion PEDOT/PSS. This ink has been specifically prepared for Inkjet Printing, has already been used in printing equipment type Microdrop, Dimatix and Galaxy and is recommended for rigid or flexible substrates. Its appearance in terms of color is dark blue to very dark blue, and in terms of form is liquid. The physical properties of the ink are reported in Table 3.6.

Table 3.6 – Orgacon™ Physical Properties [3.29, 3.46].

Contains	1-5% Ethanol, 5-10% Diethylene glycol
Conductor component	PEDOT
Solid content (wt%)	0.8
Concentration	0.8% in H <sub>2</sub> O
Electrical Resistivity(Ω.m)	1x10 <sup>-6</sup>
pH	1.5-2.5
Particle size (nm)	25 - 35
Viscosity (mPa.s)	7-12
Surface tension (mN/m)	31 - 34

Note: The tabulated values are from the producer data sheet (Appendix A.7).

### 3.1.3.3. Silver-based ink

Among metallic inks, silver (Ag) nanoparticles hold the highest electrical conductivity and are resistant to oxidation [3.47], but are, also, one of the most expensive. The silver nanoparticles can be produced through chemical reduction, electrochemical, laser ablation or photochemical processes. The chemical reduction process consists in the reduction of silver nitrate or silver acetate in presence of a stabilizer. The Ag nanoparticles are stabilized in ink solutions by organic ligand shells, i.e., the nanoparticles are encapsulated with an organic material, called a capping agent, to form a uniform and stable dispersion, preventing particles agglomeration. This capping agent can be removed after printing through curing or sintered to allow physical contact between nanoparticles, forming continuous connectivity, i.e., a percolation path for electrical conductivity. Thus, sintering consist on welding the particles to each other below their melting point [3.48], by exposure of the printed pattern to: laser sintering [3.17], microwave radiation [3.49], by applying an electrical voltage [3.50], by a chemical agent at room temperature (RT sintering) [3.51], or, the most conventional approach, by heating (thermal sintering) [3.47, 3.52, 3.53]. In the case of thermal sintering, the temperature (typically between 100 to 400° C) where the nanoparticles form the percolation path must be below the softening temperature of the polymeric substrate. The presence of a few nanometers organic layer between the silver particles is enough to block the movement of electrons from one particle to the other [3.47], thus reducing electrical conductivity. If this happens, the removal of this organic layer is required at high temperatures. For this reason, the sintering temperature of the nanoparticle based

inks has extreme importance in plastic electronic applications where materials such as polyethylene terephthalate [3.52, 3.53] and polycarbonate [3.53] are widely used but, have low ( $T_g$ ) (98 °C and 148 °C respectively).

The lowest resistivity at the lowest temperature is another important property. The conductivity of a printed Ag layer also depends on the shape and size of the Ag nanoparticles. The amount of sintering temperature and time required depends upon how easy the organic encapsulation breaks, particle size and on the thickness of the ink film. The smaller the particle size (2 to 10 nm) the lower the temperature required to sinter the particles, the short is the process and a higher conductivity is achieved. Typically, the nanoparticle loading inks is higher than 20 wt%. All these features make silver based inks suitable for IPT on flexible substrates [3.52, 3.54, 3.55]. Table 3.7 presents silver ink dispensing possibilities and limitations for IPT.

Table 3.7 – Major ink requirements for IPT [3.56].

Percentage of silver filler	40-60%
Viscosity (unheated)	~0.5 to 34 mPa.s
Particle size	< 100 nm
Sintering temperature	130-300 °C
Surface Tension	28.5-34 mN/m
Resistivity	~3 $\mu\Omega$ .cm

The Ag-IJ10 from Applied Nanotech, Inc. is the trade name of the silver based ink is designed for piezoelectric inkjet printing of conductive features on several substrates. This nanoparticle ink can be thermally sintered to high conductivity at low temperature. The nanoparticles do not require high melting temperatures like conventional materials. The silver nanoparticles are stabilized in ink solutions by organic ligand shells, which can be removed after printing through curing or sintered to highly conductive films at low temperatures. Films surface area to volume ratio is very high, the bonds occur with low energy consumption, improving resolution, and with good mechanical properties. The low processing temperatures (100-150°C) enable applications in printed electronics using low cost flexible polymer substrates. The small sizes of the nanoparticles and uniform dispersion in Ag-IJ10 make it suitable for printing using inkjet technologies [3.57]. A less positive



factor for such inks is their tendency to sedimentation in the print heads and the necessity to use dispersants [3.58].

Table 3.8 - Ag-IJ10 silver-based ink.

Typical properties	
Particle Size	3-10 nm
Resistivity	10-50 $\mu\Omega\cdot\text{cm}^*$
Solid Content	45 wt%
Viscosity	4-5 mPa.s**
Surface Tension	28-35 mN/m
Solvent	Organic

\* Dependent on sintering temperature and time- higher temperature and longer sintering time results in lower resistivity and better adhesion to the substrate.

\*\*Measured at 100rpm and 25°C with Brookfield VLDV-II+PRO/ULA viscometer.

Note: The tabulated values are from the producer data sheet (Appendix A.7).

## 3.2. Substrates preparation method

### 3.2.1. PDMS fabrication

The used PDMS included a base polymer (part A) called siloxano oligomer and a curing agent (part B), the siloxane cross-linker. These two parts were mixed together with a proportion of 10 (A):1 (B) weight ratio and placed in a vacuum chamber (at 760 mmHg) to degas the mixture, in order to remove all of the air bubbles [3.59]. Subsequently, the liquid mixture is carefully deposited into a mold of polymethylmethacrylate (PMMA) with a defined geometry and heated in an oven at 80°C for the generation of an elastomeric solid [3.59] (Figure 3.6).

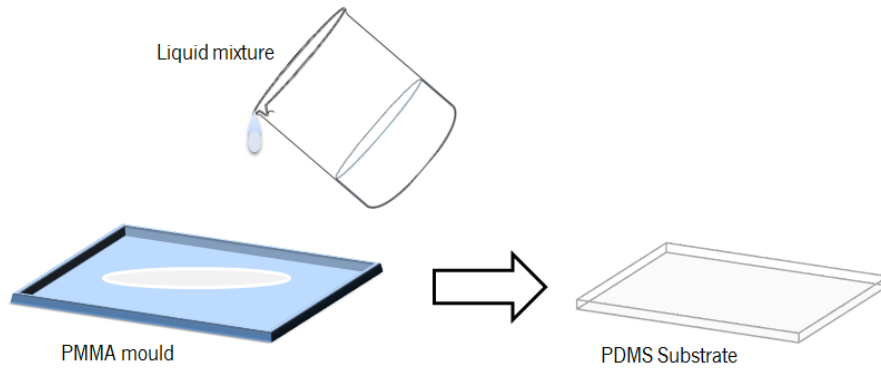


Figure 3.8 - Fabrication process flow for the development of a flexible PDMS substrate.

### 3.2.2. TPU Compression moulding procedure

The TPU pellets were placed on a metallic mold spacer with area 210mm x 125 mm and 1.5mm thick and sandwiched between two stainless steel plates covered with Teflon foil (to facilitate plates removal) at a pressure of 774 MPa for 5 min at 190°C. This time was selected to ensure that the plates would be free of air bubbles and with a uniform 1.5 mm thickness. Afterwards, the plates were quenched in water at room temperature (23°C). All specimens were kept in a controlled temperature room (23°C) for at least 3 weeks before performing any experimental tests according to ASTM 618 – 00 (Figure 3.7).

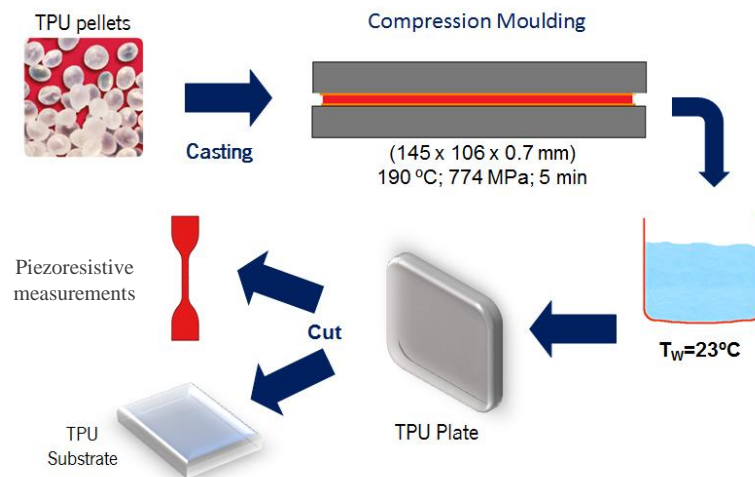


Figure 3.9– Compression moulding procedure for TPU substrates fabrication.

### 3.2.3. Substrate cleaning

Previous cleaning of the substrate is a required step, as this affects the surface wettability (see example in Figure 3.10). The objective of cleaning and deionization is to eliminate surface contaminants such as silicone mold release, dirt, dust, grease, oils, and fingerprints and inhibit new particles to stick on the surface of the substrate. The substrates are cleaned, before placing them on the printer motion system plate, using the following procedure: baths in acetone, isopropyl alcohol, then washed with deionized water and finally dried under dried nitrogen flow. Thinner substrates are more flexible than the thicker ones, which constitute an advantage in some applications where a higher flexibility is required, but they are more difficult to hand during the cleaning process. In the case of PET and PI, it was difficult to avoid scratches and pleats on the substrate surface caused by handling and cleaning of the substrate (e.g., the use of tweezers and blown dried nitrogen flow). The substrate was fixed to the plate motion system of the printer using adhesive tape. However, the use of tape originates the contamination of the substrate with glue at its edge corners.

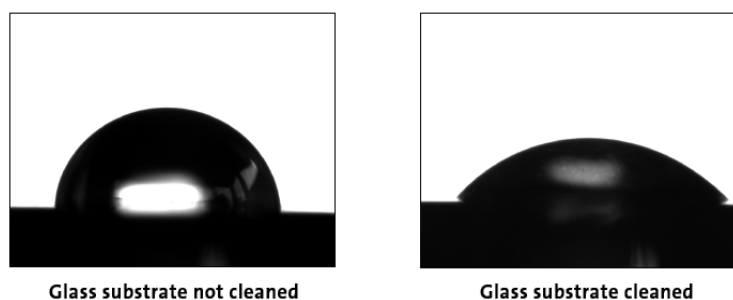


Figure 3.10 - Cleaning effect on the wettability. Cleaning the glass substrates results in a better wetting with polar liquids [3.60].

### 3.3. Technology – Xennia Carnelian

The Inkjet printer used for the fabrication of the flexible substrates reported in the experimental work is the Carnelian Printer, a piezoelectric Drop-on-Demand (DoD) printer provided by Xennia Technology Ltd. The Xennia Carnelian inkjet incorporates industrial printhead technology in a flexible, high precision printer, printhead evaluation and accurate fluid dispensing [3.61]. In Figure 3.11 shows an image of the printer used while in Figure 3.12 a block diagram of the printer system is presented.



Figure 3.11 – Xennia Carnelian Inkjet Printer.

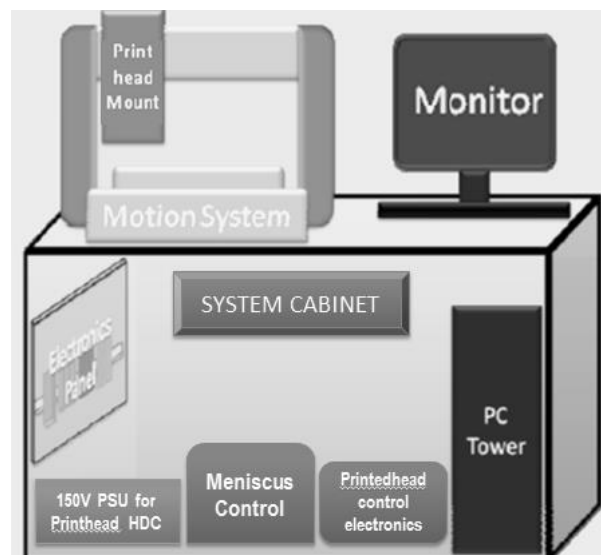


Figure 3.12 - Schematic of the main components of the Carnelian system [3.62].

The printer includes three main parts:

- **Printhead Mount:** Is the physical support for the ink supply syringe, a secondary syringe on the outlet port of the printhead for annual purge and wipe, the rotating printhead, an ink temperature control and the inspection camera which allows viewing with more detail the final printed substrate. This part represents the core of the printer.
- **Motion System:** Consists on a plate functioning as a base for substrates with a printable area of 229 mm x 305 mm (9 in x 12 in). Adhesive tape was used for holding the substrate on the plate during printing instead of a vacuum system. We found this method more effective since vacuum would cause the bending of the film in the case of very thin films.

Adhesive tape fits to all type of substrates: thin, thick, smooth, raised or flat. The plate has no temperature control of the substrate.

- **System cabinet:** Here, all the electrical components and the controlling systems are placed: The printhead and Dimatix Meniscus Control. The printing system is controlled by a METEOR software provides by Xennia Technology Ltd.

Some of main functionalities and potentialities of this printer are briefly described in the following subsections and can be easily found in the printer manual [3.62], others arose from direct experiences.

### 3.3.1. Printhead Mount

The Printhead Mount is the heart of the printing system (Figure 3.13). It supports the printhead, the inspection and alignment camera system (is a very useful tool because allows the nozzle alignment and also an evaluation of the achieved printed pattern quality).

To achieve reliable printing a suitable negative pressure needs to be applied to the ink system to enable ink to feed the print head without flooding the face plate. The required negative pressure is determined by the height of the meniscus level in the feed syringe, relative to the print head nozzle plate. The system has been set up for ink to be at the level marked on the syringe holder [3.62].

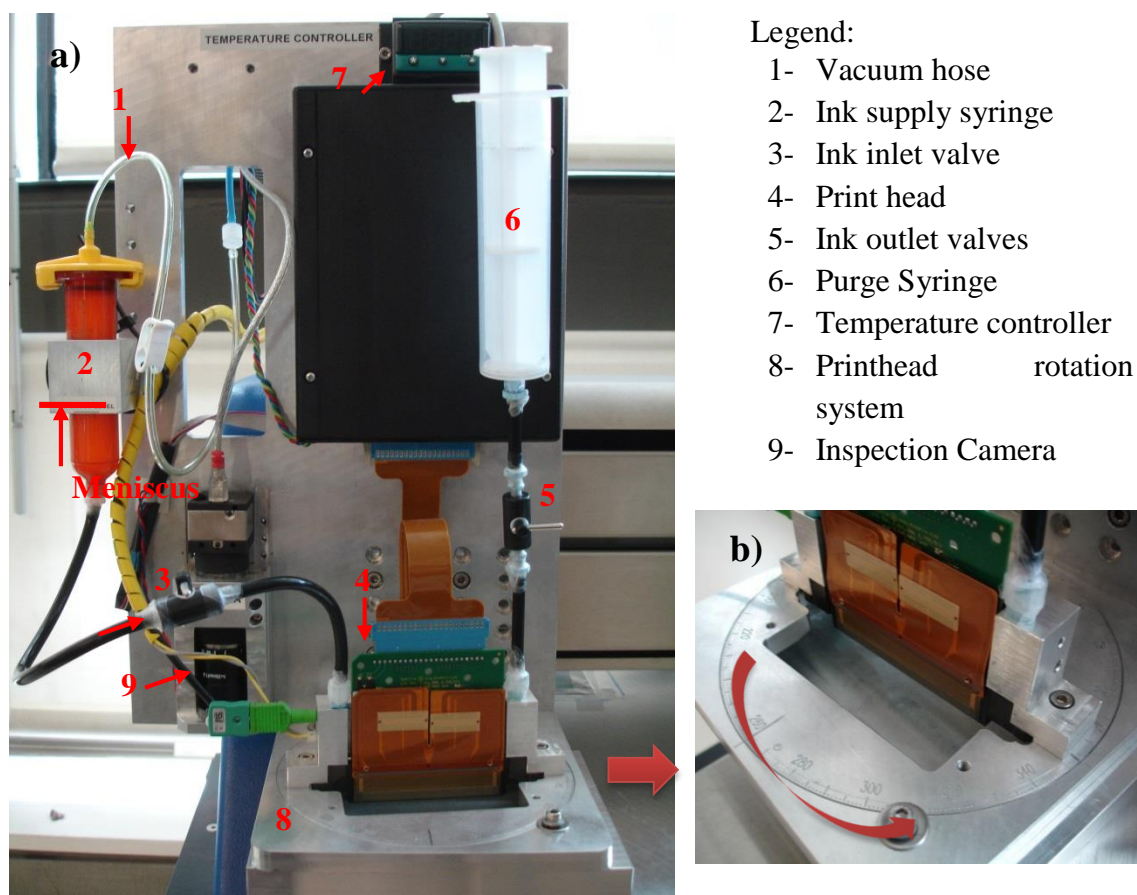


Figure 3.13 – Printhead mount: a) printhead; b) detail figure of the printhead rotation system.

In order to unclog nozzles some cleaning actions may be required which may cause material and time waste otherwise permanent damage of nozzles may occur.

The printhead Sapphire QS-256/10 AAA from Dimatix (Figure 3.14) features 256 independent channels (with two PZT modules, one driving the odd nozzles, one for the even nozzles), arranged in a single row of nozzles at 100 dots-per-inch spacing. It was programmed to eject 10 pL normal drops size [3.63]. This is done at a nominal 8 m/s drop velocity when jetting fluids in the 10 to 14 mPa.s range [3.63]. Print head operational temperature can be up to 90° C, and has an integral temperature sensor [3.63]. However, the operational temperature parameter must be defined according to the properties of operated ink, since higher temperatures may case solvents (incorporated in the ink) volatilization and nozzle clogging. For this reason, room temperature is recommended.

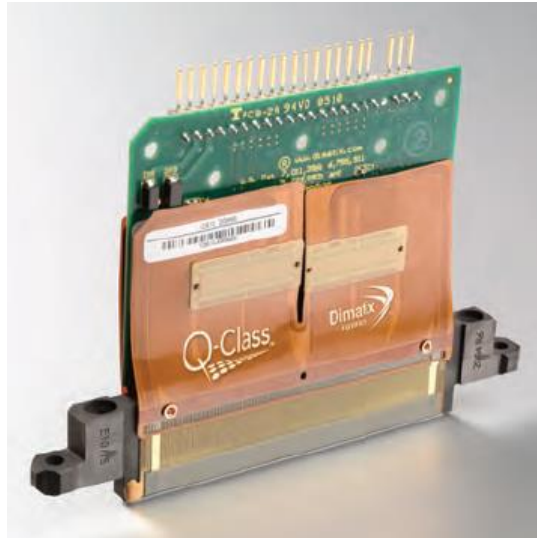


Figure 3.14 - Digital foto of a Dimatix Sapphire QS-256/10 AAA print head [3.63].

The printhead supports UV-curable [3.63], either IMS (e.g., industrial mentholated spirits/ethanol) or Isopropyl alcohol (IPA) cleaning solvents and aqueous-based inks [3.63]. The recommend producer fluid physical parameters for best printing performance are the following:

- Fluid Viscosity range: 8 – 20 mPa.s (10 - 14 mPa.s recommend);
- Surface Tension: 30 -35 mN/m;
- Ultrasonic agitation
- Filtering the fluids with a 0.45  $\mu\text{m}$  pore size Glass microfiber filter before filing the ink supply syringe.

### 3.3.2. Motion System

The machining head can move along 3 axes. These axes are defined as the X, Y and Z axes. The print head movements are: Vertically direction (Z-Axis) moving toward the substrate, thereby defining the distance between the nozzle and the substrate (depending on the substrate thickness); Horizontal direction (X-Axis) above the substrate; the platen motion is responsible for the horizontal shift (Y-Axis). Summarizing, the printing process results in horizontal scans of the print head, and subsequent horizontal shifts of the substrate as schematized in Figure 3.15.

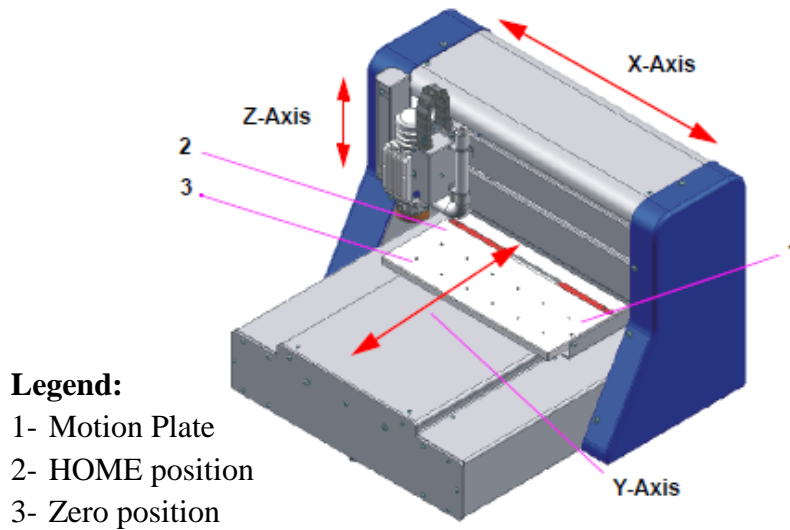


Figure 3.15 - Print head and motion plate direction movements [3.62].

The quality of ink deposition on the substrate strongly depends on this printing procedure and on the chosen printing parameters.

### 3.3.3. Drop-spacing and resolution

The drop -spacing is the distance between the center of two subsequent drops, both in X and in Y direction. The drop size and line width are dependent on the interaction between the ink-jetted droplets and the used substrate. The used model of piezo-driven jetting from Dimatix has a nominal volume value (the effective volume of a jetted drop depends on the used firing voltage and the jetting frequency). A 40  $\mu\text{m}$  size drop can be produced on a polymeric substrate with a 10 pL drop.

According to an encoder signal and to the image resolution corresponding to the drop spacing settled, the printer manages the ejection of a drop from the nozzle in the X direction. In the Y direction, the distance between two subsequent drop is determined by the printhead rotation angle (see Table 3.9), but also by the distance between two subsequent nozzles in the nozzle plate, in this case, 254  $\mu\text{m}$  [0.010 in.] (100 DPI). This is set manually through the rotation of the printhead system which allows the operator to rotate the printhead at the desired angle by means of a graduated scale (Figure 3.13). As the mounting angle decreases, the print resolution increases (Figure 3.16).



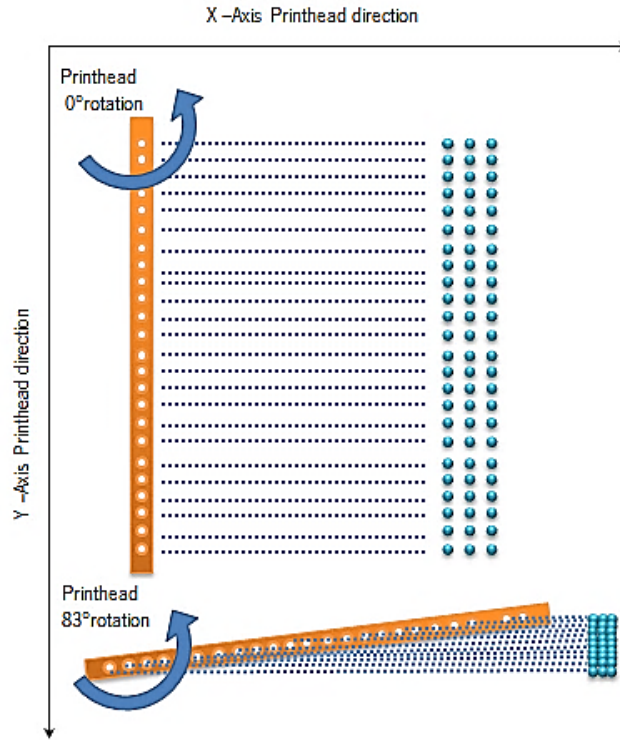


Figure 3.16 – Pattern resolution in X-Axis and Y- Axis.

The mathematical equation used to determine the printhead rotation according to desired drop spacing and resolution is reported in Equation 3.1.

$$Drop - spacing (\mu m) = \frac{25400}{resolution(dpi)} \quad \text{Equation 3.1}$$

Table 3.9 – Resolution setting according to rotation angle.

Rotation	Drop Spacing	Resolution (DPI)
0°	254 $\mu m$	100 DPI
70°	84.67 $\mu m$	300 DPI
80°	42.33 $\mu m$	600 DPI
83°	28.22 $\mu m$	900DPI

### 3.3.4. Jet controls

In order to achieve the best print quality it is crucial to control and monitor the ink droplets ejection and nozzle maintenance. The control and monitoring operations are supported by software (METEOR software and Xenjet 4000 application) of the printer:

- **Firing Voltage:** It corresponds to the stress wave (electric current) applied to deform the piezoelectric crystal for the droplet's ejection. The firing voltage affects drop-shape. For different inks, different firing voltages are required in order to reach the optimal jetting performances. A high firing voltage results in a short time of flight and produces compact drops but with a long tail (These are highly undesirable for the quality of the print). The droplets are required to have a certain speed, typically several m/s. Conversely, reducing the firing voltage the tails length are reduced, also reducing the drop velocity avoiding droplets scattering at the impact with the substrate (thereafter, obtaining a better print quality). However, a low firing voltage may misdirect the jets which increase dot position errors and the probability of clogging nozzles during printing.

- **Jetting Frequency:** It's the frequency of ejected droplets from the nozzles. It affects the print velocity, the print precision and it is strictly dependent on the particular pattern as described afterwards.

- **Number of Jetting Nozzles:** As the jetting frequency, also the choice of the number of nozzles used is strictly dependent on the specific pattern and precision required.

The maintenance is supported by hardware along with cleaning foam swabs, which has the function of soaking up the excess ink that may be present in proximity of the nozzles. This operation is important to perform before pattern printing in order to prevent puddle of ink around the nozzles that may cause misdirection of the ink and, consequently, the presence of satellite-drops around the printed pattern. Important operations are:

- **Purging:** After every ink supply syringe filling and before initial use of the printhead (mandatory to achieve satisfactory printing performances), purging is a required procedure to push air out of the ink path (air bubble may cause nozzle clogging). The ink is pushed out of the nozzles (pump button with air pressure). During printing, also during resting time, purging cycles are recommended in order to clear the nozzles and to keep ink path surfaces wet.

- **Meniscus Control:** In order to prevent the ink from flowing out a low vacuum is applied to the ink supply syringe.

Checking the filling of all nozzles just before printing is an important step to guaranty a good jetting performance.

### **3.3.5. Check of the printed pattern quality**

The inspection camera is a tool consisting of a camera, mounted on the printhead mount, able to frame selected parts of the substrate (7.680 mm x 5.760 mm with a resolution of 768 x 576 Pixel (0.44 Megapixel)). The operator can select three different light operation modes: bright field, dark field; adjustable by the operator. The camera is used after printing, to check the print quality. This inspection camera, do not allows the measurement of the size of single drops or printed lines.

The camera does not have enough resolution to evaluate each drop individually, so the evaluation of print quality was assessed according to the quality of the printed pattern.

### **3.3.6. Printhead working principle**

The printhead goal is to fire billions of drops. Before a drop is fired, a lot of proceeding steps must take place. Before each printing and during printing when required the following cycle procedure was conducted in order to effectively fill the printhead:

- Fill the ink supply syringe fully with ink;
- Open both the inlet and outlet valves and draw through about half the volume of ink in the ink supply syringe into the 2<sup>nd</sup> (clear) syringe;
- Close the inlet and outlet valve and refill the 1<sup>st</sup> syringe;
- Close the 1<sup>st</sup> syringe and press the purge button to purge the printhead;
- Close the inlet valve and open the outlet valve and push ink back into the printhead to purge in the reverse direction;
- Close the outlet valve and open the inlet valve and purge the system again.

This process is repeated (of forward and reverse purging) while taking care not to, at any time, apply suction to the printhead from the 2<sup>nd</sup> syringe until the printhead is full. Also ensure that the 1st syringe is kept filled up with ink.

A study for identification and control of the best inkjet printing parameters for the conductive ink was conducted. For enhanced printing resolution and uniformity of the printed layer it is necessary to know the effect of all the process variables (e.g., DPI, printing temperature, number of printed layers, etc.), on different substrates and how they affect the print quality and the possible causes of surface defects. For improved performance it is necessary to investigate the relationships between the fabrication variables and the final achieved properties, e.g., the electrical conductivity.

Figure 3.17 shows a flowchart of the steps followed for definition of the inkjet printing parameters of the conductive ink. This optimization process consists of multiple iteration steps of experiments to reach an optimized parameter. The timeline for the three different conductive inks is not linear, so, the printing process had to be optimized for all the inks separately.

Printing was undertaken in a non-standard laboratory environment with no temperature or humidity control, non-particle filtered enclosure in order to determine the extent to which the devices could be fabricated in a basic processing facility

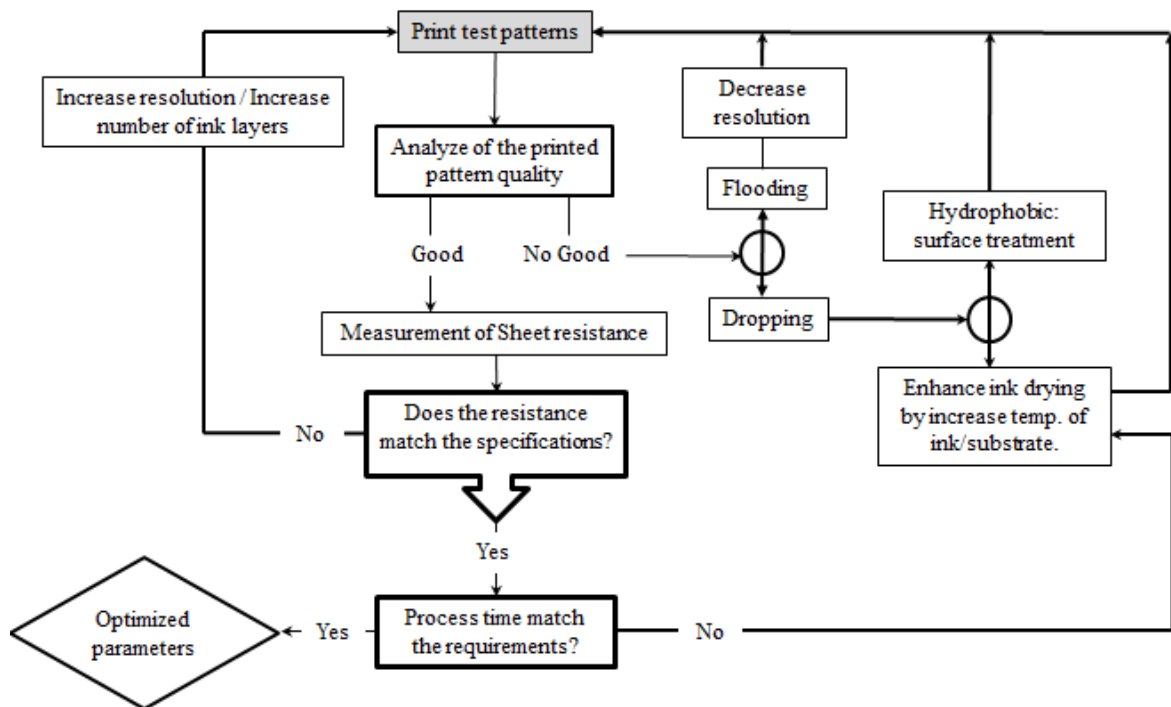


Figure 3.17 – Steps for testing the inkjet printing parameters.

### 3.4. Characterization Techniques

In the IP technique, a previous evaluation of the material fundamental properties as well as the compatibility between them for printing quality control it is very important, in order to meet the desired final properties. A proper characterization of the substrate enables an evaluation of which envelop and dependent variables can dictated the possible limitations of the process in order to anticipate problems and causes of defects and to optimize the manufacturing process A previous study of the surface properties of the substrate can predict its compatibility with the ink and ensure that during the jet printing, the ink absorption occurs

through the substrate. A proper characterization of the materials, before and after superficial treatments (when needed), to assess whether or not improvements were obtained is necessary.

### 3.4.1. Critical Substrate Superficial Tension (ST) measurements

The characterization of substrates is the starting point for the study in question, because knowing the properties of these materials can help to predicted and/or understand the causes or effects of the final properties. Substrate superficial tension (ST) was measured by contact angle (using a Contact angle measurement equipment Dataphysics OCA15 plus to evaluate the substrate with more receptive of the inks.

There is no direct method for measuring the surface energy of a solid substrate. Instead, what is determined is the critical surface tension. The standard procedure for determination of the critical surface tension of a solid substrate consists on the measurement the contact angles between the substrate and a number of test liquids with various surface tensions (known from literature, see Table 3.10), at room temperature, while the values of the contact angle are directly measured.

A preliminary cleaning of the surface using isopropyl alcohol at room temperature must be initially performed and subsequently washed with distilled water and dried with dried nitrogen. A drop of the pattern liquid with 5  $\mu\text{L}$  of volume is released on the substrate by a micro syringe by "sensile drop" method and the contact angle between the substrates and the liquid is measured. This procedure is repeated with the 3 different liquids (water, ethylene glycol and diiodmethane). The measured results are plotted: contact angle vs. surface tension coordinates. The procedure was repeated six times for each sample.

Table 3.10 - Surface energy components for the test liquids (Source: DataPhysics Instruments GmbH, Filderstadt manual).

Liquid	$\gamma$ (mN/m)
Water	72.8
Ethylene glycol	48.0
Diiodmethane	50.8

### **3.4.2. Thermalgravimetric analysis (TGA) of the conductive inks**

Investigation of the thermal properties of the inks was performed. The mass loss as a function of the temperature was measured using TGA TA Instruments Q500 under nitrogen atmosphere. The sample was heated from 20 °C to 700 °C with a heating rate of 10 °C.min<sup>-1</sup>.

### **3.4.3. Detail characterization of the surface treated substrates and of the printed ink**

The effect of the surface treatment of the substrates was analyzed by adhesion tests, SEM and AFM. Defect-free printing pattern is obviously a prerequisite for any ideal printed substrate. After IP a detailed characterization of the printed substrate, in terms of structure and behavior was performed for pattern resolution, and electromechanical evaluation of the obtained transducing properties. Adhesion between the substrate and ink was evaluated. The thickness of the printed ink will be characterized by SEM and AFM. In order to evaluate the printing quality of the printing method, samples were characterized in terms of microscopic analyze to evaluate patterning quality (measurement of the width and spacing of the embedded lines).

#### **3.4.3.1. Adhesion tests**

The evaluation of the adhesion between substrate-ink was performed through the Cross-cut Tape test (according to ASTM D3359). Classified as a destructive tests, as the name suggests, allows analyzing compliance systems through damage [3.64]. For these adhesion tests an appropriate tool for this purpose was used (See Appendix A.8). The multi-blades, consisting of six cutting edges, are made of hardened steel alloy and are designed to maintain the tip of the sharp cutting zone, this way reducing the frequency of replacement of the blade. With the cutting tool shown in Figure 3.18, cuts were made on the longitudinal and transverse of the sample.



Figure 3.18 - The TQC Cross Cut Adhesion Test KIT (CC2000) at the left and Cutting tool accessory at right.

The cuts should be perpendicular to each other. Subsequently an adhesive tape was applied over this zone and pulled from the surface. The qualitative evaluation (according to ASTM - D3359, method B) of the results was performed through the visual analysis of remaining ink on the substrate, on a scale of evaluation of adhesion (see Comparison Chart in Appendix A.8). If the level of adhesion between the substrate and the coating is low, delamination occurs [3.64].

The adhesion of the ink film to the substrate is rated on a 0 - 5 scale as follows:

**Classification:**

- 0 - None of the square is removed.
- 1 - Small squares of the coating are removed at the intersections, less than 5% the area is affected.
- 2 - Small squares of the coating are removed at the intersections, the area affected is 5-15% of the coating.
- 3 - Small squares of the coating are removed at the intersections, the area affected is 15-35% of the coating.
- 4 - Small squares of the coating are removed at the intersections, the area affected is 35-65% of the coating.
- 5- For removal of the coating more than 65% of the area.

There's no defined value for the velocity of removal of the adhesive tape test adhesion ink-substrate, being the test carried out by a quick and manual tug of the tape. One drawback of this test, is dealing with different materials, such as substrate, the coating and tape, which influence the result [3.64].

### 3.4.3.2. Optical Microscopy (OM)

Optical Microscopy was used for a qualitative evaluation of the samples tested in order to assess the adhesion between substrate-ink. For this purpose, micrographs of remaining ink on the substrate and of the removed ink on the adhesion tape were acquired using an Olympus stereomicroscope with a Leica DFC 280 Digital Camera and analyzed with the LAS V4.4 Image Analysis software.

### 3.4.3.3. Scanning electron microscopy (SEM)

Microscopy investigation was used to check the level of dispersion of micro/nanosized particles on the polymeric substrate. Defect-free printing pattern is obviously a prerequisite for any ideal printed substrate. SEM was also performed to determine inks thickness of the printed layers. The final thickness of a printed conductive trace is determined by the printing conditions, the ink properties, and the amount of ink solution being transferred to the printing surface, the ink and surface affinities. The coating thickness and uniform distribution of the ink can affect the properties of the printed layer as well as on end-user application of the printed pattern. Thereby, evaluation of the surface morphology and pattern thicknesses of the printed ink indicates if an improvement and optimization of the fabrication step is required. It also helps to stabilize the thickness of embedded patterns and achieve precise and complex electrical design. In order to evaluate the patterning quality of the printing method, SEM was used to characterize the uniformity measuring the size and average spacing of the printed pattern in terms of inks spreading precision. The SEM micrographs were acquired with a NanoSEM - FEI Nova 200 (FEG/SEM). In order to avoid electrostatic charging the fractured (in liquid nitrogen) surface specimens were previous coated with Gold - Palladium (Au-Pd).

### 3.4.3.4. Atomic force microscopy (AFM)

In contrast to SEM, the AFM allows to analyze the sample surface in the three directions x, y and z. A Multimode da Digital Instruments AFM was used to analyze the topography of the samples in tapping mode. The 1x1cm samples were recorded in ambient conditions (RH=50%, T=23°C) using a rectangular cantilever (Model: TESP da Bruker) and a scan speed of 1,001 Hz. The AFM images were processed with Nanoscope III software and the roughness parameters root mean square (RMS) roughness and mean roughness (Ra) were calculated from the measured topography. The resolution in the x and y directions topographical was 10x10µm.



The Ra is the arithmetic average of the absolute values of the roughness profile ordinates [3.65, 3.66]. Ra is one of the most effective surface roughness measures and is commonly adopted in general engineering practice. It gives a good general description of the height variations in the surface:

$$R_a = \frac{1}{L} \int_0^L |Z(x)| dx \quad \text{Equation 3.2}$$

Where Z(X) is the profile height function and L is the evaluation length.

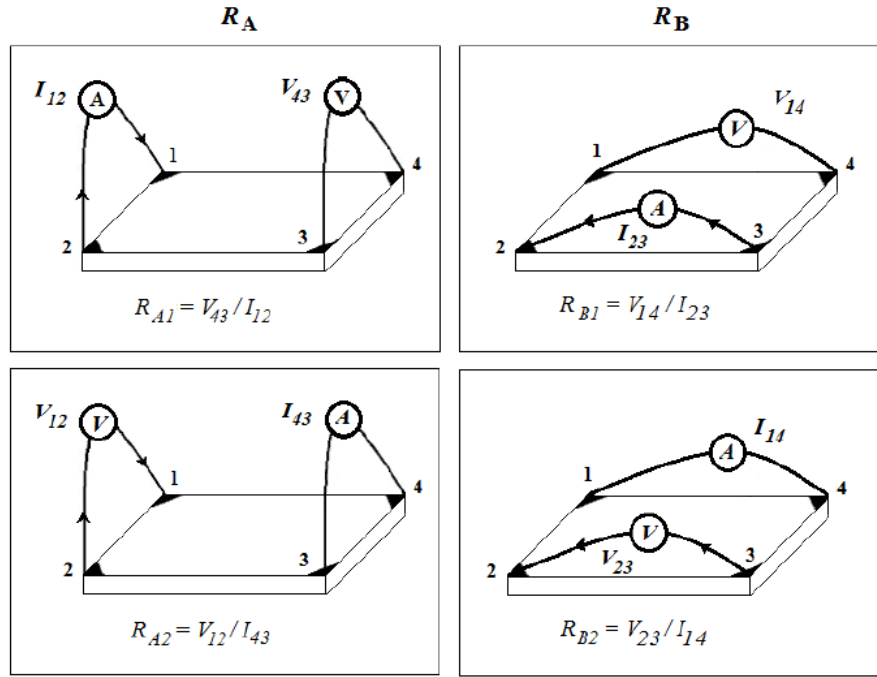
The RMS roughness, also known as Rq, is the root mean square average of the roughness profile ordinates:

AFM provided increased magnification and resolution in 3D [3.67, 3.68] and was used to measure the roughness of the treated surface layer thickness and to study the changes in the new surfaces with the printed layer deposition.

#### **3.4.3.5. Electrical conductivity measurements**

The electrical properties of a printed structure are affected by the homogeneity of the ink's chemical and physical properties, the structure geometry (thickness, edge definition, surface morphology, etc.) and the interfacial properties between different materials. For the printed substrate to effectively work as a sensing element, good electrical conductivity is required. The pattern quality evaluation results were used to select the optimal materials and optimize the processing steps and achieve precise and complex electrical design.

Printed substrates electrical conductivity measurements were performed based on the Van der Pauw technique [3.69]. Specimens with square geometry were used and four very small ohmic contacts were placed in the corners and, subsequently the resistance was measured as illustrated in Figure 3.19.



$$R_A = \frac{(R_{A1} + R_{A2})}{2} \text{ and } R_B = \frac{(R_{B1} + R_{B2})}{2}$$

Figure 3.19 - Schematic representation of a Van der Pauw configuration used in the measurements of the two characteristic resistance  $R_A$  and  $R_B$ .

The Van der Pauw method output is the sheet resistance ( $R_S$ ). According to Van der Pauw,  $R_A$  and  $R_B$ , are two characteristic resistances associated with the corresponding terminals shown in Figure 3.19 and are related to the sheet resistance  $R_S$  through the Van der Pauw equation that can be solved numerically for  $R_S$ :

$$e^{-\pi R_A / R_S} + e^{-\pi R_B / R_S} = 1 \quad \text{Equation 3.3}$$

The electrical resistivity ( $\rho$ ) can be determined through the following equation,

$$\rho = R_S \cdot d \quad \text{Equation 3.4}$$

where  $d$  is the thickness of the sample.

The electrical conductivity ( $\sigma$ ) is defined as the inverse of resistivity and is given by:

$$\sigma = \frac{1}{\rho} \quad \text{Equation 3.5}$$

The two characteristic resistances are obtained during the tests, where two consecutive measurements are performed, in which an applied dc current ( $I_{12}$ ) into contact 1 and out of contact 2, allows determining the voltage  $V_{43}$  from the contact 4 to contact 3. Then, applying the current ( $I_{23}$ ) into contact 2 and out of contact 3, the voltage  $V_{14}$  is obtained from the contact 1 to contact 4.

Electrical conductivity measurements were performed at ambient temperature. A total of 7 samples were tested using an Agilent 34410A 6 ½ Digit Multimeter/USB/GPIB Interface and a programmable DC source. The MATLAB software was used to automatically switch the polarity of the current in all Van der Pauw measurements, allowing obtaining the values of the current  $I_{12}$ ,  $I_{43}$ ,  $I_{23}$  and  $I_{14}$  (as illustrated in Figure 3.19) and to automatically record and calculate the  $R_S$ . The experimental test setup is shown in Figure 3.20.

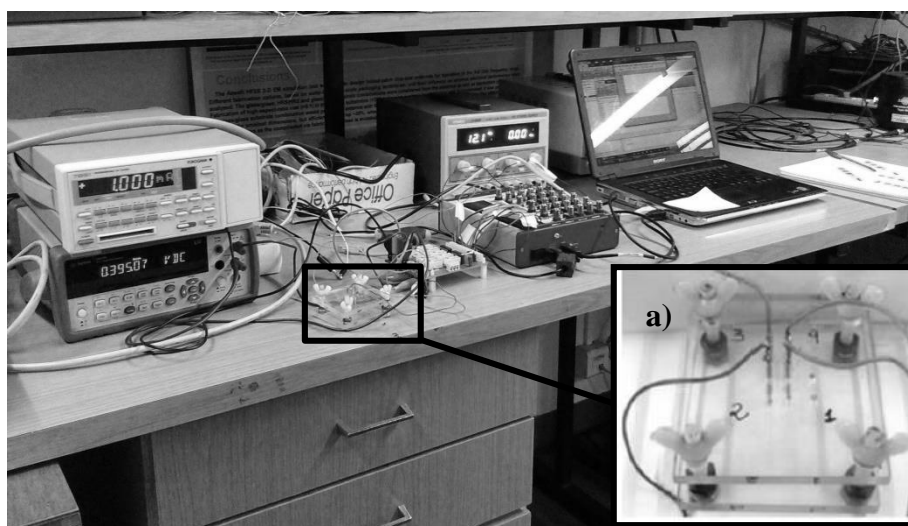


Figure 3.20 – Digital image of the experimental test setup. a) Sample assembly jig with four ohmic contact probes from the resistivity measurement system.

#### 3.4.3.6. Measurement of piezo-resistive effect of the printed ink

Minimization of resistance change under externally applied stress is one of the most important factors for highly reliable and stable electrical operation. For the coated substrate to effectively work as electrodes or sensing elements in the sensor system, good electrical conductivity is naturally desired. So, electrical resistivity has to be characterized.

The piezo-resistive behavior (evaluation of the mechanical response and measuring the electrical resistivity under tension loading conditions) is crucial. The piezo-resistive properties of the flexible printed pattern (required for a sensor design and its response), is an important

characteristic of the printed conductors. Understanding and characterization of the piezo-resistive behavior can enhance future applications on flexible sensors.

From a printed substrate (1.5 mm of thickness), six tensile test specimens shape (Figure 3.21) were cut using a compression moulding plate and tested. The piezo-resistive tests of the printed substrates were performed with a *Universal type Instron 4505* mechanical materials testing machine at room temperature (at 23°C and 55% RH). All samples were clamped in pneumatic grips with a crosshead speed of 7.5 mm.min<sup>-1</sup> (nominated strain rate of 3x10<sup>-1</sup> s<sup>-1</sup>), with a load cell of 1 kN and a gage length of 25 mm.

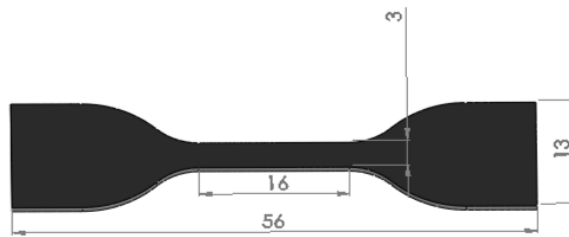


Figure 3.21 – Standard (according to ISO527- 2:1993) geometry shape (in mm) used for the piezo-resistive tests.

The grips contact surface was covered with a dielectric tape (in order to insulate the metal grips). A conductor wire was used to establish contact, at one end with the test sample and at the other end to an Agilent 34410A 6 ½ Digit Multimeter/USB/GPIB Interface. This multimeter (controlled by the Matlab code), in turn, establish a direct connection to the computer and performs the measurement of resistivity during the test. The experimental test setup is shown in Figure 3.22.

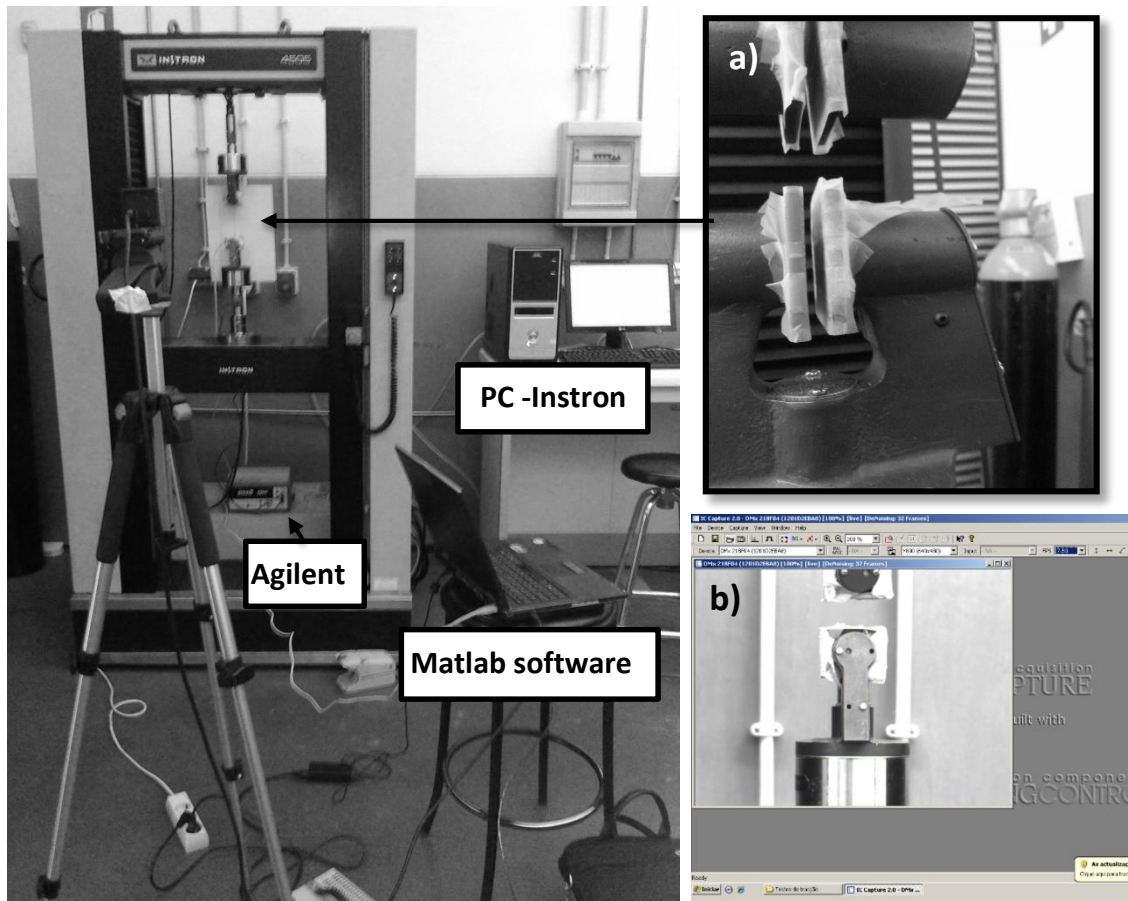


Figure 3.22 - Piezo-resistive measurements setup: a) metal grip isolation; b) IC Capture 2.0 interface.

**REFERENCES**

- [3.1] “Website of DuPont company: [www2.dupont.com](http://www2.dupont.com).” .
- [3.2] P. W. Hum, “Exploration of Large Scale Manufacturing of Polydimethylsiloxane (PDMS) Microfluidic Devices by SUBMITTED TO THE DEPARTMENT OF MECHANICAL ENGINEERING IN PARTIAL FULFILLMENT OF THE REQUIREMENTS FOR THE DEGREE OF Exploration of Large Scale Manufacturing o,” 2006.
- [3.3] A. Frick and A. Rochman, “Characterization of TPU-elastomers by thermal analysis (DSC),” *Polym. Test.*, vol. 23, no. 4, pp. 413–417, Jun. 2004.
- [3.4] W. G. Randall D., Lee S., “Introduction to flexible foams. In: The Polyurethanes Book.,” in *The polyurethanes book.*, John Wiley & Sons, Ltd. United Kingdom., 2002, pp. 180 – 181.
- [3.5] “Nanofil 5 online: [www.sud-chemie.com](http://www.sud-chemie.com).”
- [3.6] H. K. Kammler, G. Beaucage, R. Mueller, and S. E. Pratsinis, “Structure of Flame-Made Silica Nanoparticles by Ultra-Small-Angle X-ray Scattering,” no. 12, pp. 1915–1921, 2004.
- [3.7] “AEROSIL 200 online: [www.aerosil.com](http://www.aerosil.com).”
- [3.8] B. Li, S. Santhanam, L. Schultz, M. Jeffries-EL, M. C. Iovu, G. Sauvé, J. Cooper, R. Zhang, J. C. Revelli, A. G. Kusne, J. L. Snyder, T. Kowalewski, L. E. Weiss, R. D. McCullough, G. K. Fedder, and D. N. Lambeth, “Inkjet printed chemical sensor array based on polythiophene conductive polymers,” *Sensors Actuators B Chem.*, vol. 123, no. 2, pp. 651–660, May 2007.
- [3.9] R. D. R. Tian-An Chen , Xiaoming Wu, “Regiocontrolled Synthesis of Poly(3-alkylthiophenes) Mediated by Rieke Zinc: Their Characterization and Solid-State Properties,” *J. Am. Chem. Soc.*, vol. 117, no. 1, pp. 233–244, 1995.
- [3.10] G. Xie, Y. Jiang, X. Du, H. Tai, and W. Li, “Fabrication and properties of an OLED-based gas sensor with poly ( 3-hexylthiophene ) sensing film,” in *IMCS 2012 - The 14th International Meeting on Chemical Sensor*, 2012, pp. 1130–1133.
- [3.11] S. Mansouri, L. El Mir, A. a. Al-Ghamdi, O. a. Al-Hartomy, S. a. F. Al Said, and F. Yakuphanoglu, “Characterization and modeling of TIPS-pentacene-poly(3-hexyl) thiophene blend organic thin film transistor,” *Synth. Met.*, vol. 185–186, pp. 153–158, Dec. 2013.
- [3.12] S. E. San, T. Ozdal, and E. Aslan, “Manufacturing of inorganic-organic hybrid solar cells by screen,” in *6th Nanoscience and Nanotechnology Conference (NanoTRVI)*, 2010, vol. 34, pp. 261–264.
- [3.13] S. P. Speakman, G. G. Rozenberg, K. J. Clay, W. I. Milne, A. Ille, I. A. Gardner, E. Bresler, and J. H. G. Steinke, “High performance organic semiconducting thin films : Ink jet printed polythiophene [ rr -P3HT ],” *Org. Electron.*, vol. 2, pp. 65–73, 2001.

- [3.14]C.-T. Lin, C.-H. Hsu, I.-R. Chen, C.-H. Lee, and W.-J. Wu, "Enhancement of carrier mobility in all-inkjet-printed organic thin-film transistors using a blend of poly(3-hexylthiophene) and carbon nanoparticles," *Thin Solid Films*, vol. 519, no. 22, pp. 8008–8012, Sep. 2011.
- [3.15]P. Lo, P. Li, Z. Pei, J. Hou, and Y. Chan, "Enhanced P3HT OTFT Transport Performance Using Double Gate Modulation Scheme," vol. 30, no. 6, pp. 629–631, 2009.
- [3.16]C.-T. Lin, C.-H. Hsu, C.-H. Lee, and W.-J. Wu, "Inkjet-Printed Organic Field-Effect Transistor by Using Composite Semiconductor Material of Carbon Nanoparticles and Poly(3-Hexylthiophene)," *J. Nanotechnol.*, vol. 2011, pp. 1–7, 2011.
- [3.17]S. H. Ko, H. Pan, C. P. Grigoropoulos, C. K. Luscombe, J. M. J. Fréchet, and D. Poulidakos, "All-inkjet-printed flexible electronics fabrication on a polymer substrate by low-temperature high-resolution selective laser sintering of metal nanoparticles," *Nanotechnology*, vol. 18, no. 34, p. 345202, Aug. 2007.
- [3.18]P. Morvillo, I. A. Grimaldi, R. Diana, F. Loffredo, and F. Villani, "Study of the microstructure of inkjet-printed P3HT:PCBM blend for photovoltaic applications," *J. Mater. Sci.*, vol. 48, no. 7, pp. 2920–2927, Oct. 2012.
- [3.19]Y. Yang, W. Guo, Y. Zhang, Y. Ding, X. Wang, and Z. L. Wang, "Piezotronic effect on the output voltage of P3HT/ZnO micro/nanowire heterojunction solar cells.," *Nano Lett.*, vol. 11, no. 11, pp. 4812–7, Nov. 2011.
- [3.20]J. B. Chang, "Functionalized polythiophene thin-film transistors for low-cost gas sensor arrays," University of California at Berkeley, 2006.
- [3.21]R. S. Loewe, S. M. Khersonsky, and R. D. McCullough, "A Simple Method to Prepare Head-to-Tail Coupled, Regioregular Poly(3-alkylthiophenes) Using Grignard Metathesis," *Adv. Mater.*, vol. 11, no. 3, pp. 250–253, Mar. 1999.
- [3.22]R. Tipnis, D. Laird, and M. Mathai, "Polymer-based Material for Printed Electronics:Enabling High Efficiency Solar Power and Lighting," *Material Matters*, 2008. [Online]. Available: <http://www.sigmaaldrich.com/technical-documents/articles/material-matters/polymer-based-materials.html#sthash.UUnf8Thc.dpuf>.
- [3.23]"Plextronics, Inc. Plexcore -Technical bulletin AL-251."
- [3.24]J. W. McBride and L. Lam, "A Review of Conducting Polymers in Electrical Contact Applications," in *International Conference of Polymeric Materials in Power Engineering (ICPMPE)*, 2007.
- [3.25]A. Elschner, S. Kirchmeyer, W. Lövenich, U. Merker, and K. Reuter, *PEDOT-Principles and Applications of an Intrinsically Conductive Polymer*. Taylor and Francis Group, LLC, 2011, p. 353.
- [3.26]J. R. Groenendaal, L. Jonas, F. Freitag, D. Pielartzik, H. Reynolds, "Poly(3,4-ethylenedioxythiophene) and its derivatives: past, present, and future," *Adv. Mater.*, vol. 12, no. 7, pp. 481–494, 2000.

- [3.27]S. Material and S. Data, “Transparent ORGACON™ Transparent Conductive Inkjet Ink: IJ Orgacon inkjet inks are highly transparent conductive inks based on conductive polymer PEDOT / PSS. IJ-1005 was tested with different piezo inkjet platforms such as Microdrop, Dimatix DMP-28.”
- [3.28]Y. H. Kim, C. Sachse, M. L. Machala, C. May, L. Müller-Meskamp, and K. Leo, “Highly Conductive PEDOT:PSS Electrode with Optimized Solvent and Thermal Post-Treatment for ITO-Free Organic Solar Cells,” *Adv. Funct. Mater.*, vol. 21, no. 6, pp. 1076–1081, Mar. 2011.
- [3.29]“Sigma Material Safety Data Sheet.” [Online]. Available: <http://www.sigmaaldrich.com/medium/structureimages/79/mfcd07371079.png>.
- [3.30]T. Deutschmann, “micro structured electrochromic device based on poly(3,4-ethylenedioxythiophene) (PEDOT).”
- [3.31]C.-C. Tseng, Y.-H. Chou, T.-W. Hsieh, M.-W. Wang, Y.-Y. Shu, and M.-D. Ger, “Interdigitated electrode fabricated by integration of ink-jet printing with electroless plating and its application in gas sensor,” *Colloids Surfaces A Physicochem. Eng. Asp.*, vol. 402, pp. 45–52, May 2012.
- [3.32]Y. Wang, W. Jia, T. Strout, Y. Ding, and Y. Lei, “Preparation, Characterization and Sensitive Gas Sensing of Conductive Core-sheath TiO<sub>2</sub>-PEDOT Nanocables,” *Sensors (Basel)*, vol. 9, no. 9, pp. 6752–63, Jan. 2009.
- [3.33]H. Bai and G. Shi, “Gas Sensors Based on Conducting Polymers,” *Sensors*, vol. 7, no. 3, pp. 267–307, Mar. 2007.
- [3.34]a. Phongphut, C. Sriprachuabwong, a. Wisitsoraat, a. Tuantranont, S. Prichanont, and P. Sritongkham, “A disposable amperometric biosensor based on inkjet-printed Au/PEDOT-PSS nanocomposite for triglyceride determination,” *Sensors Actuators B Chem.*, vol. 178, pp. 501–507, Mar. 2013.
- [3.35]A. Määttänen, U. Vanamo, P. Ihalainen, P. Pulkkinen, H. Tenhu, J. Bobacka, and J. Peltonen, “A low-cost paper-based inkjet-printed platform for electrochemical analyses,” *Sensors Actuators B Chem.*, vol. 177, pp. 153–162, Feb. 2013.
- [3.36]Y. Wang, “Research progress on a novel conductive polymer–poly(3,4-ethylenedioxythiophene) (PEDOT),” *J. Phys. Conf. Ser.*, vol. 152, p. 012023, Mar. 2009.
- [3.37]L. Fan, N. Zhang, and K. Sun, “Flexible patterned micro-electrochemical capacitors based on PEDOT,” *Chem. Commun. (Camb)*, vol. 50, no. 51, pp. 6789–92, Jun. 2014.
- [3.38]U. S. Bhansali, M. a. Khan, and H. N. Alshareef, “Organic ferroelectric memory devices with inkjet-printed polymer electrodes on flexible substrates,” *Microelectron. Eng.*, vol. 105, pp. 68–73, May 2013.
- [3.39]F. Greco, A. Zucca, S. Taccola, A. Menciassi, T. Fujie, H. Haniuda, S. Takeoka, and V. Mattoli, “Ultra-thin conductive free-standing PEDOT/PSS nanofilms,” *R. Soc. Chem.*, vol. 7, pp. 10642–10650, 2011.



[3.40]T. M. Schweizer, “Electrical characterization and investigation of the piezoresistive effect of PEDOT : PSS thin films Electrical characterization and investigation of the piezoresistive effect of PEDOT : PSS thin films,” Georgia Institute of Technology, 2005.

[3.41]M. Zirkl, A. Sawatdee, U. Helbig, M. Krause, G. Scheipl, E. Kraker, P. A. Ersman, D. Nilsson, D. Platt, P. Bodö, S. Bauer, G. Domann, and B. Stadlober, “An all-printed ferroelectric active matrix sensor network based on only five functional materials forming a touchless control interface.,” *Adv. Mater.*, vol. 23, no. 18, pp. 2069–74, May 2011.

[3.42]Y. Yoshioka and G. E. Jabbour, “Desktop inkjet printer as a tool to print conducting polymers,” *Synth. Met.*, vol. 156, no. 11–13, pp. 779–783, Jun. 2006.

[3.43]J. H. Chen, C.-A. Dai, and W.-Y. Chiu, “Synthesis of highly conductive EDOT copolymer films via oxidative chemical in situ polymerization,” *J. Polym. Sci. Part A Polym. Chem.*, vol. 46, no. 5, pp. 1662–1673, Mar. 2008.

[3.44]T. Stöcker, A. Köhler, and R. Moos, “Why does the electrical conductivity in PEDOT:PSS decrease with PSS content? A study combining thermoelectric measurements with impedance spectroscopy,” *J. Polym. Sci. Part B Polym. Phys.*, vol. 50, no. 14, pp. 976–983, Jul. 2012.

[3.45]H. E. Katz and J. Huang, “Thin-Film Organic Electronic Devices,” *Annu. Rev. Mater. Res.*, vol. 39, no. 1, pp. 71–92, Aug. 2009.

[3.46]G. Disario, “for Flexible Organic Photovoltaics for Flexible Organic Photovoltaics,” vol. 55, no. September 2010, 2011.

[3.47]A. Kamyshny, J. Steinke, and S. Magdassi, “Metal-based Inkjet Inks for Printed Electronics,” *Open Appl. Phys. J.*, vol. 4, pp. 19–36, 2011.

[3.48]M. Nir, D. Zamir, I. Haymov, L. Ben-Asher, O. Cohen, B. Faulkner, and F. de la Vega, “Electrically conductive inks for inkjet printing. In: Magdassi S, Ed. The chemistry of inkjet inks.,” World Scie., New Jersey-London-Singapore, 2010, pp. 225–54.

[3.49]J. Perelaer, B.-J. de Gans, and U. S. Schubert, “Ink-jet Printing and Microwave Sintering of Conductive Silver Tracks,” *Adv. Mater.*, vol. 18, no. 16, pp. 2101–2104, Aug. 2006.

[3.50]G. Xie, O. Ohashi, N. Yamaguchi, and A. Wang, “Effect of Surface Oxide Films on the Properties of Pulse Electric-Current Sintered Metal Powders,” vol. 34, no. NOVEMBER, pp. 2655–2661, 2003.

[3.51]D. Wakuda, M. Hatamura, and K. Suganuma, “Novel method for room temperature sintering of Ag nanoparticle paste in air,” *Chem. Phys. Lett.*, vol. 441, no. 4–6, pp. 305–308, Jun. 2007.

[3.52]B. J. Perelaer, A. W. M. de Laat, C. E. Hendriks, and U. S. Schubert, “Inkjet-printed silver tracks: low temperature curing and thermal stability investigation,” *J. Mater. Chem.*, vol. 18, no. 27, p. 3209, 2008.

- [3.53]J. Perelaer, C. E. Hendriks, A. W. M. De Laat, and U. S. Schubert, “One-step inkjet printing of conductive silver tracks on polymer substrates,” vol. 20, 2009.
- [3.54]U. Altenberend, F. Molina-Lopez, A. Oprea, D. Briand, N. Bârsan, N. F. De Rooij, and U. Weimar, “Towards fully printed capacitive gas sensors on flexible PET substrates based on Ag interdigitated transducers with increased stability,” *Sensors Actuators B Chem.*, vol. 187, pp. 280–287, Oct. 2013.
- [3.55]S. B. Fuller, E. J. Wilhelm, and J. M. Jacobson, “Ink-jet printed nanoparticle microelectromechanical systems,” *J. Microelectromechanical Syst.*, vol. 11, no. 1, pp. 54–60, 2002.
- [3.56]J. Mei, “Formulation and processing of conductive inks for inkjet printing of electrical components.,” p. 130, *Doctoral Dissertation, University of Pittsburgh*. 2005.
- [3.57]“Ag-IJ10 Application data sheet : Ag-IJ10 Nanosilver Ink, Applied Nanotech, Inc.” AUSTIN, TX.
- [3.58]U. Caglar, “Studies of Inkjet Printing Technology with Focus on Electronic Materials,” Universidade de Tampere, 2009.
- [3.59]Www.dowcorning.com, “PDMS data sheet- Dow Corning ®.”
- [3.60]“DataPhysics Instruments GmbH -OCA 15EC DataPhysics manual . www.dataphysics.de.”
- [3.61]“Xennia Technology, Ltd: Inkjet printing solutions.” [Online]. Available: www.xennia.com.
- [3.62]“Carnelian Printer User Manual, Xennia Technonology Ltd,” 2006. .
- [3.63]“FUJIFILM Holdings America Corporation <www.dimatix.com>.” .
- [3.64]R. Lacombe, *Adhesion Measurement Methods: Theory and Practice*. Taylor & Francis, 2005.
- [3.65]“The Home Of Surface Measurement <<http://www.rubert.co.uk/faqs/roughness-parameters/>>.”
- [3.66]“Harrisonep <<http://www.harrisonep.com/electropolishing-ra.html>>.”
- [3.67]V. I. Inc., “Scanning Probe/Atomic Force Microscopy: Technology Overview and Update.” 2005.
- [3.68]M. Raposo, Q. Ferreira, and P. A. Ribeiro, “A Guide for Atomic Force Microscopy Analysis of Soft- Condensed Matter,” pp. 758–769, 2007.
- [3.69]L. J. van der Pauw, “A method of measuring specific resistivity and Hall effect of discs of arbitrary shape,” in *Philips Reseach Report, Vol. 13, No. 1.*, 1958, pp. 1–9.



# Chapter 4

## **Inkjet Printing of Poly (thiophene-3-[2-(2-methoxyethoxy)ethoxy]-2,5-diyl) sulfonated conductive ink (P3HT)**

In this Chapter, special attention is placed on P3HT ink. Here, all the results concerning the P3HT printing and the characterization of the fabricated printed patterns for use as electrodes are presented. First, the results for printability on the substrate are presented, which is followed by the results for adhesion of the ink and the electrical performance of the pattern printed on the flexible substrates.



## 4.1. Inkjet printing of polymer conductive ink

### 4.1.1. Material's properties

- **Conductive ink**

Table 4.1 presents the summarized physical properties of the commercial grade of the used P3HT.

Table 4.1 - Plexcore® OC RG-1100 physical properties [4.1].

Conductor component	Conductive Polymer
Solid content (wt%)	2
Concentration	0.8% in H <sub>2</sub> O
Electrical Resistivity ( $\Omega$ .m)	0.25-2.5
pH	2.2-2.8
Viscosity (mPa.s)	7-13
Surface tension (mN/m)	35 - 38

Note: The tabulated values are from the producer data sheet (Appendix A7).

- **Determination of the annealing temperature of the P3HT conductive ink.**

A 23.49 mg P3HT size sample was evaluated by thermal-gravimetric analyses (TGA) for determination of the optimal annealing temperature. Figure 4.1 shows the weight loss variation with temperature. The mass of the polymeric conductive ink starts to decrease at 36.04°C till 75°C (with 37.15% of the total weight loss) and between 75°C till 126°C (with 49.26% of the total weight loss). The 1<sup>st</sup>. step of the TGA curve can be associated to the initial temperature of weight loss of the solvents and little molecules or unstable side chains, which degrade at lower temperature. This indicate no need for annealing at high temperate after printing. The degradation of the ink occurs between 120°C and 126°C. The 2<sup>nd</sup> step is believed to be related to the conductive polymer itself. No expressive weight loss was register between 126°C to 350°C. From this evaluation, one can concluded that the ink annealing temperature should be between 75°C and 126°C.

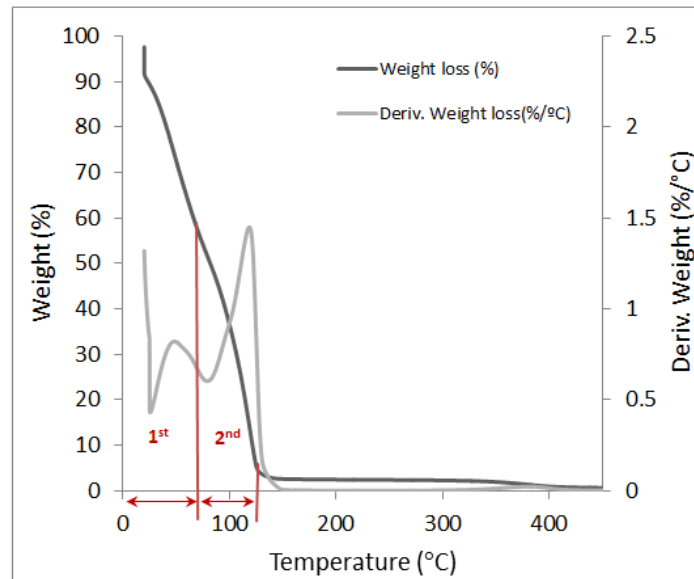


Figure 4.1 – P3HT mass loss analysis for optimal annealing temperature evaluation.

- **Substrate vs. Ink surface tensions**

Before starting the printing, the critical surface tensions (ST) of the substrates were measured in order to evaluate its receptivity to the ink. The ideal ST of a substrate should be at least 7 to 12 mN/m higher than the ST of the liquid with which it will interact [4.2, 4.3]. According to the supplier, the ST of the P3HT *Plexcore*® ink is around 35-38 mN/m. The ability of a liquid to spread on a surface was measured by the contact angle between the liquid and the surface. The smaller the contact angle is, the greatest is the spreading of the liquid on the surface and, therefore, higher is the surface energy of the substrate. The ST measurements of the substrates and their difference with the ink ST,  $\Delta$ ST, are summarized in Table 4.2.

Table 4.2– ST of the Substrates vs. ST of the ink (35-38 mN/m).

Substrate	ST* (mN/m)	$\Delta$ ST(mN/m)
PI	39.32	1.32
PET	43.31	5.31
PDMS	13.23	-24.77
TPU	32.49	-5.51

\*according to OWRK [4.4, 4.5].

This result allows predicting that the adhesion of the P3HT ink (35-38 mN/m), particularly to a clean PDMS substrate (13.23 mN/m) and TPU (32.49 mN/m) will be very difficult ( $\Delta ST = -24.77$  mN/m and  $-5.51$  mN/m, respectively). Also, the surface energy of PI and PET substrates isn't high enough to promote good wetting and a homogeneous dispersion of the ink. From these results it was concluded that surface treatment is required to achieve good adhesion of the ink to the mentioned substrates.

#### 4.1.2. Ink Preparation

Before printing, the P3HT ink underwent an ultrasonic vibration bath for 3 hours, in order to minimize sedimentation and precipitation of ink solid particles (preventing the precipitation in the nozzle and in the final printed pattern). Then, the inks were filtered by a 1  $\mu\text{m}$  pore size glass fiber filter before filling the ink supply syringe of the inkjet printer. Filling procedure of the ink supply syringe was conducted as described before in Chapter 3.

#### 4.1.3. Preliminary Inkjet printing

Simple rectangular and circular patterns of various sizes were printed on the substrates (Figure 4.2). At this stage, high resolution is not essential for large printed areas but high conductivity is required for the electrode pattern. All the available 256 nozzles were used in this printing study in order to get the highest possible throughput and overlapping from 1 to 10 ink-jetted layers at drop spacing of 254  $\mu\text{m}$  (100 DPI), 84.67  $\mu\text{m}$  (300 DPI), 42.33  $\mu\text{m}$  (600 DPI) and 28.22  $\mu\text{m}$  (900 DPI) was tested. Other printhead settings were adjusted according to the results of the iteration steps of experiments with this type of ink, and used substrate.

- **Printed patterns**

After few seconds, still during printing, it was observed that the conductive ink starts to form visible drops on the substrate, indicating a fast joint of the ink printed drops in large drops (Figure 4.2). Unsuccessfully, several printing attempts were performed for increasing temperature of the ink and temperature of the substrate in order to speed up the solvents evaporation and improve the printing pattern quality. Similar results were achieved with the different substrates. Figure 4.2 shows a clean PDMS after printing the 1<sup>st</sup>. layer at 900 DPI.

The modification of the ink formulation could be a solution for this problem [4.6], however, studding new ink formulations is entering in a new set of research fields. The addition of solvents/additives will dilute the conducting polymer concentration and will affect



the conductivity properties. The printing ink did not have the expected dispersion, and this led to the need of including an additional study. The most used solution for the lack of wettability is substrate surface treatment.

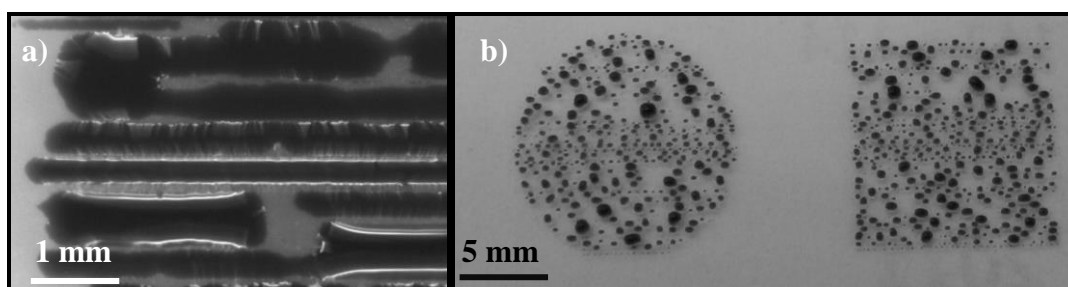


Figure 4.2 – Printed substrates: a) Inspection camera image of a clean PDMS substrate with flooding of the P3HT ink; b) Digital image of TPU with drop formation of the P3HT ink (few seconds after printing).

Studies [4.7, 4.8] show that substrates can be plasma treated to change the surface energy and eliminate surface contaminants. These contaminants also inhibit the shape of the drops, worsening the image quality [4.9] and the adhesion. Although, the hydrophilic surface is temporary, specially when we are dealing with polymers, the exposure to air quickly induces hydrophobic recovery [4.10]. Therefore, it is recommended to bond, coat, ink, or decorate the product as soon as possible after pretreatment. However, this requirement, along with the very small space inside the vacuum chamber used for plasma treatment, was automatically restricting the size of the samples, forcing to work with small sized substrates.

For this reason, a different solution was pursued to allow the study to continue within the available laboratory conditions. The surface roughness could be controlled in order to increase or decrease surface energies. Therefore, the spread of clay or silica particles on polymer surface was considered as a way to increase the surface roughness resulting in the increase of the surface contact area.

#### 4.1.3.1. Surface roughness control

Particles were spread manually on the substrate surface, and then heated below the polymer melting temperature to sink the particles on the polymer surface, achieving a better particle-polymer interaction at their interfacial region. This procedure was tested on TPU, PI and PET substrates, with their respective softening temperature.

- **Clay Particles (CP)**

Figure 4.4 shows the result of the CP Nanofil 5 mechanical dispersion on the TPU surface after 15 minutes in the woven at 120°C (thermal treatment for thermal cross-linking at TPU softening temperature) followed by careful rinsing with distilled water to clean loose particles. The extent of the particles dispersion was evaluated through microscopy analysis. Figure 4.3 shows the top substrate surface and the cross section obtained by cryogenic fracture, respectively, of neat TPU (for comparison).

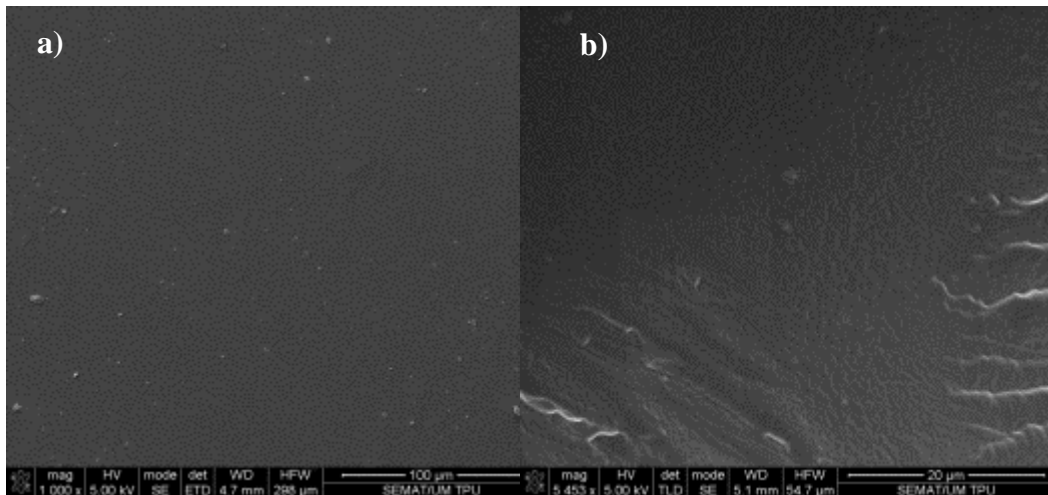


Figure 4.3 - SEM images of neat TPU: a) top substrate surface; b) cross section by cryogenic fracture.

Figure 4.4 depicts some experiments with CP. Several loose CP particles of micron size can be observed and the TPU and the PET surfaces area not completed covered. The SEM pictures depict poor CP distribution, with no adhesion to the substrate PET surface. Also no satisfactory adhesion of the CP was achieved by PI substrates. For PET substrates, reaching the material softening temperature caused deformation.

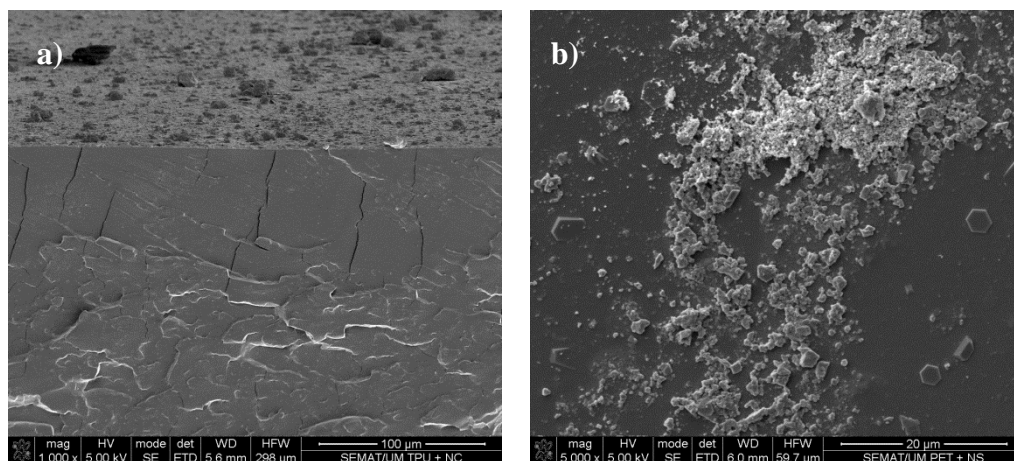


Figure 4.4 - SEM images the substrate with CP after 15 min at 120°C: a) fracture surface of TPU with CP; b) PET surface with CP.

The homogeneous deposition of CP on the polymer surface was further complicated by factors such as the topography of the particle, the material nature (the higher inter-aggregate attractive forces (Van der Waals forces) between nanoparticles) had greater tendency, when compared to the SP, to aggregate creating a high secondary structure and increasing agglomerate particles size. These results indicated that CP isn't a suitable solution for surface roughness modification.

- **Silica Particles (SP)**

As described for CP, AEROSIL 200 hydrophilic fumed SP particles were, also, manually dispersed on the surface of the substrates, and then heated below the polymer melting temperature for thermal cross-linking and SP sink-in on the polymer surface (to achieve a higher particle-polymer interaction at their interfacial region). Figure 4.5 presents an illustration of the expected particle-polymer interaction and final surface roughness.

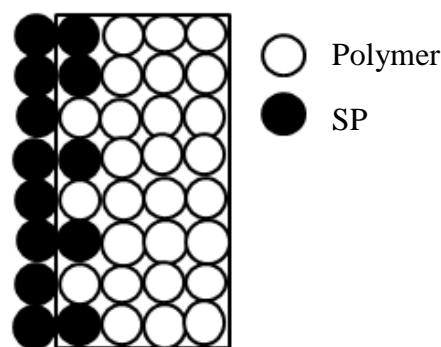


Figure 4.5 - Result structure of the SP-polymer interaction created by mechanical depositor

The extent of the particles dispersion was evaluated through microscopic analysis. The microstructure of the specimens is shown in Figure 4.6 and Figure 4.7. The Figure 4.6 depicts the SP manually dispersed on the TPU surface without any thermal treatment, followed by careful rinsing to clean the excess of particles. Many loose particles of micron size are present and the TPU surface is not completely covered by the SP. This experiment was conducted with both, clay and silica, to corroborate the importance of the thermal treatment to achieve the sinking, the thermal cross-linking, and thus, the adherence of the particles to the TPU surface.

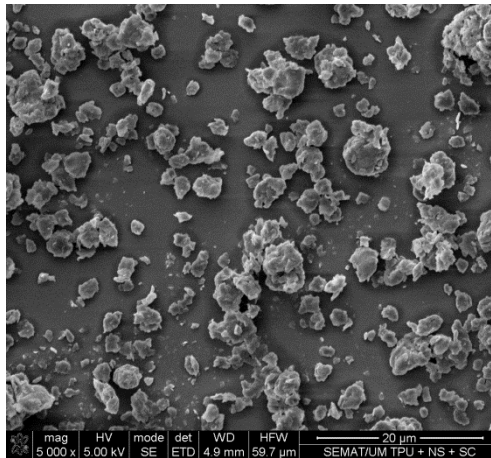


Figure 4.6 - SEM images of the top surface of the SP-TPU substrate SP without thermal treatment.

Figure 4.7 shows the SP manually dispersed on the TPU surface after 15 minutes in the woven at 120 °C (TPU softening temperature), followed by careful rinsing with distilled water (to clean loose particles). The TPU surface is well covered by the SP. Some particles agglomerations with medium 5 μm size are detected, mainly because it is difficult to homogeneously disperse material such as nanoparticles. Figure 4.7 b) shows a good interaction between SP and the polymeric substrate (SP-TPU), resulting in a good adhesion between them. Summarizing, the SEM images depict an acceptable SP distribution, taking into account the preparation process used, and a fairly good adhesion of fillers to TPU surface. Overall, to a certain level, a homogeneous roughness form was achieved.

The same procedure was tested with other substrates, PI and PET. No satisfactory adhesion of the SP was achieved.

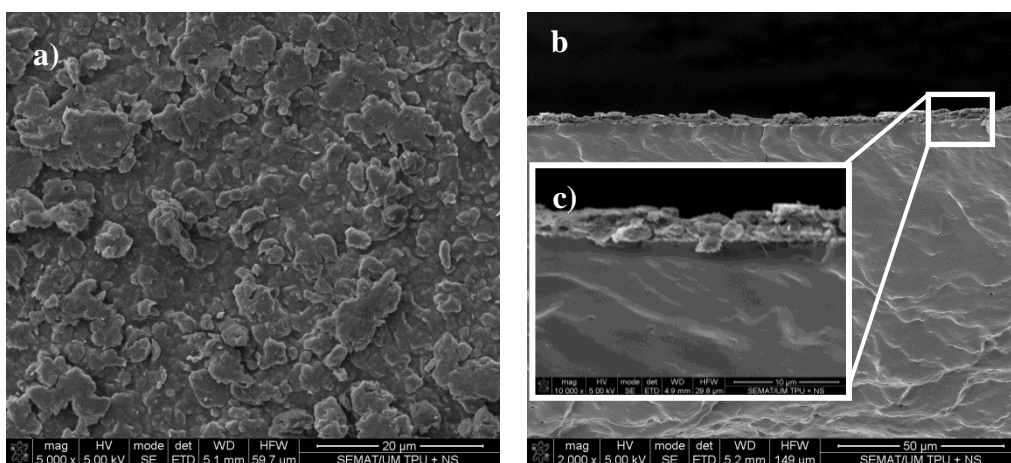


Figure 4.7 - SEM images of SP-TPU: a) Top substrate surface b) Fractured surface; c) detail of Figure 4.7 b).

The extent of the particles sink-in was evaluated through AFM analysis. The AFM topographical images of the neat TPU surface before SP deposition and after SP deposition plus thermal treatment are shown in Figure 4.8. According to the TPU roughness analysis (Figure 4.8 a)), the root-mean-square (RMS) roughness and the mean roughness (Ra) of the TPU surface are 27.056 nm and 19.574 nm, respectively. These values are considerably smaller than the RMS and Ra roughness of the SP-TPU (Figure 4.8 b)), 194.94 nm and 152.40 nm, respectively. These percentage increase of 86.12% and 87.16%, respectively, are an indication of the great increase of the TPU surface roughness induced by the propose method.

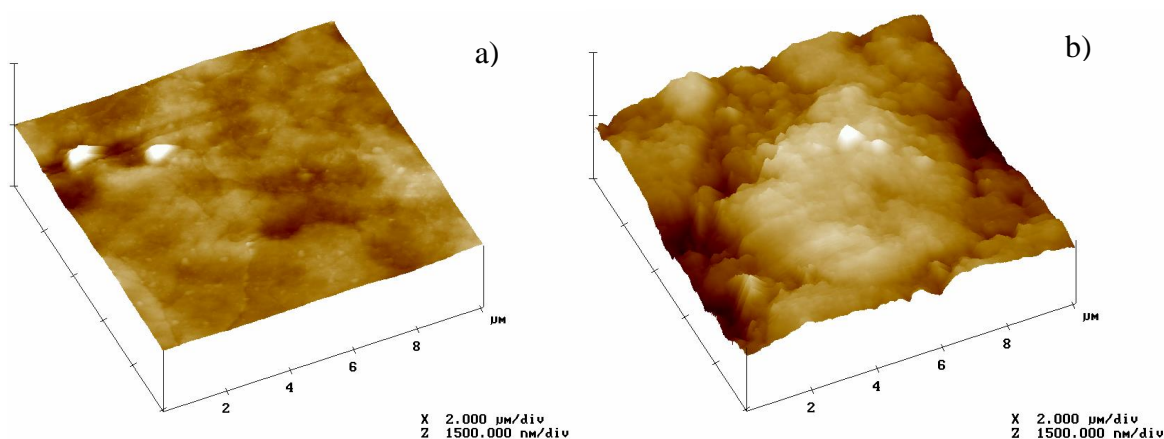


Figure 4.8 –AFM topographical images of the TPU surface: a) neat TPU and b) SP-TPU. The image size is 10  $\mu\text{m}$  x10  $\mu\text{m}$ .

- **Effect of SP on the TPU surface tension**

The effect of SP on the surface energy of the TPU was evaluated through the determination of substrates surface tension (as described in Chapter 3). As shown in Table 4.2, TPU substrate has a ST of 32.49 mN/m and the TPU with SP treatment resulted in a ST increase, to 47.11 mN/m (an increase of c.a. 31.07%). Figure 4.9 shows a drop of water on the TPU substrate, before and after the treatment, where it is easily visible the effect of SP on the TPU wettability.

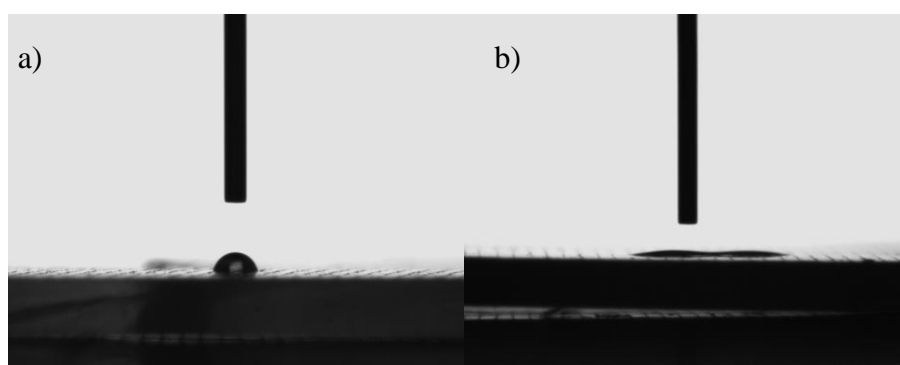


Figure 4.9 – Drop of water on the: a) neat TPU substrate; b) SP-TPU substrate.

#### 4.1.4. Inkjet printing on modified substrate

After the analysis of the nanoparticles dispersion on the TPU surface roughness, the inks were applied to the treated surface for the evaluation of the effect of SP on the ink dispersion. The SP ensured a good surface wetting, has created bond interactions, increased the surface roughness resulting in the increment of the surface contact area, and made an effective transition interphase between the ink layer and the substrate. Table 4.3 reports the optimized printhead main settings used with P3HT printing.

Table 4.3 - Main printhead settings used for P3HT ink.

Main settings	
Drop size	10 pL
Printhead height	3mm
Substrate Temperature	RT
Printhead Temperature	40 °C
Head speed	60 mm/s
Drop spacing	28.22 $\mu\text{m}$
Maximum Jetting Frequency range	50 kHz

Figure 4.10 shows a digital image of the P3HT appearance, printed in the SP-TPU substrate before and after annealing treatment. According to Figure 4.10 a) and to [4.11], the appearance of the printed pattern suggests that the morphology of the drop impact on the dry SP-TPU substrate surface is determined as *Deposition* with an effective deposition of the ink drop on the substrate surface. *Deposition* is considered when the drop, during the impact, deforms without breaking up in smaller drops, and stays attached to the substrate surface.

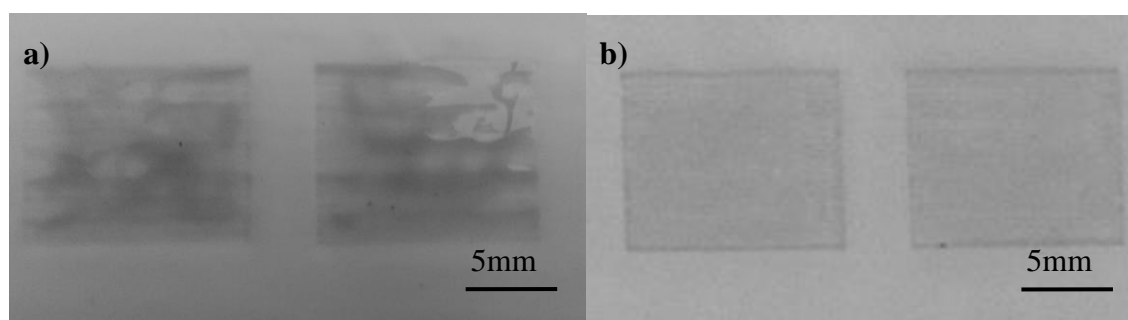


Figure 4.10 – Image of the P3HT printed in the SP-TPU substrate: a) before annealing; b) after annealing.

Between two subsequent prints, 3 minutes were needed to allow the drying of the ink before printing the next printed layer. Since this process was too long, heated air flow was used to accelerate the drying between layers and purging of the printhead was conducted every 3 ink layers in order to avoid nozzle clogging as previously referred in Chapter 3.

After printing, the samples were annealed at 80 °C in oven for at least 8 h to allow complete evaporation of the solvent. This temperature avoids the yellowing of the substrate and its deformation. Obviously, a higher annealing temperature leads to faster drying of the solvent and consequently to shorter time of manufacturing.

Figure 4.11 depicts the top SP-TPU substrate surface with different layers of inkjet printed P3HT ink. The ink wasn't homogenous dispersed since the achieved thickness isn't homogeneous along the printed pattern. This was expected, as the surface modification treatment resulted in a roughness variation along the surface. Therefore, the ink thickness variation is a consequence of the substrate roughness. On the first layers (1 to 5 layers) of ink, the measurement of its thickness was difficult because, from SEM image contrast, it was impossible to distinguish the ink from the substrate. However, from the top surface image is possible to observe that the roughness aspect of the SP-TPU (before printing) decreases with the increase of the ink layers, indicating an embedment of ink into the substrate.

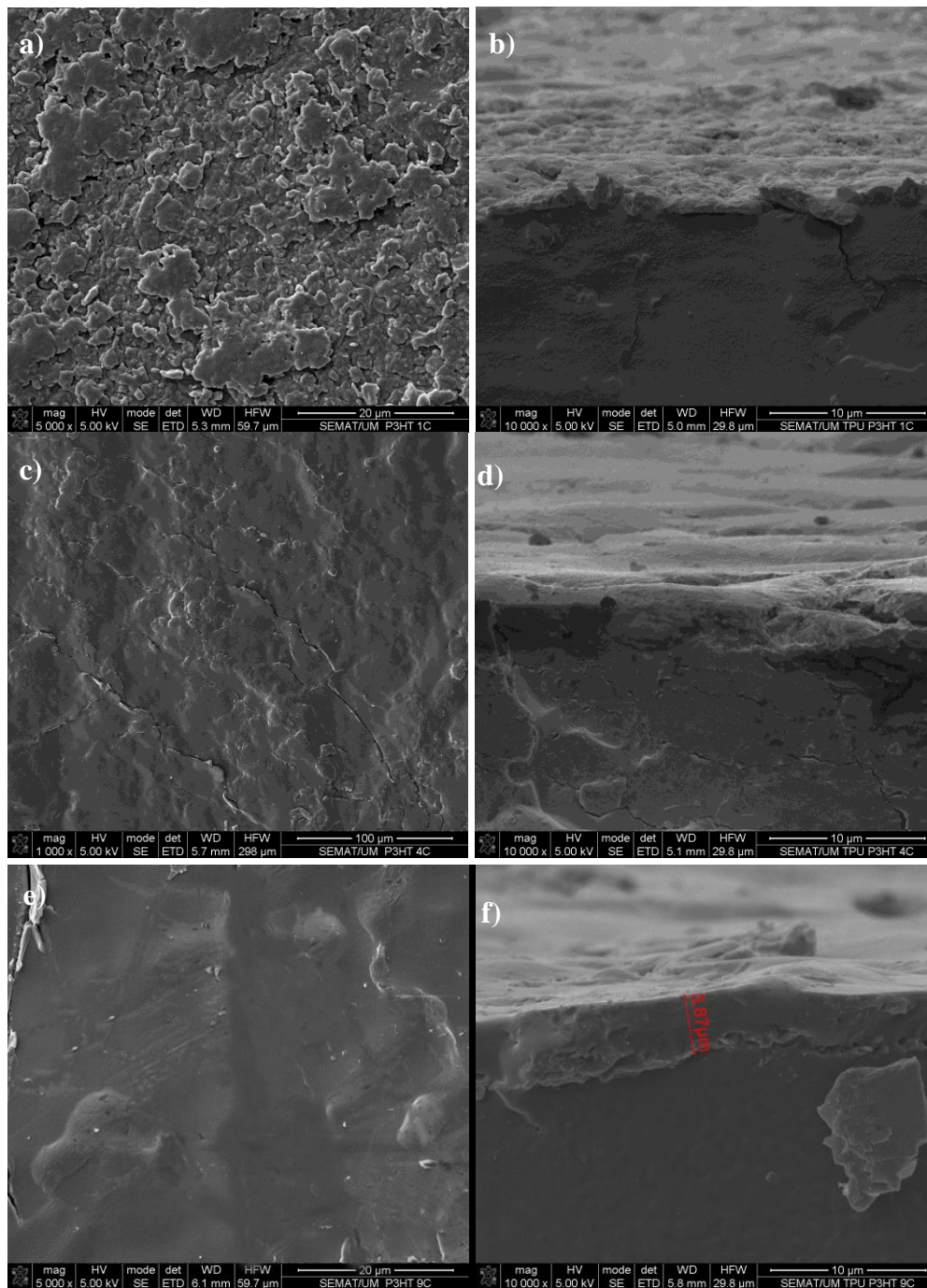


Figure 4.11 – SEM images of SP-TPU with inkjet printed P3HT ink: a) and b) Top and fractured cross section substrate surface, respectively, with one layer of ink; c) and d) Top and fractured cross section substrate surface, respectively, with four layers of ink; e) and f) Top and fractured cross section substrate surface, respectively, with nine layers of ink.

Figure 4.12 shows the cross-section of SP-TPU with nine and ten layers of printed P3HT ink. The ink film thickness increases with the number of layers,  $3.76 \mu\text{m}$  to  $4.76 \mu\text{m}$ , respectively. These values are purely indicative, since with the roughness of the TPU the thickness of the ink is not homogeneous along the printed area. Note that the ink doesn't



crack in its normal state, but the cracked ink on the above image is a result of the used method (fractured surface by liquid nitrogen) for sample preparation for SEM analysis.

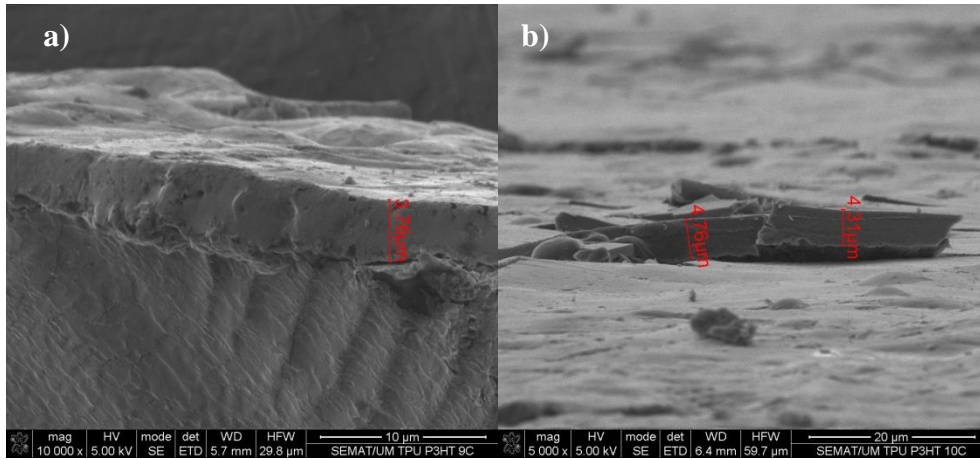


Figure 4.12 - SEM images of SP-TPU fractured surface with inkjet printed P3HT ink: a) nine layers; b) ten layers.

The AFM topographical image in Figure 4.13 shows the surface morphology of the printed SP-TPU. According to Figure 4.8 b)), the RMS and Ra roughness analysis of the SP-TPU surface was, respectively, 194.94 nm and 152.40 nm. With the six layers of P3HT ink, the measured RMS and Ra has changed to 240.69 nm and 182.38 nm, respectively, in the new surface, indicating an increase of the surface roughness (23.5% and 19.7%, respectively).

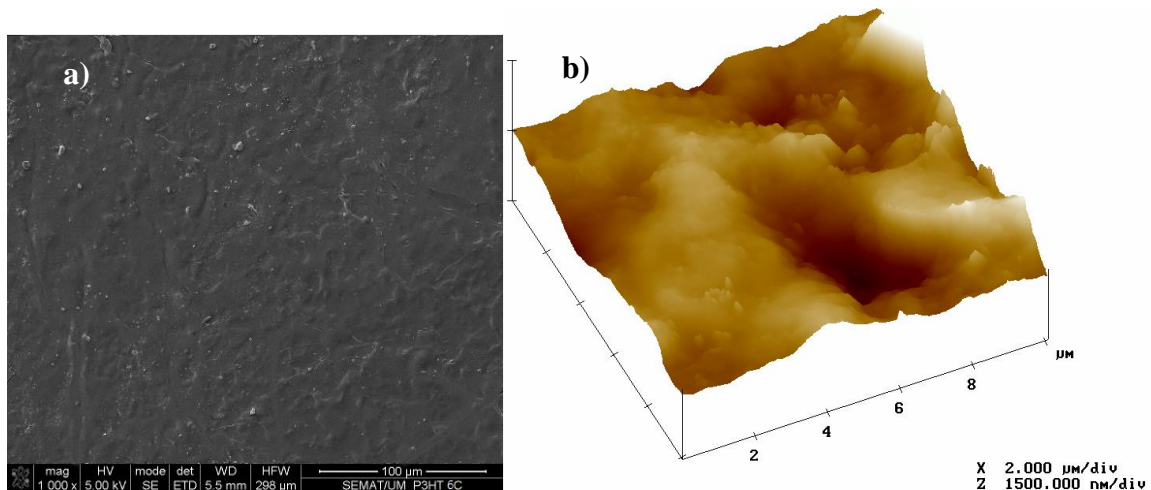


Figure 4.13 –Printed SP-TPU surface with six layers of P3HT: a) SEM image; b) AFM topographic image (image size is 10 μm x10 μm).

## 4.2. Adhesion and electrical resistivity characterization of printed substrates

### 4.2.1. Adhesion tests

There are several variables that might affect the adhesion of the printed ink to the substrate:

- a) surface energy between substrate and the ink,
- b) annealing parameters, and in this specific case,
- c) the possible chemical interaction with the SP.

Optical Microscopy (OM) was used for the qualitative evaluation of the samples tested, in order to assess the substrate-ink adhesion. Figure 4.14 shows images of remaining ink on the substrate and an image of the removed ink on the adhesion tape after the Cross-cut Tape test. Through the visual analysis of the remaining ink on the substrate and according to the ASTM - D3359, method B) qualitative evaluation scale (see Comparison Chart in Appendix 8), the level of adhesion of the ink to the substrate is high. A visual evaluation doesn't detect any delamination; the cross-cut didn't affect the ink layer, that present 0% of removed area. The adhesion of the ink film to the substrate is rated in 0 on a 0-5 scale, where 0 is 0% of removed area and 5 is more than 65% of the removed area.

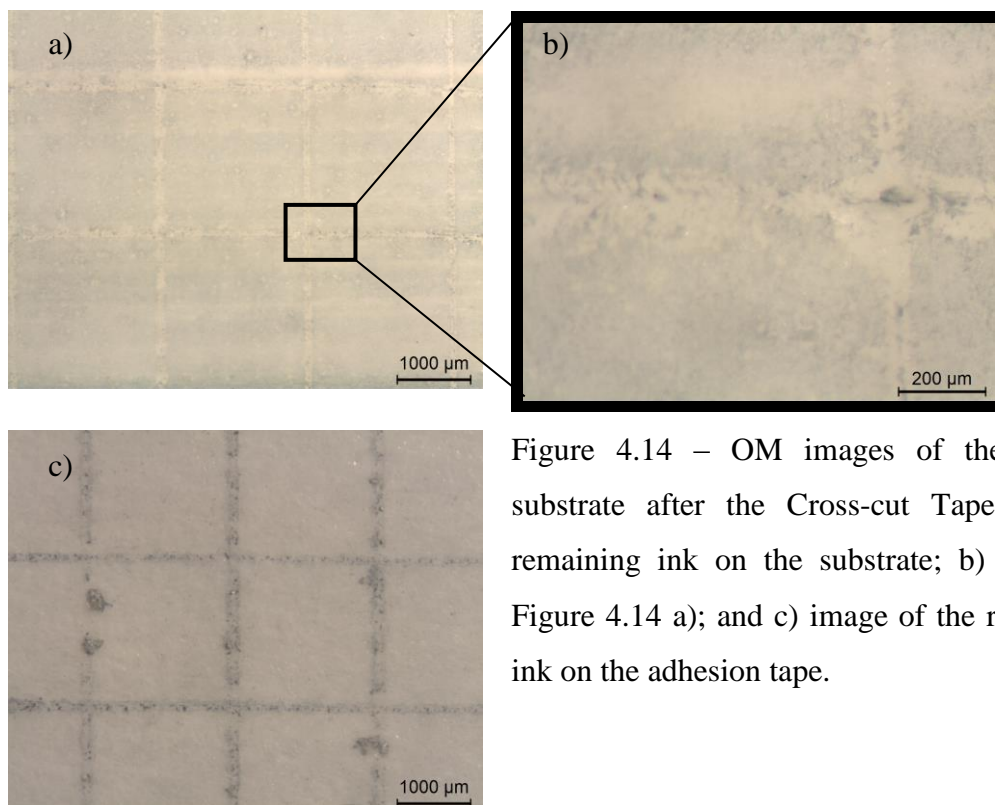


Figure 4.14 – OM images of the printed substrate after the Cross-cut Tape test: a) remaining ink on the substrate; b) detail of Figure 4.14 a); and c) image of the remaining ink on the adhesion tape.

#### 4.2.2. Electrical resistivity measurements

Figure 4.15 shows the variation of the sheet resistance measurement, through Van der Pauw method, according to the number of P3HT layers. As expected, the sheet resistance decreases as the number of printed layers increased, ranging from  $2.01 \times 10^6 \text{ } \Omega/\text{sq}$  to  $1.65 \times 10^5 \text{ } \Omega/\text{sq}$  for 1 to 10 layers, respectively. The amount of used ink is directly related to the electrical performance. These values are much higher when compared to most conducting materials. Despite the low conductivity, this ink could be used to fabricate electrodes for a capacitive sensing configuration. However, this implies the use of several layers of ink, which results in a substantial increase on the material resources, printing costs, and production time. The rather low conductivity does not compromise the development of the printed polymer, but P3HT isn't the most suitable ink to be employed for conductive electrodes, and would certainly have implications on the design, e.g. of the sensing application.

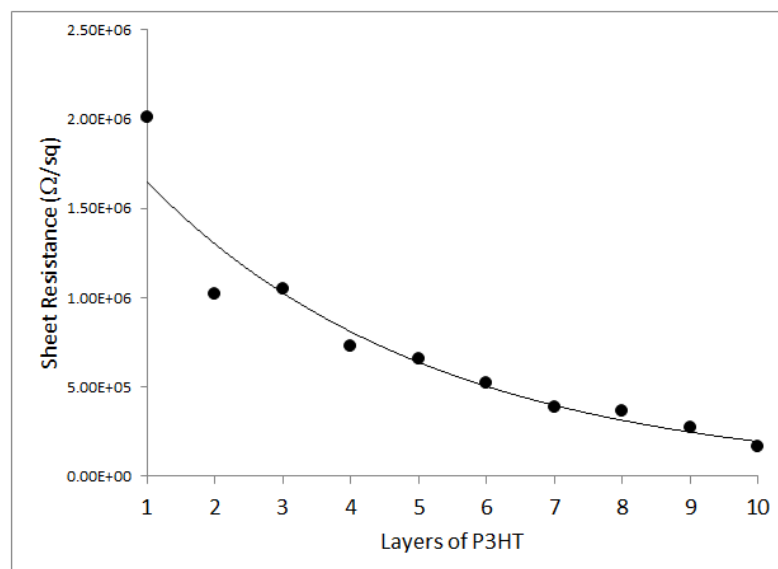


Figure 4.15 –Sheet resistance measurement, through Van der Pauw method, according to the number of P3HT layers.

### 4.3. Summary

The Poly (thiophene – 3 - [2 - (2-methoxyethoxy) ethoxy] - 2,5 - diyl), P3HT, sulfonated ink was inkjet printed on a polymeric substrate, and evaluated to be used as an electrode for sensing applications. Achievement of the desired electrical properties through the selected materials (conductive ink, substrate) and fabrication technology (IPT) was a target. Therefore, multiple iterative steps of experiments were followed for definition of the inkjet printing parameters for enhanced printing resolution and uniformity of the printed layer.

The work with this ink showed that it is an easy ink to work with: it has slow evaporation, it passes through the IJP nozzle without obstruction, it is easy and fast to clean from machine parts with minimal effort.

This Chapter covered, in five sections, the results obtained through experiments:

- The achieved optimized parameters for the inkjet printing of the polymer conductive ink;
- Morphological characterization of the printed ink;
- Thermal characterization of the printed ink;
- The adhesion characterization of the printed ink; and
- The electrical characterization of the printed ink.

The wettability of the substrates was found to be a main obstacle for the ink receptivity. For this reason, a surface treatment of the substrate was needed. A new method was developed in order to increase the substrate surface energies. The method is environmental friendly and low cost. So, in the proposed surface treatment method, micro/nanosized particles (Clay or Silica particles) were spread over the substrate surface and then thermally fixed. This latter step allowed the micro/nanosized particles sinking-in on the polymer surface, resulting in a higher polymer-particle interaction at their interfacial region. The addition of micro/nanosized particles onto the polymer surface increases surface roughness and promotes intermolecular interactions. SP shows a high affinity with the TPU due to the hydrogen-bond interactions between the silanol groups on the silica surface and the soft segments of the TPU [4.12, 4.13]. This improves the intermolecular interactions between SP and the TPU substrate, anticipating a good adhesion between them. Therefore, the developed treatment was effective on:

- increasing the surface roughness of the substrate (by 86%),
- increasing on the critical surface tension of the substrate (by 31 %).

The SP treated surface ensured good surface wetting, creating hydrogen-bond interactions, and making an adequate interphase between SP and the substrate. This novel surface treatment of thermoplastic polymers was applied to the inkjet printing of TPU substrates with conductive inks, and significant improvements on the printability were obtained.

What concerns the printed substrates characterization, the cross-cut OM images revealed that the substrate surface changes didn't affect the ink adhesion. No delamination of the ink layers was detected, presenting less than 5% of removed area. The adhesion of the ink film to the substrate is rated in 0 on a 0-5 scale (where 0 is 0% of removed area and 5 is more than 65% of the removed area). Regarding the electrical characterization, the sheet resistance decreases as the number of printed layers increased, ranging from  $2.01 \times 10^6 \text{ } \Omega/\text{sq}$  to  $1.65 \times 10^5 \text{ } \Omega/\text{sq}$ , for 1 to 10 layers, respectively. The achieved results raised a main concern about the feasibility of P3HT ink to be used for electrodes fabrication on the sensing application. The rather high measured resistivity may be strongly correlated to the final deposited film morphology (no homogeneity of the ink thickness due to the surface roughness). This can be improved either by an increase of the printed layers, using multiple print layers to overcome the high surface roughness and the low electrical conductivity. However, this solution represents a substantial increase of material resources, printing costs, and production time with no increased additional benefit (since the sheet resistance difference between 6 and 10 layers is low).

## REFERENCES

- [4.1] “Plextronics, Inc. Plexcore -Technical bulletin AL-251.”
- [4.2] “[http://www.revistatecnologiagrafica.com.br/index.php?option=com\\_content&view=article&id=92:problemas-comuns-na-impresao-de-filmes-lasticos&catid=39:impresao&Itemid=180](http://www.revistatecnologiagrafica.com.br/index.php?option=com_content&view=article&id=92:problemas-comuns-na-impresao-de-filmes-lasticos&catid=39:impresao&Itemid=180).”
- [4.3] “<http://www.jorplast.com.br/jpset01/pag10.html>.”
- [4.4] “Owens, Wendt, Rabel and Kaelble (OWRK) method. Online <<http://www.kruss.de/services/education-theory/glossary/owens-wendt-rabel-and-kaelble-owrk-method/>>.” [Online]. Available: <http://www.kruss.de/services/education-theory/glossary/owens-wendt-rabel-and-kaelble-owrk-method/>.
- [4.5] S. S. Technical, N. Tn, and T. December, “Practical Contact Angle Measurement ( 5 ),” vol. 49, no. 5, pp. 1–6, 2008.
- [4.6] J. Mei, “Formulation and processing of conductive inks for inkjet printing of electrical components.,” p. 130, *Doctoral Dissertation, University of Pittsburgh*. 2005.
- [4.7] J. S. EOM and S. H. KIM, “Plasma surface treatment of polyimide for adhesive Cu/80Ni20Cr/PI flexible copper clad laminate,” *Elsevier, Amsterdam, PAYS-BAS (1967) (Revue)*, vol. 516, no. 14, pp. 4530–4534, 2008.
- [4.8] J. Lai, B. Sunderland, J. Xue, S. Yan, W. Zhao, M. Folkard, B. D. Michael, and Y. Wang, “Study on hydrophilicity of polymer surfaces improved by plasma treatment,” *Appl. Surf. Sci.*, vol. 252, no. 10, pp. 3375–3379, 2006.
- [4.9] S. Mohanty, C. Ylitalo, and O. S. Woo, “Modeling Drop Shape on Contaminated Surfaces or Surfaces with Physical Structures,” *Langmuir*, vol. 20, no. 6, pp. 2277–2281, 2004.
- [4.10] J. C. McDonald and G. M. Whitesides, “Poly(dimethylsiloxane) as a Material for Fabricating Microfluidic Devices,” *Acc. Chem. Res.*, vol. 35, no. 7, pp. 491–499, 2002.
- [4.11] R. Rioboo and C. Tropea., “Outcomes from a drop impact on solid surfaces.,” *At. Sprays*, vol. 11:, pp. 155–165, 2001.
- [4.12] J. Vega-baudrit, S. M. Carballo, L. De Adhesión, U. De Alicante, and C. Rica, “Thermoplastic Polyurethanes-Fumed Silica Composites: Influence of NCO / OH in the Study of Thermal and Rheological Properties and Morphological Characteristics,” in *Thermoplastic - Composite Materials*, P. A. El-Sonbati, Ed. InTech, 2012, pp. 12–24.
- [4.13] J. Vega Baudrit, M. Sibaja Ballester, P. Vázquez, R. Torregrosa Maciá, and J. M. Martín Martínez, “Properties of thermoplastic polyurethane adhesives containing nanosilicas with different specific surface area and silanol content and silanol content,” *Int. J. Adhes. Adhes.*, vol. 27, no. 6, pp. 469–479, 2007.



# Chapter 5

## **Inkjet Printing of the Poly (3,4-ethylenedioxythiophene) - poly (styrenesulfonate) (PEDOT:PSS) conductive ink**

In this Chapter special attention is placed on the PEDOT:PSS ink. Here, all the results concerning the PEDOT:PSS printing and the characterization of the fabricated printed pattern for use as electrodes are presented.





## 5.1. Inkjet printing of the polymer conductive ink

### 5.1.1. Material's properties

#### • Conductive ink

Table 5.1 presents the summarized physical properties of the commercial grade of the ink used (PEDOT:PSS Orgacon™ IJ-1005).

Table 5.1 – Orgacon™ Physical Properties [5.1, 5.2].

Contains	1-5% Ethanol, 5-10% Diethylene glycol
Conductor component	PEDOT
Solid content (wt%)	0.8
Concentration	0.8% in H <sub>2</sub> O
Electrical Resistivity (Ω.m)	1x10 <sup>-6</sup>
pH	1.5-2.5
Particle size (nm)	25 - 35
Viscosity (mPa.s)	7-12
Surface tension (mN/m)	31 - 34

Note: The tabulated values are from the producer data sheet (Appendix A.7).

#### • Determination of the annealing temperature of the PEDOT:PSS conductive ink

A 24.09 mg PEDOT:PSS sample was evaluated by TGA analyses for assessment of the optimal annealing temperature. Figure 5.1 shows the weight loss variation with temperature. The mass of the polymeric conductive ink starts to decrease at 62.07 °C till 104 °C (with 84.03% of the total weight loss) and between 104 °C till 126°C (with 5.531% of the total weight lost). The 1<sup>st</sup> step of the TGA curve can be associated with the initial temperature at which there are losses of the solvents, little molecules or unstable side chains, that degrades, at lower temperature (indicating no need for annealing at high temperate after printing), and the 2<sup>nd</sup> which its believed to be related to the conductive polymer. The degradation of the ink occurs between 104 °C and 130 °C. No expressive weight loss was registred between 130 °C to 400 °C. From this evaluation, one can concluded that the ink annealing temperature should be between 62.07 °C and 104°C.

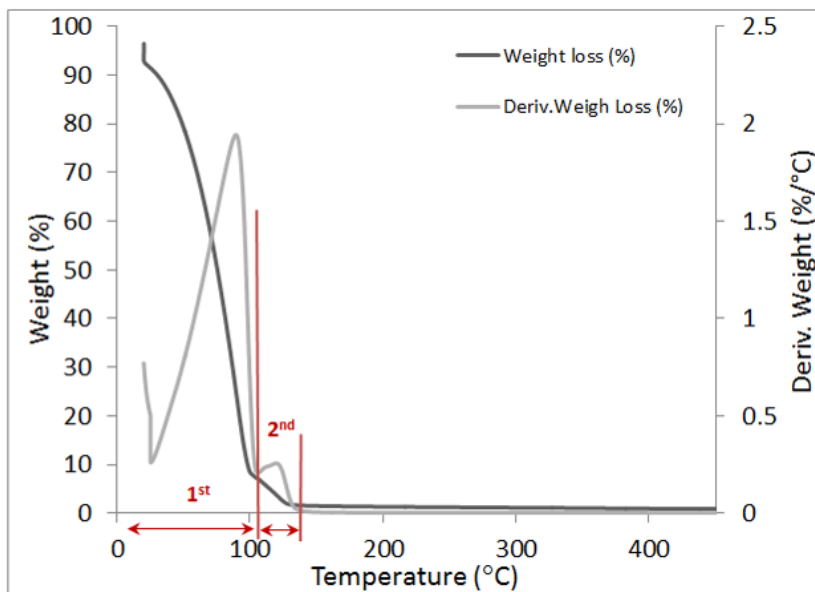


Figure 5.1 - PEDOT mass loss analysis for optimal annealing temperature evaluation.

- **Substrate vs. Ink surface tension**

The ideal critical ST of a substrate should be, at least, 7 to 12 mN/m higher than the ST of the liquid with which it will interact [5.3, 5.4]. According to the suppliers, the ST of the PEDOT:PSS ink is around 31-34 mN/m. The ST measurements of the substrates and the difference with the ink ST,  $\Delta$ ST, is summarized in Table 5.2.

Table 5.2 – ST of the Substrates and of the PEDOT:PSS ink.

Substrate	ST (mN/m)	$\Delta$ ST (mN/m)
PI	39.32	5.32
PET	43.31	9.31
PDMS	13.23	-20.77
TPU	32.49	1.51

\*according to OWRK [5.5, 5.6].

This result allows predicting that the adhesion of the PEDOT:PSS ink (31-34 mN/m), in particular to a clean PDMS substrate (13.23 mN/m) and TPU (32.49 mN/m) will be very difficult ( $\Delta$ ST = -20.77 mN/m and 1.51 mN/m, respectively). The surface energy of PI and PET substrates are good indicators of good wetting and a homogeneous dispersion of this ink.

### 5.1.2. Ink Preparation

For the same reasons described before for the P3HT ink experiments (Chapter 4), before printing, the ink underwent an ultrasonic vibration bath for 3 hours. Then, the inks were filtered by a 0.45  $\mu\text{m}$  pore size glass fiber before filling the ink supply syringe. The ink filtration generated a large amount of foam. After the filtering operation, the ink in the ink supply syringe was kept in rest for about 30 minutes for the complete dissolution of the foam. With the use of a 0.45  $\mu\text{m}$  pore size filter longer nozzles lifetime was observed. Filling procedure of the ink supply syringe was conducted as described in Chapter 3.

### 5.1.3. Preliminary Inkjet printing

Simple rectangular and circular patterns of various sizes were printed on the substrates (Figure 5.2). At this stage, high resolution is not essential for large areas but high conductivity is required for the electrode pattern. All the available 256 nozzles were used in this printing study in order to get the highest as possible throughput and overlapping from 5 to 8 ink-jetted layers at drop spacing of 254  $\mu\text{m}$  (100 DPI), 84.67  $\mu\text{m}$  (300 DPI), 42.33  $\mu\text{m}$  (600 DPI) and 28.22  $\mu\text{m}$  (900 DPI) was tested. Other printhead settings were adjusted according to the results of the iteration steps of experiments with this type of ink, and used substrate.

- **Printed patterns**

Resembling what happened with P3HT ink, and regardless of the substrate, after few seconds (still during printing), the PEDOT:PSS ink printed drops quickly started to join into larger drops (Figure 5.2). This indicates that all substrates have a poor wettability. Once again, several printing attempts with, changes on the temperature of the substrate (in order to speed up the solvents evaporation and improve the printing pattern quality) and the printing parameters were performed, but without any success.

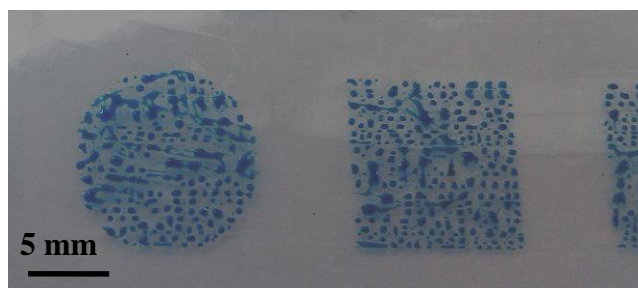


Figure 5.2 - Digital image of TPU with drop formation of the PEDOT:PSS ink (few seconds after printing).

#### 5.1.4. Inkjet printing on the modified substrate

The PEDOT:PSS study proceeded with the SP-TPU substrate (to increase the surface roughness resulting in the increase of the surface contact area) to ensure good surface wetting, and to achieve an adequate transition interphase between the ink layer and the substrate. Table 5.3 reports the optimized printhead main settings used with PEDOT:PSS ink printing.

PEDOT:PSS ink revealed to be quite problematic in terms of jetting performances and reproducibility. As described in Chapter 3, purging procedures are essential and necessary in order to avoid undesired nozzle clogging. The cleaning frequency depends on the inks physical properties (such as density, viscosity, surface tension, volatility and shelf life). These actions cause some material and time waste. The ink with solvents with higher volatility, require higher cleaning frequency. Despite all these cares, permanent damage of nozzles was inevitable.

Table 5.3 - Main printhead settings used for PEDOT:PSS ink.

Main settings	
Drop size	10 pL
Printhead height	3 mm
Substrate Temperature	$\pm 80$ °C*
Printhead Temperature	23 °C
Head speed	60 mm/s
Drop spacing	28.22 $\mu$ m
Maximum Jetting Frequency range	50 kHz

\*80°C was selected because is a temperature below the softening temperature of the TPU, so that the substrate suffers no physical or optical change.

Figure 5.3 shows a digital image of the PEDOT:PSS appearance, printed in the SP-TPU substrate before and after annealing treatment. According to Figure 5.3 a) and to [5.7], the appearance of the printed pattern suggests that the morphology of the drop impact on the dry SP-TPU substrate surface is determined as *Deposition* with an effective deposition of the ink drop on the substrate surface. *Deposition* is considered when the drop, during the impact, deforms without breaking up in smaller drops, and stays attached to the substrate surface.

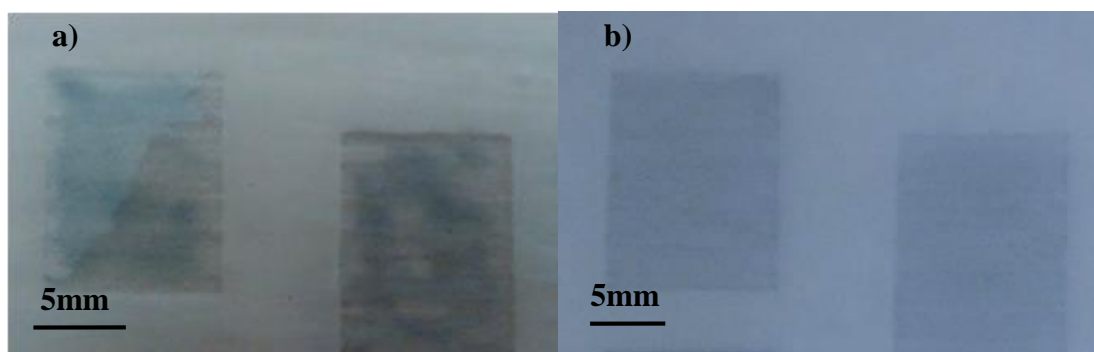


Figure 5.3 - Digital images of the PEDOT:PSS ink printed in the SP-TPU substrate: a) Before annealing; b) After annealing.

With respect to the reproducibility, whenever a new layer was deposited, the solvent slightly affected the previous layer. In other words, incompatibility between layers of the same ink used in multilayered structures was observed. An incompatibility between layers can cause re-dissolution or re-suspension of the previously printed layer preventing uniform and uncontaminated layers [5.8].

Between two subsequent printings, five minutes were required to allow ink drying before printing the next layer. To avoid a long lasting process, heated air flow was used to accelerate the drying between layers and the purging of the printhead was conducted every ink layer printing for the same reason as referred to in the Chapter 4. Five to eight layers of ink were printed. At the nozzles, PEDOT:PSS solvent evaporation revealed to be very quick, causing misdirected jets risking the nozzle clogging. To achieve satisfactory performance, printing pauses between layers were avoided. For the same reason, the temperature of the printhead was kept lower than 23 °C.

After printing, the samples were annealed at 80 °C in oven for at least 8 h in order to allow the complete evaporation of the solvent and to avoid yellowing of the substrate and its deformation.

The use of SP increased the surface roughness and the surface contact area ensured good surface wettability. Figure 5.4 depicts how the SP made an adequate interphase between the ink layer and the substrate.

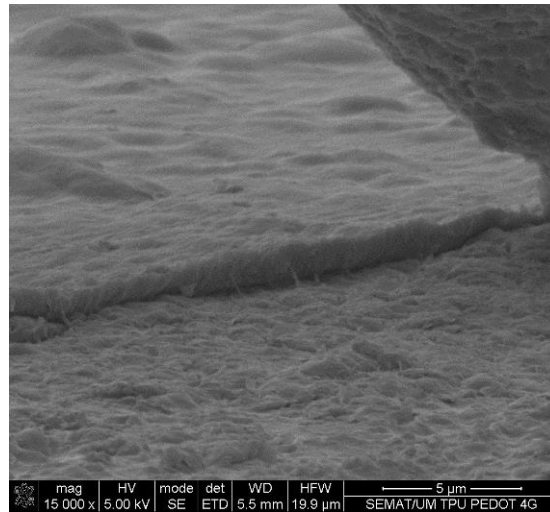


Figure 5.4 - Detail of the interface between ink and modified substrate.

In Figure 5.6 different layers of PEDOT:PSS ink printed on the SP-TPU are observed. The ink thickness increases with the number of layers, between  $\pm 0.9$  to  $1.71 \mu\text{m}$  for five to seven layers, respectively. The mean roughness of the SP-TPU substrate (see Figure 5.5) clearly decreases with the increase of printed layers. This indicates good dispersion and embedment of the ink on the substrate.

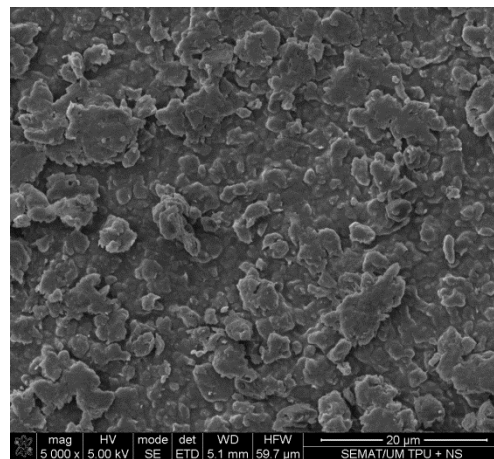


Figure 5.5 - SEM images of SP-TPU top substrate surface.

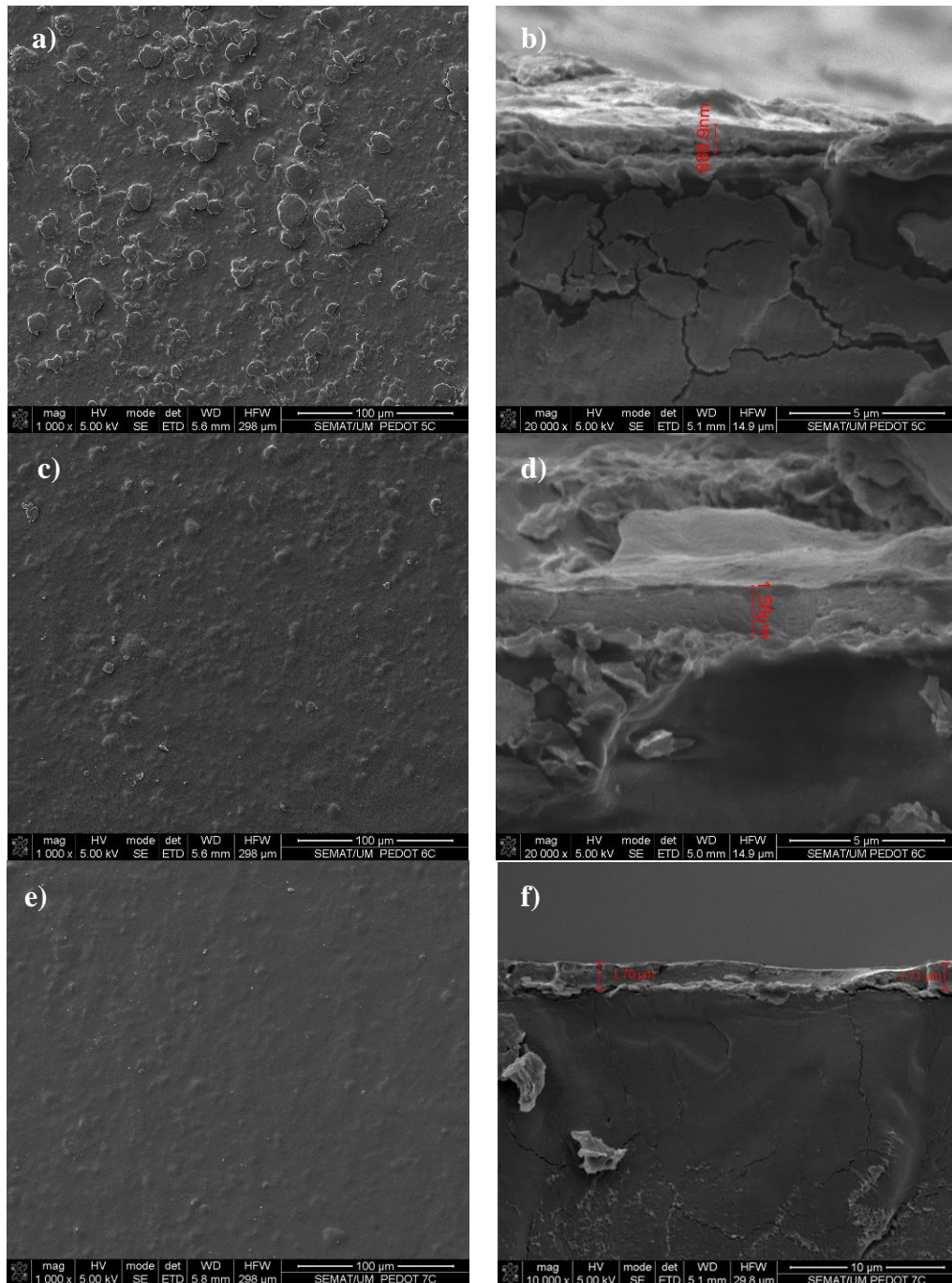


Figure 5.6 - SEM images of SP-TPU substrate with inkjet printed PEDOT:PSS ink: a) top surface with five layers of ink; b) fractured cross section surface with five layers of ink; c) top surface with six layers of ink; d) fractured cross section surface with six layers of ink; e) top surface with seven layers of ink ;f) fractured cross section surface with seven layers of ink.

The AFM topographical image in Figure 5.7 shows the surface morphology of the printed SP-TPU with PEDOT:PSS ink. As previously measured (Figure 4.8 b from Chapter 4) the RMS roughness and mean Ra of the SP-TPU surface is 194.94 nm and 152.40 nm, respectively. With six layers of PEDOT, the measured RMS and Ra changed to 49,519 nm and 40.466 nm, respectively, in the new surface. These results indicate that the ink layers greatly contributed for



the decreased of the surface roughness. These percentage reductions of 74.6% and 73.45%, respectively, are an indication of the great decrease of the SP-TPU surface roughness with the increase of ink layers.

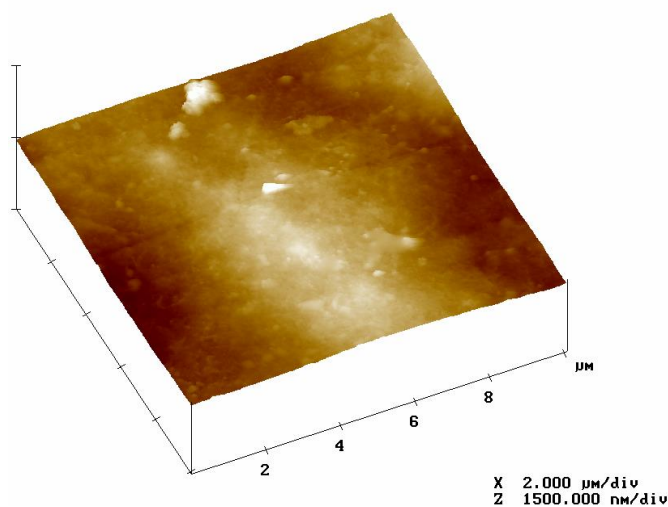


Figure 5.7 - AFM topographic image of the printed SP-TPU surface with six layers of PEDOT. The image size is 10  $\mu\text{m}$  x 10  $\mu\text{m}$ .

## 52. Adhesion and electrical characterization of the printed substrates

### 5.2.1. Adhesion test

OM was used for the qualitative evaluation of the samples tested to assess the adhesion between substrate and ink. Figure 5.8 shows the remaining ink on the substrate and the removed ink on the adhesion tape after the Cross-cut Tape test. Through the visual analysis of remaining ink on the substrate and according to ASTM - D3359, method B) qualitative evaluation scale (see Comparison Chart in Appendix A.8), the level of adhesion of the ink to the substrate is high. A visual evaluation doesn't detect any delamination; the cross-cut didn't affect significantly the ink layer, presenting less than 5% of removed area. The adhesion of the ink film to the substrate is rated in 1 on a 0-5 scale, where 0 is 0% of removed area and 5 is more than 65% of the removed area.

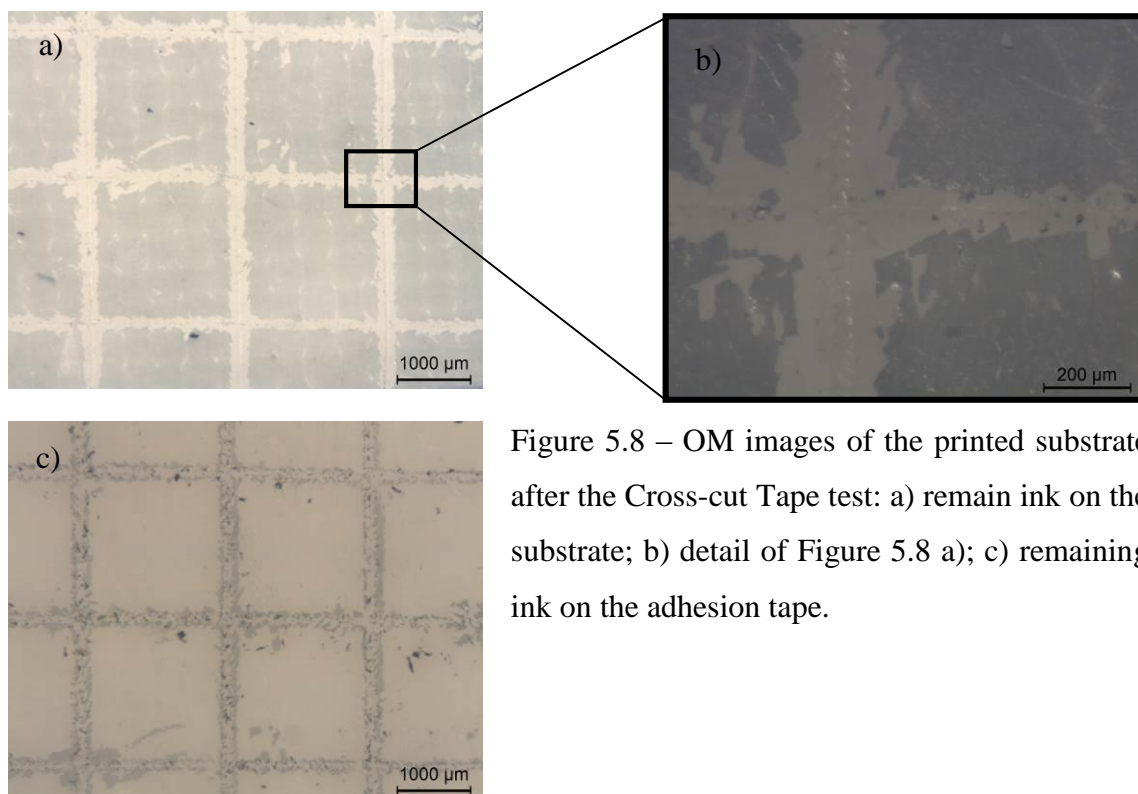


Figure 5.8 – OM images of the printed substrate after the Cross-cut Tape test: a) remain ink on the substrate; b) detail of Figure 5.8 a); c) remaining ink on the adhesion tape.

### 5.2.2. Electrical resistivity measurements

The electrical performance of the printed TPU films was also evaluated. Figure 5.9 shows the variation of the sheet resistance measurement, according to the number of PEDOT:PSS layers. With the increase of ink layers no visible change was observed in the sheet resistance. The measured sheet resistance ranges between  $2 \times 10^3 \Omega/\text{sq}$  to  $1 \times 10^4 \Omega/\text{sq}$  for 5 to 8 layers, respectively. In contrast to the P3HT results, the amount of used ink isn't directly related to the electrical performance. From these results one can conclude that the layer thickness has no effect on electrical resistivity. Nevertheless, the sheet resistance range measured on the printed PEDOT:PSS ink proved to be a suitable ink to be used as conductive electrodes for sensing applications without needing many layers of ink, saving material resources, printing costs, and production time.

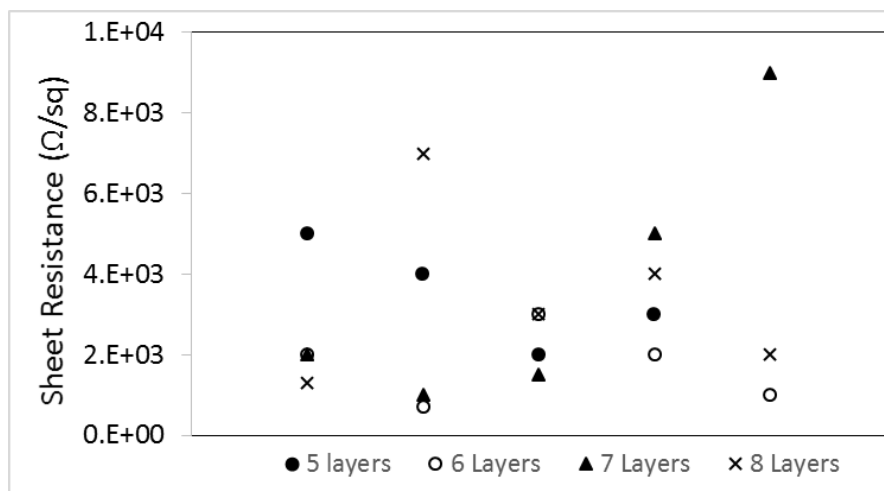


Figure 5.9 - Sheet resistance measurement, according to the number of PEDOT:PSS layers.

### 5.2.3. Piezo-resistive measurements

A conductive ink layer on a substrate with a good flexibility and stretchability needs to be able to respond mechanically to the applied stress while preserving the integrity of the printed structures, as well as the respective mechanical and electrical properties (required for sensing application). Therefore, it is of paramount importance to prove that the ink is able of following the flexibility and deformations along with the substrate, without breaking or losing adhesion and its conductivity properties. Also, if large conductivity variations occur for applied strain, it indicates that the pair ink/substrate might be used for sensing applications using the piezo-resistive effect. Measurements of the piezo-resistive effect on the printed flexible electrodes, checks whether the printed ink meets the requirements of the envisaged application, establish their limits, and shows the potential of the material to be used in sensing applications.

Figure 5.10 shows a typical SP-TPU tensile curve. The SP-TPU deformation till rupture is very high, approximately 2500%. Figure 5.11 depicts the mechanical properties of the SP-TPU substrate (for comparison) and SP-TPU inkjet printed substrate (with 6 layers of PEDOT:PSS). These measurements were conducted in order to determine if the ink affects the substrate mechanical properties.

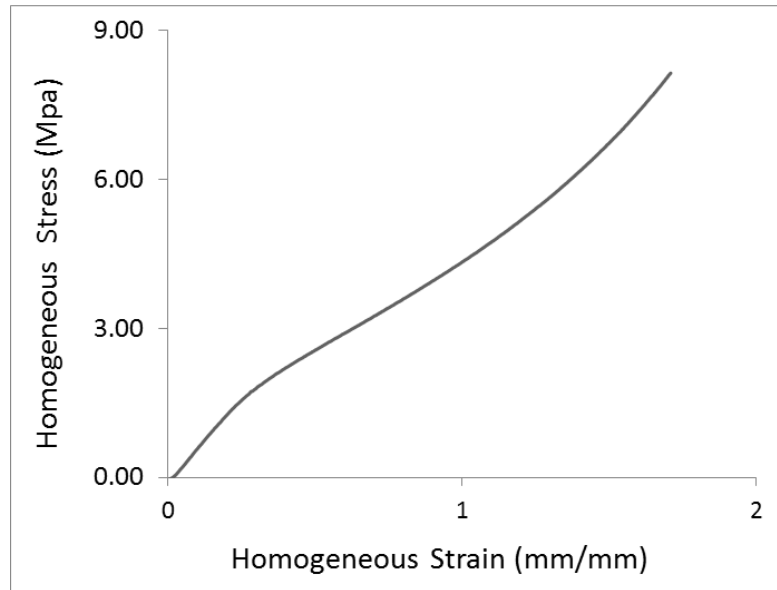


Figure 5.10 – Typical TPU Stress vs. Strain Curve.

Figure 5.11 depicts the stress-strain curves in the strain range where piezo-resistive measurements were made. The experimental results indicate that the SP-TPU has a Young's Modulus and a Yield stress of  $6.23 \pm 0.44$  MPa and  $8 \pm 0.2$  MPa, respectively, and the printed substrate have a Young's Modulus and a Yield stress of  $5.8 \pm 0.55$  MPa and  $1.5 \pm 0.05$  MPa (the rupture stress is considered at the moment the ink breaks), respectively. These results demonstrate a linear behavior and that the mechanical performance of the substrate wasn't affected by the presence of the polymer conductive ink.

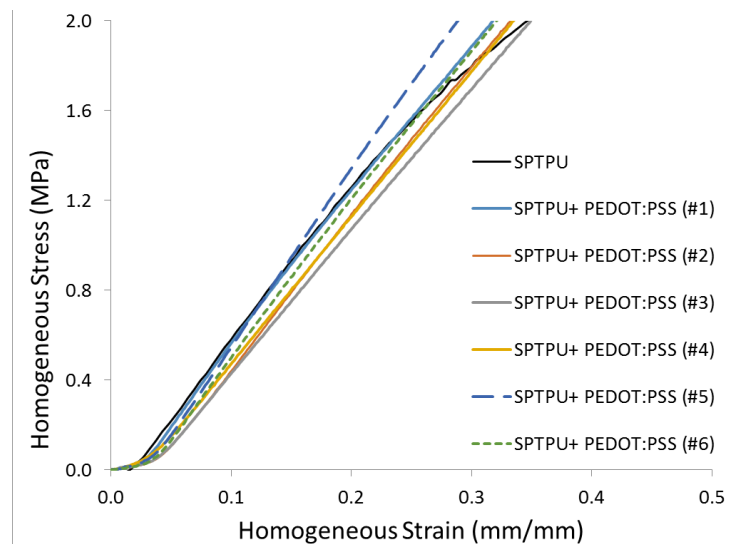


Figure 5.11 – Mechanical properties of the SP-TPU substrate (for comparison) and SP-TPU substrate inkjet printed (with 6 layers of PEDOT:PSS).

The results of the piezo-resistive measurements of SP-TPU substrate inkjet printed with 6 layers of PEDOT:PSS are presented below. Figure 5.12 and Figure 5.13 present the variation of the electrical resistance with the Homogeneous stress and Homogeneous Strain, respectively. The initial electrical resistance is of  $\pm 295.85 \Omega$ . During the mechanical tests, it was possible to observe that the PEDOT:PSS ink had good deformation properties, as it was able to follow the deformation of the SPTPU substrate without visible rupture of the ink. No significant resistance change was observed till  $\sim 0.5$  MPa of the applied stress (around 11.7 % of deformation) showing great linear behavior and confirming the high reliability and operation stability of the printed electrodes. After 0.5 MPa of the applied stress, the electrical resistance increases and presents a wide variation between specimens, and the loss of electrical contact occurs around  $\sim 50.8\%$  of deformation. Despite the wide variation between specimens, the rate of resistance change is very similar between samples, which is a good indication if one wants to use the measured piezo-resistive effect for sensing applications. This observed variation of electrical resistance from specimens with the same number of ink layers may be explained by a not homogeneous distribution of the conductive polymer particles present in the conductive path. This heterogeneous distribution may have occurred during the printing process or could be influenced by the adopted surface treatment.

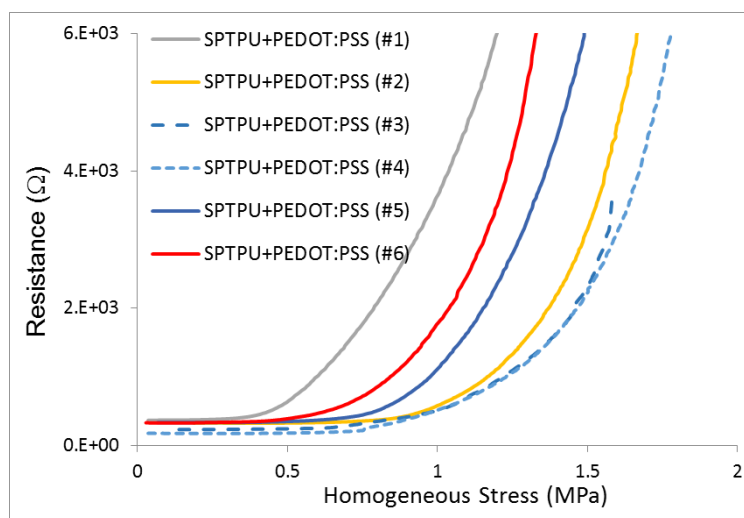


Figure 5.12 - Electrical resistance vs. Homogeneous Stress.

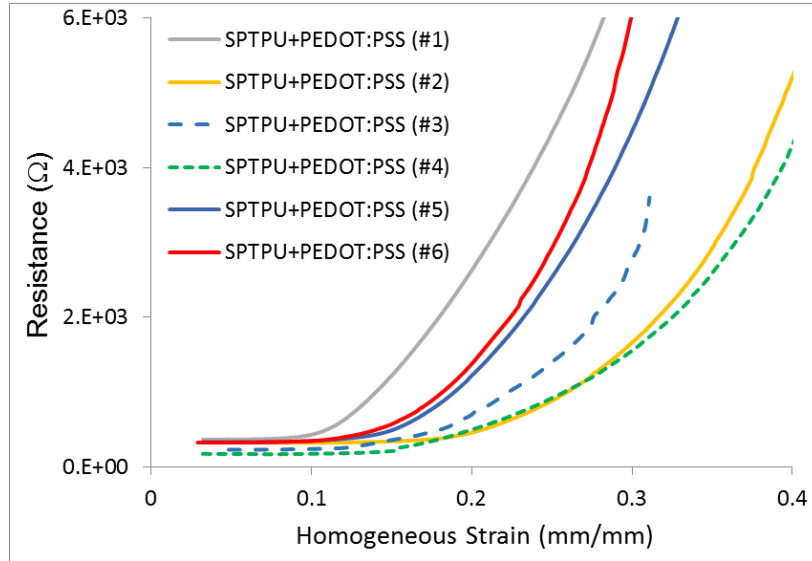


Figure 5.13 - Electrical resistance vs. Homogeneous Strain.

The *Gauge Factor (GF)*, an adimensional parameter, which is defined as the fractional change in resistance per deformation unit, translates the resistance changes in the material as a function of the deformation caused by the applied mechanical stress [5.9], and is given by:

$$GF = \frac{\frac{R-R_0}{R_0}}{\varepsilon} , \quad \text{Equation 5.1}$$

where  $R_0$  is the resistance of the material before deformation.

For the study of the piezo-resistive effect of the ink, the electrical resistance  $R$  of the PEDOT:PSS was measured during the tensile tests. From the measured resistance ( $R$ ) and strain ( $\varepsilon$ ),  $GF$  was determined by Equation 5.1. Rearranging this equation:

$$\frac{\Delta R}{R_0} = GF \cdot \varepsilon , \quad \text{Equation 5.2}$$

A linear relationship between  $\Delta R/R_0$  and  $\varepsilon$  is obtained with slope  $GF$ .

Figure 5.14 presents the measured resistance difference vs. applied strain for specimen five (with results close to the average behavior of all specimens).

The relationship between  $\Delta R/R_0$  and  $\varepsilon$  is non-linear, reflecting a varying  $GF$  with strain level. To determine the  $GF$ , the curve was divided in three regions. The 1<sup>st</sup> region was considered in the lower strain range (<15%), a 2<sup>nd</sup> region between 15% - 40%, and the 3<sup>rd</sup> region for a higher strain range, between 40% - 60%. The  $GF$  was calculated by fitting the curve in each section,

designate by GF1, GF2 and GF3, respectively, by Equation 5.2. In the lower strain range, the PEDOT:PSS showed a GF of 5.21 indicating that the ink conductivity is changing with deformation (if resistance changes in the material were just a function of the deformation caused by the applied mechanical stress, the GF would be  $1+2\nu$ , with  $\nu$  being the Poisson's Ratio, i.e.,  $R$  would increase due to the decrease of cross-section area and increase of length of the PEDOT:PSS film). On the 2<sup>nd</sup> region (intermediate strain level) GF2 was ~88. In the high strain range the determined GF3 was ~437. In all three regions a clear contribution of the intrinsic piezo-resistive effect of the ink layer over the geometrical factor is observed. The huge GF observed on the second and third region show that this material, and despite the non-linearity, has high potential for sensing applications using the piezo-resistive effect. The high GF achieved may be related to the surface treatment. With the increase of roughness, better wettability is achieved, and since the final surface morphology is not uniform it may induce large resistance variation with strain.

Due to some technical difficulties (sample sliding in the beginning of the test together with high contact resistance) the piezo-resistive effect still needs to be better characterized. Also extended tests are required to check reliability (repetition tests) and stability of the huge piezoresistive effect observed.

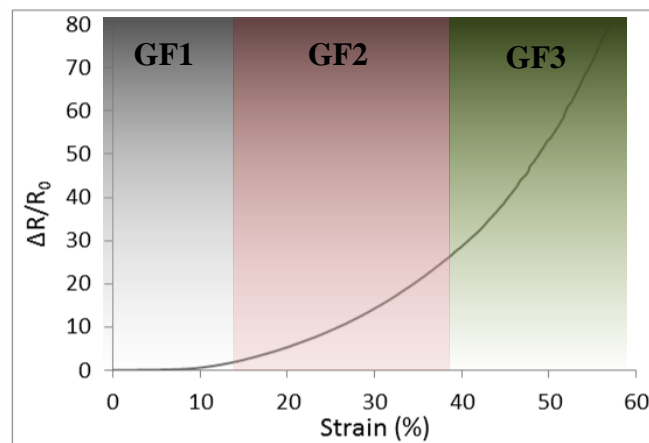


Figure 5.14 – Curve profile of the PEDOT:PSS measured resistance changes during tensile mechanical tested, with an initial resistance ( $R_0$ ) of  $\pm 295.85 \Omega$ .

### 5.3. Summary

The Poly (3,4-ethylenedioxythiophene) - poly (styrenesulfonate) (PEDOT:PSS) conductive ink was inkjet printed in a polymeric substrate, aiming its use in a flexible application. The challenge was the development of a printed pattern with suitable electrical properties. This includes the selection of appropriated materials (conductive inks, substrates) and fabrication technology (in this case, IPT). Through multiple iterative steps of experiments, the inkjet printing parameters were defined in order to achieve an enhanced printing resolution and uniformity of the printed layer. Working with this ink was complicated, when compared to the P3HT, due to its fast evaporation, increasing the risk of nozzle obstruction, and the need of a more cleaning effort.

The obtained experimental results are covered in six sections: achieved optimized parameters for the inkjet printing, ink thermal characterization, determination of the level of adhesion of the printed ink to the surface-treated substrate, electrical characterization of the printed ink and piezo-resistive effect evaluation of the printed substrate.

Once again, the proposed substrates revealed to have poor wettability when working with PEDOT:PSS ink. For this reason, a surface treatment of the substrate was needed. Good surface wetting was achieved with the SP treated surface and an adequate transition interphase between the PEDOT:PSS ink layer and the substrate was achieved.

What concerns the printed substrates characterization, the cross-cut tests revealed that substrate surface changes didn't affect the ink adhesion. No delamination of the ink layers was detected, presenting less than 5% of removed area. The adhesion of the ink to the substrate is rated in 1 on a 0-5 scale, according to ASTM - D3359, method B.

Regarding the electrical characterization, no effect on the number of layers was observed in the sheet resistance. In contrast to the P3HT results, the amount of used ink isn't directly related to the electrical performance. Nevertheless, the sheet resistance range measured (between  $2 \times 10^3 \Omega/\text{sq}$  to  $1 \times 10^4 \Omega/\text{sq}$  for 5 to 8 layers, respectively.) on the printed PEDOT:PSS ink makes this material interesting for the sensing application.

Tensile test of the printed substrates were performed in order to characterize its mechanical properties. PEDOT:PSS ink had good deformation properties, as it was able to follow the deformation of the SP-TPU substrate without visible rupture of the ink, demonstrating a high reliability and operation stability of the printed pattern. Comparatively to the P3HT, PEDOT has a more difficult processability, but offers a best compromise between electrical conductivity and stability. Also, the huge piezo-resistive effect measured reveals this material to have high potential in sensing applications, acting as standard piezo-resistive gauge for example. The



achieved pattern properties (electrical resistivity and low Young Modulus), resulting from the combination of the high flexible material, a conducting polymer material, and the manufacturing technique are the prominent factor for the design and development of a flexible sensor with high strain capabilities.

**REFERENCES**

- [5.1] “Sigma Material Safety Data Sheet.” [Online]. Available: <http://www.sigmaaldrich.com/medium/structureimages/79/mfcd07371079.png>.
- [5.2] G. Disario, “for Flexible Organic Photovoltaics for Flexible Organic Photovoltaics,” vol. 55, no. September 2010, 2011.
- [5.3] “Revista tecnologia gráfica <[http://www.revistatecnologiagrafica.com.br/index.php?option=com\\_content&view=article&id=92:problemas-comuns-na-impressao-de-filmes-elasticos&catid=39:impressao&Itemid=180](http://www.revistatecnologiagrafica.com.br/index.php?option=com_content&view=article&id=92:problemas-comuns-na-impressao-de-filmes-elasticos&catid=39:impressao&Itemid=180)>.”
- [5.4] “Jorplast <<http://www.jorplast.com.br/jpset01/pag10.html>>.”
- [5.5] “Owens, Wendt, Rabel and Kaelble (OWRK) method. Online <<http://www.kruss.de/services/education-theory/glossary/owens-wendt-rabel-and-kaelble-owrk-method/>>.” [Online]. Available: <http://www.kruss.de/services/education-theory/glossary/owens-wendt-rabel-and-kaelble-owrk-method/>.
- [5.6] S. S. Technical, N. Tn, and T. December, “Practical Contact Angle Measurement ( 5 ),” vol. 49, no. 5, pp. 1–6, 2008.
- [5.7] R. Rioboo and C. Tropea., “Outcomes from a drop impact on solid surfaces,” *At. Sprays*, vol. 11:, pp. 155–165, 2001.
- [5.8] U. Caglar, “Studies of Inkjet Printing Technology with Focus on Electronic Materials,” Universidade de Tampere, 2009.
- [5.9] S. Beeby, G. Ensell, M. Kraft, and N. White, *MEMS Mechanical Sensors*, Artech Hou. Boston, 2004.



# Chapter 6

## **Inkjet Printing of the Silver-based conductive ink**

In this Chapter special attention is placed on the silver-based ink. Here, all the results concerning the silver-based ink printing and the characterization of the fabricated conductive lines are discussed.



## 6.1. Inkjet printing of the silver-based inks

### 6.1.1. Material's properties

- **Conductive ink**

Table 6.1 presents the summarized physical properties of the commercial grade of the used Silver ink. Ag-IJ10, from Applied Nanotech, Inc., is the trade name of the silver-based ink, designed for piezoelectric inkjet printing of conductive features on several substrates.

Table 6.1 - Ag-IJ10 silver-based ink physical properties [6.1].

Typical properties	
Solvent	Organic
Solid Content	45 wt%
Electrical Resistivity	10-50 $\mu\Omega$ -cm*
Viscosity	4-5 mPa.s**
Surface Tension	28-35 mN/m

\*Dependent on sintering temperature and time - higher temperature and longer sintering time results in lower resistivity and better adhesion to the substrate;\*\* Measured at 100 rpm and 25°C with Brookfield VLDV-II+PRO/ULA viscometer. Note: The tabulated values are from the producer data sheet (Appendix A.7).

- **Preliminary determination of the sintering temperature of the Silver-based ink**

A 25.206 mg silver-based ink sample was evaluated by TGA for assessment of the optimal sintering temperature. Figure 6.1 shows the weight loss variation with temperature. No expressive weight loss was observed between 30°C to 45°C. The mass of the silver-based ink starts to decrease significantly around 130.36 °C. The 17.79 % weight of material left is believed to be the remained silver nanoparticles. The 82.21% of material loss reported by the TGA result is believed to be related to additives, solvents, and the organic ligand shells, which the silver nanoparticles are encapsulated, called a capping agent, to form a uniform and stable dispersion, preventing particles agglomeration. This capping agent is removed after printing through curing or sintering to allow physical contact between nanoparticles. Hereupon, it is understood that at 130.36 °C, the capping agent present in the ink composition starts to degrade. Although, this temperature may not be sufficient for consolidation of the printed pattern and welding the silver nanoparticles to each other,

forming continuous connectivity, i.e., the percolation network that will assign the aspired conductivity.

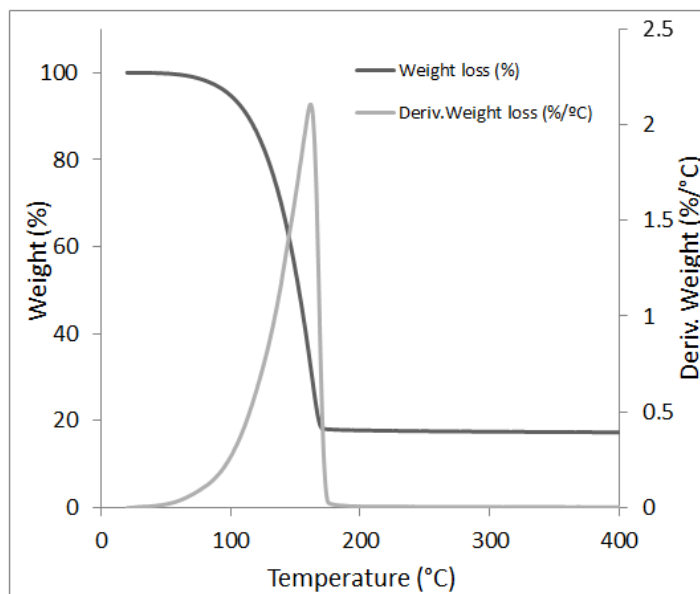


Figure 6.1 – Silver-based ink mass loss analysis for optimal annealing temperature evaluation.

The electrical resistance over a single layer inkjet printed line was measured, during heating (on an oven), at the same heating rate as used for the TGA, i.e.  $10\text{ }^{\circ}\text{C}\cdot\text{min}^{-1}$ . Figure 6.2 shows TGA measurements vs. surface resistivity. Until  $80\text{ }^{\circ}\text{C}$  no electrical resistivity change was registered. The resistance shows a sharp decrease around  $100\text{ }^{\circ}\text{C}$ , where the surface resistivity ( $\rho_s$ ) of the printed line decreases drastically from  $2.1 \times 10^{11}\ \Omega$  to  $750\ \Omega$ . This means that, for this ink, it is possible to convert the organometallic silver ink into metallic silver (particles) at relatively low temperatures, depending on the substrate. Upon further heating, the resistance continues to decrease, but in a gradual way, until  $0.3\ \Omega$  at  $200\text{ }^{\circ}\text{C}$ , indicating the binding of the silver ink particle's agglomerates into larger clusters, forming denser silver networks.

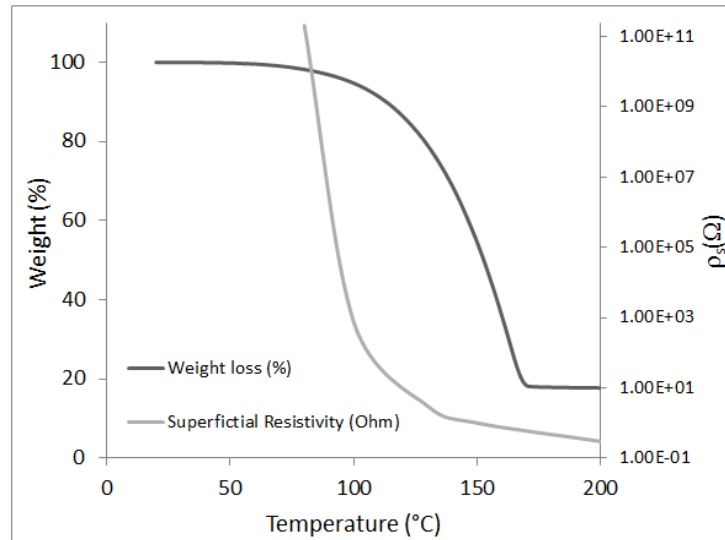


Figure 6.2 – TGA measurements vs. Surface Resistivity ( $\rho_s$ ).

Preliminary sintering tests (Temperature vs. Time), conductive measurements and morphological analysis of the printed silver-based ink were performed. Figure 6.3 shows the temperature and time influence on the sintering of the silver-based ink on a glass substrate. For this purpose, printed silver ink on a cleaned glass substrate was sintered in a oven at different temperatures (100°C, 130°C, 150°C and 200°C) and the surface electrical resistivity measured every 10 min for evaluation of temperature and time influence. At 100 °C a decrease of the surface resistivity, from  $10^{11} \Omega$  to  $10^3 \Omega$ , is observed but this value remains even for long periods of time, indicating that at 100 °C, time is not the determining factor for conductivity achievement, even for longer periods of time. At higher temperatures (from 130 °C to 200 °C), lower resistivity (with the capping agent degradation and the welding of the silver nanoparticles) is achieved with shorter periods of time. As expected, for higher temperatures, less sintering time is needed. As observed in Figure 6.3, after 20 minutes of sintering, the variations of resistivity between 130 °C and 200 °C of sintering temperature are not significant, which leads to the conclusion that 130 °C of sintering temperature should be enough, leading to an acceptable conductivity. The detail SEM image shown in Figure 6.3, testify the silver network formation of the printed ink with 60 minutes of sintering at 130 °C. Furthermore, the small voids observed in the SEM image, are believed to be formed by evaporation of the solvent in the ink. In this image, one can clearly observe the welding of the silver nanoparticles forming continuous connectivity, i.e., a percolation path.



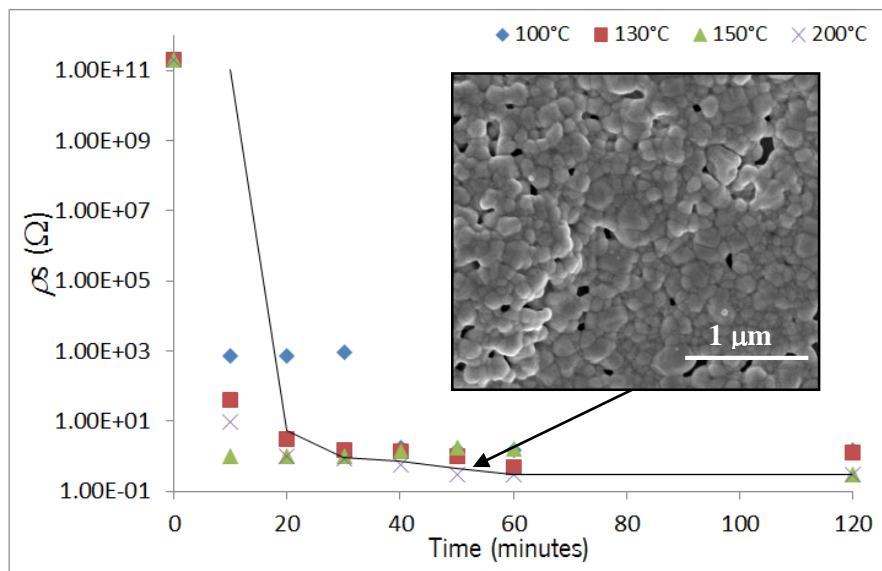


Figure 6.3 – Temperature and time influence on the sintering of the Silver-based ink on glass substrate. Detail SEM image of the printed ink with 60 minutes of sintering at 130 °C.

- **Substrate vs. Ink surface tension (ST)**

According to the suppliers, the ST of the silver-based ink is around 28-35 mN/m. As mentioned before, the ideal critical ST of a substrate should be at least 7 to 12 mN/m higher than the ST of the liquid with which it will interact [6.2, 6.3]. The ST measurements of the substrates and their difference with the ink ST,  $\Delta ST$ , are summarized in Table 6.2.

Table 6.2 - ST of the Substrates and of the silver-based ink (28-35 mN/m).

Substrate	ST (mN/m)	$\Delta ST$ (mN/m)
KAPTON	39.32	11.32
PET	43.31	15.31
PDMS	13.23	-14.77
TPU	32.49	4.49

\*according to OWRK [6.4, 6.5].

The adhesion of the silver-based ink (28-35 mN/m), particularly to a clean PDMS (13.23 mN/m) and TPU (32.49 mN/m) substrate will be very difficult ( $\Delta ST = -14.77$  mN/m and 4.49mN/m, respectively). A surface treatment is required. The surface energies of PI and PET substrates are good indicators of good wetting and homogeneous dispersion of the ink.

### 6.1.2. Ink Preparation

Before printing, the silver-based ink underwent an ultrasonic vibration bath for 3 hours. Then, the ink was filtered by a 0.45  $\mu\text{m}$  pore size glass fiber filter before filling the ink supply syringe. After the filtering operation, the ink in the syringe was kept in rest for about 30 minutes for the complete dissolution of the foam eventually present in the ink because of the filtering process. Filling procedure of the ink supply syringe was conducted as described in Chapter 3.

### 6.1.3. Preliminary Inkjet printing

Line patterns (for electrical path testing) with distinct thickness (Figure 6.4) and different distance between them were printed on PI, PET, PDMS, and TPU substrates. For electrical connection lines, high resolution and high conductivity are required. All the available print head 256 nozzles were used in this printing study in order to get the highest possible throughput and overlapping at drop spacing of 254  $\mu\text{m}$  (100 DPI), 84.67  $\mu\text{m}$  (300 DPI), 42.33  $\mu\text{m}$  (600 DPI) and 28.22  $\mu\text{m}$  (900 DPI) was tested. Other printhead settings were adjusted according to the results of the iteration steps of experiments with the silver-based ink and to the used substrate.

- **Printed patterns**

Printing of silver channels lines is much more problematic since high resolutions are required. Thinner lines require less space, giving more freedom for patterning. On the other hand, an increased number of layers may be required to achieve enough conductivity for the electrical connections, making it more difficult to obtain higher resolutions with printed overlays. Figure 6.4 shows a schematic of the printing pattern used to test the resolution of printed Ag lines.

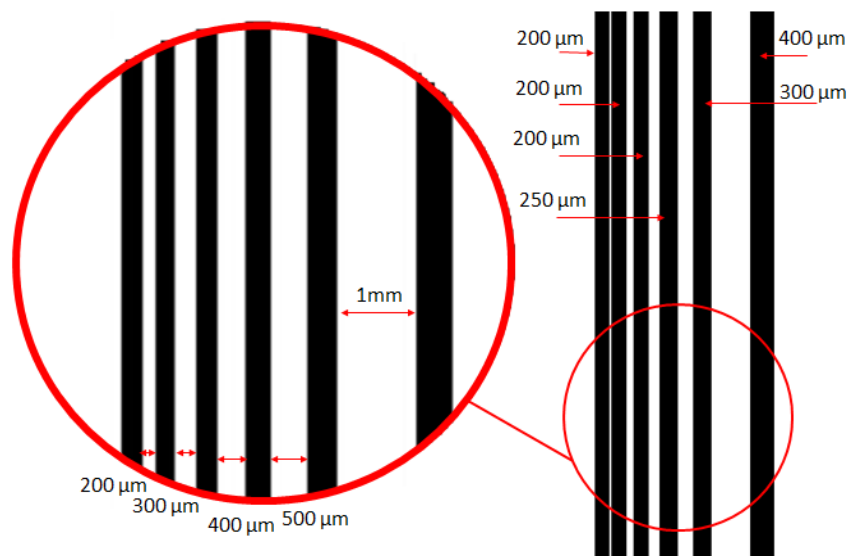


Figure 6.4 – Schematic of the printing pattern to test the resolution for Ag lines printing.

Multiple iterative steps of experiments were performed. Next, some results of these trials are presented:

- Silver-based ink printed on the PDMS substrate had good print quality (in all drop spacing range), although, as predicted by the ST measurements, the ink adhesion was notoriously weak. During sample handling, the printed pattern was peeled off very easily. Adhesion tests became an unnecessary test. PDMS material without an effective surface treatment is unsuitable to be used as substrate.
- Silver-based ink printed on the PI substrate had a very poor printing quality (in all drop spacing ranges). A printed layer with a drop spacing of 254  $\mu\text{m}$  (100 DPI) revealed to be insufficient to achieve a complete printing line. Decreasing the drop spacing (between 84.67  $\mu\text{m}$  and 28.22  $\mu\text{m}$ ) also lead to unsatisfactory results. With only 84.67  $\mu\text{m}$  (300 DPI) flooding was observed. Figure 6.5 shows a digital image of the printed pattern. Several attempts were made to obtain thinner lines, but all failed. Fluctuations in the direction of the droplets induce irregularities on the printed pattern, leading to the formation of short circuits between lines. Enhancement of the ink drying by increasing the temperature of the ink was not an option due to the high risk of nozzle clogging. The increase of the substrate temperature was not effective.

Contrary to what the ST measurements indicated, the adhesion tests revealed a poor adhesion of the ink to the PI substrate (Figure 6.6). The adhesion of the ink film to the substrate is rated as 5 on a 0-5 scale, where 0 is 0% of removed area and 5 is more than 65% of the removed area. An increase of the surface energy using surface treatment is need, although, as explained in Chapter 4, the limitation of space inside of the available vacuum chamber for plasma treatment, restricting the size of the sample, among other reasons, makes this a not possible solution, and therefore, this study didn't proceed with PI substrates.



Figure 6.5 - Example of flooding of one layer of the printed silver-based ink (with drop spacing of 28.22  $\mu\text{m}$  (900 DPI)) on a clean PI substrate.

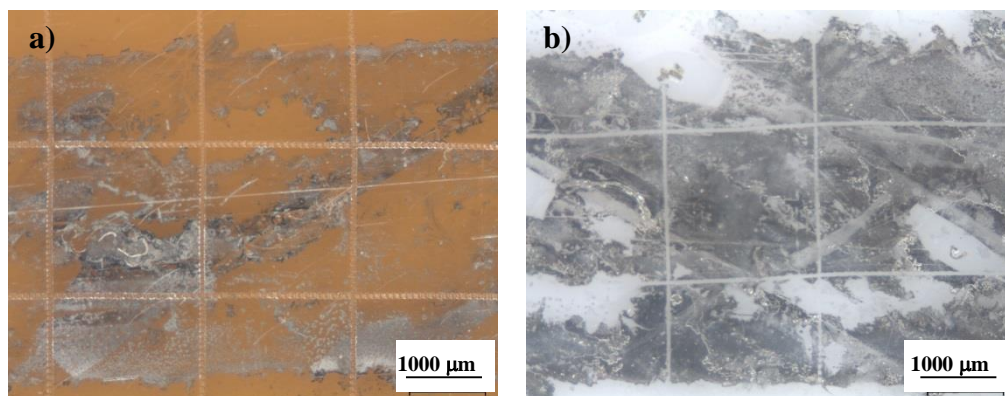


Figure 6.6 - OM images of the sintered silver-based ink printed on a PI substrate after the Cross-cut tape test: a) remain ink on the substrate; and b) image of the remaining ink on the adhesion tape.

- Silver-based ink printed on the PET substrate had once again a very poor print quality. A printed layer with a drop spacing of 254 μm (100 DPI) revealed to be insufficient to achieve a complete printing line. Decreasing the drop spacing (between 84.67 μm and 28.22 μm) also lead to unsatisfactory results. In this case, dropping was observed. The indicated iterative steps from the flowchart (Chapter 3 Figure 3.15) were followed, but with no success. For this reason, it was also impossible to proceed this study with the PET substrate.
- Silver-based ink printed on a clean TPU substrate showed good wettability. One printed layer with a drop spacing of 254 μm (100 DPI) revealed unsuitable, without full padding achievement (Figure 6.7a)). Increasing the number of layers of silver ink didn't guarantee a complete printed pattern. One layer of the silver-based ink with drop spacing of 28.22 μm (900 DPI) resulted on the flooding of the ink. Several printing attempts were made changing the temperature of the substrate (in order to speed up the solvents evaporation and improve the printing pattern quality), but without success. Silver-based ink printed on a clean TPU substrate with a drop spacing of 84.67 μm was tested and its results are presented next.

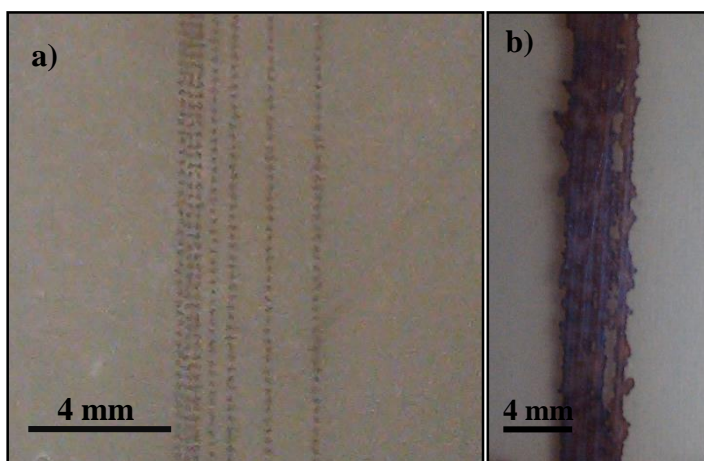


Figure 6.7 – Image of clean TPU substrate: a) one layer of printed silver-based ink lines with drop spacing of 254  $\mu\text{m}$  (100 DPI); b) flooding of one layer of the silver-based ink (with drop spacing of 28.22  $\mu\text{m}$  (900 DPI)).

#### 6.1.4. Inkjet Printing on TPU substrates

Good surface wetting (an adequate transition interphase between the ink layer and the substrate) was achieved with a drop spacing of 84.67  $\mu\text{m}$  (300 DPI) on a clean TPU substrate. This ink revealed to be quite problematic in terms of filtering, jetting performances, and reproducibility due to the high solid particle content (resulting on temporary clogging of the nozzle, also causing drop deviations (Figure 6.8 b)). For this reason, the temperature of the printhead was kept lower than 23 °C and purging procedures were essential and necessary in order to avoid undesired nozzle clogging. These actions caused some material and time wastes. Table 6.3 reports the main optimized printhead settings used with silver-based ink printing.

Table 6.3 - Main printhead settings used for silver-based ink printing.

Main settings	
Drop size	10 pL
Printhead height	3 mm
Substrate Temperature	RT
Printhead Temperature	23 °C
Head velocity	60 mm/s
Drop spacing	84.67 $\mu\text{m}$
Maximum jetting frequency range	50 kHz

Figure 6.8 shows an image of the Silver based ink appearance, printed in the TPU substrate. Drops are observed outside the printed line. This appearance of the printed pattern suggests that temporary clogging of the nozzle may cause a drop deviation or could be a morphology result from the drop impact on the dry TPU substrate surface. According to the drop impact phenomena [6.6 - 6.8], in the beginning or during the spreading phase, the drop may eventually be breaking into smaller droplets. This splashing is characterized as *Prompt Splash* or *Corona Splash*.

With respect to the resolution quality, and considering the new drop formation and the impossibility of using thinner lines with more than one layer of ink (because flooding of the ink occurs), the line with width of 400  $\mu\text{m}$  was selected for this study. For Thinner lines, a different printhead where drop size is lower than 10 pL is need. In Figure 6.8 it is possible to observe that the width along the line remained approximately the same.

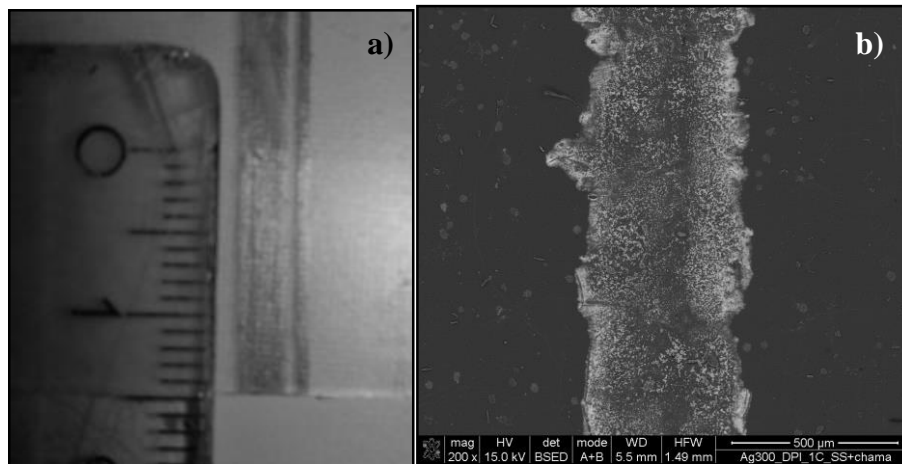


Figure 6.8 - Printed silver-based ink (with a drop spacing of 84.67  $\mu\text{m}$ ) in the TPU substrate (before sintering): a) Image of the printed pattern of testing lines; b) SEM images with detail of one layer line with width of  $\sim 400 \mu\text{m}$ .

Figure 6.9 shows a digital image of the Silver based ink appearance, printed in the SP-TPU substrate before and after annealing treatment. After printing, the samples were sintered at 130°C in an oven for 2 hours to allow complete evaporation of the solvent and capping agent degradation. Yellowing of the substrate couldn't be avoided once the sintering temperature was much higher than TPU softening temperature. This yellowing of the TPU substrate may indicate some optical and mechanical properties change. Figure 6.9 shows the printed TPU substrate before and after sintering.

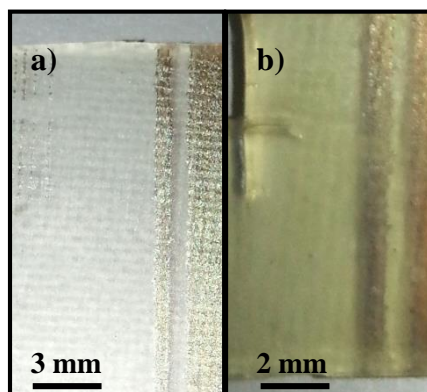


Figure 6.9 – Image of a printed sample: a) Before sintering; b) After sintering.

Figure 6.10 shows the TPU substrate fracture cross section with one layer of Inkjet printed silver-based ink, before and after sintering. Note that, after sintering, the ink layer thickness slightly decreases from 200.7 nm to 178.6 nm, losing 11% of its initial thickness. Also, the initial smooth printed layer has now a roughened surface, with the exposure of the silver particles. This is due to the evaporation of the solvent and degradation of the capping agent.

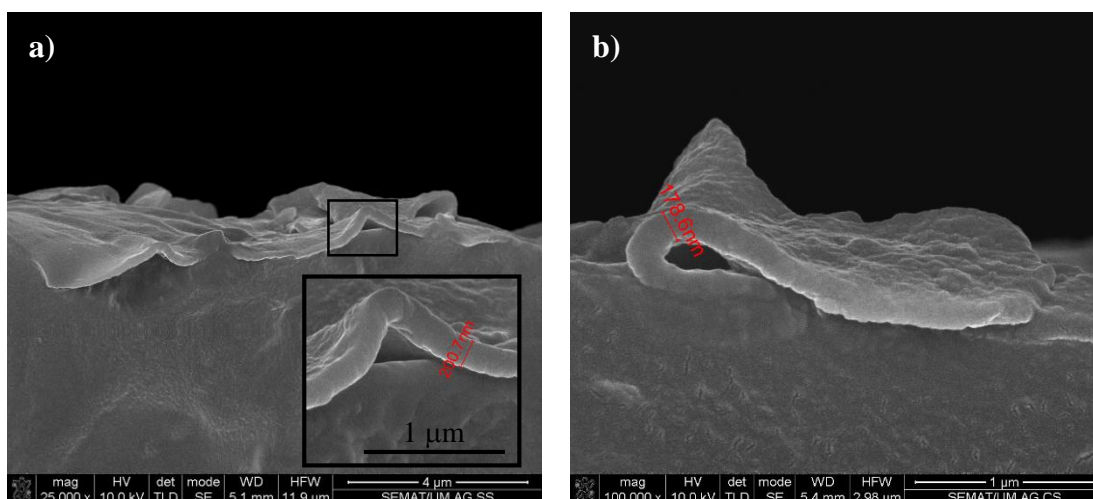


Figure 6.10 – SEM images of the TPU substrate fracture cross section with one layer of inkjet printed silver-based ink: a) before sintering; and b) after sintering.

The AFM topographical images in Figure 6.11 show the surface morphology of the printed TPU substrate with one layer of silver-based ink. According to Figure 6.11 a), the root-mean-square (RMS) roughness and mean roughness (Ra) analysis of the printed ink without sintering is, respectively, 125.72 nm and 95.331 nm. With sintering, the measured RMS and Ra values are now of 233.13 nm and 203.43 nm (a percentage increase of 85.44% and 113.4%, respectively). As expected, with the evaporation of the solvent and degradation of the capping agent, the sintered printed surface has a higher roughness consisting of a silver particles network.



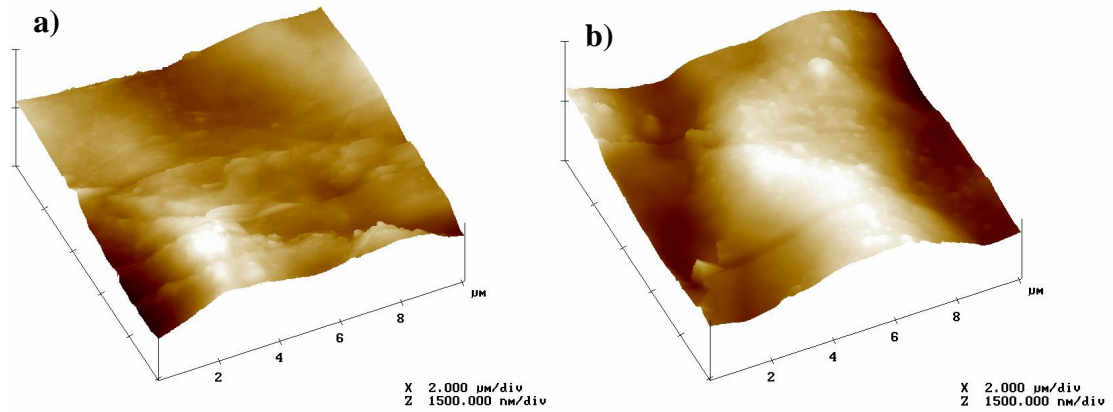


Figure 6.11- AFM topographic images of the printed TPU surface with one layer of silver-based ink: a) without sintering; and b) with sintering. The image size is 10  $\mu\text{m}$  x 10  $\mu\text{m}$ .

## 6.2 Adhesion and electrical characterization of the printed substrates

### 6.2.1. Adhesion tests

OM was used for the qualitative evaluation of the samples tested in terms of the adhesion between the TPU substrate and the silver-base ink. Figure 6.12 and Figure 6.13 show the images of the remaining ink on the substrate and the removed ink on the adhesion tape after the cross-cut tape test, before and after sintering. In relation to the test performed before sintering, the visual analysis of remaining ink on the substrate and according to ASTM - D3359, method B) qualitative evaluation scale (Comparison Chart in Appendix A.8), the level of adhesion of the ink to the substrate is poor. A visual evaluation detects large delaminations affecting significantly the ink layer, presenting more than 65% of removed area. The adhesion of the ink film to the substrate is rated in 5 on a 0-5 scale, where 0 is 0% of removed area and 5 is more than 65% of the removed area.

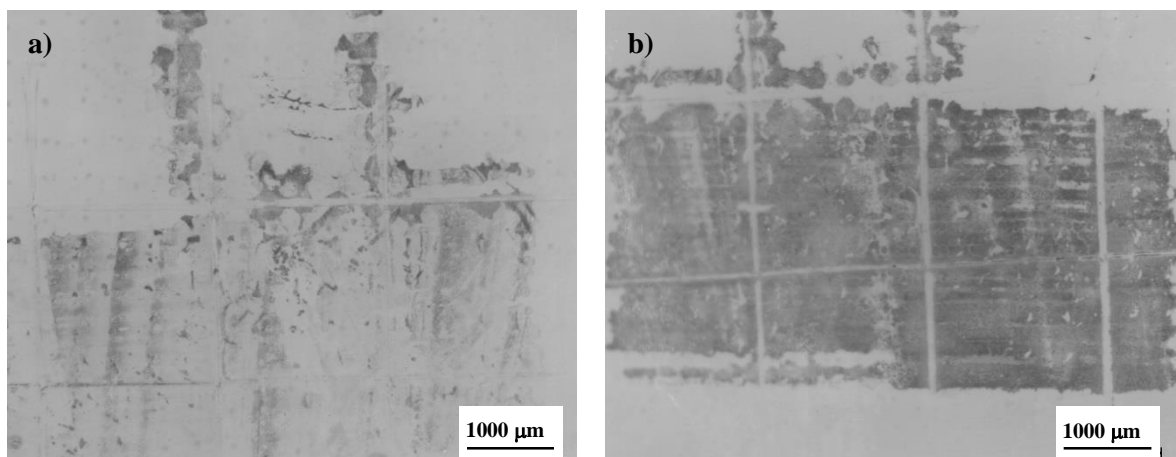


Figure 6.12 - OM images of the printed TPU substrate (before sintering) after the cross-cut tape test: a) remain ink on the TPU substrate; and b) remaining ink on the adhesion tape.



Relatively to the test performed after sintering, through the visual analysis of remain ink on the TPU substrate and according to the Comparison Chart in Appendix A.8, the level of adhesion of the ink to the substrate is high. A visual evaluation doesn't detect any delamination; the cross-cut didn't affect significantly the ink layer, presenting less than 5% of removed area. The adhesion of the ink film to the substrate is rated as 0 on a 0-5 scale, where 0 is 0% of removed area and 5 is more than 65% of the removed area.

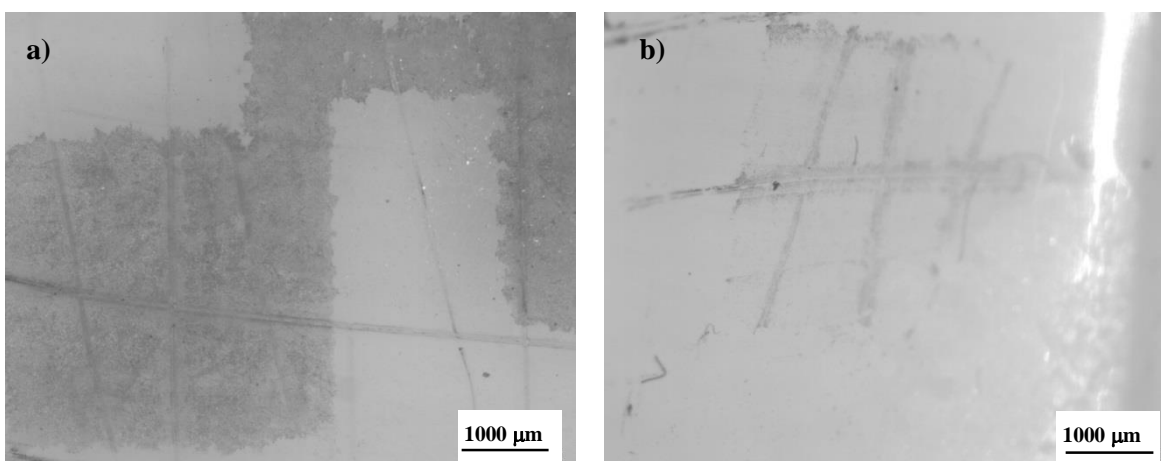


Figure 6.13- OM images of the printed TPU substrate (after sintering) after the cross-cut tape test: a) remain ink on the TPU substrate; and b) remaining ink on the adhesion tape.

### 6.2.2. Electrical resistivity measurements

The electrical performance of the printed lines was evaluated. The preliminary sintering study in 6.1.2 indicated that 1h hour at 130 °C of temperature treatment was enough to an acceptable conductivity. After the sintering on the TPU samples, none change on the electrical resistance was achieved (for 130 °C). With the increase of temperature and sintering time, no improvements were achieved either. Figure 6.14 shows the printed ink before sintering for comparison.

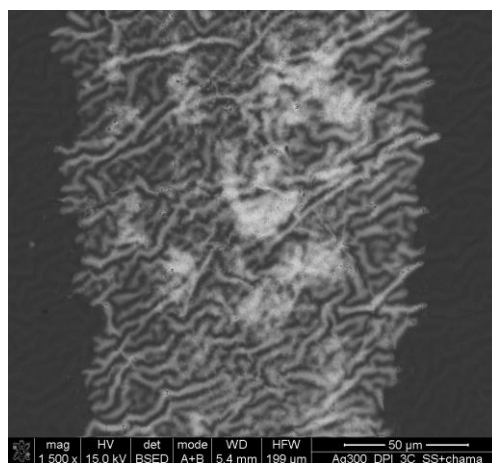


Figure 6.14 – SEM image of the printed ink, before sintering.

Figure 6.15 and Figure 6.16 show the printed ink after sintering. Cracking of the ink layer upon thermal treatment is observed, both for lower (Figure 6.15) or higher (Figure 6.16) temperatures. This could explain the low electrical conductivity measured (due to the lack of a network path formation of the metallic particles). Before thermal treatment, no cracking is observed. This indicates that permanent microstructure changes occur during the sintering process. The ink cracking may have its origin on the mismatch on the coefficient of thermal expansion (CTE),  $\alpha$ , between the silver-based ink layer and the TPU substrate. The CTE of silver is of 20 ppm/°C [6.9] and the typical CTE for TPU is 153 ppm/°C [6.10]). Therefore, the  $\Delta$ CTE is around 127 ppm/°C. The glass CTE is of 8.5 ppm/°C, so the  $\Delta$ CTE between glass and silver is much lower ( $\Delta$ CTE is around -11.5 ppm/°C), which could explain why cracking wasn't observed in the ink printed on glass substrates. As reported by Greer et al. [6.11], cracking of the silver ink occurs most likely due to the inhomogeneous stress distribution throughout the film thickness and due to the materials CTE mismatch.

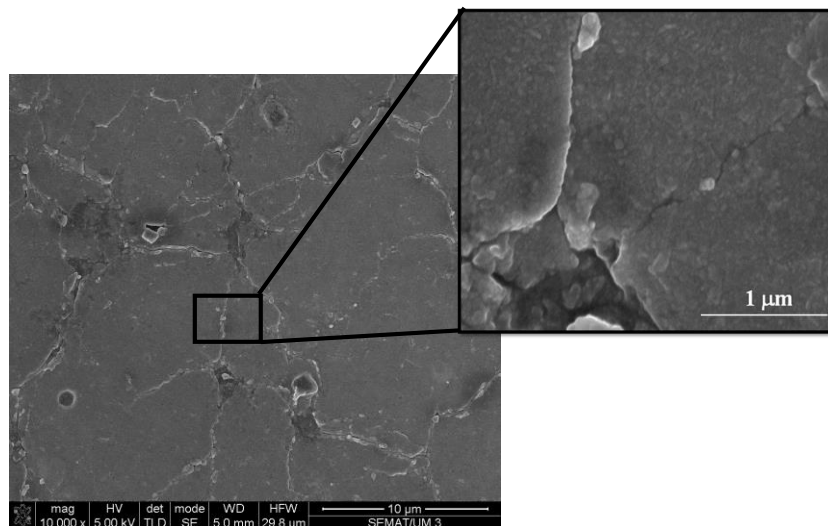


Figure 6.15– SEM images with a detail of the cracked Silver based ink on TPU substrate, after sintering at 130 °C.

For 150 °C sintering temperature, small voids are observed (Figure 6.16 b)). A quick rise of the temperature may force a quick evaporation of the solvent in the ink, contributing for voids formation, and to large strain formation leading to the observed fractures. This leads immediately to an increase in the ink's electrical resistivity.

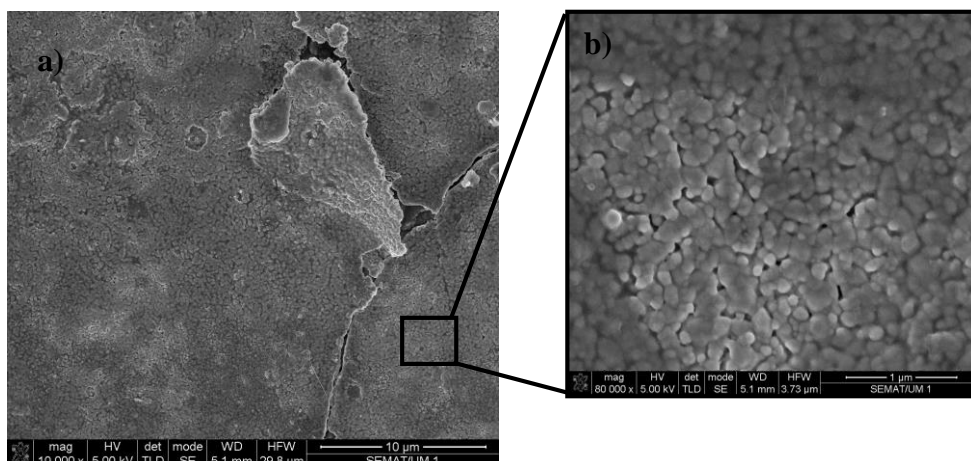


Figure 6.16 - SEM image of the TPU printed substrate after sintering at 150°C: a) with detail of the cracked Silver-based ink; b) physical contact between nanoparticles forming a silver network.

### 6.3. Summary

The silver-based ink was inkjet printed on a polymeric substrate, aiming its use as conductive tracks on a flexible electronic application. The challenge was to develop the connecting lines with suitable electrical properties on a flexible substrate. Through multiple iterative steps of experiments, the inkjet printing parameters were defined in order to achieve enhanced printing resolution and uniformity of the printed conductive lines. This silver-based ink was problematic in terms of filtering and jetting performance, and reproducibility, due to the high solid particle content (resulting partial and temporary clogging of the nozzle, also causing drop deviation).

Good surface wetting was achieved with the TPU substrate, as well as an adequate transition interphase between the silver-based ink and the substrate.

What concerns the printed substrates characterization, the cross-cut tests revealed that, without sintering, the ink presents very poor adhesion to the substrate surface, with more than 65% of removed area. After sintering no delamination was detected, for TPU, presenting less than 5% of removed area.

Preliminary study of the thermal treatment with a glass substrate indicated that 130 °C of sintering temperature would be enough to reach an acceptable electrical conductivity. When using TPU substrates these results weren't reproduced, due to permanent microstructure changes occurring during the sintering process. These results raise a main concern about the feasibility of the selected silver-based ink for use as conductive lines on a flexible sensing application. In this case, the careful selection of metallic inks with a low sintering or activation temperature wasn't

the most reliable factor for electrical conductive achievement. The limited structure elasticity of the ink upon thermal treatment (due to the CTE difference) led to extensive cracking, thereby, seriously affecting the electrical integrity, dictating the limitations of this silver-based ink for the fabrication of conductive lines. IPT revealed a suitable technology for the fabrication of high resolution conductive line, although, an alternative ink must be envisaged to overcome above mentioned technical difficulty.

**REFERENCES**

- [6.1] “Ag-IJ10 Application data sheet: Ag-IJ10 Nanosilver Ink, Applied Nanotech, Inc.,” AUSTIN, TX.
- [6.2] “[http://www.revistatecnologiagrafica.com.br/index.php?option=com\\_content&view=article&id=92:problemas-comuns-na-impressao-de-filmes-elasticos&catid=39:impressao&Itemid=180](http://www.revistatecnologiagrafica.com.br/index.php?option=com_content&view=article&id=92:problemas-comuns-na-impressao-de-filmes-elasticos&catid=39:impressao&Itemid=180).”
- [6.3] “<http://www.jorplast.com.br/jpset01/pag10.html>.”
- [6.4] “Owens, Wendt, Rabel and Kaelble (OWRK) method. Online <<http://www.kruss.de/services/education-theory/glossary/owens-wendt-rabel-and-kaelble-owrk-method/>>.” [Online]. Available: <http://www.kruss.de/services/education-theory/glossary/owens-wendt-rabel-and-kaelble-owrk-method/>.
- [6.5] S. S. Technical, N. Tn, and T. December, “Practical Contact Angle Measurement ( 5 ),” vol. 49, no. 5, pp. 1–6, 2008.
- [6.6] R. Rioboo and C. Tropea., “Outcomes from a drop impact on solid surfaces.,” *At. Sprays*, vol. 11:, pp. 155–165, 2001.
- [6.7] A. L. Yarin, “DROP IMPACT DYNAMICS: Splashing, Spreading, Receding, Bouncing...,” *Annu. Rev. Fluid Mech.*, vol. 38, no. 1, pp. 159–192, Jan. 2006.
- [6.8] R. Rioboo, M. Marengo, and C. Tropea, “Time evolution of liquid drop impact onto solid, dry surfaces,” *Exp. Fluids*, vol. 33, no. 1, pp. 112–124, Jul. 2002.
- [6.9] “DuPont <sup>TM</sup> Kapton <sup>®</sup> HN, Technical Data Sheet <Website of DuPont company: [www2.dupont.com](http://www2.dupont.com)>.”
- [6.10] T. LIIMATTA, “INKJET PRINTING IN MANUFACTURING OF STRETCHABLE,” TAMPERE UNIVERSITY OF TECHNOLOGYI, 2013.
- [6.11] J. R. Greer and R. a. Street, “Mechanical characterization of solution-derived nanoparticle silver ink thin films,” *J. Appl. Phys.*, vol. 101, no. 10, p. 103529, 2007.

## **Ink-Jet Printed Pressure Sensing Platform for Postural Imbalance Monitoring**

In this Chapter, a low cost, printed pressure sensing platform is introduced. The sensing platform consists of a flexible PCB (Printed Circuit Board) manufactured using conventional technology (defining the electrical connections and the capacitors dimensions) together with two flexible polymeric membranes made from a thermoplastic polyurethane (TPU) printed with conductive ink (PEDOT:PSS) for definition of the electrodes. A Capacitance to Digital Converter (CDC) was used to measure the capacitance of the sensors, and a graphical interface in MATLAB allows real-time visualization of data. A prototype sensing platform was designed, fabricated and tested in terms of noise, repeatability, etc., for validation, and also to demonstrate the applicability of the selected manufacturing technology and the sensors potential for clinical applications.



## 7.1. Introduction

In the electronics industry, the manufacture of electronic circuits is an area in constant development and expansion. During the last decade [7.1], the engineers has been inspired in the sense to revolutionize the applications. Thanks to novel and flexible materials combined with PE several commercial applications are being addressed, enabling a new generation of stretchable, conformal and lightweight and lower cost sensors [7.2].

Flexible pressure mapping systems (FPMS) for non-planar surfaces is an example of application for flexible, large deformation sensors. FPMS have gained increasing importance in several application areas such medical and healthcare [7.3, 7.4] as reported in the literature [7.5 - 7.9]. The need for conformability, ability to stretch and low thickness (thick sensors tend to provide erroneous readings [7.10]) require the use of flexible pressure sensors [7.10]. Depending on the spatial resolution needed for the intended application, the sensitive area of the sensors range from  $1 \times 1 \text{ mm}^2$  to  $10 \times 10 \text{ mm}^2$  [7.10].

Flexible pressure sensors (FPS) can be classified by working range, operating conditions, size, shape, base materials and fabrication method. Several materials have been used and have provided sensors increasingly intelligent, able to be integrated in complex environments [7.6, 7.8, 7.11]. New technologies that can be used to produced FPS in large-scale, with low cost, are therefore required. Inkjet printing technology (IPT) has attracted great attention [7.12 -7.15] due to a number of features that makes a compelling argument for an interesting alternative to the conventional PE technologies, therefore, a competitive and appropriate technology for production of low to medium volume sensors from small to large sensitive area.

PE technology enables savings up to 40% of the final product cost, space, and weight [7.16] when compared to traditional devices. IPT is capable of covering electronic medical implants, patches, stretchable, flexible, wide area, and low cost disposable electronics. Ink-jet print [7.17] of intrinsically conducting polymers [7.18] onto flexible substrates for humidity and gas sensing applications [7.19, 7.20] are two of many of the rapidly emerging IPT applications. However, only a few examples of IPT pressure sensors combining IPT, polymer conductive ink printed on polymer substrate have been reported so far in the literature.

The difficulties in posture control and balance treatment are an undeniable reality in physical rehabilitation. A weakened balance is translated into a more serious problem, sometimes ending in injury, disability and even death resulting from falls. The major causes of falls are related to an incipience walking stability, also leading to decreased quality of life [7.21]. According to health professionals, falls in the older adults are one of the biggest problems in health, with significant medical and economic consequences [7.21]. Mobility assessments may help to



identify who is at a high risk of falling during activities of daily living [7.22 - 7.25] providing a more objective, accurate, and reliable clinical treatment of balance problems that occur during walking [7.26 -7.28].

In 2010, according to the U.S. Department of Health & Human Services in a forthcoming *National Vital Statistics Report*, after examining the population in more detail on leading causes of death, concluded that, in a total of 180,811 deaths (classified as injury related) where, four major mechanisms of injury e.g., fall, motor vehicle traffic, or poisoning accounted for 74.7% of all injury deaths. 26,009 persons died as the result of falls, 14.9% of all injury deaths (Table 7.1) and the majority (96.9%) was unintentional. The fall related deaths increases with the increase of age [7.29] and with elderly population increase, the healthcare costs associated with falls will increase as well.

Table 7.1– Number of deaths by Accidents (unintentional injuries) cause: fall (selected from 113 causes), by age: United States, 2010 [7.29].

Cause of death	All ages	Age group (years)							Not stated
		Under 1	1-14	15-24	25-44	45-74	75-84	85 and over	
Accidents (unintentional injuries):Falls	26,009	10	52	211	792	6282	7,249	11,402	1

Face to this reality, the intervention and assessment of balance is important, especially in the elderly, since balance affects the ability of the individual to be mobile and functionally independent [7.21], and is essential to put a brake to these increasing costs. Balance assessment will provide a more objective, accurate, and reliable clinical treatment of balance problems that occur during walking to counteract the elderly quality of life decrease and death by fall [7.26 - 7.28]. Mechanical stability of a body refers to the “forces opposing any position or motion disturbing influence; static stability is concerned with the production of restoring forces, while dynamic stability is concerned with the oscillations that are set up in the system as a result of the restoring forces” [7.30].

The movement coordination and balance control involves the center of mass on the support base. The control of the center of mass is based on the assessment of the central plantar pressure (CPP) [7.22]. Present proposal is to develop a platform composed of flexible pressure mapping sensors capable of measuring the CPP. This sensing platform consists of an array of flexible capacitive pressure sensors in the millimeter range and uses a simple manufacturing process. The use of ink-jet printed electrodes over polymers results in highly deformable electrodes of the pressure sensors enabling:

- Higher sensitivities and better linearity;
- Reasonable density of sensors in the active zone;
- With reading and resolution accuracy;
- Capable of making field readings in real time;
- Cost-effective: high performance with low cost.

## 7.2. System Overview

In an initial phase, an intensive bibliographic review in physical rehabilitation was conducted in order to identify and determinate the device specifications and requirements. After this, it was done a market research to evaluate the existing devices, their operation range, their main advantages and disadvantages.

These sensors to be developed consist of an array of pressure sensor elements that are incorporated in the carrier substrate with the particularity of being flexible, providing good reading accuracy, weightlessness, and with the ability to fold/roll. Since the sensory area must be able to detect which areas are under pressure due to the balance of the user (front, back, left and right) for both feet, sensory zone must have multiple pressure sensors. The targeted FPMS have the form of a carpet with four equal sensing areas as shown in Figure 7.1. The sensing zones are approximately 12 cm x 9 cm. The capacitive sensors are placed in these regions having about 1 cm<sup>2</sup>.

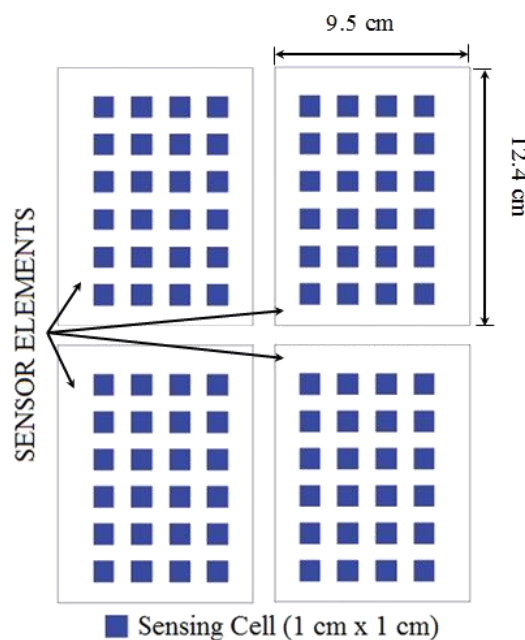


Figure 7.1- Sensorial platform scheme (the dimensions are in cm).

The capacitive readout electronics is placed next to the carpet. Each sensor element consists of a flexible Printed Circuit Board (PCB) for definition of the electrical connections and capacitor dielectric dimensions and two flexible membranes with ink-jet printed electrodes. This approach enables the fabrication of highly flexible electrodes (with low Young's Modulus) that enable pressure sensors with high sensitivity and improved linearity (achieved by the pressure dependent dielectric due to large deformation of the electrodes). It can be integrated in complex atmospheres, allowing the monitoring of the balance during physical therapy sessions, indicating the regions of the foot that are exerting force. The key elements of the sensing platform are the individual pressure sensors. A mathematical model for the flexible pressure sensors is presented in the next section.

### 7.3. Sensor Modelling

The properties of the materials and inks defined in previous chapters were very important for the definition of the final specifications of the system.

Capacitive pressure sensors are typically based on square-plate (diaphragm) electrodes separated by a dielectric (frequently of air) of separation  $d_0$  at pressure  $P_0$ . Changes on the outside pressure ( $P_{out}$ ) will deform the square plate and consequently will generate a capacitive change. Figure 7.2 shows a schematic of a square-plate (side length of  $2a$ ) pressure sensor. The behavior of the sensor is defined by its electromechanical response. A cross section of the generic square diaphragm is shown in Figure 7.3 (section cut B-B from Figure 7.2), considering only the mechanical domain.

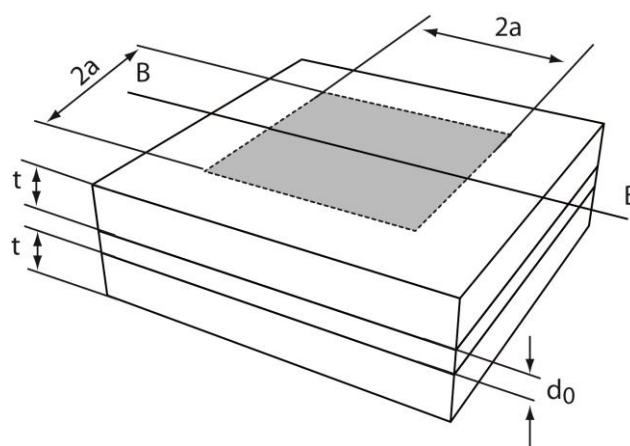


Figure 7.2 - 3D view of a square (side length =  $2a$ ) pressure sensor.

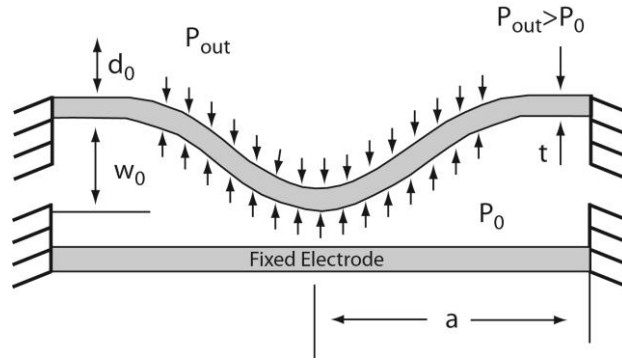


Figure 7.3 - Cross section of a generic deflectable diaphragm.

The diaphragm has clamped edges, where  $2a$  is the side length, thickness  $t$  and central deflection  $w_0$ . For a clamped diaphragm under an uniform load (such as pressure), the deflection angle is equal to zero at the center and at the edge of the diaphragm and therefore, for these defined boundary conditions, the deflection of an isotropic linear-elastic square diaphragm under a pressure load can be modeled by [7.31] (considering both bending and stretching effects):

$$P_{out} - P_0 = \left( Et^4 / (1 - \nu^4) a^4 \right) \left( 4.20 (w_0 / t) + 1.58 (w_0^3 / t^3) \right), \quad \text{Equation 7.1}$$

where  $\nu$  is the Poisson's ratio,  $E$  is the Young's Modulus and  $\Delta P = P_{out} - P_0$  is the pressure load.

While the deflection at the center of the diaphragm, for a given pressure load, is given by equation (Equation 7.1), the deflection along the diaphragm length is required to model the capacitive changes. The deflection of the whole diaphragm is usually described using trial functions [7.32], due to the complexity of the mechanical deflection calculation. In this work, the trial function presented in equation (Equation 7.2) has been used to model the diaphragm deflection, satisfying the boundary conditions:

$$w(x, y) = w_0 \left[ \left( \cos(\pi x / 2a) \right) \left( \cos(\pi y / 2a) \right) \right] \quad \text{Equation 7.2}$$

Mechanical deflections generated by pressure originate changes of the capacitor response (electrostatic domain). A capacitor is defined as being an electronic component with two electrodes, separated by a dielectric. In the absence of any displacement and for the simple case of a parallel plate capacitor, the capacitance is given by (neglecting fringe fields):

$$C = \epsilon_0 \epsilon_r (w_c l_c / d_0), \quad \text{Equation 7.3}$$

where  $\epsilon_0$  is the permittivity of free space ( $8.8546 \times 10^{-12}$  F/m),  $\epsilon_r$  is the relative permittivity,  $w_c$  and  $l_c$  are, respectively, the width and length of the capacitor electrodes (in this case  $2a$ ), and  $d_0$  is the gap between the electrodes. The double-plate capacitive sensor described here uses diaphragm electrodes with a complex bending profile. The calculation of the total capacitance requires the integration over the effective area of the electrodes as:

$$C = \int_0^{2a} \int_0^{2a} \epsilon_0 \epsilon_r / [d_0 - w(x, y)] dx dy \quad \text{Equation 7.4}$$

where  $w(x, y)$  is the distance between electrodes due to the diaphragm bending at position  $x, y$ . The integration of (Equation 7.4) is solved here numerically, allowing the calculation of the capacitance for a given pressure change.

Previous work on FPS using low Young's Modulus diaphragms [7.33] demonstrated that the large deformations of the diaphragm need to be taken into account in the electromechanical model of the sensor response. Since small pressure changes in the outside ( $P_{out}$ ) cause large diaphragm deformations, and large deformations cause volume changes of the dielectric material (air), the pressure ( $P_0$ ) inside the dielectric will change (from the ideal gas law,  $P_i V_i = P_f V_f$ ). In order to capture this behavior the model previous presented was extended and an iterative model using the flow chart presented in Figure 7.4 was implemented in Matlab and used for the pressure sensors design.

Table 7.2 shows the final parameters of the individual pressure sensors. Incorporation of pressure dependent dielectric due to bending of the electrodes is new and greatly improves accuracy of the model as demonstrated by the comparison between experimental and model results.

Table 7.2 – Main design parameters of the pressure sensor.

<i>Parameter</i>	<i>Value</i>
2a (side length)	10 mm
t (diaphragma thickness)	1.5 mm
d <sub>0</sub> (gap)	0.195 mm
E (TPU Young's Modulus)	7.5 MPa
$\nu$ (TPU Poisson's ratio)	0.5
P <sub>0</sub> (dielectric initial pressure)	100 kPa
Dynamic range (P <sub>out</sub> )	100 – 180 kPa
C <sub>0</sub> (Rest capacitance)	4.8 pF

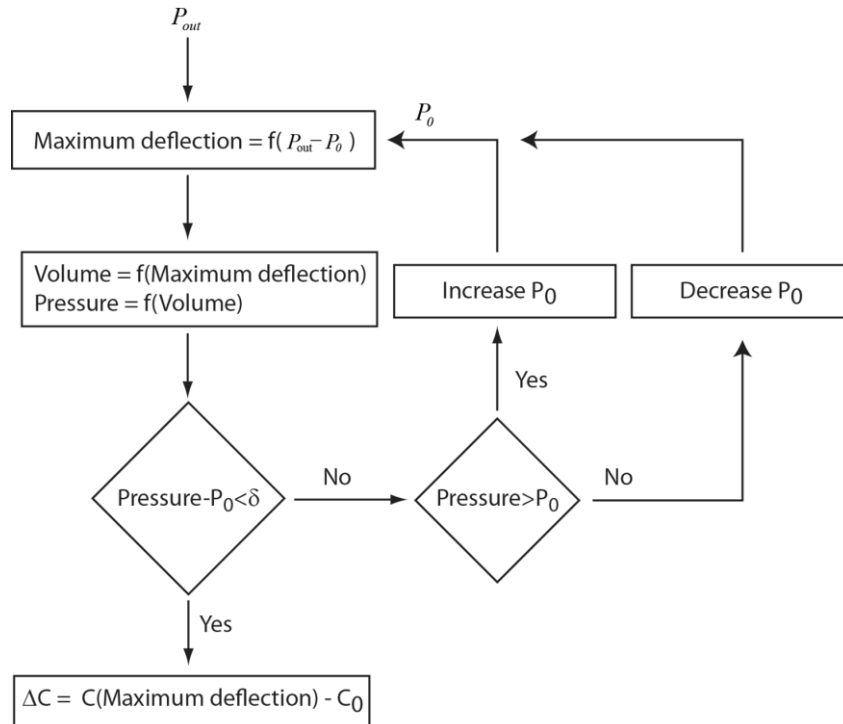


Figure 7.4 - Iterative algorithm to compute the capacitive changes of flexible capacitive pressure sensors.

## 7.4. Manufacturing Process

Technology selection is made according to the type of electronic component or device being made (small, thin, lightweight, flexible, disposable, etc.) the production cost, the batch volume and throughput. Essential to the success of any type of PE device is the processability, performance and long-term reliability of the materials used [7.34, 7.35].

The proposed fabrication process for the flexible pressure sensing platform used three main steps: (8.4.1.) fabrication of the flexible membranes with conductive ink; (8.4.2.) fabrication of a flexible PCB; and (8.4.3.) an assembly step. An overview of the full process is presented in Figure 7.5.

### 7.4.1. Flexible Membranes with Conductive Inks

The superficial treated Thermoplastic polyurethane (TPU), AVALON 65 AB grade, from Huntsman, was selected for the flexible substrate. PEDOT:PSS ORGACON™ IJ-1005 grade from Agfa was selected for the fabrication of the electrodes. Their quality adhesion along with resistivity results of the printed inks makes them the preferable pair for the conductive membranes. Moreover TPU is a material that offers the hyper-elasticity of rubber, but with

improved mechanical properties: good flexibility, strength and durability, an impact resistance superior to thermoplastics, excellent wear properties and elastic memory.

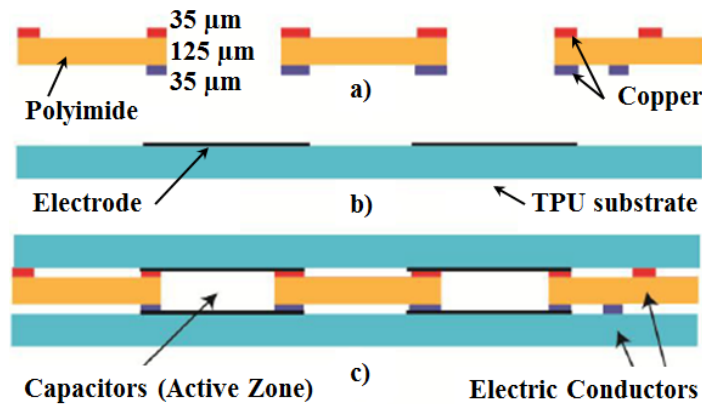


Figure 7.5 -Sensor elements manufacturing process in which: a) Flexible PCB (the geometry of copper conductors and the capacitor dielectric were defined using a PCB flexible process); b) Flexible substrate (the electrodes of the capacitors are inkjet printed on the TPU using conductive ink) and c) Assembled prototype sensor where the two flexible substrates with electrodes (one for the TOP and a second one for the BOTTOM (Figure 7.6), were assembled using conductive glue to the flexible PCB, Figure 7.7).

A high-definition printer (Xennia Carnelian) was used for drop-on-demand printing and definition of the electrodes of the capacitive sensors. Printing was undertaken in a non-standard laboratory environment with no temperature or humidity control, non-particle filtered enclosure in order to determine the extent to which the devices could be fabricated in a basic processing facility. The conductive ink was printed in two TPU flexible membranes with superficial treatment (Figure 7.6); a substrate for the TOP electrodes and another for the BOTTOM electrodes.

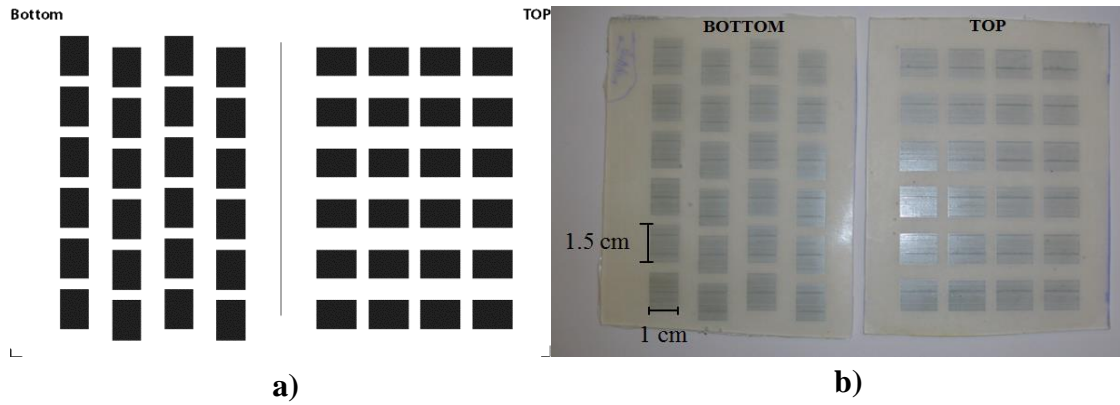


Figure 7.6- Conductive electrodes: a) Drawing pattern for electrodes definition; b) Inkjet printed flexible substrates (with conductive inks electrodes on a 1.5mm thick TPU substrate).

#### 7.4.2. Flexible PCB's

Due to the technical difficulty described in Chapter 6, and due to time constrains, the flexible PCBs with flexible conductive lines was designed and fabricated externally. These flexible PCBs consist of a substrate of polyimide (PI), 125  $\mu\text{m}$  thick with copper on both sides (35  $\mu\text{m}$  thick). The copper was subsequently machined to define the conductive lines, and then the substrate is open in certain regions to define the dielectric (air) of the capacitors. Each sensing platform has 24 capacitive pressure sensors. Figure 7.7 shows an image of the flexible PI substrate and respective conductive lines. The size of the capacitors was selected to reach a nominal capacitance of 5 pF. In order to minimize connection lines on the flexible PCB, a multiplexing strategy to read the individual sensors was adopted (synchronizing both the sensors excitation and reading). The electrical connections for sensors excitation are placed on the TOP side of the PCB, while the electrical connections for the sensors reading are placed in the BOTTOM side. In order to reduce possible cross-coupling effect between sensors, only two sensors share the same excitation, and simultaneously only two sensors share the same reading channel (that have different excitations). Noteworthy, is the line next to the dielectrics for electrical connection of the printed conductive electrodes. This line enables the electrical connections to the capacitive electrodes during the assembly process. Also, while TOP electrodes are horizontally oriented, the BOTTOM electrodes are vertically oriented. This design compensates for some misalignments between TOP and BOTTOM electrodes and minimizes parallel parasitic capacitances between the electrodes. The column offset pattern in the BOTTOM electrodes has to do with the arrangement of the lines on the flexible PCB for electrical connection.



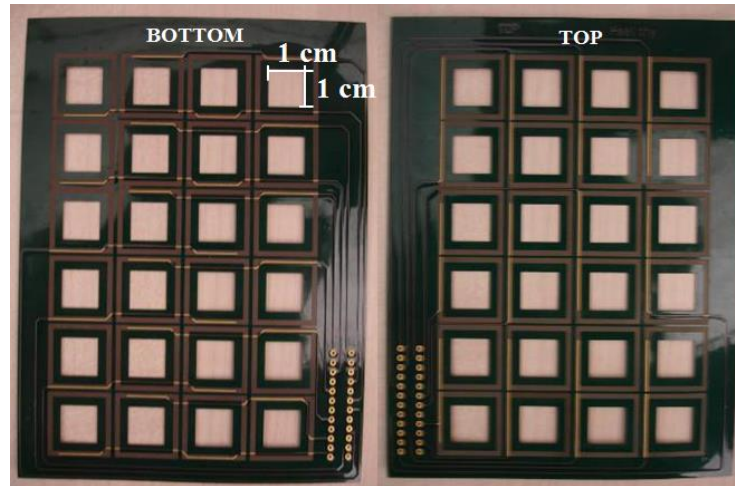


Figure 7.7 - The top side (on the left) and bottom side (on the right) of the flexible PI substrate and the respective dielectric areas. The PCB size is 124 mm x 95 mm.

### 7.4.3. Prototype Sensor Assembly

Finally, the flexible TPU membranes were bonded with ELECOLIT 414 (a polyester-based, electrically conductive adhesive) in zones of the substrate (delimiting each sensing cell) to the flexible PCB in order to establish contact and manufacture the capacitive sensors. The process was simple and can easily be automated for medium to high volume production batches.

### 7.5. Electronics Interface

The sensors' readout interface was designed taken into account the modelling results and the expected capacitive changes. The capacitive measurement is performed using a 12-bit Capacitance to Digital Converter (CDC), AD7150, for each sensitive zone allowing direct interface with the capacitive sensors. The converter consists of a second-order sigma-delta ( $\Sigma\text{-}\Delta$ ) modulator. This low-power IC, 100  $\mu\text{A}$ , has 2 input channels, with a conversion time of approximately 10 ms and 1fF resolution, for a dynamic range of 4 pF. Since excitation channel is shared by two sensors and reading channel is shared by two sensors, but with different excitation, there is the need to multiplex the reading channel and demultiplex the excitation channel, to correctly acquire all the sensors. The use of four (8-Channel) multiplexers enables sequential reading of the 24 sensors for each sensitive area. Two were used as demultiplexers to select the excitation of the sensors and were connected to the excitation channels of the converter. The other ones were used to select the sensors reading channels and were connected to the input channels of the converter. A microcontroller controls the multiplexers, enabling the synchronization between excitation and reading of the sensors.

The reading of the corresponding digital capacity value for each sensor, as well as CDC configuration was performed using I<sup>2</sup>C communication between the converter and microcontroller. The digitized data was transmitted to a computer via a serial interface. A graphical interface implemented in MATLAB provided real time readings and allowed data manipulation. An overview of the readout circuit is presented in Figure 7.8.

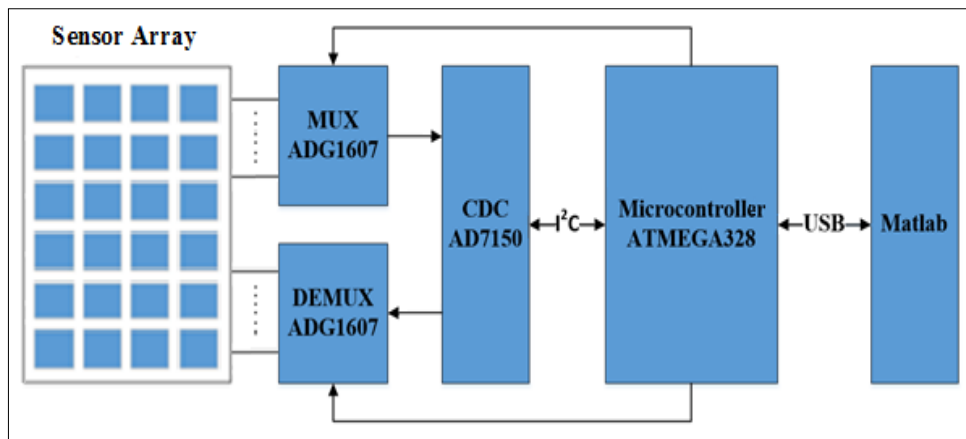


Figure 7.8 - Schematic of the sensing-array system.

## 7.6. Experimental results and discussion

The individual response of a set of sensors was performed by placing the assembled prototype and the readout electronic PCB (Figure 7.11) inside an in-house assembled pressure chamber (Figure 7.9). Initially, positive pressures were applied (ranging between 100-180kPa) and the pressure inside the pressure chamber was acquired using a reference pressure sensor (TECSIS P3297). A control loop using a reference pressure sensor and an electronic valve maintains the desired pressure with an uncertainty around 100 Pa.

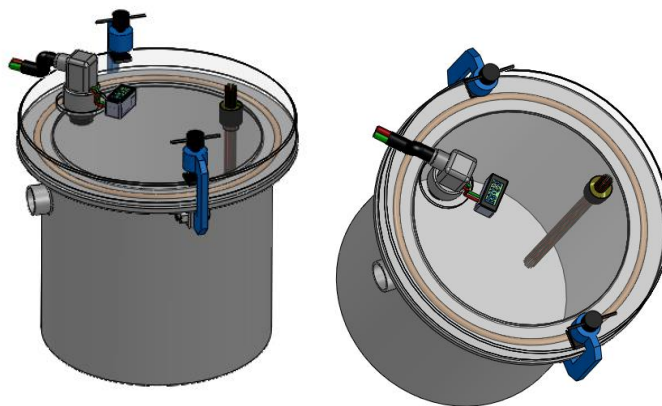


Figure 7.9 - 3D illustration of the used pressure chamber to measure the capacitive changes of the flexible pressure sensors.

Three cycles of increasing/decreasing pressure were conducted to each sensor in order to evaluate the hysteresis characteristic of the sensor. Sensors noise evaluation was performed by acquiring the sensor response (at constant ambient pressure) with a sampling rate of 100 Hz during a 64 hours period. The sensor repeatability was also verified, by performing a daily measurement test (during 21 days) with and without a load (the same load was used during the 21 days period).

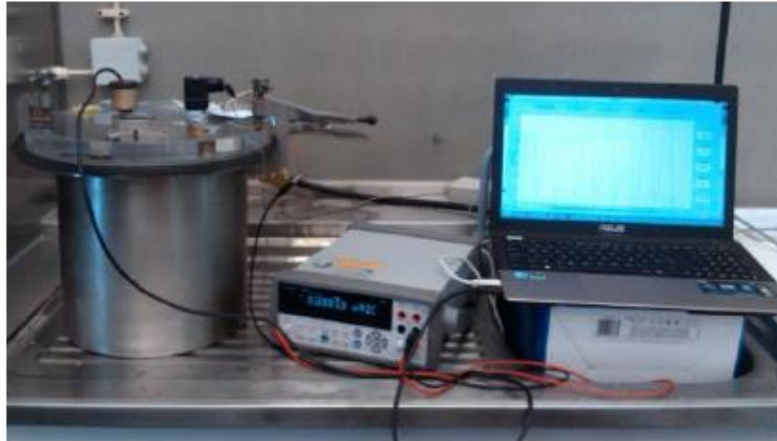


Figure 7.10 – Digital image of the test setup.

Figure 7.11 shows the assembled sensing platform prototype. The platform was successfully bended for curvature radius below 1 cm without loss of performance (the middle sensors saturate during bending, but completely recover their value when returning to the original configuration). The stretching capabilities of the sensing platform are limited by the stretchability of the flexible PCB that cannot stretch more than 0.5%.

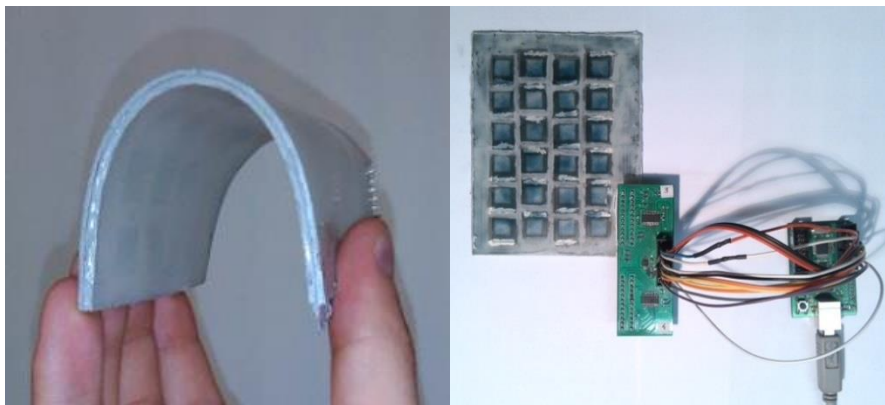


Figure 7.11 - Assembled Prototype Sensors (left) and the reading system (right).

Figure 7.12 shows the variation of the sensors' capacity vs. pressure for 10 different sensors within a sensing platform. The measured response was consistent with what one would expect, i.e., the increase in pressure resulted in increased capacity of the sensors. The sensors showed a fair linearity (in the tested range) and sensitivity around 40-50 fF/kPa. The observed differences in the sensors response is probably due to the manual assembly of the sensors (resulting in a distance variation between the electrodes), and due to the existing cross-coupling capacitances between sensors (Figure 7.13).

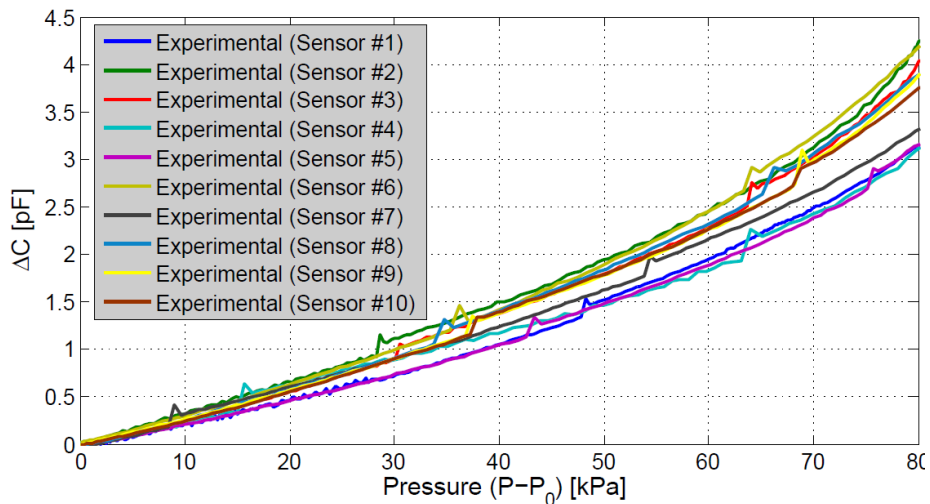


Figure 7.12 - Sensors response to pressure.

The multiplexing strategy was designed to minimize cross-coupling between capacitors, but still, some cross-coupling between the sensors sharing the same excitation channel and between the sensors that share the same reading channel was observed. The cross-coupling capacitances are attributed to the capacitances between the connection lines. Tests performed using a fixed load (0.2 kg) showed that the contribution of the sensor sharing the same excitation channel (C3 in the example provided in Figure 7.13) was around 20% of the sensor variation (for instance, while applying a load of 0.2 kg to C1 a capacitance change of 0.8pF was measured, applying the same load to C3 a 0.16pF capacitance change is measured). The contribution of the sensor sharing the same reading channel (C2 in the example provided in Figure 7.13) was around 10% of the variation.

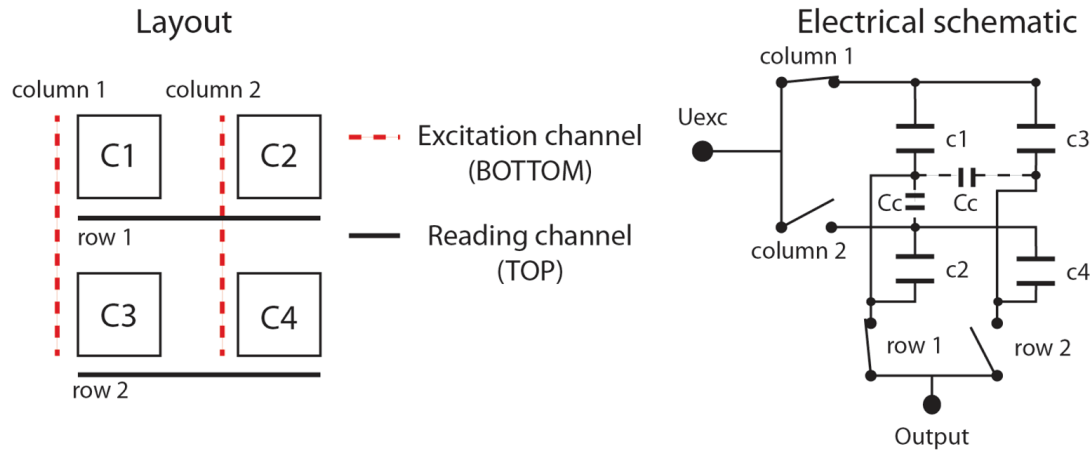


Figure 7.13 - Layout and electrical schematic of the connections for sensor reading, including cross-coupling capacitances ( $C_c$ ).

Figure 7.14 shows a comparison between the measured sensor response and the expected capacitance change given by the analytical model presented. Since the nominal capacitances of the measured sensors were around 10 pF (5 pF more than the expected ones), a parallel capacitance of 5 pF was added to the model for better comparison. The parallel capacitances on the fabricated sensors were due to the wider electrodes used and capacitances introduced by the connectors. For the 10 tested sensors the average nominal capacitances at zero pressure was 9.4 pF with a standard deviation of 2.2 pF.

The agreement between the model and experimental results was very good (especially when the cross-coupling was taken into-account on the model) and validates the assumption that the pressure on the dielectric changes for large diaphragm deflection. It also shows that the proposed model is a valid tool for flexible pressure sensors design that are based on low Young's Modulus electrodes, like the ones introduced here.

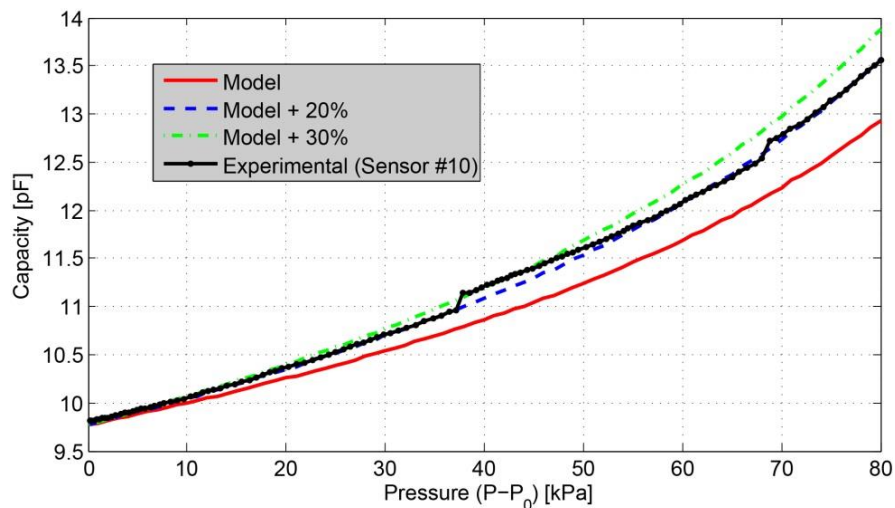


Figure 7.14 - Experimental results and comparison with analytical model.



Figure 7.15 shows the response of the sensors for increasing and decreasing pressures (different cycles). The repeatability was excellent, both for the increasing and decreasing cycle. After each cycle, the sensors capacity returns to the initial capacity value. A small hysteresis (<5%FS) was observed and was mainly due to the CDC used (a dynamic feature of the converter was used, CAPDAC, that automatically sets the dynamic range of the converter, introducing the observed jumps).

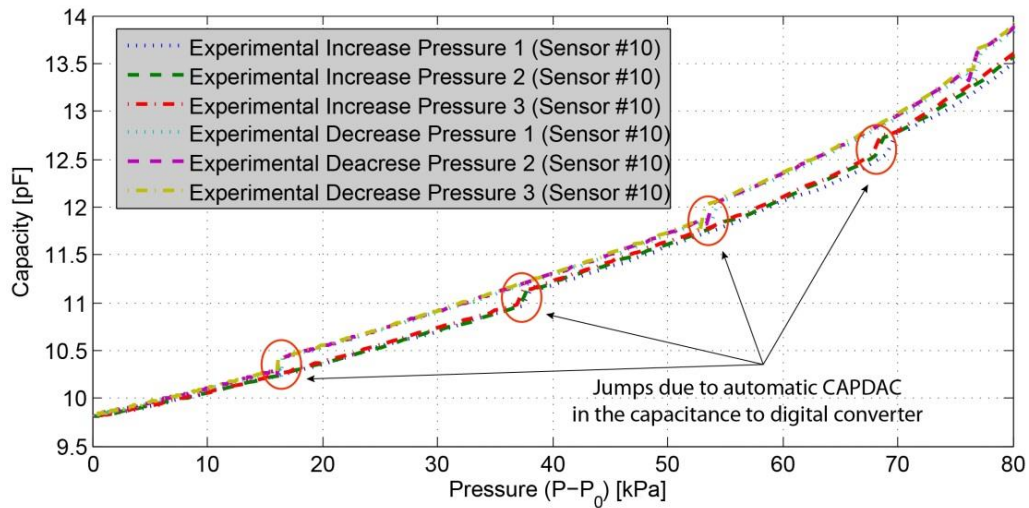


Figure 7.15 - Sensor response for increase/decrease pressure cycles.

Measurements were performed (Figure 7.16) during 64 hours to access the noise characteristics of the sensors plus readout electronics. The CDC converter takes around 10 ms (while integrates the signal) to do a conversion, and therefore only the frequencies lower than 100 Hz contribute to noise. Assuming a Gaussian noise distribution, the standard deviation of the measurements gives the total noise of  $\sigma = 12$  fF. Since the CDC has a resolution of 1fF, the measured noise is mainly due to the sensor and therefore, the total sensors noise is  $1.2\text{fF}/\sqrt{\text{Hz}}$ .

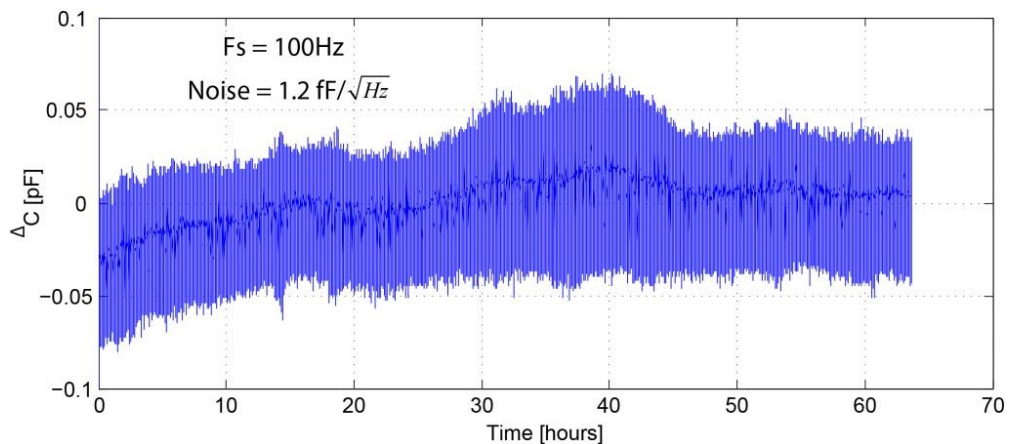


Figure 7.16 - Noise measurement during 64 hours.

The results of the repeatability/stability tests are presented in Figure 7.17. In terms of repeatability, the sensor response, with or without load, was consistent and showed a repeatability around 1.5%FS (Full Scale), for the range 100-180kPa.

Regarding the total system response time, tests results have demonstrated that the developed reading system is capable to follow the expected physical movements (average response time of 0.3 seconds) during therapy sessions. Simple equilibrium exercises include maintaining a stable position (standing with feet hip-width apart and with weight equally distributed on both legs for instance, or standing on one leg only) during 30 seconds and therefore the system sampling frequency of 3Hz is adequate for these equilibrium exercises.

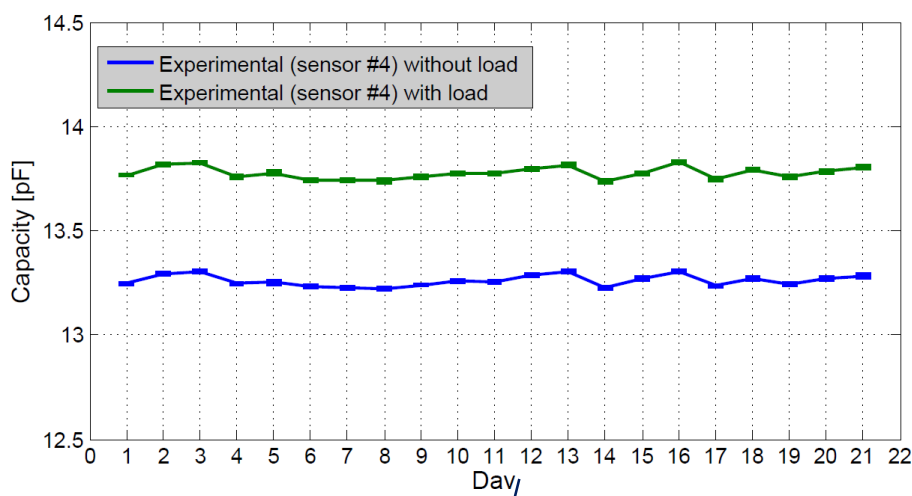


Figure 7.17 - Example of sensor repeatability with/without load.

## 7.7. Summary

The design, fabrication and experimental results of a flexible pressure mapping system and its readout electronics interface were presented here. The proposed solution enables a large density of capacitive flexible sensors with a simple and inexpensive process, capable to measure balance during physical therapy. Especial attention was given to process simplicity and high throughput in order to have a low-cost technology that can deliver good performance flexible sensors.

The capacitive sensors showed a sensitivity of 50 fF/kPa in the region of operation, a noise of 1.2 fF/ $\sqrt{\text{Hz}}\sqrt{\text{Hz}}$  and a stability greater than 1.5% FS. The proposed pressure sensor platform has the potential to integrate multiple sensing parameters for ubiquitous environment monitoring.

A comparison of capacitive pressure sensors from the literature and the one developed is presented in Table 7.3. Although this sensor has lower range (100-180 kPa), it has higher

sensitivity and higher initial capacitance, making it suitable for CPP measurements. The developed sensor was also compared with commercial sensors with similar sizes (Table 7.4). Our sensor compares extremely well in terms of repeatability and hysteresis. Regarding resolution, the commercial sensors do not include electronic circuit (just the sensing element) and performance will be dependent on the electronic circuit used, but typically, being resistive sensors, noise tends to be high.

Table 7.3 – Comparison of different pressure sensors

	Developed Sensor	Lei et al.[7.7]	Lee et al.[7.38]
Sensitivity	12.5 %/N	6.8 %/N	$3 \times 10^{-3}$ %/N
Range	100-180 kPa	0-945 kPa	0-250 kPa
Initial value	10 pF	0.95 pF	0.18 pF
Dielectric material	Air	PDMS	Air
Fabrication	Inkjet Print	Photolithography	Molded/etching
Application	Pressure measurement	Plantar pressure measurement	Artificial skin for robot

Table 7.4 - Comparison with commercial sensors.

	Our Sensor	A301 [7.36]	FSR 400 [7.37]
Range	8N	4.4N	20N
Repeatability	$\pm 0.75\%$	$\pm 2\%$	$\pm 2.5\%$
Hysteresis	$< 5\%$	$< 4.5\%$	$< 10\%$
Resolution (10Hz Bandwidth)	0.008N	Continuous (analogue)	Continuous (analogue)

The proposed sensor model was able to accurately predict the sensor response and it proves that the inclusion of an iterative algorithm to deal with the pressure changes in the dielectric is key in modelling low Young's Modulus diaphragms. Moreover, the pressure changes in the dielectric greatly improve the linearity of the sensor, a major drawback on existing pressure sensors. The sensor characterization showed that the flexible polymeric capacitive sensor presents good repeatability (taken into account the manual procedures used for sensor fabrication). The measured stability is also good and these sensors can be a suitable low-cost approach for flexible pressure sensing platforms.

Nevertheless, there are some issues that must be improved in the future. The assembly of the sensors still requires a better control and the connection between sensor platform and readout



electronics needs improvement (some connections in the flexible PCB were broken in the contact region). Also, the measured cross-coupling is still high and it can create false readings on the sensors. Individual reading of the sensors can be a solution, at the expense of increased connection lines density. Unevenly assembly of the sensing elements may be another way to mitigate the cross-coupling.

**REFERENCES**

- [7.1] F. G. Tseng, C. J. Kim, and C. M. Ho, "A microinjector free of satellite drops and characterization of the ejected droplets. Symposium on Applications of Micro-fabrication of Fluid Mechanics, ASME International Mechanical Engineering Congress and Expositions," 1998.
- [7.2] B. Andò and S. Baglio, "Inkjet-Printed Sensors: A Useful Approach for Low Cost, Rapid Prototyping," no. October, pp. 36–40, 2011.
- [7.3] "Xsensor Technology Corporation." [Online]. Available: <http://www.xsensor.com>.
- [7.4] T. V Papakostas, "Tactile sensor: stretching the limits," in *Intelligent Environments, 2007. IE 07. 3rd IET International Conference on, 2007*, pp. 472–476.
- [7.5] E. Pritchard, M. Mahfouz, B. Evans, S. Eliza, and M. Haider, "Flexible capacitive sensors for high resolution pressure measurement," in *Sensors, 2008 IEEE, 2008*, pp. 1484–1487.
- [7.6] D. Zhou and K. Jax, "Design of pressure sensor array with reduced number of wires," *2010 IEEE Int. Conf. Inf. Autom.*, pp. 900–905, Jun. 2010.
- [7.7] K. F. Lei, K.-F. Lee, and M.-Y. Lee, "Development of a flexible PDMS capacitive pressure sensor for plantar pressure measurement," *Microelectron. Eng.*, vol. 99, pp. 1–5, Nov. 2012.
- [7.8] C. Hailin and P. Tingrui, "Microfabrication of conductive PDMS on flexible substrates for biomedical applications," in *Nano/Micro Engineered and Molecular Systems, 2009. NEMS 2009. 4th IEEE International Conference on, 2009*, pp. 731–734.
- [7.9] T. V Papakostas, J. Lima, and M. Lowe, "A large area force sensor for smart skin applications," in *Sensors, 2002. Proceedings of IEEE, 2002*, vol. 2, pp. 1620–1624 vol.2.
- [7.10] C. M. A. Ashruf, "Thin flexible pressure sensors," *Sens. Rev.*, vol. 22, no. 4, pp. 322–327, 2002.
- [7.11] H. B. Muhammad, C. M. Oddo, L. Beccai, C. Recchiuto, C. J. Anthony, M. J. Adams, M. C. Carrozza, D. W. L. Hukins, and M. C. L. Ward, "Development of a bioinspired MEMS based capacitive tactile sensor for a robotic finger," *Sensors Actuators A Phys.*, vol. 165, no. 2, pp. 221–229, 2010.
- [7.12] B. News, "'Scientists use inkjet printing to produce solar cells,'" *BBC News Technology*. [Online]. Available: <http://www.bbc.co.uk/news/technology-13977038>.
- [7.13] C. Griggs, J. Sumerel, and D. Ph, "Opportunities for Inkjet Printing in Industrial Applications," *Industrial + Specialty Printing* <<http://www.industrial-printing.net>>, no. C, 1899.
- [7.14] K. E. Paul, W. S. Wong, S. E. Ready, and R. a. Street, "Additive jet printing of polymer thin-film transistors," *Appl. Phys. Lett.*, vol. 83, no. 10, p. 2070, 2003.
- [7.15] F. V. López, A. Diez, and A. Odriozola, "Inkjet Printing of Conductive and Resistive Coatings," *Int. Polym. Process.*, vol. 22, no. 1, pp. 27–32, 2007.

- [7.16] D. P. Harrop, "Printed Electronics for Healthcare, Cosmetics and Pharmaceuticals 2014-2024: IDTechEx," *"In 2014, the global market for biochemical sensors alone is over \$8.8 billion dollars,"* 2013. [Online]. Available: <http://www.idtechex.com/research/reports/printed-electronics-for-healthcare-cosmetics-and-pharmaceuticals-2014-2024-000361.asp>.
- [7.17] Y. Li, R. Torah, S. Beeby, and J. Tudor, "An all-inkjet printed flexible capacitor for wearable applications," 2012, no. April, pp. 25–28.
- [7.18] M. V. Kulkarni, S. K. Apte, S. D. Naik, J. D. Ambekar, and B. B. Kale, "Ink-jet printed conducting polyaniline based flexible humidity sensor," *Sensors Actuators B Chem.*, vol. 178, pp. 140–143, Mar. 2013.
- [7.19] U. Altenberend, F. Molina-Lopez, A. Oprea, D. Briand, N. Bârsan, N. F. De Rooij, and U. Weimar, "Towards fully printed capacitive gas sensors on flexible PET substrates based on Ag interdigitated transducers with increased stability," *Sensors Actuators B Chem.*, vol. 187, pp. 280–287, Oct. 2013.
- [7.20] V. Matic, L. Liedtke, T. Guenther, A. Buelau, A. Ilchmann, J. Keck, B. Polzinger, W. Eberhardt, and H. Kueck, "Inkjet printed differential mode touch and humidity sensors on injection molded polymer packages," *IEEE SENSORS 2014 Proc.*, pp. 2234–2237, Nov. 2014.
- [7.21] P. K. Yim-Chiplis and L. A. Talbot, "Defining and measuring balance in adults.," *Biol. Res. Nurs.*, vol. 1, no. 4, pp. 321–331, 2000.
- [7.22] A. Biswas, E. D. Lemaire, and J. Kofman, "Dynamic gait stability index based on plantar pressures and fuzzy logic.," *J. Biomech.*, vol. 41, no. 7, pp. 1574–81, Jan. 2008.
- [7.23] J. L. Patton, Y. Pai, and W. a Lee, "Evaluation of a model that determines the stability limits of dynamic balance.," *Gait Posture*, vol. 9, no. 1, pp. 38–49, Mar. 1999.
- [7.24] C. D. Ceria-Ulep, J. Grove, R. Chen, K. H. Masaki, B. L. Rodriguez, T. a Donlon, J. Guralnik, B. J. Willcox, D. C. Willcox, C. Nigg, and J. D. Curb, "Physical aspects of healthy aging: assessments of three measures of balance for studies in middle-aged and older adults.," *Curr. Gerontol. Geriatr. Res.*, vol. 2010, p. 849761, Jan. 2010.
- [7.25] M. H. Woollacott and P. F. Tang, "Balance control during walking in the older adult: research and its implications.," *Phys. Ther.*, vol. 77, no. 6, pp. 646–60, Jun. 1997.
- [7.26] M. E. Tinetti and J. S. Brach, "Translating the fall prevention recommendations into a covered service: can it be done, and who should do it?," *Ann. Intern. Med.*, vol. 157, no. 3, pp. 213–4, Aug. 2012.
- [7.27] Mary E. and Tinetti M.D., "Making Prevention Recommendations Relevant for an Aging Population," *Ann. Intern. Med. Ed. Am. Coll. Physicians*, vol. 153, no. 12, pp. 843–845, 2010.
- [7.28] K. Berg, S. Wood-Dauphinee, J. I. Williams, and D. Gayton, "Measuring balance in the elderly preliminary development of an instrument.pdf," *Physiother. Canada*, vol. 41, no. 8, pp. 304–311, 1989.
- [7.29] S. L. Murphy, J. Xu, and K. D. Kochanek, "National Vital Statistics Reports Deaths : Final Data for 2010," USA, 2013.

- [7.30] P. H. Considine, G.D., Kulik, “Van Nostrand’s Scientific Encyclopedia, Wiley-Interscience, Wiley, New York.” in *Van Nostrand’s Scientific Encyclopedia, Wiley-Interscience, Wiley, New York.*, 2002, p. ninth ed., vol. 2.
- [7.31] H.-L. Chau, M. Ann Arbor, and K. D. Wise, “Scaling limits in batch-fabricated silicon pressure sensors,” *IEEE Trans. Electron Devices*, vol. 34, no. 4, pp. 850 – 858, 1987.
- [7.32] S. D. Senturia, “Microsystem Design,” *New York Kluwer Acad. Publ.*, p. 689, 2001.
- [7.33] A. T. Sepúlveda, R. G. De Villoria, J. C. Viana, A. J. Pontes, B. L. Wardle, and L. A. Rocha, “Flexible Pressure Sensors: Modeling and Experimental Characterization,” *Procedia Eng.*, vol. 47, pp. 1177–1180, Jan. 2012.
- [7.34] T. Adcock and D. Fenner, “Printed Electronics : Traditional Technology Addresses Today’s Smaller , Faster , Lower Cost Requirements,” <<http://www.henkel.com/electronics.htm>>, 2012. .
- [7.35] L. Basiricó, “Inkjet Printing of Organic Transistor Devices,” University of Cagliari, 2012.
- [7.36] *Tekscan, FLX-A301 force sensor datasheet, Rev. E\_9.30.13. .*
- [7.37] “Interlink Electronics. FSR 400 Series data sheet.”
- [7.38] H. Lee, S. Chang, and E. Yoon. (2006, December). A Flexible Polymer Tactile Sensor : Fabrication and Modular Expandability for Large Area Deployment. *JMEMS* [Online]. 15 (6), pp. 1681–1686. Available: <http://ieeexplore.ieee.org/stamp/stamp.jsp?tp=&arnumber=4020266>



# Chapter 8

## **Conclusions and Future Work**

The summarized objectives, achievements, and the main conclusions of the work presented in this thesis are addressed here. Some guidelines regarding the potential research and development work that can be performed in the future are given at the end.



## 8.1. Conclusions

In this thesis, the feasibility of IPT for flexible pressure sensors has been evaluated through literature review and experimental work. The advantages of IPT compared with the conventional printing methods were presented. The process parameters of IPT, the homogeneous dispersion of the ink and absorption from different substrates, and the electrical conductivity of the printed layer were studied. The work performed shows that the optimization process has a key role in the development of printed sensors using polymer substrates.

The objective of this work was to develop a new generation of good performance and low cost FPS. The applied research was focused from a materials science point of view (selectively applying commercially available and compatible flexible materials, enabling the conformability of the sensor to a complex contact surface, or defining viable material alternatives), processing the materials with a simpler, lower cost and larger scale manufacturing technology and exploring its potential to be integrated into electronic applications, in particular, for use in monitoring applications related to health and rehabilitation.

To meet this objective it was necessary to develop an array of sensors built from printed polymer substrates:

- With high reading and resolution accuracy;
- Capable of making field readings in real time;
- Capable of static and dynamic measurement in the whole range of movement.
- Cost-effective: high performance with low cost.

The morphology of printed pattern depended on several critical factors. The volume of the ejected droplet determined by voltage and the firing frequency were fixed parameters once only one printhead was available, therefore, these parameters were limited characteristics of the used printhead. The type of substrate, the substrate temperature, the type of ink, the printhead temperature, the printhead height, the head speed, and the drop spacing were the variables of this study.

Before moving on to the IP process itself, an investigation of the materials properties like superficial tension, and compatibility between them to ensure the adhesion of ink to the substrate was performed. A proper characterization allowed an evaluation of which surrounding and dependent variables can dictate the possible limitations of the material/process in order to anticipate problems and causes of defects and to optimize the manufacturing process.



The main conclusions to be drawn from the work performed with the different inks and from the overall work are presented next:

A major challenge tackled during the Ph.D. work was the dispersion and adhesion of conductive inks onto polymeric substrates (known for their hydrophobic nature). A new surface treatment of the substrate was developed, to the best of our knowledge never attempted before, in order to increase the substrate surface energies. The method is environmental friendly and low cost. So, in the proposed surface treatment method, micro/nanosized particles are spread over the substrate surface and then thermally fixed. This latter step allowed the micro/nanosized particles sinking-in on the polymer surface, resulting in a higher polymer-particle interaction at their interfacial region. The addition of micro/nanosized particles onto the polymer surface increases surface roughness and promotes intermolecular interactions. SP shows a high affinity with the TPU due to the hydrogen-bond interactions between the silanol groups on the silica surface and the soft segments of the TPU. This improves the intermolecular interactions between SP and the TPU substrate, anticipating a good adhesion between them. The SP treated surface ensured, therefore, good surface wetting, creating hydrogen-bond interactions, and made an adequate interphase between SP and the substrate. This novel surface treatment of thermoplastic polymers was applied to the inkjet printing of TPU substrates with conductive inks, and significant improvements on the printability were obtained without affecting the ink adhesion.

After inkjet printing parameters definition and depending on the ink and substrate, the characterization of the printed system was conducted for pattern resolution, adhesion and electromechanical properties evaluation.

The P3HT ink was easy to work with due to:

- slow evaporation,
- capability of passing through the IJP nozzle without obstruction,
- fast and easy cleaning of machine parts with minimal effort.

What concerns the electrical characterization, the P3HT sheet resistance decreases as the number of printed layers increase. The achieved resistivity level was high, and therefore, this ink has limited applicability on sensing applications. The rather high measured resistivity may be strongly correlated to the final deposited film morphology. The electrical properties of a printed structure may be affected by the no-homogeneity of the ink thickness (due to the surface roughness), edge definition, surface morphology and the interfacial properties at the interface

between ink and the SP particles. An increase of the printed layers may overcome the high surface roughness and the low electrical conductivity. However, this solution represents a substantial increase of material resources, printing costs, and production time with no increased additional benefit evidencing the unsuitability of the P3HT for electrodes fabrication.

Compared to the P3HT ink, PEDOT:PSS ink was more complicated to work with due to:

- fast evaporation,
- increase risk of nozzle obstruction,
- need for more cleaning effort.

The low measured resistivity (even for few layers of ink) makes this ink interesting for the sensing application. PEDOT:PSS ink showed good deformation properties, as it was able to follow the deformation of the SP-TPU substrate without visible rupture of the ink. Has demonstrating a high reliability and operation stability of the printed pattern, and behaves as standard piezo-resistive gauge with a huge gauge factor. The achieved pattern properties (electrical resistivity and low Young Modulus), resulting from the combination of the high flexible material, a conducting polymer material, and the manufacturing technique are the prominent factor for the design and development of a flexible sensor with high strain capabilities.

For the Silver based ink, good surface wetting was achieved with the neat TPU substrate as well as an adequate transition interphase between the Silver based ink and the substrate. The cross-cut tests revealed that, without sintering, the ink presents very poor adhesion to the substrate surface, with more than 65% of removed area. After sintering no delamination was detected presenting less than 5% of removed area. The sintering treatment for conductive percolation wasn't achieved on the printed TPU. These results raise a main concern about the feasibility of the selected Silver based ink for its use as conductive lines for a flexible application. The limited structure's elasticity upon temperature treatment (due to the CTE) lead to extensive cracking, thereby, seriously affecting the electrical integrity, dictating the limitations of this Silver based ink for the conductive lines fabrication. IPT revealed a suitable technology for the fabrication of high resolution conductive lines, although, an alternative ink must be envisaged to overcome above mentioned technical difficulty.

Table 8.1 summarize the results. The work presented here demonstrates the suitability of PEDOT:PSS/SP-TPU in terms of IPT appropriateness, and demonstrate the applicability of the selected manufacturing technology and its potential to meet the needs of the electronic industry.

A compromise between several criteria was performed in order to get the desired sensor performance (to achieve the desired sensor characteristics like resolution and bandwidth). The mechanical performance of the selected materials was demonstrated, ink adhesion to the substrate, achieved electrical properties and large deformation.

Table 8.1 – Summary of the results.

<b>Ink</b> <b>Substrate</b>	<b>P3HT</b>	<b>PEDOT:PSS</b>	<b>Silver based</b>
PDMS	NW & NA	NW & NA	W&NA
PET	NW & NA	NW & NA	NW & NA
PI	NW & NA	NW & NA	W&NA
TPU	NW & NA	NW & NA	W&A&NC
SPTPU	W&A&LC	W&A&GC	W&A&NC

A- Adhesion; NA-No adhesion,  
W-Wettability; NW-Non wettability;  
GC-Good conductivity; LC-Low conductivity; NC-No conductivity.

Also, inkjet printing exhibited to be a simple and reliable printing procedure for obtaining robust working devices. Direct printing of conductive ink in the manufacture of electronic devices can greatly reduce the production cost. IPT is competitive and oriented for printing both, small and large areas. The premium prices of large area sensing platforms available in the market constitute a problem for a faster wide spread of new products. Given the growing interest in pressure mapping systems technology, if the price is lowered down, new products such as postural balance devices can become a volume product usable by almost anyone. This FPS have numerous advantages over rigid pressure sensors, as, high compression, and contact area thanks to its ability to fold/roll, lightness, thinner, can be transparent, so it has greater design freedom.

The recognition of tactile information is very important for humans use in daily life. The design, fabrication and experimental results of a FPS system and its readout electronics interface were presented here. The developed sensing platform to assess the patients balance consists of an array of flexible capacitive pressure sensors, in the millimeter range and uses a simple manufacturing process (enabling a reasonable density of sensors in the active zone). Thus, it is possible to achieve good performance results (comparable to existing solutions in the industry), with the particularity of offering an economically viable alternative, allowing its use in rehabilitation activities. The proposed pressure sensor platform has the potential to integrate multiple sensing parameters for ubiquitous environment monitoring. The first prototype results

are very promising and encouraging. The sensor characterization showed that flexible polymeric capacitive sensors present good sensor to sensor response (taken into account the manual procedures used for sensor fabrication). The FPMS is capable of measuring and analyze the medical process pattern, overcoming some of the difficulties found in today's Physical Rehabilitation. The measured stability is also good and these sensors can be a suitable low-cost approach for FPMS.

This work features an effort to simplify the manufacturing process, using low cost flexible materials, reduce materials waste and to improve the performance of flexible pressure sensors. Finally, the collaboration between different fields of science and technology allowed achieving the objectives of this dissertation.

## 8.2. Future work

Nevertheless, there are some issues that must be improved in the future.

- Material for IPT needs further development. Different formulations for conductive inks, specifically applicable to the printer that was used in this work, should be studied.
- With regard to improving the adhesion between the ink and the substrate, and willing to continue working with this type of substrates, in particular, it would be advisable to perform another type of surface treatment (e.g., chemical treatments, corona treatment and plasma treatment, etc.).
- Work with printheads with different characteristic (e.g., different drop-size) to produce more narrow and sharp-edged connections lines.
- The results achieved with the Silver based ink raise a main concern about the feasibility of the select commercial ink for its use as conductive lines for the flexible application. The limited structure's elasticity upon temperature treatment lead to extensive cracking, thereby, seriously affecting the electrical integrity. An alternative ink must be envisaged to overcome the problem, or substitute the TPU substrate with a substrate with a CTE compatible with the CTE of the ink.
- The assembly of the sensors still requires a better control and the connection between sensor platform and readout electronics needs improvement (some connections in the flexible PCB were broken in the contact region). Also, the measured cross-coupling is still

high and it can create false readings on the sensors. Individual reading of the sensors can be a solution, at the expense of increased connection lines density.

- The inks undergo various processes and phases of use in their lifetime. At the end the printed pattern must be resistant to handling. During all these phases, the ink composition changes over time, therefore, it is critical that the ink must resist and keep its initial properties. The same applies to the other materials involved in the sensor structure (e.g., substrate, etc). Therefore, a demonstration of the reliability and durability of the flexible printed structure in terms of mechanical performance and applicability of the selected materials to the application is still required.
- The use of the develop platform in real clinical environments is also a very important task that should be addressed in the near future and that should be strongly emphasized.
- An experimental comparison with other existing pressure sensor systems should be performed.
- Potential new application may be manufactured with this materials and technology and be the integrated into future systems such as temperature and gas sensors, etc. for biomedical applications, biomechanics, robotics touch.
- Development of manuals and study of the production process in large series.

# Appendix

**A1. Other fabrication techniques**

**A2. Piezoelectric heads**

**A3. Inkjet Printer information**

**A4. Datasheet of the used printhead**

**A5. Datasheet of the substrates**

**A6. Datasheet of the micro/nanosized particles**

**A7. Datasheet of the inks**

**A8. Characterization Kit and Comparison Chart**

**A9. Adhesive datasheet**

**A10. Pressure Chamber accessories**

**A11. List of Publications**

## A1. Other fabrication techniques

### *Spin coating*

Spin coating is a common manufacturing technique that consists of a uniform application of thin films by depositing a few drops of fluid in the center of a flat substrate and then the substrate is spin at high speed (typically around 3000 rpm). The centrifugal force causes the liquid to spread, eventually, out of the edges of the substrate leaving a thin layer on the surface, until the desired film thickness is achieved. Higher the speed, the thinner is the film. The thickness and final properties depend on the nature of the liquid (viscosity, volatilization rate of the solvent, surface tension, solids percent, etc.) the parameters chosen for the centrifugation process, such as rotational speed, acceleration. Is the combination of rotational speed and time which generally defines the final thickness. One of the most important factors in spin coating is reproducibility. Small variations in process parameters can result in drastic variations in the final film. In general, longer times and higher speeds of rotation produce thinner films. This step may take from 10 seconds to several minutes.

Sometimes an additional drying step is carried out without rotation to prevent reducing the thickness. The substrate speed (rpm) affects the degree of applied centrifugal force to the fluid as well as the characteristic velocity and turbulence of the air immediately above it. The drying rate depends on the nature of the fluid (volatility of the solvent system used) and the air around the substrate during the centrifugation process.

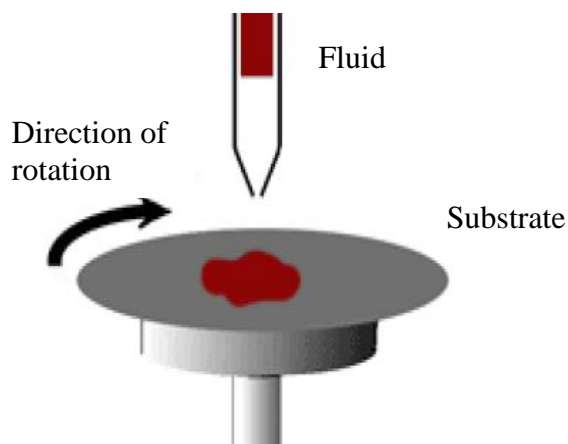


Figure A1.1 –*Spin coating process.*

It is, therefore, important to minimize or at least control the airflow over the substrate during the process. The drying rate also affects the viscosity of the fluid as the fluid dries there is an increase in viscosity associated with drying until the force of the centrifugation process can no longer move appreciably on the surface. Reached this point, the film thickness will not suffer significant changes that increase the turnaround time. Since about 50% of the common constituents of the ink fluid solvent is lost by evaporation during the first few seconds of the process, it is important to accurately control the acceleration. Therefore, plays an important role in the final properties of the coating. Inks with low viscosity and low rates of incorporation of particles are the most suitable for use in processes such as spin coating.

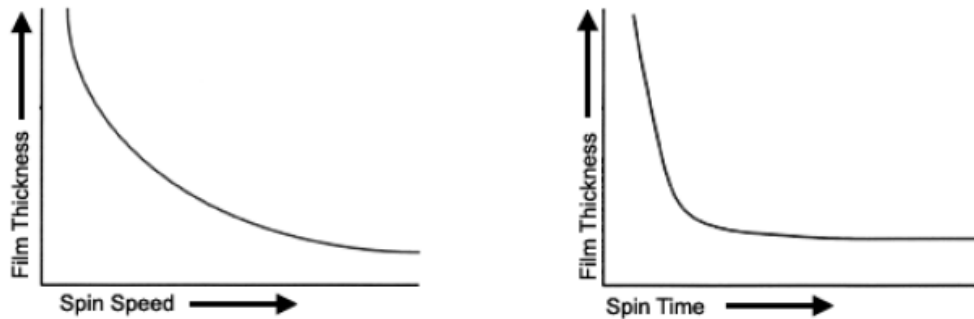


Figure A1.2 – Process tendency.

These charts represent the general trends for the process parameters. For most materials the final thickness is inversely proportional to the velocity and the rotation time.



## A2. Piezoelectric heads

The selected technology for this study was DoD system - piezoelectric heads. The different DoD system -piezoelectric heads are described in detail in this subsection

### A.2.1. Shear mode

The printhead of the Shear mode system uses an electric field perpendicular to the polarization of the piezoelectric crystal, which differentiate them from the other types. In this case the electric charge causes a cutting action on the distortion of the piezoelectric elements against the ink, thereby ejecting ink droplets through nozzle ejectors (Figure A2.1). There are many brands that have adopted this system in particular, the Spectra, Xaar, Nu-Kote MIT, Brothers and Olympus.

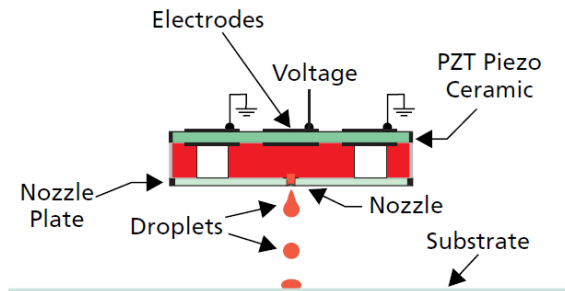


Figure A2.1 – Shear mode Piezoelectric DoD InkJet printhead [1].

The Shear mode system has proven its performance with high reliability, robust process capability, and a broad range of choice of inks with viscosity higher (20-25 mPa.s) than what usually is used in piezoelectric heads. It's possible to conduct some alterations on the mode system to give specific properties depending on the application [1]. You can also get these systems quite compact with small piezo crystals, having a higher market price [1]. This type of piezoelectric head was used in this study.

### A.2.2. Bend mode

The Bend mode system is based on the stimulation of the piezoelectric crystal plate that expands to cause a pressure on the ink channel, forcing the ink moving to the nozzles of the printer and leaving outwards in droplet form (Figure A2.2). The electric field between the electrodes is in parallel to the polarization of the piezoelectric plate. The plates are coupled to the transducer diaphragm printhead, and opposed to the nozzles.

This system is used by Epson printers since 1997 in printers like Color Stylus, as the P50. In our days Epson combines the old technology with a new microwave algorithm, managing to eliminate the difference in banding for uniformity of ink droplets, greatly improving the printing quality [1].

Its resolution is around 1440 Dots Per Inch (DPI) and has a great accuracy of circular drops which gives high quality and speed printing at a low cost. The major drawbacks is that the multi-layer piezo system is very sensitive can only support low viscosity inks around 1.6 to 3 mPa.s [1].

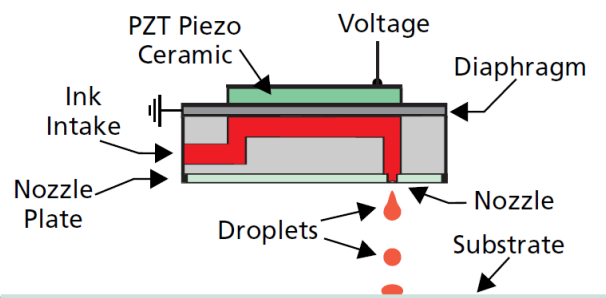


Figure A2.2 – Bend mode Piezoelectric DoD InkJet printhead [1].

### A.2.2.3. Push mode

The Push mode system is similar to Bend mode in a way that the electric field between the electrodes is parallel to the polarization of the piezo plates and is the piezoelectrical crystal itself that pushes the transducer, which causes the sufficient pressure in the ink to eject the droplets (Figure A2.3).

Initially, Dataproducts, Trident and Epson adopted this system. Although improvements had to be made once its high-energy system form quite elongated drops. It is distinguished by its robustness and can use inks with viscosities between 10-20 mPa.s, but nevertheless the obstacle of the possibility of satellite formation [1].Epson used this system in the print heads of his first Stylus Color printers (1994) and Stylus II (1995), each one having 64 nozzles [1].

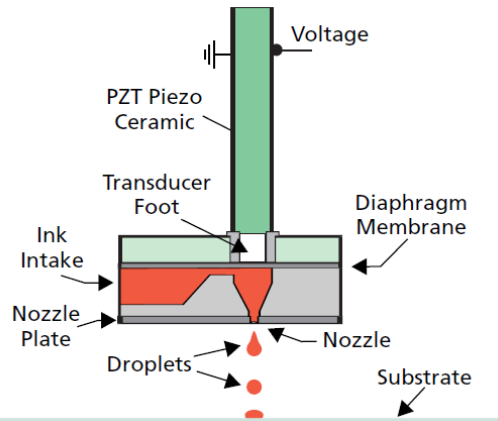


Figure A2.3 – Push mode Piezoelectric DoD InkJet printhead [1].

#### A.2.2.4. Squeeze mode

The Squeeze mode system refers to a technology developed in the company Clevite in 1972 and Siemens used it later in the printer PT-80 (1977). In this mode the application of an electrical load causes the deformation of a piezoelectric tube, pressing the ink in that tube, forcing it out through the nozzle end (Figure A2.4). Note that Siemens successfully commercialized this system for conventional printing office equipment [2].

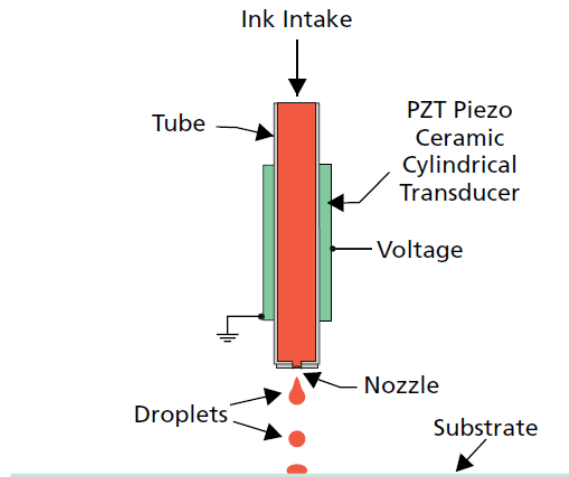



Figure A2.4 – Squeeze mode Piezoelectric DoD InkJet printhead [1].

#### REFERENCES A.2

- [1] V. Cabbill, "Introduction to Digital Printing Technology. Graphic Artists," *Pre-Press Pers.*, 1998.
- [2] M. Junfeng, M. R. Lovell, and M. H. Mickle, "Formulation and processing of novel conductive solution inks in continuous inkjet printing of 3-D electric circuits," *Electron. Packag. Manuf. IEEE Trans.*, vol. 28, no. 3, pp. 265–273, 2005.

## A3. Inkjet Printer information

**CARMINE**  
THE RANGE OF XENNIA DEVELOPMENT PRINTING SYSTEMS



# Xennia Carnelian

## Flexible inkjet development system

The Xennia Carnelian inkjet dispenser incorporates industrial printhead technology in a flexible, high precision 3-axis printer for fluid & process development, printhead evaluation and accurate fluid dispensing.

**Ideal for fluid & process development**

The Xennia Carnelian is the ultimate industrial fluid development and printhead evaluation tool for printed electronics, biotechnology/pharmaceutical or other fluid development applications, allowing developers to get to grips with industrial inkjet technology quickly and cost effectively. The Carnelian comes with a choice of industrial piezo printheads, and can even be fitted with two different types of printhead to allow technology comparison. The combined industrial and low volume syringe ink system allows evaluation of small quantities of fluid, while enabling scaling to a larger volume for extensive testing or pilot production.

**Powerful performance with flexible options**

The Carnelian uses a robust fully programmable XY motion stage with sub-micron resolution and repeatability of  $\pm 5 \mu\text{m}$  over an A4 printable area. An optional programmable Z axis allows print height to be easily adjusted for 3D substrates. The Carnelian is also available with an optional integrated vacuum table top and alignment camera system for advanced substrate handling and positioning, and with an optional integrated scanning UV lamp for inline pinning of UV fluids.

**Industrial-scale process development made simple**

The Xennia Carnelian is a small-scale development tool built around industrial-scale printhead and fluid control technology, meaning that fluid development can be completed using the Carnelian and then ported onto a production printer using the same technology, without the need for reformulation.


**Intuitive printing with detailed control**


Powerful Xenjet print software is integrated into the Carnelian, allowing simple one click operation of the printer, or engineering level access to the detailed operation of the system if that is required. The software can also print fully variable data and process DXF/Gerber file formats with optional upgrades.

**Application development support**

Xennia offers a full application development and support service, including fluid formulation and process optimisation along with inkjet training, to help customers successfully implement inkjet technology into their production process.

- Functional materials dispensing
- Fluid testing and development
- Industrial printhead evaluation







## Xennia Carmelian

### Specifications

<b>Fluid type</b>	Wide range of aqueous, solvent and UV fluids
<b>Printheads</b>	Up to 2 (most types of industrial piezo printheads)
<b>Printable area</b>	229 mm x 305 mm (9 in x 12 in)
<b>Motion resolution</b>	0.25 $\mu\text{m}$ (XY), 0.5 $\mu\text{m}$ (Z)
<b>Repeatability</b>	$\pm 5 \mu\text{m}$ (XY)
<b>Print speed</b>	Up to 150 mm/s (6 in/s)
<b>XY positioning</b>	Stepper motors
<b>Z positioning</b>	Stepper motor (38 mm (1.5 in) travel)
<b>Fluid control</b>	Combined industrial and low volume syringe system (most printheads) Small volume recirculating ink management system (recirculating printheads)
<b>Printhead maintenance</b>	Manual purge and wipe
<b>Software</b>	XenJet print software with integrated user interface Variable data capability and DXF/Gerber capability available as an option.
<b>Dimensions (WxDxH)</b>	1.2 m x 0.75 m x 1.6 m (47 in x 30 in x 63 in) (approx)
<b>Power supply</b>	120/230V, 50-60Hz, single phase
<b>Optional accessories</b>	Integrated vacuum table top Alignment camera system Integrated scanning UV lamp Programmable Z axis Variable data capability DXF/Gerber file processing

Subject to technical modification without notice



Xennia Technology Ltd  
Monroe House • Works Road • Letchworth • Hertfordshire SG6 1LN • UK  
telephone: +44 (0) 1462 705220 • facsimile: +44 (0) 1462 705221 • email: enquiries@xennia.com  
[www.xennia.com](http://www.xennia.com)



Xennia is part of Royal Ten Cate  
[www.tencate.com](http://www.tencate.com)

uEye Camera Manual Version 3.90

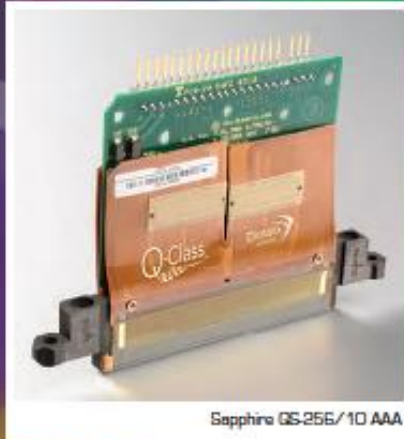
**UI-112x/UI-512x**

<b>Sensor specification</b>				
Sensor type	CMOS			
Shutter system	-			
Characteristic	Logarithmic			
Readout mode	Progressive scan, rolling readout			
Resolution class	CCIR			
Resolution	768 x 576 Pixel (0.44 Megapixel)			
Aspect ratio	4:3			
<a href="#">Bit depth</a>	14 bit A/D converter, 12 bit transfer			
Optical sensor class	1/2 inch			
Exact sensitive area	7.680 mm x 5.760 mm			
Exact optical sensor diagonal	9.60 mm (1/1.67 inch)			
Pixel size	10.0 µm, square			
Sensor name, monochrome	NCS0806-M			
Special features	<ul style="list-style-type: none"> <li>• HDR sensor with logarithmic characteristic</li> <li>• The sensor does not possess an exposure time.</li> </ul> See also chapters <a href="#">Functionality of the uEye HDR sensor (NCS0806)</a> and <a href="#">UI-112x/UI-512x application notes</a> <ul style="list-style-type: none"> <li>• Sensor internal controls for gain (AGC)</li> </ul>			
<b>Gain</b>				
Monochrome model (master gain)	-			
Analog gain boost	-			
<b>Camera timing</b>				
		USB uEye	GigE uEye SE/RE	GigE uEye HE
Pixel clock range (allowed/recommended)	MHz	5-31/10-15 <sup>*1)</sup>	5-31/10-15 <sup>*1)</sup>	5-31/10-15 <sup>*1)</sup>
Pixel clock for optimal image quality	MHz	14 <sup>*1)</sup>	14 <sup>*1)</sup>	14 <sup>*1)</sup>
Max. pixel clock with subsampling/binning	MHz	-	-	-
Frame rate (freerun mode)	fps	50.0 <sup>*2)</sup>	50.0 <sup>*2)</sup>	50.0 <sup>*2)</sup>
Frame rate (trigger mode, 1 ms exposure)	fps	48.0 <sup>*2)</sup>	48.0 <sup>*2)</sup>	48.0 <sup>*2)</sup>
Exposure time in freerun mode	ms	-	-	-
Exposure time in trigger mode	ms	-	-	-
<b>AOI</b>				
Mode	-			
<b>Binning</b>				
Mode	-			
<b>Subsampling</b>				
Mode	-			



## A4. Datasheet of the used printhead

## Sapphire QS-256/10 AAA

256-Channel  
Inkjet Printhead

Sapphire QS-256/10 AAA

**Features:**

- 10 picoliter nominal drop size
- 256 individually addressable, inline nozzles
- Incorporates VersaDrop™ binary and grayscale jetting modes
- Excellent channel-to-channel uniformity
- High frequency continuous operation
- Precise alignment features facilitate drop-in replacement
- Lightweight with thin profile
- Supports UV-curable, solvent, and aqueous-based inks
- Integral temperature sensor
- Dual-ported with minimal wetted surface area
- OEM accessible non-volatile memory area for tracking purposes
- Easy to integrate

*The Performa™ Sapphire QS-256/10 AAA printhead delivers best-in-class jetting accuracy combined with versatile grayscale operation. Its lightweight, thin-profile design and configurability plus support for a broad range of ink formulations makes this printhead model particularly suited to scanning printer architectures and applications.*

Dimatix continues building upon its long history of excellent dot placement accuracy, channel-to-channel uniformity, low cross talk, and high-frequency/high-productivity with the Q-Class Sapphire printhead family.

The Sapphire QS-256/10 AAA printhead features 256 independent channels, arranged in a single row of nozzles at 100 dots-per-inch spacing. It is designed to eject adjustable 10 to 30 picoliter drops in binary jetting mode or a 10-picoliter fundamental drop in grayscale mode. This is done at a nominal 8-meter per second drop velocity when jetting fluids in the 10 to 14 centipoise range.

Dimatix' breakthrough VersaDrop™ jetting technology is featured within the Sapphire QS-256/10 AAA printhead. It allows unparalleled flexible modes of operation including adjustable binary drop size and grayscale capability at unprecedented throughput rates.

The rugged, field proven material set selected for the Sapphire QS-256/10 AAA printhead deliver long service life and consistent output.

Using tailored waveforms and a durable, inert silicon nozzle plate to provide best-in-class drop placement accuracy, a wide range of ink formulations are accommodated including UV-curable, organic solvent and aqueous-based inks and associated maintenance fluids.

Precision registration points have been added to the printhead to provide absolute reference to the nozzles to within a few microns. This makes it possible to nest printheads together for high packing densities.

Shared physical features and identical interfaces as other Q-Class products allow the Sapphire QS-256/10 AAA to be intermingled with the same or complementary printhead models to create a multitude of single and multiple-color configurations.

Each 256-channel Sapphire printhead is offered with an integral temperature sensor and a configurable, dual-ported fluid interface comprised of O-ring face mounts or barbed fittings to facilitate fast flushing or recirculation of inks.

Printhead operational temperature can be up to 90° C. The driver chip is double buffered to support the Sapphire QS-256/10 AAA high-speed jetting capability.



www.dimatix.com

POB00050 Rev. 06 05/15/10

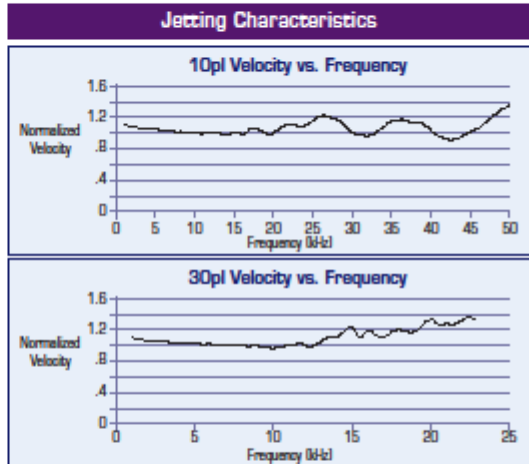
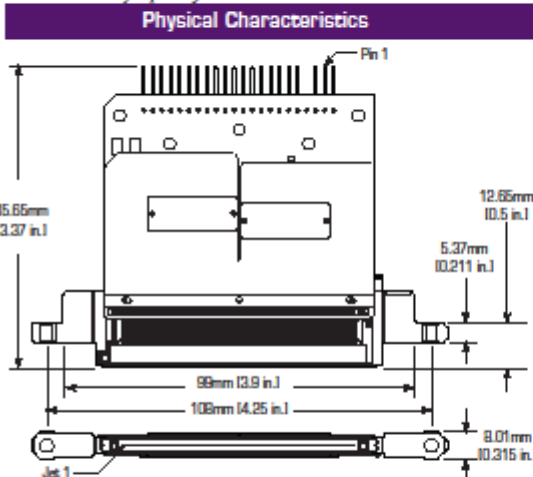
**Performa**

Sapphire GS-256/10 AAA

Product Data

Parameter	Sapphire GS-256/10 AAA								
Number of addressable jets	256								
Print width	64.77 mm [2.550 in.]								
Nozzle spacing	254 microns [0.010 in.] (100 dpi)								
Typical jet straightness, 1 sigma*	1.5 mrad [0.085°]								
Typical drop velocity variability, 1 sigma*	5%								
Ink operating temperature range	up to 90° C [194° F]								
Fluid viscosity range (at jetting temperature)	8 - 20 cP (10 - 14 cP recommended)								
Compatible jetting fluids	UV curable, Organic solvents, and aqueous inks								
<b>BINARY OPERATION:</b>									
Adjustment for drop size	10 - 30 picoliters								
Productivity	<table border="1"> <thead> <tr> <th>Drop Size</th> <th>Maximum Frequency</th> </tr> </thead> <tbody> <tr> <td>10 pl</td> <td>50 kHz</td> </tr> <tr> <td>20 pl</td> <td>25 kHz</td> </tr> <tr> <td>30 pl</td> <td>16 kHz</td> </tr> </tbody> </table>	Drop Size	Maximum Frequency	10 pl	50 kHz	20 pl	25 kHz	30 pl	16 kHz
Drop Size	Maximum Frequency								
10 pl	50 kHz								
20 pl	25 kHz								
30 pl	16 kHz								
<b>GRayscale OPERATION:</b>									
Number of levels	up to 4								
Fundamental drop size	10 picoliters								
Productivity	<table border="1"> <thead> <tr> <th>Largest Drop Size</th> <th>Maximum Frequency</th> </tr> </thead> <tbody> <tr> <td>20 pl</td> <td>25 kHz</td> </tr> <tr> <td>30 pl</td> <td>16 kHz</td> </tr> </tbody> </table>	Largest Drop Size	Maximum Frequency	20 pl	25 kHz	30 pl	16 kHz		
Largest Drop Size	Maximum Frequency								
20 pl	25 kHz								
30 pl	16 kHz								
OEM accessible non-volatile memory	Two 256-bit pages, write once								

\*at constant frequency



Product data presented above are for guideline purposes only. For design and engineering work using this product, please contact Dimatix Technical Support for the appropriate Product Manual containing full Product Specifications.



<p><b>Corporate Office:</b> FUJIFILM Dimatix, Inc. 2320 Martin Avenue Santa Clara, CA 95050 USA</p> <p>Tel: (408) 565-9150 Fax: (408) 565-9151 Email: info@dimatix.com</p>	<p><b>New Hampshire Facility:</b> FUJIFILM Dimatix, Inc. 109 Etna Road Lebanon, NH 03766 USA</p> <p>Tel: (603) 443-5300 Fax: (603) 448-9870 Email: info@dimatix.com</p>	<p><b>Japan Office:</b> Advanced Marking Business Division FUJIFILM Corporation Midtown West, 7-3, Akasaka 9-Chome Minato-ku, Tokyo 107-0002 Japan</p> <p>Tel: +81 3 6271 1091 Fax: +81 3 6271 1165 E-mail: front.amb@fujifilm.co.jp</p>	<p><b>European Office:</b> Tel: +44 7739 863 505 Fax: +44 870 167 4329 Email: euro@dimatix.com</p> <p><b>Korean Office:</b> Tel: +82 2 6242 6012 Fax: +82 2 6247 6012 Email: korea@dimatix.com</p>	<p><b>China Office:</b> Email: china@dimatix.com</p>
--	---	--	--	--

www.dimatix.com

PO300050 Rev. 06 05/15/10



## A5. Datasheet of the substrates

### *Kapton*



#### Technical Data Sheet

DuPont™ Kapton® HN general-purpose film has been used successfully in applications at temperatures as low as -269°C (-452°F) and as high as 400°C (752°F). HN film can be laminated, metalized, punched, formed or adhesive coated. Kapton® HN is the recommended choice for applications that require an all-polyimide film with an excellent balance of properties over a wide range of temperatures.

#### Applications

- Mechanical parts
- Electronic parts
- Electrical Insulation
- Pressure sensitive tape
- Fiber optics cable
- Insulation blankets
- Insulation tubing
- Automotive diaphragms sensors and manifolds
- Etching
- Shims

#### Product Specifications

Kapton® HN is manufactured, slit and packaged according to the product specifications listed in H-38479, Bulletin GS-98-7.

#### Certification

Kapton® HN meets ASTM D-5213 (type 1, item A) requirements.



**Table 1**  
**Physical Properties of DuPont™ Kapton® HN at 23°C (73°F)**

Property	Unit	1 mil 25µm	2 mil 50µm	3 mil 75µm	5 mil 125µm	Test Method
Ultimate Tensile Strength at 23°C, (73°F) at 200°C (392°F)	psi (MPa)	33,600(231) 20,000(139)	33,600(231) 20,000(139)	33,600(231) 20,000(139)	33,600(231) 20,000(139)	ASTM D-882-91, Method A*
Ultimate Elongation at 23°C, (73°F) at 200°C (392°F)	%	72 83	82 83	82 83	82 83	ASTM D-882-91, Method A
Tensile Modulus at 23°C, (73°F) at 200°C (392°F)	psi (GPa)	370,000 (2.6) 290,000 (2.0)	370,000 (2.6) 290,000 (2.0)	370,000 (2.6) 290,000 (2.0)	370,000 (2.6) 290,000 (2.0)	ASTM D-882-91, Method A
Density	g/cc	1.42	1.42	1.42	1.42	ASTM D-1606-90
MIT Folding Endurance	cycles	285,000	65,000	6,000	6,000	ASTM D-2176-89
Tear Strength-propagating (Elmendorf), N (lbf)		0.07 (0.02)	0.21 (0.02)	0.38 (0.02)	0.68 (0.02)	ASTM D-1922-89
Tear Strength, Initial (Graves), N (lbf)		7.2 (1.6)	16.3 (1.6)	26.3 (1.6)	46.9 (1.6)	ASTM D-1004-90
Yield Point at 3% at 23°C, (73°F) at 200°C (392°F)	MPa (psi)	69 (10,000) 41 (6,000)	69 (10,000) 41 (6,000)	69 (10,000) 41 (6,000)	69 (10,000) 41 (6,000)	ASTM D-882-91
Stress to produce 5% elong. at 23°C, (73°F) at 200°C (392°F)	MPa (psi)	90 (13,000) 61 (9,000)	90 (13,000) 61 (9,000)	90 (13,000) 61 (9,000)	90 (13,000) 61 (9,000)	ASTM D-882-92
Impact Strength at 23°C, (73°F)	N•cm•(ft lb)	78 (0.68)	78 (0.68)	78 (0.68)	78 (0.68)	DuPont Pneumatic Impact Test
Coefficient of Friction, kinetic (film-to-film)		0.48	0.48	0.48	0.48	ASTM D-1894-90
Coefficient of Friction, static (film-to-film)		0.63	0.63	0.63	0.63	ASTM D-1894-90
Refractive Index (sodium D line)		1.70	1.70	1.70	1.70	ASTM D-642-90
Poisson's Ratio		0.34	0.34	0.34	0.34	Avg. three samples, elongated at 5, 7, 10%
Low temperature flex life		pass	pass	pass	pass	IPC-TM-650, Method 2.6.18

\*Specimen size 25 x 150 mm (1.6 in); jaw separation 100 mm (4 in), jaw speed, 50mm/min (2 in/min). Ultimate refers to the tensile strength and elongation measured at break.

**Table 2**  
**Thermal Properties of DuPont™ Kapton® HN Film**

Thermal Property	Typical Value	Test Condition	Test Method
Melting Point	None	None	ASTM E-794-85 (1989)
Thermal Coefficient of Linear Expansion	20 ppm/°C (11 ppm/°F)	-14 to 38°C (7 to 100°F)	ASTM D-696-91
Coefficient of Thermal Conductivity, W/m•K $\frac{\text{cal}}{\text{cm}\cdot\text{sec}\cdot^\circ\text{C}}$	0.12 2.87 x 10 <sup>4</sup>	296K 23°C	ASTM F-433-77 (1987)
Specific Heat, J/g•K (cal/g•°C)	1.09 (0.261)		Differential calorimetry
Heat Sealability	not heat sealable		
Solder Float	pass		IPC-TM-650 Method 2.4.13A
Smoke Generation	D <sub>m</sub> < 1	NBS smoke chamber	NFPA-258
Shrinkage, % 30 min at 150°C 120 min at 400°C	0.17 1.25		IPC-TM-650 Method 2.2.4A; ASTM D-5214-91
Limiting Oxygen Index, %	37-45		ASTM D-2863-87
Glass Transition Temperature (T <sub>g</sub> )	A second order transition occurs in Kapton® between 360°C (680°F) and 410°C (770°F) and is assumed to be the glass transition temperature. Different measurement techniques produce different results within the above temperature range.		

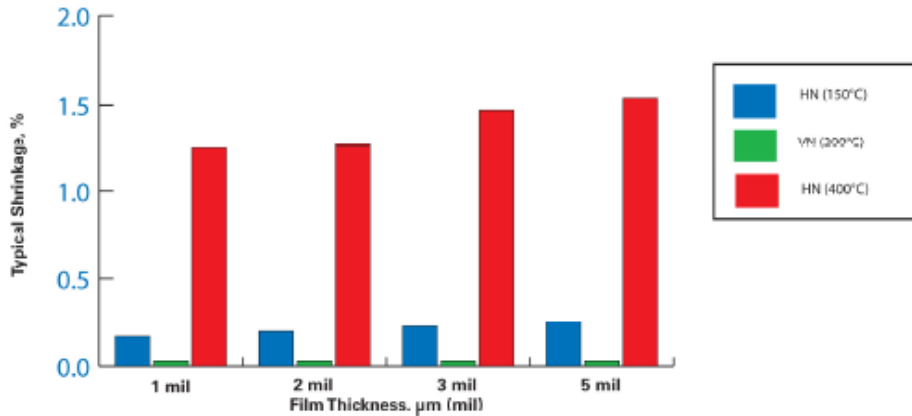
**Table 3**  
**Typical Electrical Properties of DuPont™ Kapton® HN Film at 23°C (73°F), 50% RH**

Property Film Gage	Typical Value		Test Condition	Test Method
<u>Dielectric Strength</u>	<u>V/m kV/mm</u>	<u>V/mil</u>	60 Hz 1/4 in electrodes 500 V/sec rise	ASTM D-149-91
25 µm (1 mil)	303	(7700)		
50 µm (2 mil)	240	(6100)		
75 µm (3 mil)	205	(5200)		
125 µm (5 mil)	154	(3900)		
<u>Dielectric Constant</u>			1 kHz	ASTM D-150-92
25 µm (1 mil)	3.4			
50 µm (2 mil)	3.4			
75 µm (3 mil)	3.5			
125 µm (5 mil)	3.5			
<u>Dissipation Factor</u>			1 kHz	ASTM D-150-92
25 µm (1 mil)	0.0018			
50 µm (2 mil)	0.0020			
75 µm (3 mil)	0.0020			
125 µm (5 mil)	0.0026			
<u>Volume Resistivity</u>	*cm			ASTM D-257-91
25 µm (1 mil)	1.5 x 10 <sup>17</sup>			
50 µm (2 mil)	1.5 x 10 <sup>17</sup>			
75 µm (3 mil)	1.4 x 10 <sup>17</sup>			
125 µm (5 mil)	1.0 x 10 <sup>17</sup>			

**Dimensional Stability**

The dimensional stability of DuPont™ Kapton® polyimide film depends on two factors—the normal coefficient of thermal expansion and the residual stresses placed in the film during manufacture. The latter causes Kapton® to shrink on its first exposure to elevated temperatures as indicated in the bar graph in **Figure 1**. Once the film has been exposed, the normal values of the thermal coefficient of linear expansion as shown in **Table 4** can be expected.

**Figure 1. Residual Shrinkage vs. Exposure Temperature and Thickness, DuPont™ Kapton® HN and VN Films**



**Table 4**  
**Thermal Coefficient of Expansion,**  
**DuPont™ Kapton® HN Film, 25 µm (1 mil),**  
**Thermally Exposed**

Temperature Range, °C, (°F)	ppm/°C
30–100 (86–212)	17
100–200 (212–392)	32
200–300 (392–572)	40
300–400 (572–752)	44
30–400 (86–752)	34

**PET****Product Information****Mylar<sup>®</sup> A 12 - 36 $\mu$ m****Product Description**

MYLAR<sup>®</sup> polyester film is a flexible, strong and durable film with an unusual balance of properties making it suitable for many industrial applications. Type MYLAR<sup>®</sup> A is a tough general purpose film which is transparent in 12 $\mu$ m through 23 $\mu$ m and translucent in heavier thickness.

Type MYLAR<sup>®</sup> A is primarily used for release applications, office supplies, electrical insulation and industrial laminations with other flexible materials. Type MYLAR<sup>®</sup> A is also available in 50 $\mu$ m through 500  $\mu$ m thickness range.

**Film Properties (typical values)**

Type MYLAR<sup>®</sup> A has a tensile strength that averages 190 MPa, has excellent resistance to moisture and most chemicals and can withstand temperature extremes from -70°C to 150°C. Because it contains no plasticisers MYLAR<sup>®</sup> A does not become brittle with age under normal conditions.

Property	Test Method		Value					
			12	15	19	23	30	36
Thickness	---	micron	12	15	19	23	30	36
Tensile Strength (Mpa)	ASTM D 882	MD	200	200	210	21	230	230
		TD	220	220	230	230	260	260
Modulus (Mpa)	ASTM D 882	MD	4200	4200	4200	4100	4100	4100
		TD	4200	4200	4300	4300	4300	4300
Elongation (%)	ASTM D 882	MD	100	110	110	130	120	130
		TD	100	100	110	110	100	110
Shrinkage 150°C for 30 min (%)	ASTM D 1204	MD	1.5	1.3	1.3	1.3	2.5	2
		TD	0	0	1	1	1.7	1.7
Shrinkage 200°C for 30 min (%)	ASTM D 1204	MD	4.5	4	4	4	8	7
		TD	1.5	1	3	3	7	6.5
Haze (%)	ASTM D 1003 Gardner Hazemeter		5	7	11	15	20	22
Dielectric Strength (minimum) (kV)	ASTM D 149		2.5	2.7	3	4	4.8	5.5

1mm = 1 micron = 0.001 mm approx 4 gauge, MD = Machine Direction, TD = Transverse Direction

**PDMS**

Produto	Descrição	Características	
<b>Encapsulantes de Silicone</b>			
<i>Sylgard</i> <sup>®</sup> 160 Elastômero de Silicone	Baixo custo; boa condutividade térmica	Bicomponente; mistura de 1:1; cura em temperatura ambiente ou acelerada com calor; Contração mínima; não libera calor durante a cura; sem solventes ou subprodutos de cura; reparável, boas propriedades dielétricas; cura em seção profunda; elastômero flexível.	
<i>Sylgard</i> <sup>®</sup> 165 Elastômero de Silicone	Cura rápida; baixo custo; boa condutividade térmica		
<i>Sylgard</i> <sup>®</sup> 170 Elastômero de Silicone	Baixa Viscosidade		
<i>Sylgard</i> <sup>®</sup> 170 Elastômero de Silicone de Cura Rápida	Cura rápida; baixa viscosidade		
<i>Dow Corning</i> <sup>®</sup> Encapsulante 96-082 A & B	Viscosidade baixíssima; retardador de chamas; não derrete; Auto-extinguível; "pot-life" é extremamente longo; ampla faixa de temperatura	Bicomponente; mistura em 10:1; contração mínima; não libera calor durante a cura; sem solventes ou subprodutos da cura; cura em seção profunda; reparável; boas propriedades dielétricas; elastômero flexível	
<i>Sylgard</i> <sup>®</sup> 182 Elastômero de Silicone	Transparente, "pot-life" longo; cura por calor		
<i>Sylgard</i> <sup>®</sup> 184 Elastômero de Silicone	Transparente; cura em temperatura ambiente e/ou acelerada com calor		
<i>Sylgard</i> <sup>®</sup> 186 Elastômero de Silicone	Incolor; cura em temperatura ambiente e/ou acelerada com calor; alta resistência ao rasgo		
<i>Dow Corning</i> <sup>®</sup> 3-6121 Elastômero Encapsulante	Desempenho em temperaturas abaixo de -65°C (-85°F); Incolor; alta resistência ao rasgo e tração; cura em temperatura ambiente e/ou acelerada com calor; alto índice de refração		
<b>Encapsulantes de Silicone Sem Primer</b>			
<i>Dow Corning</i> <sup>®</sup> 3-6642 Adesivo Termicamente Condutivo	Excelente condutividade térmica; auto-aderente; líquido de baixa viscosidade; elastomérico		Bicomponente; mistura de 1:1; cura por calor; contração mínima; não libera calor durante a cura; sem solventes ou subprodutos; reparável; boas propriedades dielétricas.
<i>Dow Corning</i> <sup>®</sup> 3-8264 Adesivo de Silicone Sem Primer	Excelente adesão sem primer; cura por calor; elastomérico		
<i>Dow Corning</i> <sup>®</sup> 567 Encapsulante de Silicone Sem Primer	Cura por calor; adesão sem primer; elastomérico		
<b>Encapsulantes Bicomponentes com Cura por Condensação em Temperatura Ambiente</b>			
<i>Dow Corning</i> <sup>®</sup> 255 Elastômero Sem Primer	Cura rápida em temperatura ambiente e em seção profunda; auto-aderente; boa adesão em temperatura ambiente para a maioria dos substratos; adesão aumenta com o tempo.	Bicomponente; mistura de 10:1; não corrosiva; boas propriedades dielétricas; elastômero flexível; não requer cura por calor; refrigerar o agente de cura para uma vida útil mais longa; catalisador de estanho não pode ser inibido; possível reversão com calor e pressão em ambientes fechados.	

## Appendix

Produto	Usos Potenciais	Métodos de Aplicação	Cura <sup>1,2</sup>
<b>Encapsulantes de Silicone</b>			
<i>Sylgard</i> <sup>®</sup> 160 Elastômero de Silicone	Aplicações genéricas de proteção; fontes de energia; conectores; sensores; controles industriais; transformadores; amplificadores; módulos de resistores de alta voltagem; relés.	Fornecido em kits de dois componentes líquidos, contendo Parte A/Parte B para serem misturados em proporção 1:1 (volume ou peso); permite mistura e utilização automatizada e/ou manual.	24 horas à 25°C (77°F) 10 minutos à 100°C (212°F) 5 minutos à 150°C (302°F)
<i>Sylgard</i> <sup>®</sup> 165 Elastômero de Silicone		Fornecido em kits de dois componentes líquidos, contendo Parte A/Parte B para serem misturados em proporção 1:1 (volume ou peso); permite mistura e utilização automatizada e/ou manual.	5 minutos à 25°C (77°F)
<i>Sylgard</i> <sup>®</sup> 170 Elastômero de Silicone		Fornecido em kits de dois componentes líquidos, contendo Parte A/Parte B para serem misturados em proporção 1:1 (volume ou peso); permite mistura e utilização automatizada e/ou manual.	24 horas à 25°C (77°F) 20 minutos à 70°C (158°F) 15 minutos à 85°C (185°F) 10 minutos à 100°C (212°F)
<i>Sylgard</i> <sup>®</sup> 170 Elastômero de Silicone de Cura Rápida		Fornecido em kits de dois componentes líquidos, contendo Parte A/Parte B para serem misturados em proporção 1:1 (volume ou peso); permite mistura e utilização automatizada.	10 minutos à 25°C (77°F)
<i>Dow Corning</i> <sup>®</sup> Encapsulante 96-082 A & B	As aplicações que requeiram profunda impregnação, possível somente com uma resina de viscosidade muito baixa.	Fornecido em kits de dois componentes líquidos, contendo Parte A/Parte B para serem misturados em proporção 1:1 (volume ou peso); permite mistura e utilização automatizada e/ou manual.	30 minutos à 150°C (302°F)
<i>Sylgard</i> <sup>®</sup> 182 Elastômero de Silicone	Aplicações genéricas de proteção; fontes de energia; conectores; sensores; controles industriais; transformadores; amplificadores; módulos de resistores de alta voltagem; relés; adesivo/encapsulante para células solares.	Fornecido em kits de dois componentes líquidos, contendo Base/Agente de cura para serem misturados em proporção 10:1 (volume ou peso); permite mistura e utilização automatizada e/ou manual.	45 minutos à 100°C (212°F) 20 minutos à 125°C (257°F) 10 minutos à 150°C (302°F)
<i>Sylgard</i> <sup>®</sup> 184 Elastômero de Silicone			-48 horas em temperatura ambiente 45 minutos à 100°C (212°F) 20 minutos à 125°C (257°F) 10 minutos à 150°C (302°F)
<i>Sylgard</i> <sup>®</sup> 186 Elastômero de Silicone			-48 horas em temperatura ambiente 30 minutos à 100°C (212°F) 15 minutos à 150°C (302°F)
<i>Dow Corning</i> <sup>®</sup> 3-6121 Elastômero Encapsulante			-48 horas à temperatura ambiente 20 minutos à 100°C (212°F) 10 minutos à 150°C (302°F)
	Aplicações de encapsulamento em baixas temperaturas; aplicações ópticas que requerem um alto índice de refração		

Produto	Proporção de Mistura	Cor	Viscosidade, em Centipoise ou mPa • s	Dureza, Shore A	Gravidade Específica	Tempo de Trabalho à Temperatura Ambiente	Adesão Sem Primer, Cisalhamento			Condutividade Térmica		Coeficiente Linear da Expansão Térmica $\mu\text{m} / \text{m} \cdot ^\circ\text{C}$ ou ppm	Vida Útil a partir da data de fabricação, à temperatura ambiente, em meses
							psi	MPa	kgf/cm <sup>2</sup>	Watt-meter-°K	cal/cm.sec.°C		
<b>Encapsulantes de Silicone</b>													
<i>Sylgard</i> <sup>®</sup> 160 Elastômero de Silicone	1:1	Cinza	8775	60	1,57	30 min	NA	NA	NA	0,58	$1,4 \times 10^{-3}$	240	18
<i>Sylgard</i> <sup>®</sup> 165 Elastômero de Silicone	1:1	Cinza	5.000	52	1,57	<2 min	NA	NA	NA	0,58	$1,4 \times 10^{-3}$	230	18
<i>Sylgard</i> <sup>®</sup> 170 Elastômero de Silicone	1:1	Cinza escuro para preto	2.900	40	1,37	15 min	NA	NA	NA	0,40	$9,6 \times 10^{-4}$	270	24
<i>Sylgard</i> <sup>®</sup> 170 Elastômero de Silicone de Cura Rápida	1:1	Cinza escuro para preto	2.850	42	1,37	<5 min	NA	NA	NA	0,40	$9,6 \times 10^{-4}$	-	18
<i>Dow Corning</i> <sup>®</sup> 96-082 A & B Encapsulante	1:1	Preto	1.100	31	1,21	14 dias	NA	NA	NA	0,30	$7,2 \times 10^{-4}$	285	12
<i>Sylgard</i> <sup>®</sup> 182 Elastômero de Silicone	10:1	Incolor	3.900	50	1,03	>8 horas	NA	NA	NA	0,18	$4,3 \times 10^{-4}$	310	24
<i>Sylgard</i> <sup>®</sup> 184 Elastômero de Silicone	10:1	Incolor	3.900	50	1,03	>2 horas	NA	NA	NA	0,18	$4,3 \times 10^{-4}$	310	24
<i>Sylgard</i> <sup>®</sup> 186 Elastômero de Silicone	10:1	Transparente	65.000	24	1,12	2 horas	NA	NA	NA	0,2	$4,8 \times 10^{-4}$	330	12
<i>Dow Corning</i> <sup>®</sup> 3-6121 Elastômero Encapsulante	10:1	Transparente	25.000	30	1,13	2 horas	NA	NA	NA	0,18	$4,3 \times 10^{-4}$	290	18

## Appendix

Produto	Certificações UL		Especificações Militares		Rigidez Dielétrica		Constante Dielétrica à 100 Hz	Constante Dielétrica à 100 kHz	Resistividade Volumétrica ohm-cm	Fator de Dissipação à 100 Hz	Fator de Dissipação à 100 kHz
	Classificação de Flamaabilidade	Índice UL de Temperatura, Elétrica/ Mecânica, °C	Especificação	Tipo, Classe, Grupo	volts/ mil	kV/ mm					
<i>Sylgard</i> <sup>®</sup> 160 Elastômero de Silicone	94 V-0	105/105	NA	NA	530	20,9	3,30	3,20	1,0x10 <sup>15</sup>	0,01	0,002
<i>Sylgard</i> <sup>®</sup> 165 Elastômero de Silicone	94 V-0	105/105	NA	NA	530	20,9	3,30	3,20	1,0x10 <sup>15</sup>	0,01	0,002
<i>Sylgard</i> <sup>®</sup> 170 Elastômero de Silicone	94 V-0	170/170	MIL-PRF-23586F (Grau B2)	Tipo I, Classe II, QPL	480	18,9	3,17	3,16	3,1x10 <sup>13</sup>	0,003	<0,001
<i>Sylgard</i> <sup>®</sup> 170 Elastômero de Silicone de Cura Rápida	94 V-0	170/170	NA	NA	530	20,9	2,97	2,90	1,4x10 <sup>15</sup>	0,005	<0,001
<i>Dow Corning</i> <sup>®</sup> 96-082 A & B Encapsulante	94 V-0	170/170	NA	NA	500	19,7	3,14	3,12	9,5x10 <sup>14</sup>	0,0055	<0,001
<i>Sylgard</i> <sup>®</sup> 182 Elastômero de Silicone	94 V-1	130/130	MIL-I-81550C	Tipo II, QPL	540	21,2	2,65	2,65	1,2x10 <sup>14</sup>	0,0005	<0,001
<i>Sylgard</i> <sup>®</sup> 184 Elastômero de Silicone	94 V-1	130/130	MIL-I-81550C	Tipo I, QPL	540	21,2	2,65	2,65	1,2x10 <sup>14</sup>	0,0005	<0,001
<i>Sylgard</i> <sup>®</sup> 186 Elastômero de Silicone	94 HB	140/140	NA	NA	450	17,7	2,93	2,87	1,1x10 <sup>14</sup>	0,0012	<0,001
<i>Dow Corning</i> <sup>®</sup> 3-6121 Elastômero Encapsulante	NA	NA	NA	NA	415	16,3	2,92	2,92	1,4x10 <sup>14</sup>	0,01	<0,001



## TPU

**INTRODUCTION**

AVALON 65 AB is a general purpose polyester based thermoplastic polyurethane for injection moulding.

AVALON 65 AB is part of the AVALON Soft Range and offers a premium soling material for casual, sport and protective footwear.

The features offered include :

- Durability
- Excellent surface definition
- Abrasion resistance
- Slip resistance
- Phthalate free

Table 1: Typical Physical Properties <sup>(1)</sup>			
Property	Method	Unit	Value
Density	DIN 53479	g/cm <sup>3</sup>	1.18
Hardness, Shore A	DIN 53505	A	67
Hardness, Shore D	DIN 53505	D	-
Tensile Strength	DIN 53504	MPa	30
Elongation at Break	DIN 53504	%	700
100% Modulus	DIN 53504	MPa	2.5
300% Modulus	DIN 53504	MPa	5
Tear Strength (Angle)	DIN 53515	kN/m	40
Compression Set @ 23°C	DIN 53517	%	20
Abrasion Resistance	DIN 53516	mm <sup>3</sup>	< 60
Ross Flex @ -10°C	BS 5131	k.cycles	100

<sup>(1)</sup> : Test plates conditioned 20 hours at 100°C before testing.

**PRODUCT DATA****AVALON® 65 AB**

**Thermoplastic Polyurethane**

**HEALTH AND SAFETY ADVICE**

Before undertaking any trials with this product it is essential that all personnel are aware of the necessary precautions that must be taken. These are detailed in the relevant Safety Data Sheet that will be provided by Huntsman Polyurethanes.

**POLYMER SELECTION**

Before selecting this product it is necessary that the user ensures its performance will meet all operational and end use requirements. Having satisfied these requirements, should changes be contemplated in method of application, materials, service conditions or any other change that could affect the ultimate performance of the end product, then further tests and trials should be carried out.

For assistance with particular problems and applications, please contact the AVALON TPU Technical Service Department.

**PACKAGING & STORAGE**

AVALON TPU is supplied in 25 kg moisture guarded sacks, 40 per pallet and shrink wrapped.

AVALON Thermoplastic Polyurethanes may be stored for 24 months from the date of manufacture, sealed in the manufacturers original packaging.



## A6. Datasheet of the micro/nanosize particles

### Clay Particles

## Datasheet



### Nanofil<sup>®</sup> 5

Active nanofillers for polymer applications

**Composition:** organic modified nanodispers layered silicate

**Chemical functionality:** long chain hydrocarbon

**Typical technical data:**

Product form:	powder
Colour:	creme
Specific weight:	approx. 1,8 g/cm <sup>3</sup>
Bulk density:	150 g/l
Medium particle size:	8 µm
Primary particle size after complete dispersion:	100 - 500 nm x 1nm
Moisture content:	< 3 %
Loss on ignition:	approx. 35 %

All information given in this technical information cannot be guaranteed. Variations from the indications mentioned above are possible because of the particular production facilities.

## Silica Particles

**degussa.**  
creating essentials

## Product Information

### ▶ **AEROSIL® 200** Hydrophilic Fumed Silica

*AEROSIL® 200 is a hydrophilic fumed silica with a specific surface area of 200 m<sup>2</sup>/g.*

#### Applications and Properties

##### Applications

- Paints and coatings
- Unsaturated polyester resins, laminating resins and gel coats
- HTV- and RTV-2K-silicone rubber
- Adhesives and sealants
- Printing inks
- Cable compounds and cable gels
- Plant protection
- Food and cosmetics

##### Properties

- Rheology and thixotropy control of liquid systems, binders, polymers, etc.
- Used as anti-settling, thickening and anti-sagging agent
- Reinforcement of HTV- and RTV-2K-silicone rubber
- Improvement of free flow and anticaking characteristics of powders

#### Physico-chemical Data

Properties	Unit	Typical Value
Specific surface area (BET)	m <sup>2</sup> /g	200 ± 25
Average primary particle size	nm	12
Tapped density* (approx. value) acc. to DIN EN ISO 787/11, Aug. 1983	g/l	approx. 50
Moisture* 2 hours at 105 °C	wt. %	≤ 1.5
Ignition loss, 2 hours at 1000 °C, based on material dried for 2 hours at 105 °C	wt. %	≤ 1.0
pH in 4% dispersion		3.7 - 4.7
SiO <sub>2</sub> -content based on ignited material	wt. %	≥ 99.8

\* as plant

The data represents typical values and not production parameters.

AEROSIL® 200 / Sept 04 / www.aerosil.com

**AEROSIL®**  
Invented to improve

## A7. Datasheet of the inks

## P3HT

**SIGMA-ALDRICH**

sigma-aldrich.com

300 North Avenue, St. Louis, MO 63103 USA  
 Tel: (800) 225-0321 (618) 455-3500 Fax: (314) 997-2227  
 email: sigmaaldrich@sigmaaldrich.com

## Product Information

**Poly(thiophene-3-[2-(2-methoxyethoxy)ethoxy]-2,5-diyl), sulfonated solutions**

Catalog Numbers **699799** and **699780**  
 Store at Room Temperature  
 Technical Bulletin AL-251

**TECHNICAL BULLETIN**

CAS RN 1003582-37-3  
 Synonyms: Plexcore® OC RG-1100 and OC RG-1200

**Product Description**

Poly(thiophene-3-[2-(2-methoxyethoxy)ethoxy]-2,5-diyl), sulfonated solutions are organic conductive inks designed for spin coating applications. However, they have also been evaluated and may be used in conjunction with other film deposition techniques such as ink jet printing, slot-die, and gravure.

The inks are typically used as a hole injection layer (HIL) in organic light emitting diode (OLED) devices for lighting and display applications, and as the hole transport layer (HTL) in organic photovoltaic (OPV) devices. In addition, these inks can be used in other devices, for example organic photo-detectors, smart labels, and field effect transistors.

Two different solutions are offered (Catalog Numbers 699799 and 699780) with the following properties:

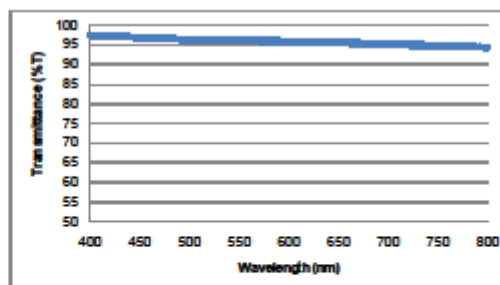
Property	Catalog Number 699799	Catalog Number 699780
Synonym	Plexcore OC RG-1100	Plexcore OC RG-1200
Solvent	2% in 1,2-propanediol/isopropanol/water	2% in ethylene glycol monobutyl ether/water (3:2)
Resistivity	25–250 Ω-cm	500–3,000 Ω-cm
Viscosity	7–13 cP (Brookfield)	4–10 cP (Brookfield)
Assay	≥99.99% (trace metal basis)	
Work Function	–5.1 to –5.2 eV	
pH	2.2–2.8	
Density	0.95 g/mL (25 °C)	
Surface Tension	35–38 dynes/cm	

Hole injection is the phenomenon of a positive charge (hole) being transferred from an electrode into a semiconducting layer within a device. The inks enable hole injection between the electrode and the neighboring semiconducting layer by reducing the energy barriers between the electrode and the semiconducting layer.

Improved hole injection implies the capability to modulate it depending on the requirement for charge balance within the device. This impacts OLED performance by improving the lifetime of the device. In addition, the effective reduction of energetic barriers at interfaces enables lower operating voltage of the OLED.

The sulfonated polythiophene inks have lower acidity compared to conventional hole injection layer (HIL) materials and form dried film which are less hygroscopic than conventional HIL materials.

**Figure 1.**  
 Plexcore OC RG-1100 – Optical Transmission  
 (100 nm film thickness)



## **PEDOT**



### **ORGACON™ Transparent Conductive Inkjet Ink: IJ-1005**

Orgacon inkjet inks are highly transparent conductive inks based on conductive polymer PEDOT/PSS. IJ-1005 was tested with different piezo inkjet platforms such as Microdrop, Dimatix DMP-2800, Spectra Galaxy 30

#### **Typical Applications**

- capacitive touch pads
- membrane switches
- smart packaging
- printed sensors
- OPV HIL

#### **Physical Properties**

- Solid content: 0.8 wt%
- Viscosity: 7 - 12 mPas
- Surface tension: 31 - 34 mN/m
- pH: 1.5 - 2.5
- Surface Resistance: 800 Ohm/square, 96% VLT excl. substrate (Dimatix DMP-2831 test)
- Shelf Life: 6 months in storage conditions

#### **Storage**

- Store the product between 5°C and 25 °C

#### **Health and Safety**

- See Material Safety Data Sheet

#### **Jetting Orgacon Ink**

- Degassing ink sample before use
- Filtering before use is not recommended due to possible air entrapment but can be performed with a syringe filter (0.2 µm) or glass fiber filter (0.4 µm)
- Contact us for more recommendations on a specific platform



Ag



**Applied Nanotech, Inc.**  
*A subsidiary of APPLIED NANOTECH HOLDINGS, INC.*

3006 LONGHORN BLVD., SUITE 107 AUSTIN, TX 78758  
 PHONE (512) 339-5020 • FAX (512) 339-5021 • WWW.APPLIEDNANOTECH.NET

**Ag-IJ10**  
*Nanosilver Ink*

ANI's Ag-IJ10 is a silver nanoparticle ink that can be thermally sintered to high conductivity at low temperature. Additional photosintering can further lower the resistivity. The low processing temperatures (100-150°C) allow for applications in printed electronics using low cost flexible polymer substrates such as PET. The small sizes of the nanoparticles and uniform dispersion in Ag-IJ10 make it suitable for printing using inkjet technologies.

**Typical properties**

<b>Part number</b>	<b>Ag-IJ10</b>
<b>Particle Size</b>	<b>3-10 nm</b>
<b>Resistivity</b>	<b>10-50 <math>\mu\Omega</math>-cm*</b>
<b>Solid Content</b>	<b>45 wt%</b>
<b>Viscosity</b>	<b>4-5 cP**</b>
<b>Surface Tension</b>	<b>28-35 mN/m</b>
<b>Solvent</b>	<b>Organic</b>

\* Dependent on sintering temperature and time- higher temperature and longer sintering time results in lower resistivity and better adhesion to the substrate.

\*\* Measured at 100rpm and 25°C with Brookfield VLDV-II+PRO/ULA viscometer

IN USA AND EUROPE

+1 (512) 339-5020 PHONE  
 +1 (512) 339-5021 FAX  
 SALES@APPLIEDNANOTECH.NET

IN ASIA

+81-3-5214-6144 PHONE  
 +81-3-5214-6148 FAX  
 MMATT@NIFTY.COM



**Applied Nanotech, Inc.**  
*A subsidiary of APPLIED NANOTECH HOLDINGS, INC.*

3006 LONGHORN BLVD., SUITE 107 AUSTIN, TX 78758  
PHONE (512) 339-5020 • FAX (512) 339-5021 • WWW.APPLIEDNANOTECH.NET

**Application Notes:**  
**Ag-IJ10 Nanosilver Ink**

**Description**

ANI's Ag-IJ10 is a silver nanoparticle ink suitable for drop on demand printing highly conductive lines and patterns for applications in the printed electronics industry. Ag-IJ10 ink can be thermally sintered at low temperatures on PET and polyimide substrates.

**Storage and Shelf Life**

Ag-IJ10 ink should be stored in a tightly sealed, leak-proof container at 3-10°C. Storage in freezers is not recommended. Ag-IJ10 may be stored for up to 3 months.

**Safety and Handling**

When working with Ag-IJ10 ink, use adequate ventilation and wear appropriate protective gear. Ag-IJ10 can cause eye and skin irritation. The following precautions should be taken when handling Ag-IJ10 ink:

- Read the Material Safety Data Sheet (MSDS)
- Avoid prolonged breathing of vapor
- Use appropriate safety equipment such as gloves and eye protection
- Wash hands thoroughly after handling
- Keep the ink container closed when not in use to prevent drying and spilling

**Processing Procedures**

*Pre-processing*

- The Ag-IJ10 ink requires ultrasonic agitation for 10 minutes.
- After sonication, the ink should be filtered by using a 0.45 micrometer pore size glass fiber filter before filling ink cartridge.

*Printing*

- Printing has been demonstrated using inkjet and wire rod drawdown. Conditions will vary based on technique and substrate.

*Drying*

- Printed ink can be air dried at room temperature for 30 min, or dried at 100°C for 10 min in ambient atmosphere.

*Sintering*

- Ag-IJ10 will reach the minimum resistivity after 30 min at 150°C
- Curing the printed sample in convection oven is recommended

*Clean-up*

- Follow appropriate cleaning procedures for equipment used to dispense Ag-IJ10 ink. Excess ink can be removed with ethanol, IPA, or acetone.

DISCLAIMER: Applied Nanotech, Inc. extends no warranties, makes no representations, and assumes no responsibility as to the accuracy of this information for this product for any use or for any consequence of its use. Users assume all risk of handling, whether or not in accordance with any statements or recommendation of Applied Nanotech, Inc.

IN USA AND EUROPE

+1 (512) 339-5020 PHONE  
+1 (512) 339-5021 FAX  
SALES@APPLIEDNANOTECH.NET

IN ASIA +81-3-5214-6144 PHONE

+81-3-5214-6148 FAX  
MMATT@NIFTY.COM



## A8. Characterization Kit and Comparison Chart



### TQC Cross Cut Adhesion Test - CC2000 SP1690, SP1691, SP1692, SP1699, SP1700

**Datasheet**

**Product description** The TQC Cross Cut Adhesion Test KIT (CC2000) is used to test the adhesion of dry coats of paint on their substrate by means of a series of cuts through the coating. Two series of parallel cuts cross angled to each other to obtain a pattern of 25 or 100 similar squares. The ruled area is evaluated by using a table chart after a short treatment with a stiff brush, or adhesive tape for hard substrates.



**Standards** ISO/DIN 2409, ASTM D3359

**Application area's** Coating/Paint Industry, Galvanise, Automotive, Laboratory, Painters, Shipping Industry, Steel Protection, Wood

**Features**

- Self-adjusting knife-holder ensures equal pressure on the cutting knife
- Ergonomically shaped handle
- Easy to change cutting knife, no extra key needed
- Wide range of knife sizes available for different coating thicknesses and substrates and according to different standards.



**Standard delivery**

**Cross Cut Adhesion Tester acc. to DIN-ISO, 6 teeth**

SP1690 TQC Cross-cut adhesion test kit CC2000, incl. blade 1mm

SP1691 TQC Cross-cut adhesion test kit CC2000, incl. blade 2 mm

SP1692 TQC Cross-cut adhesion test kit CC2000, incl. blade 3 mm.

**Cross cut Adhesion Tester acc. To ASTM, 11 teeth**

SP1699 TQC Cross-cut adhesion test kit CC2000, incl. blade 1 mm.

SP1700 TQC Cross-cut adhesion test kit CC2000, incl. blade 1,5 mm.

*The test kit contains a soft grip handle, a hardened steel cutter (type may vary, see above), a nylon brush, an illuminated magnifier and adhesive tape (adhesion to steel 4.3N/cm).*

**Optional items**

SP3007 Adhesion tape, single roll, adhesion to steel 4.3 N/cm

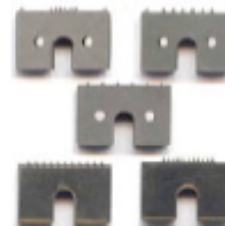
SP3010 Adhesion tape, set of 3 rolls, adhesion to steel 4.3 N/cm

SP3020 Adhesion tape, single roll, adhesion to steel 7.6 N/cm

SP1710 Nylon Brush for Cross Cut Adhesion Test

SP9700 Lighted Magnifier 2.5x


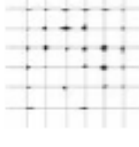
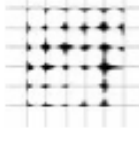
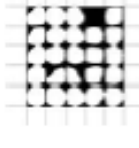
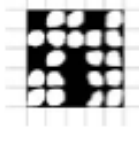
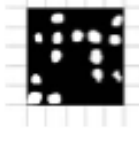
SP1702 Teeth distance 1 mm  
 SP1703 Teeth distance 2 mm  
 SP1704 Teeth distance 3 mm



**Spare TQC knife acc. to ASTM**

SP1705 Teeth distance: 1 mm  
 SP1706 Teeth distance: 1,5 mm

**Comparison Chart**

Classi- fication	Description	Appearance of surface of cross-cut area from which flaking has occurred (Example for six parallel cuts)
0	The edges of the cuts are completely smooth; none of the squares of the lattice is detached.	
1	Detachment of small flakes of the coating at the intersections of the cuts. A cross-cut area not significantly greater than 5% is affected.	
2	The coating has flaked along the edges and/or at the intersections of the cuts. A cross-cut area significantly greater than 5%, but not significantly greater than 15%, is affected.	
3	The coating has flaked along the edges of the cuts partly or wholly in large ribbons, and/or it has flaked partly or wholly on different parts of the squares. A cross-cut area significantly greater than 15%, but not significantly greater than 35%, is affected.	
4	The coating has flaked along the edges of the cuts in large ribbons and/or some squares have detached partly or wholly. A cross-cut area significantly greater than 35%, but not significantly greater than 65%, is affected.	
5	Any degree of flaking that cannot even be classified by classification 4.	



## A9. Adhesive datasheet



EXCLUSIVE DISTRIBUTORS OF  
**REINHARDT-TECHNIK**  
 Machines for the application of adhesives & sealants  
**PANACOL ELOSOL**  
 Adhesive systems



Bonham Drive, Eurolink Industrial Estate  
 Sittingbourne, Kent. ME10 3RY  
 Tel 01795 427888 Fax 01795 479685  
 Email [sales@eurobond-adhesives.co.uk](mailto:sales@eurobond-adhesives.co.uk)  
 Web [www.eurobond-adhesives.co.uk](http://www.eurobond-adhesives.co.uk)

### Technical Data - ELECOLIT 414

ELECOLIT 414 is a polyester - based, electrically conductive ink, coating and adhesive suitable for application by stamping, screen printing, dipping and syringe dispensing.

ELECOLIT 414 is formulated to provide exceptional conductivity when cured at low temperatures. Unlike conventional conductive materials, this product is very resistant to flexing and creasing. Some applications for ELECOLIT 414 include, but are not limited to, EMI/RFI shielding of polyimide flexible circuits, polymer thick film circuitry, membrane switches, electrical attachments for surface mounted devices and anode coatings for tantalum capacitors.

### TYPICAL CURED PROPERTIES

Consistency	Smooth Paste
Filler	Silver
Percent Silver, Cured	87
Crease Resistance	Excellent
Volume Resistivity (ohm-cm) (70°C)	0.00005
Sheet Resistivity(ohm/sq/mil) (70°C)	0.02
Solderable	NO
Hydrolytic Stability	Excellent
Useful Temperature Range	-65°C to + 200°C
Thermal Stability	Good to 325°C

### SUGGESTED HANDLING AND CURING

ELECOLIT 414 is ready to use as supplied. Further thinning may be accomplished by adding small amounts of Butyl Cellosolve Acetate. Prior to using, be certain to re-suspend silver by thorough mixing. Best properties for most applications, result when cured for several minutes at 125°C to 150°C. Good properties are obtained on a variety of substrates by dry and curing for 15 minutes at 70°C. End user is advised to experimentally determine temperature and time best suited for individual applications.

### STORAGE

Shelf Life: 6 months at 25°C, or 9 months at 5°C, or 12 months at -10°C

### SAFETY AND HANDLING

Use with adequate ventilation. Keep away from sparks and open flames. Avoid prolonged contact with skin and breathing of vapours. Wash with soap and water to remove from skin.

14.12.98

## A10. Pressure Chamber accessories

Technologies for Sensors Indicators and Systems

| Force | Pressure | Temperature | Switch



### Pressure sensors for industrial applications Model P3297

Non linearity 0.6% (option 0.26%)

Standard output: 4...20 mA; 2-wire  
 or 0...5 VDC; 3-wire  
 or 0...10 VDC; 3-wire  
 or 0.5...4.5 VDC; 3-wire  
 or 0.5...4.5 VDC ratiometric



#### Description

Robustness and long-term stability during operation are the strengths of this compact pressure sensor for general industrial applications.

The materials and technologies used make these sensors suitable for applications with aggressive media. Welded connections between pressure cell and process connection require no sealing elements and make the measuring system particularly resistant to mechanical shock and vibration. The compact design makes these sensors interesting for room critical applications.

A wide variety of electrical connections and pressure ports simplifies the adaptation to different applications. The pressure sensor is internationally certified and ready for global deployment.

The pressure sensors comply with electromagnetic compatibility requirements (EMC) as per EN 61326.

#### Features

- Measuring range from 0...1 bar to 0...600 bar
- Medium wetted parts of stainless steel
- High EMV-protection according to EN 61 326
- Compact instrument size
- No internal sealing elements
- Highly resistance to shock and vibration
- For dynamic or static measurements

#### Measuring range

Gauge pressure 0...1 bar to 0...600 bar  
 -1...0 bar to -1...+24 bar

#### Applications

Hydraulics and pneumatics  
 Pumps and compressors  
 Building automation  
 Test stand construction  
 Machine and apparatus construction

## Technical Data

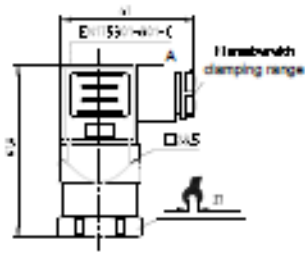
<b>Model</b>	P8287	
<b>Pressure type</b>	positive and negative gauge pressure absolut pressure on request	
<b>- Measuring range [bar]</b>	0...1 bar to 0...600 bar -1...0 bar to -1...+24 bar	
<b>- overrange limit [bar]</b>	x 2	
<b>- burst pressure [bar]</b>	x 6	
<b>Sensor element</b>	piezoresistive to 0.6 bar, thin film as of 0...10 bar	
<b>Output signal</b>	4...20 mA      2- wire 0...5 VDC      3- wire 1...5 VDC      3- wire 0...10 VDC     3- wire 0.5...4.5 VDC   3- wire 0.5...4.5 VDC   ratiometric	
<b>Non linearity<sup>1)</sup></b>	≤ 0.5% of F.S.; option: 0.25% of F.S.	
<b>Accuracy<sup>2)</sup></b>	≤ 1.0% of F.S.; option: 0.5% of F.S. <sup>3)</sup>	
<b>Hysteresis</b>	≤ 0.16% of F.S.	
<b>Non repeatability</b>	≤ 0.1% of F.S.	
<b>Stability annual</b>	≤ 0.2% of F.S. (by reference conditions)	
<b>Material</b> case medium wetted parts	stainless steel 316L stainless steel 316L (from 0...10 bar rel. 13-8PH)	
<b>Pressure connection</b>	G 1/4 according to DIN 3852-E G 1/4 according to EN 837 G 1/2 according to EN 837 1/4 NPT 1/2 NPT other pressure connection on request	
<b>Electrical connection</b>	connector DIN EN 175301-803 Form A with junction box (IP 65) connector DIN EN 175301-803 Form C with junction box (IP 65) circular plug-in connector M12x1 (4-pin) (IP 67) cable outlet: 2m (IP 67) other electrical connection on request	
<b>Power supply / load</b> 4...20 mA 0...1...5 V 0...10 V 0.5 ... 4.5 V 0.5 ... 4.5 V ratiometric	8...30 VDC 8...30 VDC 14...30 VDC 8...30 VDC 5 VDC ± 10%	$R_A [Ω] ≤ (U_A [V] - 8V) / 0.02A$ $R_A ≥ 5kΩ$ $R_A ≥ 10kΩ$ $R_A ≥ 4.5kΩ$ $R_A ≥ 4.5kΩ$
<b>Response time</b>	≤ 4ms within 10% to 90% of F.S.	
<b>RoHS-conformance</b>	yes	
<b>Approval according to</b>	cULus	
<b>CE-conformance</b>	2004/108/EC interference emission and interference resistance to EN 61 326 Interference emission limit class B 97/23/EC pressure gauge code	
<b>Electrical protections</b>	polarity, overvoltage and short-circuit protection	
<b>Temperature influence</b>	≤ 1% typ., ≤ 2.5% max. in range 0...80°C	
<b>Temperature ranges</b> compensated range storage media ambient	0...80°C -20...80°C (Option: -30...100°C) 0...80°C (Option: -30...100°C) 0...80°C (Option: -30...100°C)	
<b>Load capacity</b> shock (mechanical) vibration (under resonance)	500g acc. to IEC 60068-2-27 10g acc. to IEC 60068-2-6	
<b>Weight</b>	approx. 80g	

<sup>1)</sup> According to IEC 61208-2<sup>2)</sup> Including non linearity, hysteresis, non repeatability, variation of zero point and final value (is equal to error according to IEC 61208-2)<sup>3)</sup> By option: accuracy 0.5% and signal 0...5V is accuracy 0.6%

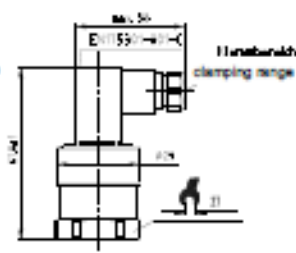
Dimension (mm)

Case

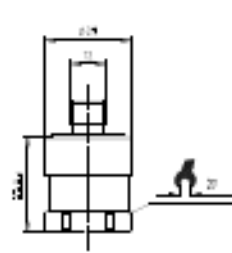
connector according to DIN EN 175301 – 803 Form A



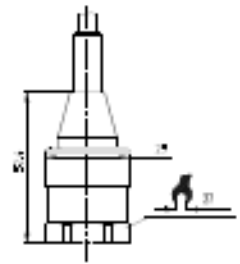
connector according to DIN EN 175301 – 803 Form C



circular plug-in connector M12x1

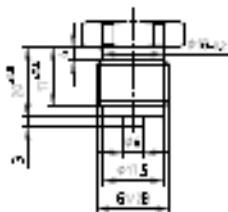


Cable outlet

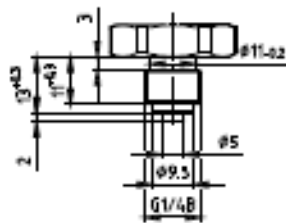


Pressure connections

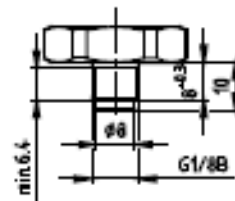
G 1/2 B



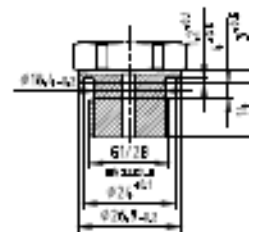
G 1/4 B



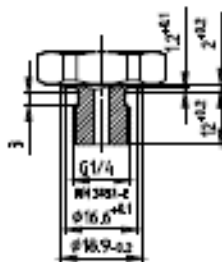
G 1/8 B



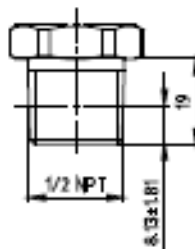
G 1/2 DIN 3852-E



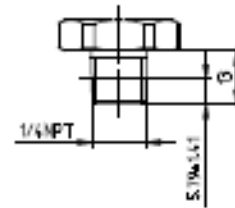
G 1/4 A DIN 3852-E



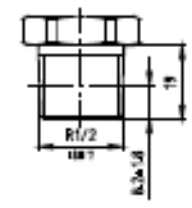
1/2 NPT



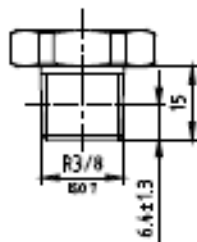
1/4 NPT



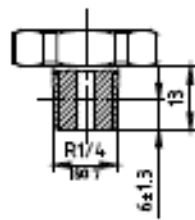
R 1/2



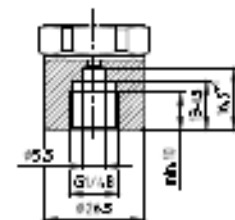
R 3/8



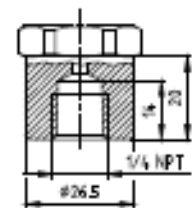
R 1/4



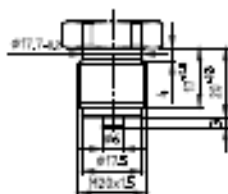
G 1/4 female



1/4 NPT female



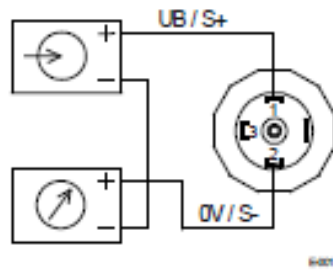
M20 x 1,5



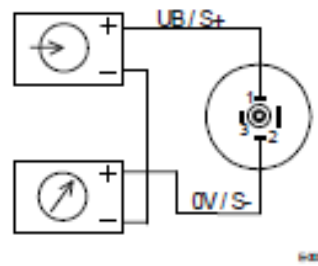
Electrical connector

Two-wire system

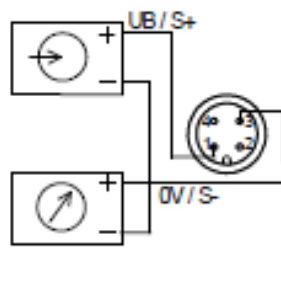
Connector according to DIN EN 175301-803 Form A with junction box



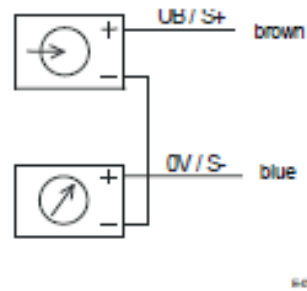
Connector according to DIN EN 175301-803 Form C with junction box



Circular plug-in connector M12x1

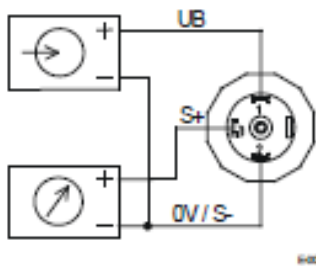


Cable outlet

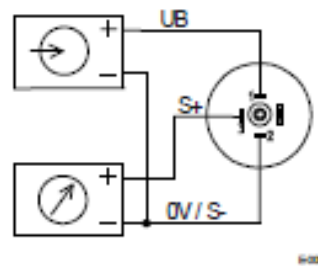


Three-wire system

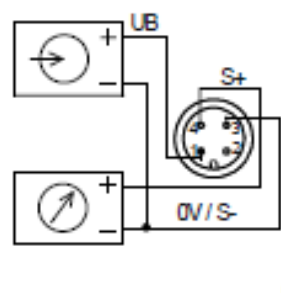
Connector according to DIN EN 175301-803 Form A with junction box



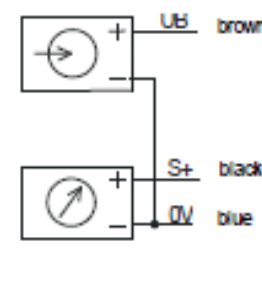
Connector according to DIN EN 175301-803 Form C with junction box



Circular plug-in connector M12x1



Cable outlet



## **A.11. List of Publications**

### **International Journals Publications**

S. Cruz, L. A. Rocha, J. C. Viana, “Novel Surface Treatment for Polymeric Substrates”, 2015 (Submitted for publication).

S. Cruz, D. Dias, J. C. Viana, L. A. Rocha, “Ink-Jet Printed Pressure Sensing Platform for Postural Imbalance Monitoring”, IEEE Sensors Journal Special Issue on “Printable Sensors and Systems”(Submitted for publication, under review).

### **Proceedings of International Conferences with acceptance based on full paper submission**

S. Cruz, D. Dias, J. C. Viana, L. A. Rocha, “Real Time Sensing Device For Health Monitoring”, IEEE MeMeA 2014 - International Symposium on Medical Measurements and Applications, 11-12 June, 2014, Lisbon, Portugal.

S. Cruz, D. Dias, J. C. Viana and L. A. Rocha, “Flexible Pressure Mapping Platform for Mobility Monitoring Applications”, PhyCS 2014 International conferences on Physiological computing Systems, 7-9 January, 2014, Lisbon, Portugal.

S. Cruz, N. J. Vieira, J. C. Viana and L. A. Rocha, “Low Cost Pressure Mapping Platform for Mobility”, I2MTC 2013 IEEE international Instrumentation and Measurement Technology Conference, 6-9 May, 2013, Minneapolis, USA.

### **Posters**

**Cruz S**, Viana JC, Rocha LA. Inkjet printing technologies for active polymeric materials. IV Annual Meeting I3N, March 9-10, 2012, Quiaios, Portugal.